

Characterising the role of Valosin Containing Protein (VCP) in autophagy and cell differentiation.

*Autophagy vs. aberrant osteoclastogenesis in the IBMPFD
mouse model*

Doctor of Philosophy
Thesis, October 2015

Milka B. Budnik-Zawilska

Project Supervisors: Dr Giles Watts, Prof Ian Clark

Norwich Medical School, Health Policy and Practice
University of East Anglia

This copy of the thesis has been supplied on condition that anyone who consults it is understood to recognise that its copyright rests with the author and that use of any information derived there from must be in accordance with current UK Copyright Law. In addition, any quotation or extract must include full attribution.

Contents

LIST OF TABLES.....	5
LIST OF FIGURES.....	6
ABSTRACT.....	9
ABBREVIATIONS.....	10
ACKNOWLEDGMENTS.....	15
CHAPTER 1: INTRODUCTION	17
1.1 Mutations in the VCP gene cause a degenerative disorder of muscle, bone and brain.....	17
1.2 VCP is implicated in diseases other than IBMPFD	21
1.3 Structure and function of Valosin Containing Protein (VCP)	23
1.4 VCP in the ubiquitin system	28
1.5 Protein quality control, stress granules and inclusion bodies	32
1.6 Autophagy in health and disease	37
1.7 Paget disease of the bone and aberrant osteoclastogenesis	46
1.8 Summary	53
CHAPTER 2: MATERIALS AND METHODS	57
2.1 Cell culture	57
2.2 Plasmids	58
2.3 Cloning	61
2.3.1 Generating pQE9 plasmids encoding His-tagged wt p62 and wt LC3B.....	62
2.3.2 Generating VCP-deletion mutants.....	66
2.4 Bacterial cell cultures.....	68
2.5 Reagents.....	68
2.6 Transfection and Autophagy induction	69
2.7 Cycloheximide-chase degradation assay	70
2.8 Co-immunoprecipitation.....	70
2.9 Western blot analysis.....	71
2.9.1 Odyssey infrared imaging system (Licor)	72
2.9.2 WesternBreeze Chemiluminescent Immunodetection (Invitrogen #WB7104 and #WB7106)	74
2.9.3 Quantification of Western Blots	74
2.10 Immunostaining	75
2.10 Light Microscopy and imaging	76
2.11 Imaris analysis	76

2.12	Filter-trap assay.....	77
2.13	VCP mouse Genotyping	78
2.14	Primary macrophages culture preparation and <i>In vitro</i> osteoclastogenesis.....	80
2.14.1	Osteoclast (OCL) differentiation ‘monocyte separation protocol’	80
2.14.2	OCL differentiation ‘quick protocol’	81
2.14.3	OCL differentiation ‘9-day protocol’	81
2.15	TRAP staining of osteoclasts	82
2.16	Detection of Active NFκB p65 in the Bone Marrow Derived Macrophages	83
2.17	Statistical Analysis.....	84
CHAPTER 3: VCP IN AGGREGATE CLEARANCE		87
3.1	Introduction	87
3.2	VCP in autophagy positive cells co-localises not only with Ubiquitin but also with p62 and LC3.....	89
3.3	VCP co-localises with ubiquitin, p62 and LC3 in cells expressing expanded polyglutamines.....	94
3.4	Cells expressing VCP mutants are more sensitive to protein aggregation	96
3.5	Overexpression of <i>wt</i> VCP in the cell culture increases clearance of poly-ubiquitinated substrates.....	102
3.6	Discussion.....	104
CHAPTER 4: VCP FORMS A COMPLEX WITH p62		110
4.1	Introduction	110
4.2	VCP directly interacts with p62 in the mTOR/ autophagy dependant manner.....	115
4.3	Discussion.....	123
CHAPTER 5: STABILITY AND DEGRADATION OF VCP.....		127
5.1	Introduction	127
5.2	VCP stability is linked to p62 instability in cells.	128
5.3	Discussion.....	136
CHAPTER 6: AUTOPHAGY AND OSTEOCLASTOGENESIS		140
6.1	Introduction	140
6.2	Inhibition of the mTOR signalling suppresses both early and late stages of osteoclast differentiation.....	146
6.3	Osteoclast differentiation from the primary Bone marrow derived macrophages.....	150
6.4	Inducers of protein aggregation lead to increased NFκB activation and p65 nuclear translocation in the primary BMDM.....	153
6.5	Discussion.....	161
CHAPTER 7: DISCUSSION.....		167

7.1	The VCP binds to p62 and is involved in the clearance of ubiquitinated protein aggregates by autophagy.....	167
7.2	VCP stability is linked to p62 instability	172
7.3	P62/VCP – dependant autophagy regulates osteoclastogenesis	175
7.4	Concluding remarks	182
	REFERENCES.....	184
	APPENDIX.....	208

LIST OF TABLES

CHAPTER 1: INTRODUCTION

Table 1.1. VCP mutations identified in patients with IBMPFD	20
-------------------------------------------------------------	----

CHAPTER 2: MATERIALS AND METHODS

Table 2.1. PCR running conditions for the Platinum Taq DNA Polymerase	62
Table 2.2. PCR running conditions for the Biomix DNA polymerase.	65
Table 2.3. Cloning primers.	66
Table 2.4. PCR running conditions.	66
Table 2.5. Formulation and concentration of the Thermo Scientific Halt TM Protease Inhibitor Cocktail	69
Table 2.6. Primary Antibodies	73
Table 2.7. Secondary Infrared Antibodies	73
Table 2.8. Primary Antibodies used for immunofluorescent staining.	75
Table 2.9. Secondary antibodies used for immunofluorescent staining.	76
Table 2.10. Sequencing primers.	79
Table 2.11. PCR running conditions for the sequencing.	80

CHAPTER 4: VCP FORMS A COMPLEX WITH p62

Table 4.1. Proposed VCP-interacting motifs and identified to date cofactors	113
Table 4.2. Experimental variables for optimizing IP results.	118
Table 4.3. Common binding partners for VCP.	125

LIST OF FIGURES

CHAPTER 1: INTRODUCTION

Figure 1.1. IBMPFD penetrance by phenotypes.	18
Figure 1.2. VCP protein structure.	23
Figure 1.3. Structural model of VCP N-domain flexibility.	25
Figure 1.4. General model for the ubiquitin system.	31
Figure 1.5. Schematic diagram of macroautophagy pathway.	39
Figure 1.6. Activation of the NF- κ B signalling cascade leads to increased osteoclastogenesis.	49

CHAPTER 2: MATERIALS AND METHODS

Figure 2.1. pcDNA3.2-p62-FLAG.	58
Figure 2.2. pcDNA3.2-VCP-V5.	59
Figure 2.3. pcDNA-DEST53-LC3B.	59
Figure 2.4. pCMX-HA-ataxin_3-Q35.	60
Figure 2.5. pCMX-HA-ataxin_3-Q79.	60
Figure 2.6. pQE-9 Vector (3439bp) Quiagen.	63
Figure 2.7. Plasmid map of pDONR221 plasmid indicating restriction sites.	67
Figure 2.8. Generation of the VCP ^{R155H/+} knock-in mice.	78
Figure 2.9. 'The 9-day osteoclast differentiation protocol'	82

CHAPTER 3: VCP IN AGGREGATE CLEARANCE

Figure 3.1. VCP R155H mutant mice show accumulation of p62 in muscle. Wild-type VCP localises to p62-positive structures in autophagy active cells.	91
-----------------------------------------------------------------------------------------------------------------------------------------------------	----

Figure 3.2. Vesicles that accumulate in autophagy active cells are positive for VCP, LC3 and ubiquitin.	93
Figure 3.3. Large vesicles accumulating in polyglutamine expressing cells are positive for VCP, ubiquitin and p62.	95
Figure 3.4. Large LC3-positive aggregates accumulate in cells expressing polyglutamines and mutant VCP.	98-99
Figure 3.5. More of large aggregates is formed in cells expressing mutant VCP.	101
Figure 3.6. Cells expressing VCP mutants are defective in aggregate clearance.	103
CHAPTER 4: VCP FORMS A COMPLEX WITH p62	
Figure 4.1. Schematic diagram showing VCP protein structure.	111
Figure 4.2. Schematic diagram showing p62 protein structure.	114
Figure 4.3. Immunoprecipitation (IP) of the VCP and autophagy markers LC3 and p62	117
Figure 4.4. Wt VCP Immunoprecipitates (IP) with wt p62 in the mTOR-dependant manner.	120
Figure 4.5. Co-immunoprecipitation (IP) of mutant VCP with wt p62.	121
Figure 4.6. Design of the VCP deletion constructs.	123
Figure 4.7. Model showing how the VCP/p62 interaction potentially is used for substrate selection and delivery to the macroautophagy pathway.	124
CHAPTER 5: STABILITY AND DEGRADATION OF VCP	
Figure 5.1. p62 and VCP stability in cells.	129
Figure 5.2. VCP stability increases in cells lacking p62.	131
Figure 5.3. Autophagy regulates VCP protein levels.	133
Figure 5.4. Overexpression of wt VCP increases stability of the endogenous p62.	135

CHAPTER 6: AUTOPHAGY AND OSTEOCLASTOGENESIS

Figure 6.1. Canonical and non-canonical NF- κ B signalling pathways.	141
Figure 6.2. Inhibition of the mTOR signalling suppresses both early and late stages of osteoclast differentiation.	148
Figure 6.3. Differentiating osteoclasts from RAW264.7 cells and Bone marrow derived	152
Figure 6.4. Disrupted regulatory pathways lead to over-activation of the NF κ B signalling cascade and increased osteoclastogenesis.	154
Figure 6.5. VCP mutant increases NF κ B activation in BMDM.	156
Figure 6.6. Autophagy inhibitors, Bafilomycin A1 and Wortmannin, increase NF κ B activation in BMDM.	158
Figure 6.7. Autophagy inhibition leads to accumulation of LC3II-positive inclusions in BMDM.	160
Figure 6.8. C/EBP β is a master switch in osteoclast differentiation.	162

CHAPTER 7: DISCUSSION

Figure 7.1. Mutations in p62 and VCP disrupt regulatory pathways resulting in over-activation of the NF κ B signalling cascade and increased osteoclastogenesis.	176
-------------------------------------------------------------------------------------------------------------------------------------------------------------------------	-----

ABSTRACT

Valosin containing protein (VCP)/p97 is a hexameric ATPase of the AAA family, which regulates a wide array of essential cellular processes. Dominant mutations in the N-domain of the VCP give rise to the complex disease syndrome known as Inclusion body myopathy with Paget disease of the bone and frontotemporal dementia (IBMPFD). VCP plays a key role in the ubiquitin-proteasome dependent protein degradation although mutations in VCP seem to result in a late stage autophagy defect. Osteoclast precursors containing VCP mutations are hyper-responsive to RANKL and M-CSF treatment. This suggests that under normal homeostasis VCP plays an important role in regulating the response of osteoclasts to bone microenvironment. However, the mechanisms by which VCP mutations stimulate osteoclast differentiation in Paget disease of the bone (PDB) are not completely understood.

To gain insight into disease phenotype associated with VCP mutations I examined the role of VCP in autophagy and the role of autophagy on osteoclastogenesis. I have shown that VCP co-localises with p62 and LC3 at the subcellular level in cells undergoing autophagy and that VCP co-immunoprecipitates with p62 in the autophagy-dependant manner. I have also examined the stability of VCP in the cell and shown that p62 has a role in stabilising the VCP protein and that the mutant protomers seem to be less stable than the normal VCP protomers. Initiation of autophagy in RAW264.7 cells in the presence of RANKL resulted in marked reduction in osteoclast formation, regardless of the time point at which the treatment begun. I also found that RANKL and TNF α induced NF κ B activation is increased (in an autophagy dependent manner) in macrophages from the heterozygous VCP mouse compared to normal macrophages.

These data together with the already existing knowledge on VCP, and the link with PDB, suggest that modulation of the autophagy pathway by VCP may represent a major regulator of bone remodelling and maintenance. Autophagy has direct effect on the fate of osteoclast progenitor cells thus regulation of osteoclastogenesis is a key process underlying the pathogenesis of PDB. This work acts to further our understanding of the pathogenic mechanism of VCP-related disease and will facilitate the search for modifiers of the disease phenotype.

ABBREVIATIONS

AD	Alzheimer's disease
Alfy	Autophagy-linked FYVE protein
ALS	Amyotrophic lateral sclerosis
ADP	Adenosine diphosphate
ANOVA	Analysis of variance
AR	Androgen receptor
ATG	Autophagy-related proteins
Atx1	Ataxin-1
Atx3	Ataxin-3
Atx7	Ataxin-7
ATPase	Adenosine triphosphatase
Baf A1	Bafilomycin A1
BECN1	Beclin 1
BMDM	Bone marrow derived macrophage
BMP6	Bone morphogenic protein 6
BP	Bisphosphonates
BSA	Bovine serum albumin
BS1	Binding site 1
CatK	Cathepsin K
C/EBP β	Transcription factor CCAAT/enhancer binding protein β
CFTR	Cystic fibrosis transmembrane conductance regulator
CHX	Cycloheximide
CIP	Calf intestinal alkaline phosphatase
CNS	Central nervous system
CRL	Cullin-RING ligase
CTHRC1	Collagen triple helix repeat containing 1
DKO	Double knockout
DMEM	Dulbecco's Modified Eagles Medium
DNA	Deoxyribonucleic acid

dNRAMP	<i>Drosophila</i> natural resistance-associated macrophage protein
DUBs	Deubiquitinating enzymes
DRIPs	Defective ribosomal products
E.coli	Escherichia coli
ELISA	Enzyme-linked immunosorbent assay
ER	Endoplasmic reticulum
ERAD	Endoplasmic reticulum-associated degradation
ESH	Expansile skeletal hyperphosphatasia
FAF1	Fas-associated factor 1
FBS	Foetal bovine serum
FEO	Familial expansile hyperphosphatasia
FIP200	Family interacting protein of 200kDa
FTD	Frontotemporal dementia
FTLD	Frontotemporal lobar degeneration
GAPARAP	GABA Receptor- Associated Protein
GATE16	Golgi-associated ATPase Enhancer of 16 kDa
GFP	Green fluorescent protein
gp78	Glycoprotein 78
HBSS	Hanks Balanced Salt Solution
HD	Huntington's disease
HDAC6	Histone deacetylase 6
HIF-1 α	Hypoxia inducible factor 1 α
HotSHOT	Hot sodium hydroxide and Tris
HRP	Horseradish peroxidase
HTT	Huntingtin protein
LB	Lysogeny broth
IBMPFD	Inclusion body myopathy with Paget disease of the bone and Frontotemporal dementia
IBM	Inclusion body myopathy
IgG	Immunoglobulin G
I κ B	Inhibitor of kappa B

IKK	I κ B kinase
IL-1	Interleukin 1
IP	Immunoprecipitation
KO	Knockout
LAMP 1 (2)	Lysosomal-associated membrane protein 1 (2)
LC3	Microtubule-associated protein (MAP) Light Chain 3
LGMD	Limb-girdle muscular dystrophic
LIR	LC3 interacting region
3-MA	3-Methyladenine
M-CSF	Macrophage colony stimulating factor
MEF	Mouse embryonic fibroblasts
α -MEM	α -minimal essential medium
Micro CT	Micro Computed Tomography
MHC	Major histocompatibility complex
MJD	Machado-Joseph disease
MMP13	Matrix metalloproteinase 13
M-PER	Mammalian protein extraction reagent
mRNA	Messenger RNA
MSP	Multisystem proteinopathy
mTOR	Mammalian target of rapamycin
NBR1	Neighbour of BR1 gene 1
NC	Nitrocellulose
NCIs	Neuronal cytoplasmic inclusions
NCL	Neuronal ceroid lipofuscinosis
NF κ B	Nuclear Factor kappa B
NFZ	Npl4 zinc finger
NIK	NF κ B-inducing kinase
OCL	Osteoclast
OPG	Osteoprotegerin
ORF	Open reading frame

PA	Phosphatidic acid
PBS	Phosphate buffer saline
PCR	Polymerase Chain Reaction
PD	Parkinson's disease
PDB	Paget's disease of bone
PE	Phosphatidylethanolamine
PEST	Proline, Glutamic Acid, Serine and Threonine
PFA	Paraformaldehyde
PFU	PLAA-family ubiquitin binding
PI3K	Phosphatidylinositol 3-phosphate kinase
polyQ	Polyglutamine
PQC	Protein quality control
PUB	PNGase/ubiquitin-associated
Q35	35-residue polyglutamine
Q79	79-residue polyglutamine
RA	Rheumatoid arthritis
RANK	Receptor activator of nuclear factor κ B
RANKL	Receptor activator of nuclear factor κ B ligand
Rheb	Ras-homologue enriched in brain
RNA	Ribonucleic acid
RNAi	RNA interference
SD	Standard deviation
SEM	Standard error of the mean
siRNA	Small interfering RNA
S1P	Sphingosine-1-phosphate
SPLM	Spleen derived macrophage
SQST1/p62	Sequestosome 1
SVIP	Small VCP-interacting protein
TBS	Tris-Buffered Saline
TDP-43	Transactivation response DNA binding protein

TGFβ	Transforming growth factor β
TIA-1	T-cell-restricted intracellular antigen-1
TLR	Toll-like receptor
TRAF6	TNF receptor-associated factor 6
TRAP	Tartrate resistant acid phosphatase
TNFα	Tumour necrosis factor alpha
Ub	Ubiquitin
UBA	Ubiquitin associated domain
UBD	Ubiquitin binding domain
UBIs	Ubiquitinated inclusions
UBX	Ubiquitin regulatory X
UPS	Ubiquitin-proteasome system
URAG	UV-radiation associated gene
V-ATPase	Vacuolar ATPase
VBM	VCP-binding motif
VCP	Valosin containing protein
VIM	VCP-interacting motif
WT	Wild-type
ZZ	Zinc finger

ACKNOWLEDGMENTS

First of all I would like to express my gratitude to my supervisor Dr Giles Watts, who has supported me throughout my PhD and whose expertise, understanding and encouragement have made this thesis possible. With his knowledge, patience and guidance I have developed research skills and techniques, whilst being able to work in my own way. I would also like to thank my secondary supervisor Prof Ian Clark and the lovely team of 'Clarkies' for letting me use their laboratory equipment and (occasionally) refer to the odd COSHH forms.

I would like to acknowledge the one and only other Watts lab member and at the same time my dearest friend Louise Cully who provided a great deal of physical and emotional support.

I would also like to thank everyone in the BMRC and BIO for everything they have helped me with - technical difficulties in one shape or another – in particular Matthew Jefferson for antibodies, reagents and cells; Prof. Tom Wileman and Dr Penny Powell for the constructive feedback and guidance I have received in their weekly lab meetings; Paul Thomas for his patience and guidance with microscopy; Dr Ernst Pöschl, Dr Helen James and Dr Jelena Gavrilovic for allowing me to gain experience in teaching and demonstrating and Laura Vaux for advice and help with Imaris analysis. I would also like to thank Jasmine Waters and Andy Loveday for daily running of the BMRC laboratories (especially tissue culture).

Lastly, I would like to say a huge thank you to my family – mostly to my dear mum: 'mamusiu dziekuje Ci za wsparcie przez ostatnie lata. Wiem ze we mnie wierzylas. Jakos przebrnelam przez ta wielka doktorancka probe!' I thank my friends (especially Agnieszka Zawadzka, Natalia Boguslawska and Johanna Nader) for all the love and support for the duration of my studies. Last but not least, I would like to acknowledge my partner Ryan Dewing, without whose love, encouragement and motivation I would not have become the person I am today.

CHAPTER 1

INTRODUCTION

CHAPTER 1: INTRODUCTION

1.1 Mutations in the VCP gene cause a degenerative disorder of muscle, bone and brain.

Autosomal dominant mutations in the gene encoding Valosin Containing Protein (VCP, also known as p97), which maps to chromosome 9p13.3, give rise to the complex disease syndrome named inclusion body myopathy (IBM) with Paget disease of the bone (PDB) and frontotemporal dementia (FTD), also known as IBMPFD (OMIM 1167320) (Watts *et al.*, 2004; Kimonis *et al.*, 2008). This hereditary multi-system disorder is characterised by three pathological phenotypes of varying penetrance – progressive adult-onset proximal and distal myopathy; early-onset PDB and premature neuro-degenerative FTD (Fig. 1.1). The combination of all three phenotypes was recognised as a genetically distinct syndrome by Kimonis and colleagues in 2000. The group found the concurrence of both a limb-girdle muscular dystrophic (LGMD) and Pagetic phenotype present in eight out of eleven family members (Kimonis *et al.*, 2000). Subsequently, using a candidate gene approach, six mutations were identified in the *VCP* gene in thirteen North American families with IBMPFD (Watts *et al.*, 2004). Today, it is known that VCP-related disease may manifest in muscle, brain and/or bone. Although patients are considered to have IBMPFD if they displayed two or more of the clinical phenotypes, diagnosis is carried out by gene sequencing.

The myopathy phenotype is the most common clinical feature in IBMPFD, presenting symptoms in over 90% of affected individuals in their 40s. Patients with IBM show an inability to raise the arms and difficulty climbing stairs; exhibit an abnormal gait eventually leading to loss of walking ability. Clinically, patients display a generalised reduction or absence of tendon reflexes, normal nerve conduction and myopathic electromyogram (Hübbers *et al.*, 2007). Muscle biopsies in affected individuals show the presence of atrophic and hypertrophic fibres with rimmed vacuoles and cytoplasmic inclusion bodies (Weihl *et al.*, 2008). The serum creatine phosphokinase levels are normal to slightly elevated (Kimonis *et al.*, 2008). In advanced cases, severe degeneration may result in death by complications of

respiratory and cardiac failure (resulting from skeletal muscle weakness rather than cardiomyopathy).

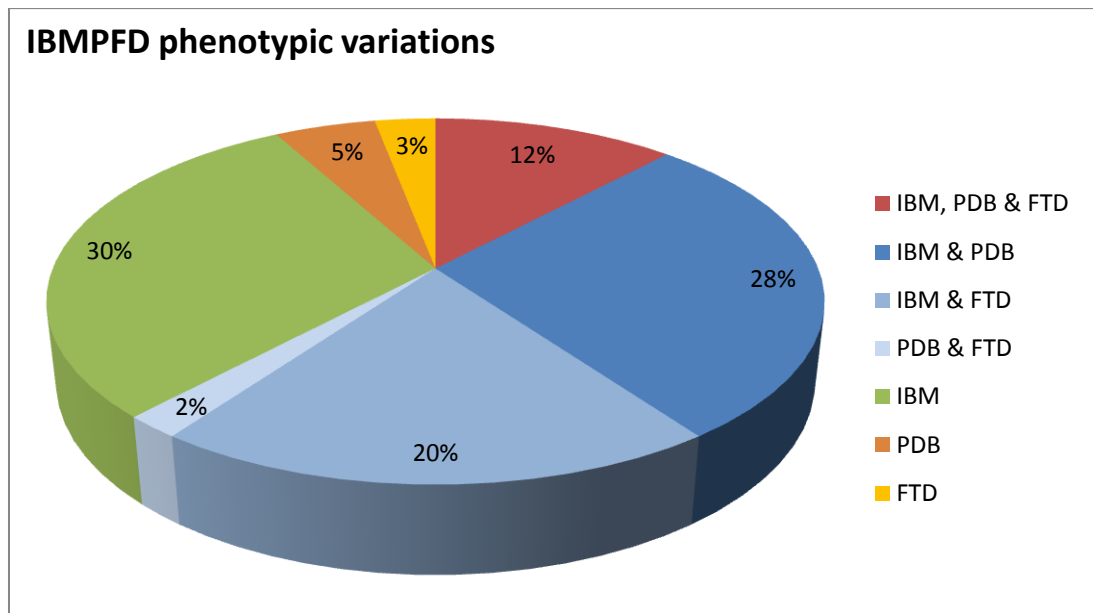


Figure 1.1. *IBMPFD penetrance by phenotypes.* Diagram is showing percentage of diagnosed IBMPFD patients with one or more of the IBMPFD-associated clinical feature. Statistics acquired from Kimonis *et al.* 2011 (GeneReviews).

PDB, characterised by abnormal bone remodelling, is observed in roughly 50% of IBMPFD patients (mean age 42 years). Pathologically increased bone resorption and formation results in abundant new bone that is highly disorganised and of poor quality. This can manifest as reduced height, bone pain, enlargement and fractures or even hearing loss due to cranial bone deformity (Kimonis and Watts, 2007). The imbalance of bone turnover is believed to result from the hyperactivity of osteoclasts – bone resorbing cells (Kimonis *et al.*, 2008). Histological analysis reveals abnormally large, multinucleated osteoclasts with nuclear inclusions of paired helical filaments similar to that seen in muscle tissue of IBM (Kimonis *et al.*, 2008). The average age of onset of bone deformity and enlargement is earlier than sporadic Paget’s disease (Hiruma *et al.*, 2008). On the other hand, the age of onset is similar to the slowly progressive distal and proximal muscle weakness seen in IBMPFD patients with myopathy.

Involvement of the central nervous system (CNS) in IBMPFD typically presents as frontotemporal dementia in 30% of cases. Affected individuals develop FTD in their

mid 50s, much later than both the IBM and PDB; manifested by prominent language and behavioural dysfunction (Mehta *et al.*, 2007; Kimonis *et al.*, 2008). Contrary to Alzheimer's disease (AD), patients with FTD develop cerebral atrophy in the frontal and anterior temporal lobes of the brain; rather than the hippocampal, posterior temporal and parietal lobes. Furthermore, AD associates with greater deficits in memory and executive function whereas individuals with FTD show relative preservation of memory (Forman *et al.*, 2006). Interestingly, a novel rare variant within the *VCP* gene (R95H on exon 2) was found to associate with Alzheimer's disease in one out of 188 sequenced individuals (Kaleem *et al.*, 2007). Other reports publish that mutations in *VCP* cause Amyotrophic lateral sclerosis (ALS) (Johnson *et al.*, 2010), with further data indicating that mutations may also cause Parkinsonism (Mizuno *et al.*, 2003). Although it is unclear if these disorders are part of the clinical spectrum of IBMPFD, the classification of *VCP*-related disease is certainly widening.

To date, 21 missense mutations in *VCP* gene have been identified in IBMPFD patients (Table 1.1), reported in more than 39 families worldwide (Nalbandian *et al.*, 2011; Komatsu *et al.*, 2013; Mehta *et al.*, 2013). The majority of mutations cluster within the interface between the D1 and N domains (Fig. 1.2). More than 50% of these mutations affect the arginine residue at position 155 resulting in a R155H, R155C or R155P change. The most common *VCP* mutation R155H (arginine to histidine) leads to increased level of ubiquitin-conjugated proteins, formation of cytoplasmic aggregates, impaired Endoplasmic Reticulum-associated degradation (ERAD) activity and increased ATPase activity (Halawani *et al.*, 2009; Manno *et al.*, 2010). Nevertheless, the most severe disease phenotype, characterised by early onset PDB and a particularly aggressive myopathy, is linked to A232E *VCP* mutant (Watts *et al.*, 2004) and shows the highest ATPase activity (Manno *et al.*, 2010; Niwa *et al.*, 2012). However, the notion that IBMPFD-associated *VCP* mutants possess the elevated ATPase activity is questionable as few have reported a normal ATPase activity in *VCP* mutants (Weihl *et al.*, 2006; Fernandez-Saiz and Buchberger, 2010).

	Amino Acid	Base Change (ORF)	Exon	Domain	No. of Families
1	I27V	79A>G	2	N terminus	1
2	R93C	277C>T	3	N terminus	4
3	R95G	283C>G	3	N terminus	2
4	R95C	283C>T	3	N terminus	1
5	P137L	410C>T	4	N terminus	1
6	R155C	463C>T	5	N terminus	5
7	R155H	464G>A	5	N terminus	8
8	R155P	464G>C	5	N terminus	1
9	R155S	463C>A	5	N terminus	1
10	R155L	464G>T	5	N terminus	2
11	G157R	469G>C	5	N terminus	1
12	G156S	466G>A	5	N terminus	1
13	R159H	476G>A	5	N terminus	2
14	R159C	476G>A	5	N terminus	2
15	R191Q	572G>A	5	Linker 1	1
16	L198W	593T>G	6	Linker 1	2
17	I206F	828A>T	6	Linker 1	1
18	A232E	695C>A	6	L1-D1 Junction	1
19	T262A	784A>G	7	AAA D1	1
20	N387H	1159A>C	10	AAA D1	1
21	A439S	1351G>T	11	Linker 2	1

Table 1.1. VCP mutations identified in patients with IBMPFD. Mutations are predominantly dispersed throughout the N-terminal domain, the N-D1 Linker region and D1 ATPase domain (not within the catalytic domain). Most of the mutated residues are adjacent and potentially interacting with each other (Watts *et al.*, 2007), suggesting that these residues have a similar and specific function within the VCP hexamer that does not affect ubiquitin or adaptor binding. In the context of the 3D protein structure it is likely that those mutants affect conformation of VCP and thus influence its affinity for ligand binding.

Disease models, carrying common VCP mutations have been generated in fruit flies (Ritson *et al.*, 2010) and mice (Weihl *et al.*, 2007; Custer *et al.*, 2010;

Badadani *et al.*, 2010). These provide insights into the human IBMPFD pathology and are useful as tools for preclinical studies and testing of therapeutic strategies. The VCP^{R155H/+} knock-in mouse, generated in the Kimonis Laboratory, expresses the mutant VCP allele at the endogenous level providing an opportunity to understand the *in vivo* effects of VCP mutations and the pathogenesis of IBMPFD. Crucially, the amino acids affected by the disease-causing mutations are highly conserved across species. Indeed, both human and mouse VCP proteins consist of 806 amino acids, and the mouse protein differs by only one amino acid residue (at position 684) when compared to the human protein containing the common R155H VCP mutation (Badadani *et al.*, 2010; Nalbandian *et al.*, 2012). The VCP^{R155H/+} knock-in mice demonstrate muscle weakness starting at approximately 6 months of age, with typical histopathology, accumulation of ubiquitin and transactivation response DNA binding protein (TDP-43) positive inclusion bodies in the muscle and brain, resembling the disease onset in humans in their 30s-40s (Badadani *et al.*, 2010). More recently, VCP mutations have also been linked to motor neuron degenerative disorder known as familiar amyotrophic lateral sclerosis (ALS) (Johnson *et al.*, 2010). Both ALS and IBMPFD lead to the deposition of ubiquitin-positive TDP-43 inclusions in diverse tissue types, including neurons of the frontal cortex (Shaw, 2011; Nalbandian *et al.*, 2011). Notably, the spinal cords of VCP^{R155H/+} mice show neuronal atrophy and astrocyte proliferation, with electrodiagnostic studies revealing a neurogenic pattern typical for ALS. Thus it would appear that VCP mutations cause the mislocalisation of TDP-43 from the nucleus and its aggregation in the cytoplasm of motor neurons which results in neurodegeneration (Johnson *et al.*, 2010; Shaw, 2011). Beside developing a significant progressive muscle weakness the Micro Computed Tomography (CT) analyses of VCP^{R155H/+} mice skeleton revealed Paget-like lesions at the ends of long bones (Nalbandian *et al.*, 2013). PDB-like lesions are patchy with increased bone activity, cortical thickness and osteoclastogenesis on bone histology resembling the distribution in humans (Nalbandian *et al.*, 2010).

1.2 VCP is implicated in diseases other than IBMPFD

While mutations in VCP lead to IBMPFD, Amyotrophic lateral sclerosis (ALS) and Motor Neuron disease (NMD), the expression levels on VCP have also been

associated with other diseases. Most notably, elevated VCP levels have been found in gastric, colon, pancreatic and hepatocellular cancers and are linked to a poor prognosis (Vij, 2008). The strongest correlation between VCP and cancer is in Nuclear Factor kappa B (NFκB) signalling which upregulation leads to increased survival and proliferation of tumorigenic cells (Hoesel and Schmid, 2013). Similar to TDP-43 and p62, VCP has been detected in some of the disease-associated inclusions of a broad array of neurodegenerative diseases such as senile plaques in Alzheimer's disease, Lewy bodies in Parkinson's disease, neuronal intranuclear inclusions in polyglutamine diseases and ubiquitin-positive inclusions in ALS (Mizuno *et al.*, 2003; Hirabayashi *et al.*, 2001).

As mentioned above, TAR DNA-binding protein 43 (TDP-43) accumulation is recognised as a pathological feature in many diseases including IBMPFD and ALS. TDP-43 is a 414- amino acid nuclear protein encoded by the *TARDBP* gene on chromosome 1; binds to DNA and RNA and regulates transcription, pre-mRNA splicing and translation. Pathological signature of TDP-43 in ALS and FTD is classified based upon ubiquitin-positive TDP-43 deposition in central nervous system (including hippocampus, neocortex and spinal cord) (McClusky *et al.*, 2009). After neuronal injury, TDP-43 redistributes to the cytoplasm where it associates with stress granules (Colombrita *et al.*, 2009). VCP and TDP-43 interact genetically and disease-causing mutations in VCP lead to this redistribution of TDP-43 to the cytoplasm (where it then accumulates), which is sufficient to induce cytotoxicity (Ritson *et al.*, 2010). The redistribution of TDP-43 to the cytoplasm contributes to degeneration initiated by mutations in VCP.

VCP has also been shown to interact with other pathological ubiquitinated substrates (including MJD and HTT proteins) in a broad array of sporadic and inherited human diseases. The MJD protein, which causes Machado-Joseph disease (MJD) - the most common inherited spinocerebellar ataxia, was identified as a substrate specifically bound by VCP (Hirabayashi *et al.*, 2001). Furthermore, the huntingtin protein (HTT), causative agent of Huntington's disease, interferes with ERAD, although it does not interact directly with VCP but with the gp78 - ER-membrane associated E3 ligase and a VCP cofactor (Erzurumlu *et al.*, 2013).

1.3 Structure and function of Valosin Containing Protein (VCP)

VCP (p97 in mice, TER94 in *Drosophila melanogaster* and CDC48 in *Saccharomyces cerevisiae*) is a 97-kDa ubiquitously expressed, highly conserved member of the type II AAA-ATPase (ATPase associated with variety of cellular activities) family (Woodman, 2003). Structurally VCP forms a homo-hexamer with each monomer consisting of an N-domain, two centrally located ATPase domains – hallmark feature of AAA-ATPase family members - D1 and D2, and a C-terminal domain (Fig. 1.2). While both ATPase domains comprise highly conserved protein motifs: Walker A (consensus sequence of GXXXXGK (T/S), associated with phosphate binding) and B (consensus sequence of (R/K) XXXXGXXXLXXXD) motifs, necessary for ATP binding and hydrolysis, respectively, the D1 domain has less ATPase activity than D2 (Wang *et al.*, 2005). The D1 domain is primarily responsible for VCP hexamerisation but this molecular assembly is not dependent on nucleotide binding (Wang *et al.*, 2003). The ATPase activity conferred by the D2 domain is utilised for VCP function as a molecular chaperone to structurally remodel or unfold client proteins in diverse cellular processes (including endoplasmic reticulum-associated degradation – ERAD, endosomal sorting and mitotic spindle disassociation). Nevertheless, either D1 or D2 domain of VCP is sufficient to carry out its unfolding activity, partially dependant on the structure of the polyubiquitinated substrate itself (Song *et al.*, 2015). Mutations in the Walker A or Walker B motifs of D2 domain are dominantly lethal (Chapman *et al.*, 2011).

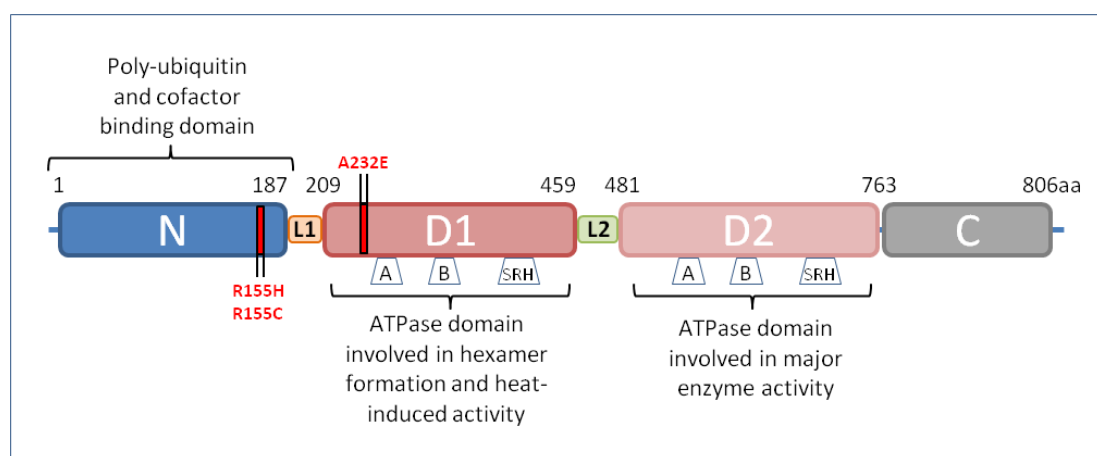


Figure 1.2. VCP protein structure. VCP functions as homo-hexamer composed of six subunits. Each subunit consists of a globular N-terminal domain (1-187) (blue), the two AAA ATPase

domains D1 (209-460) (crimson) and D2 (481-761) (blush), and a C-terminal tail (762-806) (grey). There are two linker domains in the protein: N-D1 linker (orange) and flexible D1-D2 linker (green). The two AAA domains contain the conserved Walker A, Walker B and a second region of homology (SRH). Walker A is required for nucleotide binding, whereas Walker B and SRH motifs mediate efficient ATP hydrolysis. The N domain of VCP is responsible for the cofactor and ubiquitin binding function. While the D1 domain mediates oligomerisation and independent nucleotide binding, the D2 domain confers most of the ATPase activity. The D1 and D2 form two stacked hexameric rings. The ATP binding and hydrolysis lead to changes in the conformation of the hexameric ring. This is assumed to be a driving force for VCP role as a chaperone in disassembling protein complexes and mediating extraction of ubiquitinated proteins from the ER. Mutations detected in IBMPFD patients predominantly affect evolutionarily highly conserved arginine residues in codon 155 of the N-domain. The A232E mutant is associated with the most severe disease phenotype, characterised by early onset PDB and a particularly aggressive Myopathy.

The conformational integrity of the D2 ring is altered in mutant VCP complexes resulting in increased ATPase activity (Halawani *et al.*, 2009). The N-terminal domain is proposed to be the determining factor in target binding specificity (Wang *et al.*, 2003) and mediates the binding of both adaptor proteins and ubiquitinated substrates. Electron-microscopic studies show that the VCP hexameric protein structure comprises two ring-shaped layers consisting of the D1 and D2 ATPase domains. The conformation of the N-domain and linker region with respect to the D1 and D2 regions correlates directly with the ATPase activity of VCP (Niwa *et al.*, 2012). The N-domain is connected to D1 by a flexible linker that allows it to adopt either of two conformations, named coplanar and flexible with D1. When N-domains are coplanar with the D1 ring, VCP is unable to hydrolyse ATP. In a flexible state the N-domains are released from the D1 plane, D2 domains form a compact ring and VCP hydrolyses ATP (Fig. 1.3). Besides mediating the binding of cofactors and ubiquitinated protein substrates, the N-domain is thought to regulate ATPase activity of VCP. The C-terminal region binds a subset of cofactors and may be involved in maintaining the conformation of the D2 ring (Niwa *et al.* 2012). In addition, this region includes the major tyrosine phosphorylation site implicated in the regulation of endoplasmic reticulum (ER) assembly and cell cycle dependent nuclear localization of VCP (Lavoie *et al.*, 2000; Song *et al.*, 2015).

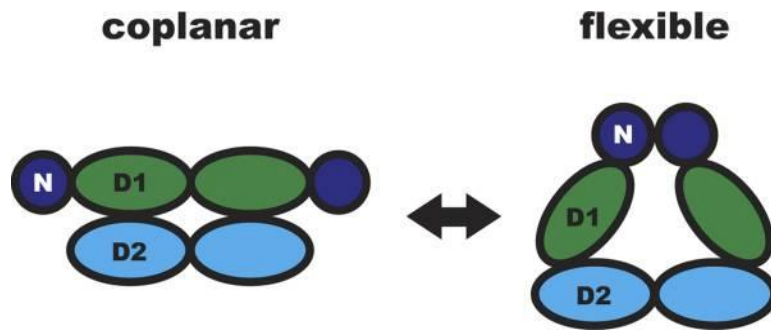


Figure 1.3. *Structural model of VCP N-domain flexibility.* During the ATPase cycle, VCP can adopt two conformations. When N-domains are coplanar with the D1 ring, VCP is unable to hydrolyse ATP. In the flexible state, when the D2 domains form a compact ring and N domains are released from the D1 plane, VCP hydrolyses ATP. Only two subunits of the hexamer are shown in a side view for clarity (Adapted from Niwa *et al.*, 2012)

Different aspects of VCP functions depend on its ability to interact with a diverse array of cofactor proteins. These cofactors contain specific interaction domains or motifs (see below) that bind to VCP either at its N-terminal domain or C-terminal tail (Meyer *et al.*, 2012). Structural studies on VCP suggest that mutations within the N-D1 domains could alter the interaction with the adaptor complexes. Moreover, the presence of ubiquitinated inclusions in the affected tissue of IBMPFD patients and the known VCP role in the UPS, suggest that these mutations may somehow disrupt normal protein degradation (Schroder *et al.*, 2005; Forman *et al.*, 2006). VCP is known to be essential for the endoplasmic reticulum-associated degradation (ERAD), a pathway in which defective or abnormally folded and short-lived ER proteins are degraded (Ballar *et al.*, 2011). The participation of VCP in this pathway depends on its binding partners Ufd1 (ubiquitin fusion degradation 1) and Npl4 (nuclear protein localisation homolog 4) (Ye *et al.*, 2003). Once substrates designed for proteasomal degradation are retrotranslocated from the ER lumen to the cytosolic face of the ER, they are bound by the VCP/Ufd1-Npl4 complex, and this triggers subsequent ubiquitination and transfer to the proteasome for degradation (Ye *et al.*, 2003). A nonubiquitinated, unfolded segment of a retrotranslocation substrate is initially recognised by VCP then, once a polyubiquitin chain has been attached, the substrate is recognised by VCP and the cofactor Ufd1-Npl4 in the complex; and this interaction may in turn activate the ATPase to pull the polypeptide chains out of the membrane (Mayer *et al.*, 2002; Ye *et al.*, 2003). Interestingly, the

VCP/Ufd1-Npl4 complex also selectively interacts with UBX domain of Fas-associated factor 1 (FAF1, an ubiquitin receptor and substrate-recruiting cofactor) (Lee *et al.*, 2013), which regulates the recruitment of polyubiquitinated substrates to FAF1 ubiquitin-associated (UBA) domain further regulating and promoting ERAD. Although almost all IBMPFD-specific VCP mutants exhibit enhanced Ufd1-Npl4 binding, the functional complexes formed show impaired substrate-processing ability resulting in ERAD substrate accumulation (Erzurumlu *et al.*, 2013). Loss of VCP activity or expression of an ATP hydrolysis-deficient mutant been shown to lead to accumulation of non-degraded ubiquitinated proteins and prevented aggresome formation in cells (Ju and Weihl, 2010). The function of VCP and its adaptor complexes described here and how this could relate to disease implies that the role of VCP within the cell is not confined but determined by the adaptor/substrate binding. At the cellular level IBMPFD has been characterised by not only the impaired ERAD but also excessive accumulation of ubiquitin-positive protein aggregates in affected tissues (Tresse *et al.*, 2010; Yamanaka *et al.*, 2012). In a subset of transfected cells, IBMPFD mutations were associated with elevated levels of endogenously expressed mutant Cystic fibrosis transmembrane conductance regulator (CFTR, a protein degraded by ERAD (Weihl *et al.*, 2006). However, the mutant CFTR protein was also shown to be degraded by autophagy (Fu and Sztul 2009). Others noted no impairment of the ERAD pathway in cells expressing disease-associated VCP mutants, but only in cells with catalytically-dead VCP (Tresse *et al.*, 2010). Therefore the current notion is that the dominant negative VCP could have a varied effect on cellular function. If the ERAD is not impaired then another ubiquitin-dependant degradation pathway is affected by VCP mutations? Seemingly, the exact role of the VCP ATPase in the pathogenesis of the IBMPFD syndrome is not yet understood.

Recent studies have helped shed light on how mutations in VCP affect the protein structure. As mentioned above, the majority of disease-associated mutations in VCP localise to the interface of the N and D1- domains. These pathogenic mutants are able to form proper hexamers just like the wild type (Weihl *et al.*, 2006; Niwa *et al.* 2012) and do not introduce apparent alterations to the part of the structure where they occur (Tang *et al.*, 2010). Instead, they alter conformational changes that cause impaired communication between the D1 and N domains and indirectly

influence the nucleotide binding pocket in D1 (Fernandez-Saiz and Buchberger 2010). IBMPFD causing mutations exhibit dysregulated N-domain conformation where they adopt an atypical N-domain conformation i.e. all six domains of the complex swing upwards (Tang *et al.*, 2010). In addition, Niwa and colleagues observed that the A232E mutation introduces a negative charge in a largely hydrophobic area, resulting in increased flexibility of the N-domain what in turn ablates its ability to assume the coplanar conformation (Niwa *et al.* 2012). The most apparent effect of this is a change in the relative affinity for ATP and ADP. Recently, Tang and colleagues found that this uniform arrangement of N-domains in mutant complexes is a secondary effect of reduced ADP binding by the D1 domain (Tang and Xia 2013). In wild type VCP the prebound ADP cannot be displaced and thus ATP can only bind to empty D1 sites, resulting in heterogenous nucleotide states within a hexamer (Tang *et al.*, 2010). Since the movement of the N-domain is controlled by the nucleotide state of the D1 domain, the heterogeneity in N-D1 domain conformation seems to be a crucial property for the function of wild type VCP. Notably, the IBMPFD-specific VCP mutants show an increase in ATPase activity and increased sensitivity to heat-induced upregulation in ATPase activity (Halawani *et al.*, 2009). This enhanced ATPase activity could be correlated with the availability of nucleotide-binding sites of the D1 domain, what in turn stimulates the ATPase activity in the D2 ring (Tang and Xia 2013).

The disease-associated mutations, through introducing conformational changes in the N-domain, also specifically alter interaction of VCP with a subset of cofactors, such as Npl4 and Ufd1 heterodimers (Fernandez-Saiz and Bunchberger, 2010). Specifically, the IBMPFD disease mutants exhibit elevated binding affinities for Ufd1-Npl4 as well as for p47 *in vitro*. However, decreased binding to a UBX cofactor – UBXD1 was observed in 293T cells expressing VCP mutants, resulting in impaired trafficking of the plasma membrane protein caveolin-1 (Ritz *et al.*, 2011). It would thus appear that binding of some but not other cofactors at the N-domain triggers a conformational change to convert D1 to the ADP-open state. This allows more ATP to bind to D1, thereby stimulating the D2 ATPase. Crucially, cofactors play a critical role in controlling VCP ATPase activity thus the lack of cofactor-regulated communication may contribute to VCP-associated disease pathogenesis (Zhang *et al.*, 2015). Nevertheless, the autosomal dominance of IBMPFD disease penetrance is indicative

of a dominant mechanism; either a toxic gain of function or dominant negative activity. Since mutant forms of VCP retain the ability to form hexamers, even the A232E mutant, and the ATPase activity of multiple VCP mutants is significantly increased, the theory that mutations in VCP result in the amplification of a native function is a believable concept (Halawani *et al.*, 2009; Niwa *et al.* 2012).

1.4 VCP in the ubiquitin system

VCP protein is highly abundant in cells and regulates a variety of cellular functions, such as nuclear envelope formation, cell cycle progression, apoptosis, nuclear envelope reconstruction and postmitotic organelle reassembly (Chapman *et al.*, 2011). These seemingly unrelated functions are at least partially regulated by the ubiquitin-proteasome system (UPS). The UPS is the major selective proteolytic pathway in eukaryotic cells defining the degradation of substrate proteins that are tagged with homopolymers of ubiquitin (Franz *et al.*, 2014). Ubiquitin (ub) is a small 8 kDa protein that is conjugated through an isopeptide bond to a lysine residue of the substrate and itself contains seven lysine residues in positions 6, 11, 27, 31, 33, 48 and 63 (Korolchuk *et al.*, 2010). It can thus either serve as monoubiquitin or be extended to create chains through ubiquitination of one of seven lysines generating different types of polyubiquitin chains. A polyubiquitin chain is attached to target proteins via the action of ubiquitin-activating (E1), ubiquitin-conjugating (E2) and ubiquitin-ligating enzymes (E3; dictates substrate specificity) into poly-lysine chains with various conformations and monoubiquitinate and multi-monoubiquitinate target proteins (Fig. 1.4) (Scheffner *et al.*, 1995; Ikeda and Dikic, 2009). In some cases ubiquitin chain elongation factors called E4 enzymes are required for efficient ubiquitination (Hoppe, 2005). Ubiquitin can attach at one or multiple sites of a client protein. The length of the ubiquitin chain and the linkages between ubiquitin molecules determines if that substrate will be degraded via the UPS (Komander and Rape, 2012). For example, lysine 11 (K11) - and lysine 48 (K48) – linked chains serve to target substrates for degradation at the proteasome (Thrower *et al.*, 2000). Conversely, monoubiquitin and other types of chains (e.g. K63-linked) primarily trigger lysosomal degradation (through endosomal sorting or autophagy) as well as non-proteolytic signalling pathways (Mukhopadhyay and Riezman, 2007). Chains of

minimum four ubiquitins interconnected via K48 (or K11) residues are optimal for delivery to the proteasome (Fushman and Walker, 2010). The proteasome (26S) is a barrel-shaped multicatalytic protease complex localised both in the cytosol and the nucleus that consists of a 20S central cylinder subunit and two 19S cap-shaped subunits (Peters *et al.*, 1994). The 19S complexes bind cargo-loaded shuttling proteins, deubiquitinate the substrates and control access to the six proteolytic sites of a central 20S subunit. The catalytic activities of the 26S proteasome are considered to be trypsin-, chymotrypsin-, peptide-glutamyl and peptide-hydrolysing-like (Peters *et al.*, 1994). The narrow size of the proteasome catalytic 20S pore requires protein substrates to be partially unfolded prior to entry, process mediated by VCP and ubiquitin binding adaptor proteins (Korolchuk *et al.*, 2010).

In association with the UPS, VCP acts as a molecular segregase and mediates ubiquitin-dependent extraction of substrates from membranes, cellular structures and multiprotein complexes for recycling or degradation by the 26S proteasome (Fig. 1.4); this is likely in flux with the alternative route of degradation via autophagy (Korolchuk *et al.*, 2009; Meyer *et al.*, 2012). The UPS selectively degrades misfolded and short-lived proteins that are covalently modified with a polyubiquitin chain. The VCP facilitates steps downstream of ubiquitination, as it directly and indirectly binds to ubiquitinated substrates (Jentsch and Rumpf, 2007; Meyer *et al.*, 2012). The degree of the requirement for VCP varies and might depend on substrate localisation, structure or solubility (Gallagher *et al.*, 2014). Whilst VCP itself has some affinity for ubiquitin, it binds to ubiquitin conjugates largely through adaptor proteins with dedicated ubiquitin-binding domains (Franz *et al.*, 2014). VCP has been associated with monoubiquitin, lysine 29 (K29), lysine 63 (K63), lysine 48 (K48) – linked chains, as well as branched lysine 11/48 (K11/K48) – linked chains (Ye, 2006; Meyer and Rape, 2014). VCP mediates the turnover of several cytosolic UPS substrates including inhibitor of kappa B (I κ B) (Dai *et al.*, 1998), UNC-45B (skeletal muscle myosin chaperone) (Janiesch *et al.*, 2007) and hypoxia inducible factor 1 α (HIF-1 α) (Alexandru *et al.*, 2008). Degradation of ubiquitinated proteins by the 26S proteasome requires continuous ATP hydrolysis. It was proposed that VCP uses the energy from ATP hydrolysis to structurally remodel target proteins in order to unfold or extract them from binding partners or cellular structures (Bug and Meyer, 2012).

More importantly however, different aspects of VCP functions depend on its ability to interact with a diverse array of cofactors. This ability to form adaptor complexes with different sets of at least 40 cofactors enables VCP to mediate a myriad of cellular processes, including targeting specific substrates for degradation (Yeung et al., 2008; Ju and Wehl, 2010; Buchberger et al., 2015). Some of these cofactors serve as ubiquitin adaptors or recruit VCP to intracellular membranes. Many of each contains UBX (ubiquitin regulatory X) or UBX-like ubiquitin-fold domains that bind to VCP N-terminal domain (Kloppsteck et al., 2012). They also contain the ubiquitin binding domains (UBDs) that recognise the client, such as ubiquitin-associated (UBA), the Npl4 zinc finger (NFZ) or the PLAA-family ubiquitin binding (PFU) domains (Meyer et al., 2012). The majority of UBDs recognise the Isoleucine 44/ Valine 70 (I44/V70) hydrophobic patch on ubiquitin, while some bind to a polar site centred on Aspartic Acid 58 (D58) or a hydrophobic patch on leucine 8 (L8) (Searle et al., 2012). The most functionally diverse of VCP's substrate recruiting cofactors is the heterodimeric complex Ufd1-Npl4, which mediates many of the proteasome-related activities of VCP. Both proteins bind to VCP in a synergistic fashion, Ufd1 via its UBX domain and Npl4 via its UBD domain (Chapman et al., 2011). The VCP-Ufd1-Npl4 complex facilitates a number of proteasomal degradation pathways such as ERAD, where it drives the dislocation of polyubiquitylated substrates from the ER membrane into the cytosol, degradation of proteins associated with chromatin and the outer mitochondrial membrane, and of important regulators of cell cycle progression and signal transduction (Buchberger et al., 2015). Other VCP-interacting motifs identified to date include the PNGase/ubiquitin-associated (PUB) domain (Madsen et al., 2009), VCP-interacting motif (VIM) (Staph et al., 2011), PUL and PFU (PLAA family ubiquitin binding) domains (Mullally et al., 2006) or BS1/SHP (binding site 1) box (Madsen et al., 2009) (More on VCP binding partners in Chapter 4). VCP also either directly or indirectly (through the UBXD7/Ubx5 adaptor) binds to ubiquitin E3/E4 ligases and deubiquitinating enzymes (DUBs) which edit the ubiquitin chains on the substrate protein (Alexandru et al., 2008; Sowa et al., 2009). This in turn results in either recycle of the substrate or improves its targeting to the proteasome, thus determining its fate. E3 ligases that interact with VCP include a large number of cullin-RING ligases (CRLs), which facilitate ubiquitin transfer from the E2 enzyme to

the substrate (Alexandru et al., 2008). Some of the CRL substrates that require VCP for extraction include hypoxia-inducible factor (HIF α - CUL2 substrate), mitotic kinase Aurora B, polymerase II catalytic subunit Rpb1 (both ubiquitinated by CUL3) and replication licensing factor Cdt1 (targeted by CUL4A) (Meyer et al., 2012). VCP also recruits ubiquitin-chain editing factors, such as E4B/Ufd2, which can extend shorter ubiquitin chains to promote substrate targeting for degradation (Jentsch and Rumpf, 2007). In contrast, DUBs remove ubiquitin, shortening ubiquitin chains, to either promote substrate recycling or facilitate proteasome recognition and subsequent degradation (Franz et al., 2014). VCP facilitates the proteasomal degradation of large cohorts of damaged or misfolded proteins in different compartments including the ER (via ERAD), the outer mitochondrial membrane and the nucleus, as well as co-translational degradation at the ribosome (see below). Thus one could say that the main function of VCP in ensuring protein homeostasis is well established.

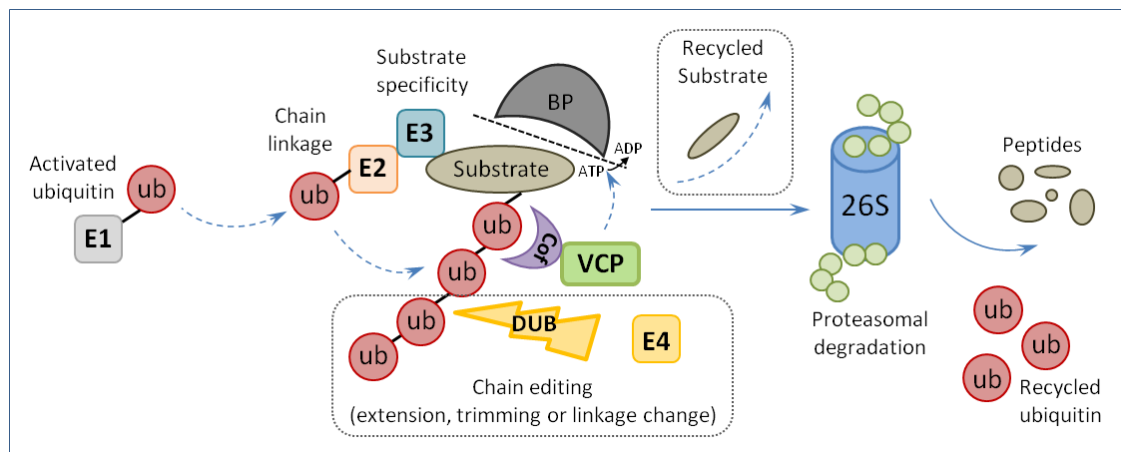


Figure 1.4. *General model for the ubiquitin system.* Substrate protein is modified by covalent attachment of ubiquitin (ub) via a cascade of the ubiquitin-activating enzyme (E1), ubiquitin-conjugating enzyme (E2) and a specific ubiquitin ligase (E3). VCP cooperates with dedicated ubiquitin-binding cofactors in substrate recognition and together with chain-elongation (E4) or deubiquitinating (DUB) enzymes in ubiquitin chain editing. VCP converts the energy of ATP hydrolysis to extract substrate protein from binding partners (BP) such as protein complexes, membranes, or chromatin. Following ubiquitin modification, after segregation from its binding partner, substrate protein may either be recycled or transferred to the 26S proteasome for degradation.

1.5 Protein quality control, stress granules and inclusion bodies

Cells respond to stresses, like heat shock or oxidative agents, which lead to protein aggregation, by activating the protein quality control and attenuating translation (Bukau *et al.*, 2006). The protein quality control (PQC) consists of molecular chaperones and degradation systems and is an essential player of the proteotoxic stress response. In order to minimize protein aggregation chaperones assist protein folding; when this is not effective, chaperones assist in targeting damaged substrates for clearance by the UPS and the lysosome-based degradation systems (Bukau *et al.*, 2006; Korolchuk *et al.*, 2009). In parallel, polysomes (or polyribosomes – a cluster of ribosomes bound to a mRNA) disassemble, releasing ribosomes, mRNAs (messenger RNAs), defective ribosomal products (DRIPs) and newly synthesised proteins, which, due to the stress, are prone to aggregation (Schubert *et al.*, 2000).

In order to maintain proper modulation of gene expression the control of mRNA (carrier of genetic code for a specific protein product) translation, as well as its localisation and degradation is particularly important. From transcription to degradation, cellular mRNAs are coated with proteins in messenger ribonucleoprotein (mRNP) complexes. The mRNP composition dictates whether the mRNA engages in translation or remains translationally inactive and is subject to either storage or degradation (Erickson and Lykke-Andersen 2011). Non-translating mRNPs in eukaryotic cells often assemble into conserved and dynamic cytoplasmic mRNP granules known as processing (P) -bodies and stress granules (Buchan and Parker, 2009; Erickson and Lykke-Andersen, 2011). Stress granules and P-bodies are highly dynamic membraneless cytoplasmic granules observed in a wide variety of eukaryotes; and are related to mRNP granules in embryos - where maternal mRNAs are stored, neurons - involved in mRNA transport and translational control at synapses, and pathological inclusions in some degenerative diseases (Nonhoff *et al.*, 2007; Buchan and Parker, 2009). Stress granules are typically observed when translation initiation is limiting and consist of translationally silent mRNAs, early initiation factors, small, but not large, ribosomal subunits, mRNA-binding proteins, kinases and signalling molecules, and thus are thought to represent a pool of mRNPs stalled in the process of translation initiation (Anderson and Kedersha, 2009; Buchan

and Parker, 2009). P-bodies, on the other hand, consist of mRNAs associated with translation repressors and the mRNA decay machinery, and while typically present in cells at modest levels, they increase when the pool of non-translating mRNPs is larger (Parker and Sheth, 2007). Under the microscope, P-bodies generally seem discrete and rounded, ranging from 100 to 300 nm in diameter, whereas stress granules can seem more diffuse and can average 100 to 200 nm (Yang et al., 2004; Erickson and Lykke-Andersen 2011). Stress granules assembly occurs in a challenging subcellular environment where aggregate-prone substrates (released by polysomes) tend to accumulate, but can also be triggered by the self-aggregation of RNA-binding proteins that contain prion-like domains, including T-cell-restricted intracellular antigen-1 (TIA-1) (Gilks *et al.*, 2004).

The formation of stress granules and P-bodies is based on two principles. First, they require non-translating RNA for their assembly. Second, individual mRNPs are brought together by dimerization or aggregation domains present on mRNP binding proteins. For example, the assembly of P-bodies in yeast is driven in part by a dimerization domain on the Edc3 protein and a “prion domain” present on the Lsm4 protein (Decker *et al.*, 2007; Reijns *et al.*, 2008). Similarly, as mentioned above, stress granule formation in mammalian cells is promoted by a prion domain on the TIA-1 protein (Gilks *et al.*, 2004), and mRNA binding proteins frequently contain such aggregation prone prion-like or low-complexity domains (Decker *et al.*, 2007; Kim *et al.*, 2013). The prevalence of such aggregation domains in RNA binding proteins as part of their normal role in forming stress granules and P-bodies suggests they provide a significant target for mutations that create pathologically aggregated proteins. In fact, mutations in known stress granule proteins which often increase their tendency to aggregation have emerged as being involved in some degenerative diseases, including such conditions as amyotrophic lateral sclerosis (ALS), frontotemporal lobar degeneration (FTLD), fragile X syndrome, spinocerebellar ataxia-2, inclusion body myopathy (IBM) and multisystem proteinopathy (MSP) (Nonhoff *et al.*, 2007; Didiot *et al.*, 2009; Ito and Suzuki, 2011; Kim *et al.*, 2013). Furthermore, a hallmark of ALS, FTLD and some other degenerative diseases is the accumulation of cytoplasmic aggregates that contain several stress granule factors and RNA (Ito and Suzuki, 2011; Dewey *et al.*, 2012). Specifically, stress granule marker

proteins were found to be additional components of trans-activation response DNA protein 43 (TDP-43) or fused in sarcoma (FUS)-positive neuronal cytoplasmic inclusions (NCIs) in patients with ALS and FTLD (Dormann *et al.*, 2010; Dewey *et al.*, 2012) and in transgenic mice expressing mutant human VCP (Rodriguez-Ortiz *et al.*, 2013). TDP-43- positive NCIs were ubiquitin-positive, whereas FUS-positive NCIs were inconsistently ubiquitin-immunoreactive in ALS and FTLD patients (Dormann *et al.*, 2010; Ito and Suzuki, 2011). This led to the hypothesis that inappropriate formation or persistence of stress granules, or some related mRNP aggregate might be related to the pathogenesis in these diseases. Therefore, since mutations in VCP cause ALS, FTLD and MSP, which are all characterised by pathological accumulation of TDP-43 and in some cases other stress granule proteins in cytoplasmic aggregates (Johnson *et al.*, 2010; Salajegheh *et al.*, 2009; Kim *et al.*, 2013), it is not surprising that VCP has been identified to be involved in clearance of stress granules (Buchan *et al.*, 2013; Seguin *et al.*, 2014).

VCP and the autophagy-lysosome pathway govern protein (and organelle) degradation and are thus key players of the protein quality control. Observations suggested that stress granules and P-bodies can be degraded by autophagy, in a process termed granulophagy, although stress granules are more commonly targeted for autophagy than P-bodies (Buchan *et al.*, 2008; Buchan *et al.*, 2013). Interestingly, inhibition of autophagy, lysosomes and VCP impairs stress granules, supporting that the PQC modulates stress granule formation and disassembly (Seguin *et al.*, 2014). In addition, silencing the VCP co-factors UFD1L and PLAA, which degrade defective ribosomal products (DRIPs) and 60S ribosomes, also impair stress granule assembly (Seguin *et al.*, 2014). Furthermore, DRIPs and 60S, which are released from disassembling polysomes and are normally excluded from stress granules, are retained within stress granules in cells with impaired autophagy, lysosome or VCP function (Seguin *et al.*, 2014). In contrast, stimulation of autophagy with either 3-MA or rapamycin increased rate at which stress granules were cleared following the relief of oxidative stress (Wu *et al.*, 2010). Since VCP utilises ATP hydrolysis to segregate ubiquitinated proteins from a variety of cellular complexes and stress granules in mammalian cells are heavily ubiquitinated (Kwon *et al.*, 2007) it would appear that stress granules and P-body dynamics is modulated via ubiquitination. Furthermore,

VCP binding partner – HDAC6 is involved in autophagic clearance of ubiquitinated proteins (Ju *et al.*, 2008) and itself binds ubiquitinated targets, but also regulates stress granule assembly in mammalian cells (Kwon *et al.*, 2008). These findings imply that deregulated autophagy, lysosomal or VCP activities, which occur in several neurodegenerative (VCP-associated) diseases, may alter stress granule morphology and composition. Persistent or partly disassembled stress granules may act as seeds for aggregation, what in turn can pose further challenge for RNA and protein homeostasis.

Although most misfolded and aggregated proteins generated in various cellular compartments, including the cytoplasm, nucleus and endoplasmic reticulum (ER), can be degraded by cellular protein quality control systems, some native and mutant proteins prone to aggregation into β -sheet-enriched oligomers are resistant to all known proteolytic pathways and can thus grow into inclusion bodies or extracellular plaques (Ciechanover and Kwon, 2015). The accumulation of protease-resistant misfolded and aggregated proteins is a common mechanism underlying protein misfolding disorders including neurodegenerative diseases such as Huntington's disease (HD), Alzheimer's disease (AD), Parkinson's disease (PD), prion diseases and Amyotrophic Lateral Sclerosis (ALS) (Mizuno *et al.*, 2003; Johnson *et al.*, 2010; Erzurumlu *et al.*, 2013). Expansion of polyglutamine (polyQ) tracts in the coding region of specific genes, such as huntingtin, atrophin-1, androgen receptor and ataxin-1, 2, 3, 6, 7 and 17 results in the accumulation of the mutant proteins into micro-aggregates/oligomers and inclusions (Pennuto and Sambataro, 2010). Expanded polyglutamine (polyQ) tracts form antiparallel β -strands held together by hydrogen bonds between the main chain of one strand and the side chain of the adjacent strand. This leads the polyQ protein to acquire a non-native β -sheet conformation, which results in the production of various aggregates (Perutz *et al.*, 1994). Micro-aggregates are relatively small species identifiable by biochemistry and atomic force microscopy and are thought to originate as intermediate products that generate during the process of aggregation and inclusion formation. Inclusions are larger species detectable by immunohistochemistry and are likely to represent a protective cellular response to the presence of misfolded protein. Inclusions can be found in the cytosol as well as in the nucleus (nuclear inclusions) of neuronal and

non-neuronal cells (Perutz *et al.*, 1994; Kopito 2000). Even though polyQ proteins are substrates of proteasome, their aggregate species, oligomers and micro-aggregates, are not efficiently degraded and accumulate in the cells causing toxicity (Demuro *et al.*, 2005). Furthermore, association of polyQ proteins with proteasome may lead to sequestration of proteasome components into aggregates.

VCP interacts with both normal length (shorter than 38 glutamines) and mutant (above a threshold length of 38 glutamines; aggregate-prone) polyQ tract sequence, although only mutant proteins affect dynamism of VCP and impair its function (Imafuku *et al.*, 1998; Fujita *et al.*, 2013). Mutant polyQ proteins such as huntingtin (HTT), ataxin-1 and 7 (Atx1 and Atx7), and androgen receptor (AR) are bound directly to VCP via polyglutamine sequence reducing the amount of VCP in the functional domains in cells (Fujita *et al.*, 2013). On the other hand however, overexpression of a *C.elegans* VCP homologue has been shown to decrease ex-polyQ aggregates in *C.elegans* (Yamanaka *et al.*, 2004). Consistently, overexpression of VCP/TERA resulted in the recovery of lifespan in polyglutamine disease flies model (Manno *et al.*, 2010). Therefore, these findings suggest that VCP is involved in the clearance of pathogenic aggregates.

Expanded polyglutamine containing proteins or other mutant, aggregate prone proteins, such as synuclein in autosomal dominant Parkinson disease, are the molecular constituents of the ubiquitinated inclusions (UBIs) (Watts *et al.*, 2004; Ju *et al.*, 2008). In some cases these UBIs contain tubulofilamentous inclusions and insoluble protein aggregates (Hubbers *et al.*, 2007). In addition, UBIs can form in the setting of impaired autophagy (Rubinsztein, 2006), and one potential point of intersection between autophagy and the UPS is the “aggresome” or inclusion body (Johnston *et al.*, 1998). An aggresome is a microtubule-dependent pericentriolar region of the cell that contains sequestered misfolded or aggregated proteins (Johnston *et al.*, 1998). Aggresome formation occurs in the setting of UPS dysfunction due to decreased proteasome activity or the overwhelming accumulation of misfolded proteins (Johnston *et al.*, 1998; Ju *et al.* 2008). Furthermore, the aggresome also contains proteins such as LC3 and p62 along with lysosomes, which would imply that these are areas of active autophagic degradation (Bjorkoy *et al.*,

2005). As a defence against polyglutamine-induced cell death, ubiquitinated and aggregated proteins are trafficked to the aggresome via interactions with HDAC6, a VCP-binding protein and dynein (Kobayashi *et al.* 2007; Ju *et al.* 2008).

In summary, protein quality control via autophagy is particularly important for the timely removal of aggregated forms of pathogenic proteins in neurodegenerative diseases (Kobayashi *et al.* 2007; Ciechanover and Kwon, 2015). Although misfolded proteins can be immediately and directly delivered to autophagosomes, excess misfolded or damaged proteins and their aggregates that accumulate beyond cellular capacity are temporarily stored in the aggresome. During this process, called aggrephagy, the HDAC 6, in association with molecular chaperones, binds untethered ubiquitinated aggregates and delivers them via microtubules to a location that minimises their toxicity until they are finally degraded by the UPS or autophagy (Ju *et al.* 2008). Therefore, one way to enhance degradation of pathogenic protein aggregates would be to increase the activities of proteolytic pathways.

1.6 Autophagy in health and disease

Living organisms developed mechanisms enabling them to capture and utilise energy from degrading parts of themselves in order to survive. The major evolutionarily conserved breakdown pathway is known as *autophagy* (Greek), meaning 'to eat oneself'. Autophagy (as a general process) is a homeostatic process that involves degradation of a cell's interior components through the lysosomal machinery (Yang and Klionsky, 2010). This 'self-cannibalisation' pathway is not only responsible for degrading cellular proteins but also degrading cellular organelles and even intracellular pathogens, which are too large for other degradation systems. It is a tightly regulated process that plays a normal part in cell growth and development, helping to maintain a balance between the synthesis, degradation, and subsequent recycling of cellular products. Autophagy is a major mechanism by which a starving cell re-allocates nutrients from unnecessary to more-essential processes to ensure cell survival.

While a variety of autophagic processes exist (microautophagy, macroautophagy and chaperone mediated autophagy), they all degrade intracellular

components via the lysosome. The most well-known mechanism of autophagy is macroautophagy (now more commonly referred to as 'autophagy'), which involves the formation of a double-membrane vesicles (autophagic vacuoles) around a targeted region of the cell, separating the contents from the rest of the cytoplasm (Mizushima *et al.*, 2008; Yang and Klionski, 2010). The resultant autophagosome then fuses with a lysosome creating autolysosome and subsequently degrades the contents. In contrast to the UPS, autophagy is restricted to the cytoplasm but is capable of degrading a much wider spectrum of substrates, which include functional or misfolded soluble proteins, protein complexes, oligomers and protein aggregates, and even whole cellular organelles (Korolchuk *et al.*, 2010). Terms like pexophagy, mitophagy or ribophagy are used to describe autophagosomal degradation of peroxisomes, mitochondria or ribosomes respectively. Autophagy comprises five distinct steps: initiation – formation of a double-layered isolation membrane (also called a phagophore), the origin of which has been reported to be the endoplasmic reticulum (ER) (Hayashi-Nishino *et al.*, 2009), Golgi (Yen *et al.*, 2010), and the mitochondria (Van der Vaart *et al.*, 2010); elongation and engulfment of cytoplasm portions containing autophagic substrates, autophagosome formation, lysosome fusion and autolysosome activation, where the engulfed content is degraded by lysosomal proteases (Fig. 1.5). Autophagy can be selective/ basal or non-selective/induced. In general, basal autophagy acts as a quality-control mechanism for specific cargo, including proteins and organelles. Basal autophagy functions mainly in the maintenance of cells, especially terminally differentiated, long-lived cells such as neurons, and tissue-dependent physiological functions (Komatsu *et al.*, 2007 2nd; Tanida and Waguri, 2010). During selective/ basal autophagy, certain autophagic substrates are specifically targeted for destruction through ubiquitination (Korolchuk *et al.*, 2010). Specifically, K63-linked and K27-linked ubiquitin chains (as well as monoubiquitin) all function in the removal of proteins and organelle via autophagy (Kirkin *et al.*, 2009). There are several adaptor proteins that serve as linkers between ubiquitinated cargo and the autophagy-lysosome degradation system. These include p62 (also called SQSTM1), neighbour of BRCA1 gene 1 (Nbr1) and autophagy-linked FYVE protein (Alfy) that recognise and form complexes with the ubiquitinated proteins or organelle through ubiquitin-binding domains (UBDs). The

most established of these adaptors, p62, is itself an autophagy substrate that sequesters ubiquitinated substrates via its ubiquitin-associated (UBA) domain and is recruited to the autophagosomal membrane through interaction with LC3 (see below) (Pankiv *et al.*, 2007; Itakura and Mizushima, 2011). Non-selective autophagy is rapidly induced upon nutrient deprivation (amino acid removal, but not growth factor removal), hypoxia or infection and the contents of the induced autophagosomes include any protein or organelle that is in the vicinity of the expanding phagophore. In mammals induced autophagy is observed mainly in the liver and muscle (Tanida and Waguri, 2010). In general, after feeding, autophagy in the liver is suppressed to store nutrients and is re-induced again several hours after feeding. Thereafter, when fasting continues for over 6 hours, autophagy in the skeletal muscles occurs and then in the heart when fasting lasts longer.

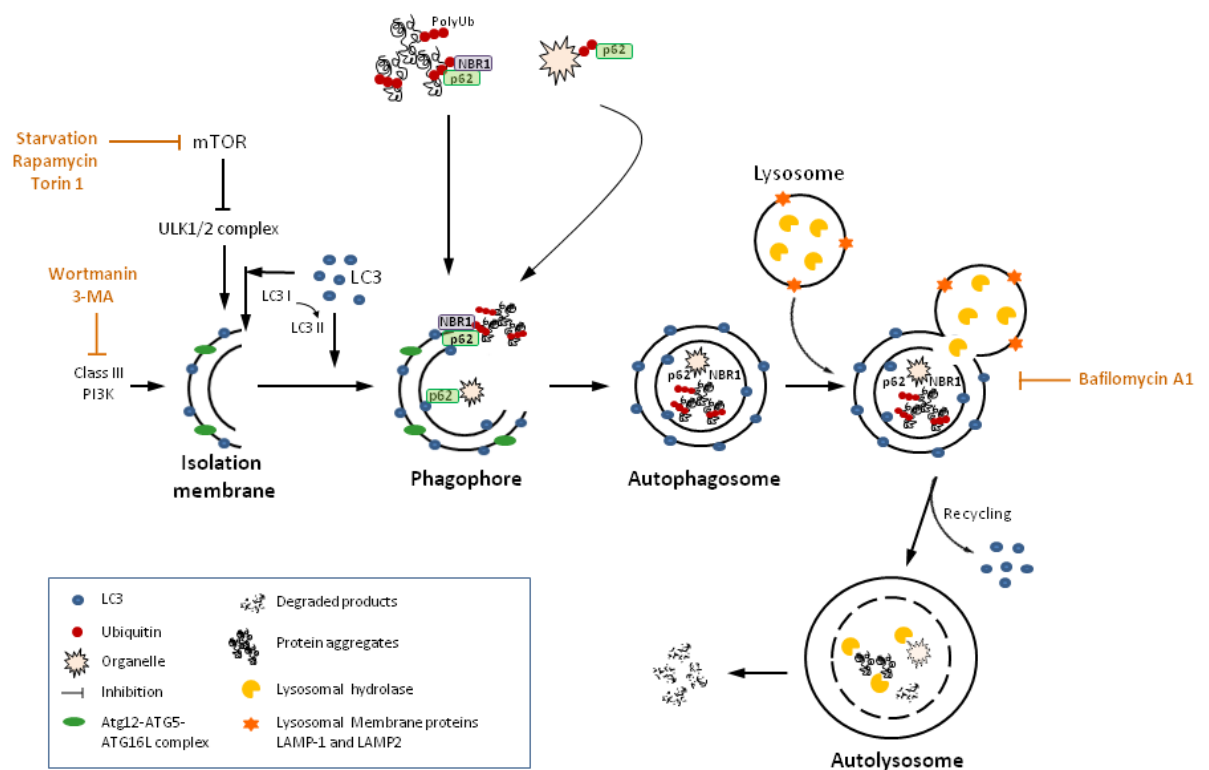


Figure 1.5. Schematic diagram of the macroautophagy pathway. In mammalian cells, the ULK1/2–Atg13–FIP200–Atg101 complex (ULK complex) is responsible for initiation of autophagy, in response to certain signals. Initiation of autophagy involves the formation of a sequestering membrane called phagophore. Atg12-ATG5-ATG16L complex conjugates to the sequestering membrane enabling the recruitment of LC3. Expansion of the phagophore allows engulfment of cytosolic components including long-lived and dysfunctional organelles

such as mitochondria and endoplasmic reticulum, protein aggregates and foreign organisms (viruses and bacteria). At the end of elongation, sequestering membrane closes and results in the formation of a double-membrane vesicle, autophagosome. Once the autophagosome is formed, it is delivered to fuse with lysosome to form autolysosome. Lysosomal hydrolases degrade the cargo together with the inner membrane of autophagosome; nutrients are recycled and reused by the cell. Autophagy can be blocked at early stages, via mTOR kinase or pharmacological inhibition of PI3Ks, or at late stage, via inhibition of lysosomes acidification with Bafilomycin A1. Conversely, pharmacological or starvation-induced inhibition of mTOR or endogenous activity of Class III PI3K positively regulates autophagy.

The formation of autophagosomes is regulated by the reversible conjugation of the ubiquitin-like (UBL) family of proteins (ATG - Autophagy-related proteins) to the sequestering double membrane during the autophagosome formation. The ATG proteins can be grouped, according to their function, into the Atg1 complex (Atg1-Atg13-Atg17) controlling autophagosomal induction, the phosphatidylinositol 3-phosphate kinase (PI3K) complex III (including PI3K, Beclin 1 and UV-radiation associated gene – UVRAG) regulating vesicle nucleation, and two interconnected conjugation systems that mediate vesicle elongation and sealing (Korolchuk *et al.*, 2010). The first conjugation system, consisting of Atg12-Atg5-Atg16L complex, localises to the phagophore and is thought to determine the sites of Atg8/LC3 lipidation (Fujita *et al.*, 2008; Yang and Klionsky, 2010). The second conjugation system (including Atg4, Atg7 and Atg3) regulates the lipidation of Atg8 in yeast, and LC3 (Light Chain 3) in mammals (Cherra *et al.*, 2010; Rabinowitz and White, 2010). Autophagy proteins undergo their own ubiquitin (ub) – like conjugation reactions that are essential for expansion of the autophagosomal membrane. Both Atg8/LC3 and Atg12 proteins are activated by the E1-like enzyme Atg7, Atg12 is conjugated to Atg5 by the E2-like Atg10 and Atg8/LC3 is conjugated to phosphatidylethanolamine (PE) by Atg3. The Atg12–Atg5 conjugate forms a complex with Atg16 and this hierarchical assembly of proteins can drive the formation of Atg8/LC3–PE in an E3-like manner (Hanada *et al.*, 2007). Following the formation of autophagosome, Atg12-Atg5-Atg16 conjugate is removed from the vesicle, while Atg8/LC3 remains attached. Autophagosomes are transported along microtubules in a dynein-dependent manner and fuse with lysosomes where contents are degraded by

lysosomal hydrolases (Ravikumar *et al.*, 2005). The lipidated form of LC3, known as LC3-II, conjugates to PE of the autophagosomal membrane and remains on mature autophagosome until after fusion with lysosome, where LC3-II is also degraded. Other mammalian homologues of Atg8/LC3 include GABARAP (GABA Receptor-Associated Protein), GABARAPL1, GATE16 (Golgi-associated ATPase Enhancer of 16 kDa), and GABARAPL3 (Klionsky and Deretic, 2011), they all share the same ubiquitin-like fold three-dimensional structure. The lysosomal turnover of LC3-II reflects starvation induced autophagy and is thus routinely monitored, via experimental methods such as immunoblotting or immunofluorescence. For example, inhibition of lysosomal function by inhibition of cathepsins or by acidification of lysosomes inhibits the final step of autophagy. This results in significant accumulation of autolysosomes and LC3-II because there is little degradation of autolysosomal content. This accumulation reflects the activity of the delivery process of LC3-II into lysosomes and can be used for measurement of autophagy flux (Tanida and Waguri, 2010). Although, in contrast to induced autophagy, there is little increase of LC3-II during basal autophagy (Komatsu *et al.*, 2007 2nd).

The identification of p62/SQSTM1 and NBR1 (neighbour of BRCA1) as adaptor proteins that simultaneously bind LC3 (via LIR) and ubiquitinated cargo (via their ubiquitin binding domains) indicated that these could allow inclusion of ubiquitinated cargo into autophagosomes and their subsequent degradation by the lysosome (Pankiv *et al.*, 2007; Kirkin *et al.*, 2009). The direct interaction of SQSTM1/p62 protein with LC3 in autophagic membranes, was described fairly recently (Bjorkoy *et al.*, 2005; Pankiv *et al.*, 2007). It was found that this interaction is dependent on LC3 first 10 N-terminal amino acids and on Phe52-Leu53 residues located within the ubiquitin core (Shvets *et al.*, 2008). Interestingly, the LC3 ubiquitin core is sufficient for its conjugation to PE, serving as a structural recognition module for interacting proteins (Shvets *et al.*, 2008). The p62 protein binds polyubiquitinated proteins via the UBA domain, polymerises via its PB1 domain and binds to LC3 via the LIR motif (Pankiv *et al.*, 2007). Once the substrate-adaptor protein complex associates with the autophagosomal membrane-bound LC3-II the cargo can be incorporated into the autophagic vesicle and further recycled by the cell. Therefore, the interaction of p62 with LC3 is essential for the selective recruitment of aggregated proteins to

autophagy for degradation (Tung *et al.*, 2010). Finally, p62 is thought to regulate the formation of protein aggregates and is itself removed by autophagy (Komatsu *et al.*, 2007). Therefore, when autophagy is impaired, the level of p62 is increased in addition to the accumulation of ubiquitinated proteins and like LC3 can also be monitored by experimental methods (such as immunoblotting or fluorescent immunostaining). Therefore levels of ubiquitin and p62 are often monitored for estimation of impairment in basal autophagy.

Autophagy acts as a mechanism to cope with the cellular stress triggered by nutrient starvation or hypoxia, allowing both yeast and mammalian cells to survive in conditions of low nutrient availability. The ability to sense low levels of nutrients and initiate autophagy is regulated by the target of rapamycin (TOR) kinase (Fig. 1.5) and thus TOR is said to be a key regulator of autophagy (Kamada *et al.*, 2000). Mammalian systems have two distinct mammalian TOR complexes (mTOR) – mTORC1 and mTORC2, characterised by the presence or absence of various subunits. In nutrient-rich conditions, mTOR has an inhibitory effect on autophagy, whereas under starvation conditions mTOR is inactivated which leads to the initiation of autophagy. The ability of mTOR to inhibit autophagy occurs via initial incorporation of mTORC1 into the ULK1/2–Atg13–FIP200–Atg101 (ULK) complex, followed by the phosphorylation of ULK1 and Atg13, thereby preventing initiation of the process (Jung *et al.*, 2009). Inhibition of TOR kinase with a chemical agent, such as rapamycin, is sufficient to induce cell cycle and growth arrest and autophagy, even in the presence of amino acids (Kamada *et al.*, 2000; Wullschleger *et al.*, 2006). The mTOR complexes differ in their sensitivity to rapamycin, namely only mTORC1 is inhibited by the drug (Wullschleger *et al.*, 2006). Rapamycin treatment acts via releasing ULK1 to phosphorylated FIP200 (family interacting protein of 200kDa) and subsequent autophagy is induced. Torin1 is another inhibitor of mTOR kinase and induces autophagy to a greater degree, as it directly inhibits both mTORC1 and mTORC2 complexes (Thoren *et al.*, 2009). Class I and class III phosphoinositide 3 kinases (PI3Ks), involved in cell growth and survival, positively regulate autophagy and when inhibited with either 3-Methyladenine (3-MA) or Wortmanin, the formation of autophagosomes is also blocked (Fig 1.4).

Autophagy-deficient tissues tend to accumulate ubiquitinated aggregates and p62- and LC3- positive inclusion bodies (Komatsu *et al.*, 2007). Therefore, the increase in ubiquitin-positive and p62-positive inclusions in tissues indicates the possibility of an insufficiency in autophagy. As mentioned above autophagy occurs at basal, constitutive levels, although the demand for basal autophagy differs among tissues. The brain is probably one of the organs which require most protection against starvation, and as one might expect neuronspecific autophagy-deficient mice show progressive neurodegeneration associated with the accumulation of ubiquitinated protein aggregates and/or inclusion bodies (Komatsu *et al.*, 2006; Hara *et al.*, 2006). The neurons in patients with neuronal ceroid lipofuscinosis (NCL) show accumulation of mitochondrial ATPase subunit C in lysosomes, indicating that impairment of mitochondrial protein degradation occurred in the patients and suggesting that mitochondria are degraded via the autophagy-lysosomal system in neurons (Koike *et al.*, 2005). In addition, mutation of *cln3*, one of the NCL-related genes, or a lack of cathepsin D, one of the major lysosomal proteases, leads to neuronal ceroid lipofuscinosis with autophagic vacuolisation (Koike *et al.*, 2005; Cao *et al.*, 2006). Studies reveal that degradation of disease-related mutant proteins, such as extended polyglutamine-containing proteins that cause Huntington's disease and spinocerebellar ataxia, and mutant forms of α -synuclein that cause familial Parkinson's disease, is highly dependent on autophagy, in addition to the ubiquitin-proteasome system (Cuervo *et al.*, 2005; Martinez-Vicente and Cuervo, 2007).

The same autophagic machinery used to selectively capture cellular organelles is used for the selective delivery of microorganisms to lysosomes in a process termed xenophagy (Yang and Klionsky, 2010). Pathogen-containing LC3-positive compartments can be considerably larger than classical autophagosomes consisting exclusively of cellular constituents (Levine and Deretic, 2007), indicating a plasticity of the autophagic process that permits it to adapt to the need to engulf microbes that are larger than its own organelles. Beyond its direct role in pathogen elimination, autophagy also mediates trafficking events required for innate and adaptive immunity. In the case of certain RNA viral infections, autophagy is required for the delivery of viral nucleic acids to the endosomal toll-like receptor TLR7, and subsequent activation of type I interferon signalling (Levine and Deretic, 2007). The

autophagic machinery is also used for the major histocompatibility complex (MHC) class II presentation of certain endogenously synthesised viral antigens (Schmid *et al.*, 2007). Given the diverse roles of autophagy in innate and adaptive immunity, it may not be surprising that Atg16-deficient macrophages produce more of the inflammatory cytokines IL-1 β and IL-18 upon stimulation with lipopolysaccharides (Saitoh *et al.*, 2008). Furthermore, single nucleotide polymorphisms in Atg16L1 have been linked to Crohn's disease, a major type of inflammatory bowel disease (Hampe *et al.*, 2007). These associations suggest that autophagy plays an important role in the innate immune response of the intestine.

One of the first diseases genetically linked to autophagy malfunction was cancer, where *Beclin 1 (BECN1)* was found to be monoallelically deleted in 40-75% of cases of human breast, ovarian and prostate cancer (Mathew *et al.*, 2007). Additionally, mice with heterozygous disruption of *beclin 1* have decreased autophagy and are more prone to the development of spontaneous tumours including lymphomas, lung carcinomas, hepatocellular carcinomas, and mammary precancerous lesions (Qu *et al.*, 2003; Yue *et al.*, 2003). Interestingly, components that enhance the autophagic activity of Beclin 1/ class III PI3K complex (Takahashi *et al.*, 2007) and additional *Atg* genes, including *atg4c* (Marino *et al.*, 2007) exert tumour suppressor effects. Conversely, downregulation of autophagy observed in cancer cells is associated with tumour progression. For example, mTOR and Class I PI3K which control cell growth, proliferation and cell survival, and inhibit autophagy are commonly activated oncogenes (promoter of oncogenesis) (Botti *et al.*, 2006). This would suggest that tumour suppression may be a shared property of autophagy proteins (ATGs). Although the tumour suppressor effects of autophagy may often be counterbalanced by its pro-survival effects that contribute to tumour cell resistance to chemotherapy, giving the necessity to differentially target autophagy in a disease-stage-specific manner (Chan *et al.*, 2005; Abedin *et al.*, 2007). Considering all of the available data, there is no doubt that autophagy may help to prevent or halt the progression of some diseases, specifically some types of neurodegeneration, heart disease and cancer, and play a protective role against infection by intracellular pathogens, but paradoxically it may also be deleterious, particularly in cells that cannot die by apoptosis (Levine and Yuan, 2005; Levine and Kroemer, 2008).

A common characteristic of all tissues with impaired autophagy is accumulation of damaged proteins and organelles, and this is even more evident with age and particularly detrimental in non-dividing differentiated cells (Choi *et al.*, 2013). Muscle biopsies from affected muscle in IBMPFD patients as well as muscle from two transgenic mouse models of IBMPFD display ubiquitinated inclusions, TDP-43 cytoplasmic aggregates and the presence of rimmed vacuoles (Weihl *et al.*, 2007; Kimonis *et al.* 2008; Custer *et al.*, 2010). The accumulation of TDP-43 observed in IBMPFD, was replicated in cells upon autophagy inhibition (Ju *et al.*, 2009; Custer *et al.*, 2010), suggesting that the accumulation of this protein in the disease state may be a consequence of autophagy deficiency. An early disease model of Chloroquine myopathy (drug poisoning induced myopathy) in rats linked the muscle atrophy and rimmed vacuole formation to accumulated autophagosomes (LC3-II positive vesicles) (Suzuki *et al.*, 2002). Further to that, the IBMPFD muscle was shown to accumulate autophagosome-associated proteins p62 and LC3-II, which localised to rimmed vacuoles (Ju *et al.*, 2009; Bug and Meyer, 2012). Additionally, myoblasts derived from IBMPFD patients show abnormal accumulation of large lysosomal-associated membrane protein 1 and 2 (LAMP1- and LAMP2) - positive vacuoles (where both LAMP1 and LAMP2 are markers for lysosomes and autolysosomes) and accumulation of LC3-II (Tresse *et al.*, 2010). Ultrastructural analysis of rimmed vacuoles from IBM patient muscle demonstrated that these were in fact autophagic vacuoles containing filamentous material (Hubberts *et al.*, 2007). The muscle pathology seen in patients and IBMPFD models implies a possible link between VCP mutations and compromised autophagy. These observations were reproduced in cell culture, either by expressing dominant-negative VCP mutant or upon siRNA-mediated depletion of endogenous VCP, suggesting that VCP may be required for the autophagosome maturation - processes that occur after autophagosome formation, through acidification, including lysosomal fusion (Ju *et al.*, 2009; Tresse *et al.*, 2010). First study noted that when VCP activity was impaired, autophagosomes (LC3-positive vacuoles) failed to localise with acidic and LAMP1 positive vesicles, suggesting that loss of functional VCP results in an impairment of the fusion of mature autophagosomes with lysosomes and final degradation of autophagic targets (Ju *et al.*, 2009). Others observed that VCP acts after the fusion of autophagosomes with lysosomes since enlarged, acidified

cathepsin B protease-positive autolysosomes were detected in VCP-mutant expressing cells (Tresse *et al.*, 2010). Therefore, Tresse and colleagues concluded that impairment of VCP function (resulting from VCP mutation) results in defective autophagosome maturation, but this is not simply a defect in autophagosome-lysosome fusion (Tresse *et al.*, 2010).

VCP is also believed to protect against the toxic effects of insoluble polyglutamine (polyQ) aggregates, since impaired polyQ aggregate clearance was observed in IBMPFD mutant expressing transgenic mouse muscle (Ju *et al.*, 2008) and in the *Drosophila's* eye degeneration (Higashiyama *et al.*, 2002, Manno *et al.*, 2010). Suggested to be responsible for delivering ubiquitinated abnormal proteins and aggregated proteins to autophagosomes for degradation (Ju and Weihl, 2010; Manno *et al.*, 2010), the full spectrum of VCP function at the interplay of autophagy and UPS remains to be elucidated. Nevertheless, there is a significant clinical overlap of IBMPFD and disease caused by mutations in other autophagy related genes, and in particular in *SQSTM1/p62* gene (Moscat and Diaz-Meco 2009). This would suggest that VCP and p62 are likely to share a common biological pathway. Noteworthy, increase in ubiquitinated aggregates (in autophagy-deficient cells) was shown to be a direct effect of the p62 overexpression, which was ablated via overexpression of wild-type VCP (Korolchuk *et al.*, 2009). Since IBMPFD-related mutations in VCP result in disrupted aggregate clearance, one may postulate that this could result from a disrupted interaction of mutant VCP with components of the autophagy pathway, and in particular with p62, given that mutations in p62 cause PDB.

1.7 Paget disease of the bone and aberrant osteoclastogenesis

Paget disease of the bone (PDB) is the second most common metabolic bone disease after osteoporosis, affecting up to 3% of adults in the UK over the age of 50 years (nhs.uk, 2014). Epidemiological studies show a varying prevalence of PDB across different ethnicities, with an enrichment of PDB in individuals of a Caucasian descent (Chung and Van Hul, 2012). It is a chronic bone disease characterised by focal regions of accelerated and disorganised bone turnover, featuring osteoclasts that are excessively large, multinucleated and overactive. Resulting new bone is highly disorganised and of poor quality. Additional features include marrow fibrosis and

increased vascularity of bone (Ralston, 2008). Pagetic bone lesions are commonly found in the pelvis, skull, spine, femur and tibia. The abnormal bone remodelling disrupts normal bone architecture and lead to the development of various complications such as bone pain, pathological fracture, bone deformity, secondary osteoarthritis or nerve compression syndromes. This can further manifest as reduced height or hearing loss due to cranial bone deformity. At the molecular level Pagetic osteoclasts contain nuclear inclusion bodies (Kimonis *et al.*, 2008).

The primary lesion in PDB involves the formation of abnormal osteoclasts (large terminally differentiated polykaryons that originate from hematopoietic precursors and whose function is bone resorption) which express a "pagetic phenotype" that includes increased osteoclast number and size, increased nuclei and increased responsivity of the osteoclast precursors to activators of NF κ B signalling; these include RANKL, tumor necrosis factor (TNF)- α , and 1,25-dihydroxy-vitamin D3 (1,25-[OH]₂D₃) (Roodman and Windle, 2005). The formation and activation of osteoclasts is regulated by binding of receptor activator of nuclear factor κ B ligand (RANKL, originally identified as TRANCE - TNF-related activation-induced cytokine) to its cognate receptor (RANK) on myeloid progenitor cells and subsequent activation of multiple intracellular pathways including AKT/PI3K, MAP kinase, and NF κ B (Otero *et al.*, 2012). The primary pathway responsible for osteoclast differentiation is the RANKL-NF κ B pathway and it's this pathway which is said to be dysregulated in PDB (Daroszewska and Ralston, 2005). The pagetic osteoclasts also express increased levels of coupling factors (including bone morphogenic protein 6 - BMP6, lipid mediator sphingosine-1-phosphate - S1P, and collagen triple helix repeat containing 1 - CTHRC1) which drive aberrant bone formation (Pederson *et al.*, 2008; Takeshita *et al.*, 2013; Galson and Roodman, 2014). The excessive focal bone formation in Paget's results in the generation of weak woven bone, with collagen fibres laid down in an irregular mosaic pattern, rather than normal lamellar bone (Ralston, 2008). The pagetic bone that is formed can bow and result in bone deformity or fracture, skull thickening, bone pain, secondary osteoarthritis, and nerve root compression. Between 15-40% of Paget's patients have a family history of the disorder with an autosomal dominant pattern of inheritance, suggesting a genetic predisposition for Paget's disease (Morales-Piga *et al.*, 1995; Galson and Roodman, 2014).

Many genetic factors have been associated with PDB and related syndromes; these include RANK (or Tumor Necrosis Factor Receptor Superfamily, Member 11a, NFKB Activator - TNFRSF11A), Osteoprotegerin (OPG or TNFRSF11B), VCP and p62/SQSTM1 (Ralston, 2008; Chung *et al.*, 2011). All of these factors are involved in RANKL-NF κ B signalling pathway (more on the pathway in Chapter 6), which increases transcription of genes responsible for the osteoclast differentiation. Therefore, mutations in such genes disrupt normal NF κ B signalling, resulting in increased osteoclastogenesis and bone resorption. In addition, increased resorptive activity of osteoclast leads to secondary increase in osteoblast activity, resulting in focal increase in bone turnover – a unique feature of PDB. While activating mutations in the first exon of the *RANK* gene cause early onset PDB (Nakatsuka *et al.*, 2003) and related conditions: FEO (familial expansile hyperphosphatasia) and ESH (expansile skeletal hyperphosphatasia) (Hughes *et al.*, 1994; Whyte and Hughes, 2002); a homozygous deletion for the gene encoding OPG (a decoy receptor for RANKL) was identified in two Navajo patients with juvenile PDB (Whyte *et al.*, 2002) (Fig.1.6). These rare genetic bone disorders display clinical, radiological or histological features in common with classic PDB, although the age of onset and the distribution of the disease are different. The nature of the genes involved in PDB indicates that the regulation of osteoclastogenesis is a key process underlying the pathogenesis of PDB.

The most commonly associated gene with PDB is sequestosome-1 (*SQSTM1*), located on chromosome 5q35, which encodes the p62 protein. P62 acts as an anchor protein and plays an important role in the NF κ B signalling pathway. It binds either TNF receptor–associated factor (TRAF)-6 in the RANK or receptor-interacting protein (RIP)-1 in the TNF signaling pathway to activate NF κ B (Daroszewska and Ralston, 2005). Mutations in the coding region of p62 are linked to hereditary and most sporadic, adult onset PDB disease (Fig.1.6). Approximately 50% of the familiar cases are due to dominant mutations that lead to loss of function of polyubiquitin binding. This is due to either deletion of the ubiquitin associated (UBA) domain or point mutations within this domain, with P392L (proline to leucine change) being the most commonly identified mutation (Hocking *et al.*, 2002; Layfield *et al.*, 2004; Chamoux *et al.*, 2009). This in turn results in elevated cytokine activation of NF κ B pathway and hyper-responsiveness to receptor activator of nuclear factor κ B ligand (RANKL)

(Chamoux *et al.*, 2009). A possible explanation for this observation would be a continuous activation of the NF κ B signalling as the mutation in the UBA domain of p62 hinders the ubiquitin dependant inactivation of TRAF6 (Sundaram *et al.*, 2011). The deubiquitinating enzyme cylindromatosis (CYLD) interacts with the p62 UBA domain to inhibit TRAF6 ubiquitination and thus negatively regulates RANK signalling and osteoclastogenesis (Sundaram *et al.*, 2011). Therefore, p62 UBA mutation (P392L) abolishes interaction with CYLD, leading to accumulation of polyubiquitinated TRAF6 and hence increased downstream activation NF κ B (Sundaram *et al.*, 2011). Interestingly the p62^{P392L} knock-in mice have increased osteoclast formation but do not develop characteristic for PDB focal osteolytic lesions (Hiruma *et al.*, 2008). More recently however, mice with a proline to leucine mutation at codon 394 of mouse *Sqstm1* (P394L) developed a PDB-like skeletal disorder (Daroszewska *et al.*, 2011). Collectively, it would appear that mutations in the UBA domain of SQSTM1 are sufficient to cause PDB in the absence of additional triggers.

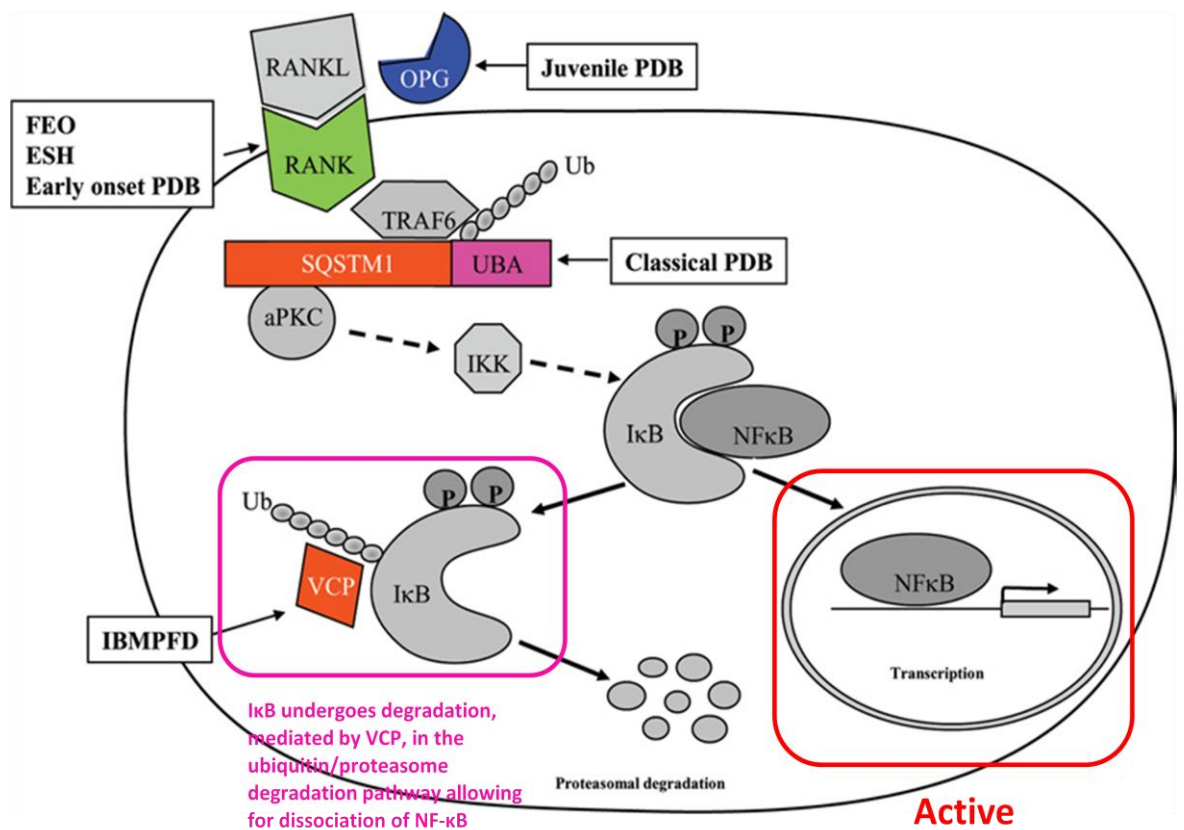


Figure 1.6. Activation of the NF- κ B signalling cascade leads to increased osteoclastogenesis. The RANKL cytokine binds to the RANK receptor in an interaction antagonised by osteoprotegerin (OPG). In the absence of inhibitors, downstream TRAF6 associates with

RANK and p62 (SQSTM1) adapter protein. Through its N-terminal PB1 domain p62 binds α PKC, stimulating activation of IKK β . This allows IKK β to enter the nucleus and activate target gene expression and initiation of osteoclast formation. VCP binds ubiquitinated I κ B α and shuttles it to the 26S proteasome for degradation. This allows dissociation of NF κ B which then enters the nucleus and activates target gene expression and initiation of osteoclastogenesis. Mutations in RANK receptor can result in Familial expansile osteolysis (FEO), Expansile skeletal hyperphosphatasia (ESH) or Early onset Paget's disease of bone (PDB). Mutations in OPG are associated with Juvenile PDB. Mutations in *SQSTM1* (*p62*) gene result in a Classical PDB; mutations in *VCP* result in the IBMPFD-associated PDB. Effects of these mutations lead to elevated cytokine activation of NF κ B. (Adapted from Daroszewska and Ralston, 2005)

Genetic factors play an important role in PDB, reflected by the fact that 15-40% of patients have at least one affected first-degree relative (Morales-Piga *et al.*, 1995; (Hocking *et al.*, 2002; Lucas *et al.*, 2006). Mutations in *VCP* gene are responsible for the Paget disease of the bone associated with inclusion body myopathy and frontotemporal dementia (IBMPFD). In the clinic, many PDB patients are diagnosed incidentally, because PDB is asymptomatic in up to 80%, and is often the case for patient with no family history of PDB (sporadic PDB) (Chung and Van Hul, 2012). In case of a sporadic PDB the onset starts later in life of the patient (over 55 years old) and disease symptoms are much milder than for familial (inherited) PDB (Lucas *et al.*, 2006; Chung and Van Hul, 2012). None of the currently characterised *VCP* mutations have been associated with sporadic PDB (Lucas *et al.*, 2006). In contrast to sporadic PDB, the inherited PDB seen in patients with IBMPFD presents earlier, at mean age of 42, with typical distribution in the spine, pelvis and skull and later progression to involve other bones (Lucas *et al.* 2005). The age of onset is similar to the slowly progressive distal and proximal muscle weakness seen in IBMPFD patients with myopathy. On the molecular level *VCP* mediates ubiquitin-proteasome degradation of phosphorylated inhibitor of κ B (I κ B)- α , allowing for dissociation of the transcription factor NF κ B and subsequent translocation to the nucleus where it activates genes responsible for osteoclastogenesis (Fig.1.6). It is postulated that expression of mutant *VCP* in bone tissue leads to increased degradation of I κ B and therefore to increased NF κ B activation (Vandermoere *et al.*, 2006). This in turn

results in formation and activation of osteoclasts, and therefore focal increase in bone resorption leading to generation of weak woven “pagetic bone”.

While both the PDB-mutant p62 and IBMPFD-mutant VCP cause an increase in osteoclast activity involving NF κ B signalling, little is known of the impact of either mutation on autophagy. Interestingly, the causative mutations in both p62 and VCP affect domains which are involved in ubiquitin binding. This might affect the ability of either p62 or VCP to regulate recycling and degradation of NF κ B signalling pathway ubiquitinated components (such as TRAF6, I κ B or other components). As there appears to be a crosstalk between the autophagy and NF κ B (Hocking *et al.*, 2012), changes in NF κ B activity and autophagic function, could be expected. For example, the IKK complex, which is an essential mediator of the RANKL/RANK- NF κ B pathway, contributes to the induction of autophagy and is activated by multiple autophagy inducers, without affecting NF κ B nuclear translocation (Criollo *et al.*, 2010; Comb *et al.*, 2011). Activation of IKK in response to cellular starvation induces expression of pro-autophagic genes *LC3*, *BECN1*, and *ATG5*; and levels of these genes are markedly decreased in IKK deficient cells (Comb *et al.*, 2011). Autophagy also appeared to regulate the levels of I κ B α (VCP substrate for the proteasomal degradation), the inhibitor of NF κ B (Colleran *et al.*, 2011). Namely, Colleran and colleagues observed that I κ B α co-localized with autophagosomal vesicles in intestinal epithelial cells after stimulation with proinflammatory cytokine TNF- α . In fact even though the first phase of I κ B α degradation was proteasome (and VCP) - dependent, the second was regulated by autophagy and was completely blocked with the type III PI3K inhibitor 3-MA (Colleran *et al.*, 2011). Furthermore, indirect evidence supports the notion that alterations in autophagy are linked to the pathogenesis of PDB. Specifically, disease-causing mutations increase osteoclast activity and autophagy positively regulates osteoclast activity (DeSelm *et al.*, 2011); and importantly p62, which is commonly mutated in PDB, is an autophagy receptor and interacts with VCP (see Chapter 4). In addition, PDB-associated mutations map to regions of p62, which are relevant for its autophagy-dependent function: principally the UBA domain (Hocking *et al.*, 2002) but also the LIR (D335E) (Falchetti *et al.*, 2009) and the KIR (S349T) domains (Michou *et al.*, 2010). Nevertheless, perhaps the best evidence of alterations in autophagic function comes from studies of the p62^{P394L} mutant mouse, which, as noted above,

develops a PDB-like bone disorder with focal bone lesions (Daroszewska *et al.*, 2011). Osteoclast precursors from the mutant animals, had not only increased sensitivity to RANKL, but also, in the presence of Bafilomycin A1, exhibit increased expression of SQSTM1, ATG5, and LC3 along with increased LC3-II protein levels (Daroszewska *et al.*, 2011) suggesting a possible increase in autophagic flux (and consistent with the known relationship between autophagic and osteoclastic activity) (DeSelm *et al.*, 2011).

Interestingly, SQSTM1 mutations, including some UBA domain mutations that are associated with PDB, have also been reported in patients with ALS (amyotrophic lateral sclerosis) and frontotemporal lobar degeneration (Rubino *et al.*, 2012). Curiously, among other recently identified genes for ALS is also VCP (Johnson *et al.*, 2010). Although, as discussed earlier, the precise role of VCP in autophagy is still unclear, in muscle cells the mutant VCP appears to be linked to alterations in autophagy (Tresse *et al.*, 2010). Indeed, IBMPFD mutant VCP expression is associated with accumulation of nondegradative autophagosomes and a failure to degrade aggregated proteins (Ju *et al.*, 2009). Similar to p62^{P394L} mouse, knock-in mouse model with mutant VCP has increased levels of LC3-II in muscle cells, osteoclast precursors exhibit increased sensitivity to RANKL, and there are focal bone lesions (Badadani *et al.*, 2010). Finally, the findings of this study (see Chapters 3-6) further imply a mechanistic link between autophagy and osteoclast formation, involving both p62 and VCP.

Although genetic and environmental factors certainly play an important role in the differentiation process, the active osteoclast needs to both regulate the secretion of hydrolytic enzymes as well as promote the intracellular digestion of peptide residues of matrix proteins. Once the terminally differentiated osteoclasts become activated they tightly adhere to the bone surface through one or more specialized structures termed podosomes. Contained within the podosome, a folding of the plasma membrane in the area facing the bone matrix is known as ruffled border (RB). The RB is formed by fusion of secretory lysosomes with the plasma membrane, and confined by an actin ring, which seals the peripheral contact site between osteoclast and bone (Teitelbaum, 2011). Osteoclasts resorb bone at the RB

extracellular resorptive space by directionally secreting hydrochloric acid – which dissolves the mineral phase of bone, and proteases; key proteases are: matrix metalloproteinase 13 (MMP13, collagenase3), tartate resistant acid phosphatase (TRAP) and cathepsin K (CatK), these hydrolyse the collagen-rich organic bone matrix (Baron, 2008). Interestingly, recent findings suggest that fusion of the secretory lysosome to the RB is in part regulated by the autophagic proteins Atg5, Atg7 and Atg4B (DeSelm *et al.*, 2011). Specifically, Atg5 and Atg7 promote bone resorptive activities both *in vivo* and *in vitro*, and serve to target lysosomes to the actin ring of the functioning osteoclast. In addition, LC3II was found to localise within the actin ring together with CatK, suggesting that the secretory lysosomes are not in fact LC3 coated (DeSelm *et al.*, 2011; Gelman and Elazar, 2011). Modulation of LC3 with Atg4B blocked both resorptive activity and expression of CatK (DeSelm *et al.*, 2011), whereas LC3 knock-down inhibited actin ring formation and resorptive activity of osteoclast (Chung *et al.*, 2012). Overall, these findings lend support to the notion that discussed above autophagy proteins are also involved in modulation of bone resorptive activity of osteoclasts. Collectively, all of these observations confirm an important, noncanonical role for autophagy in the regulation of both osteoclastogenesis and resorptive function of mature osteoclasts.

1.8 Summary

The mechanism whereby mutations in VCP lead to the pathogenesis of IBMPFD and the selective vulnerability of brain, muscle and bone remains unknown but there is a considerable amount of new evidence that points to a role for the autophagic process in the clearance of cytotoxic protein aggregates, which accumulate in disease states due to impairment of the ubiquitin-proteasome system. Importantly, the process of autophagy has been reported to decline in efficiency with age and this effect is more pronounced in terminally differentiated cells (Hubbard *et al.*, 2012). This would explain the relatively late onset of the VCP-associated diseases. In addition, since autophagy plays an essential role in cell homeostasis, and thus protects cells against stress, due to their post-mitotic nature, polarisation and size, osteoclasts could be particularly sensitive to the accumulation of damaged or aggregated proteins and rely on autophagy for survival. Indeed, aberrant, misfolded

proteins, along with chaperones, are commonly found in p62- and ubiquitin-positive aggregates which are precursors to the inclusion bodies seen in many age-related degenerative diseases (Komatsu *et al.*, 2006; Ju *et al.*, 2009). Both p62 and VCP are integral to the ubiquitin-based protein degradation pathways and among several other proteins (including ALFY/WDFY3 and NBR1) have been linked to autophagic regulation of protein aggregates (Bjorkoy *et al.*, 2005; Korolchuk *et al.*, 2009). Although, it is not clear if their involvement is limited to selective autophagy or bulk autophagy in response to starvation, some of these proteins act as autophagy cargo receptors (e.g. NBR1 and p62) (Pankiv *et al.*, 2007), while others are scaffolds (e.g. ALFY) that facilitate autophagosome membrane formation around the cargo to be degraded (Isakson *et al.*, 2013). Interestingly in osteoclasts, ALFY interacts directly with p62 (via its PH-BEACH domain), Atg5 (via its WD40 repeat domain) and phosphatidylinositol-3-phosphate (PI3P) (via its FYVE domains) and forms large cytoplasmic aggregates (Hocking *et al.*, 2010).

These new data on VCP and the link with PDB suggest that modulation of the autophagy pathway by VCP may represent a major regulator of the bone remodelling and maintenance. Crucially, the causative mutations in VCP all cluster within the N-terminal region, which is known to be involved in ubiquitin (Ub) binding (Dai and Li, 2001; Lucas *et al.*, 2006). This is relevant since PDB-causative mutations in the *p62/SQSTM1* gene also affect the Ub-binding domain of the resulting p62 protein (Hocking *et al.*, 2004), suggesting that disease processes in PDB and IBMPFD may be related. The specific aim of the current study was to determine the relationship of VCP to p62 as part of the PDB pathogenic process and evaluate the potential role of autophagy during osteoclastogenesis. The main questions addressed were:

1. To define the potential role of VCP in autophagy (particularly if VCP, p62 and LC3 have the potential to be working together in clearing of ubiquitinated protein substrates); and assess effect of VCP mutation on protein homeostasis.
2. To evaluate if VCP binds to p62 and if so, is it a direct or indirect protein-protein interaction.
3. To elucidate how the VCP is turned over in dividing and differentiated cells.

4. Finally, to determine extend that disruption of autophagy pathway has on differentiation of osteoclasts and if IBMPFD mutations in VCP affect RANKL and TNF α stimulated NF κ B signalling in a similar manner to p62.

Multi-organ involvement that occurs in patients with IBMPFD implies the importance of VCP as a mediator of protein degradation in several organ systems. In contrast, the effect of *p62* mutations seems to be more restricted to cells of the osteoclast lineage. The IBMPFD is a multisystem disease that not only affects the bone but, as mentioned above, also extends to muscle and brain. Understanding the underlying affected pathway in these different tissues will lead to better understanding of the IBMPFD as well as the sporadic counterparts FTD, IBM and PDB. With the heterozygote R155H/+ VCP mouse model, that recapitulates a full spectrum of human disease, one will be able to delineate the pathological molecular cascades that result in the clinical manifestation of the disease. Collectively, identifying the mechanisms by which VCP missense mutations cause pagetic bone lesions should also yield important insights into the pathogenesis of myopathies and neurodegenerative disorders. In this study, in addition to the already gathered evidence for the involvement of VCP in the autophagy-lysosome degradation, I show that VCP directly interacts with key components of the macroautophagy pathway, and in particular with p62. I also demonstrate that autophagy defect, resulting from mutations in VCP, significantly regulate the osteoclast differentiation.

CHAPTER 2

MATERIALS AND METHODS

CHAPTER 2: MATERIALS AND METHODS

2.1 Cell culture

HeLa, HEK293 and mouse embryonic fibroblasts (MEF) cells were cultured in DMEM (Dulbecco's modified Eagle's medium) containing 4.5 g/l glucose and supplemented with 10% heat-inactivated foetal bovine serum (FBS) and 0.5 units/ml Penicillin and 50 µg/ml Streptomycin solution.

Stable p62-KO MEF cells were provided by Dr T. Johansen from Molecular Cancer Research Group; Institute of Medical Biology; University of Tromsø; Tromsø, Norway. These immortalized p62-MEFs were established by infecting MEFs with a recombinant retrovirus carrying a temperature-sensitive simian virus 40 large T antigenand, described in Ichimura *et al.*, 2008.

The murine monocytic cell line RAW264.7 can differentiate into osteoclast-like cells in the presence of the receptor activator of nuclear factor kappa B ligand (RANKL). RAW264.7 cells were cultured in α-MEM (α-minimal essential medium) supplemented with 10% heat inactivated foetal bovine serum (FBS) and 0.5 units/ml penicillin and 50 µg/ml streptomycin solution.

All cells were propagated in a humidified incubator at 37°C in 5% CO₂ until reaching approximately 80% confluency, at which point cells were passaged (1:10 for HeLa, CHO and MEF and 1:6 for RAW264.7 cells).

Culture media and Penicillin-Streptomycin antibiotic solution were purchased from Invitrogen/ Gibco. Hanks Balanced Salt Solution (HBSS) used for starvation experiments was also purchased from Gibco.

HyClone Foetal Bovine Serum (FBS) was purchased from Thermo Scientific (product number SV80160.03), sourced from South America. Heat inactivated at 56°C for 30minutes.

2.2 Plasmids

Plasmids used in this study were either purchased from external sources or made internally by conventional restriction enzyme-based cloning. All plasmid constructs were verified by restriction digestion and/or DNA sequencing.

Plasmids encoding FLAG-tagged *wt* p62, V5-tagged *wt* and R155H VCP were constructed in pcDNATM3.2-DEST vector (Fig. 2.1 and Fig 2.2 respectively) (Dr Giles Watts's personal communication).

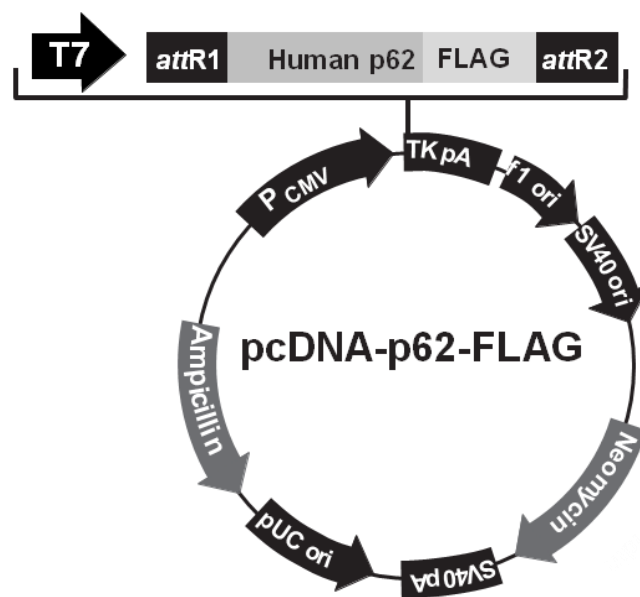


Figure 2.1. *pcDNA3.2-p62-FLAG* (7043 nucleotides). Positions of elements in bases: CMV promoter: bases 232-819, T7 promoter/priming site: 863-882, attR1 site: 911-1035; Human p62 ORF 1036-2355, FLAG epitope with STOP codon: 2356-2383, attR2 site: 2383-2507, V5 epitope (unused): 2508-2574, V5 reverse priming site: 2542-2562, TK polyadenylation signal: 2601-2872, f1 origin: 2908-3336; SV40 early promoter and origin: 3363-3671, Neomycin resistance gene: 3746-4540; SV40 early polyadenylation signal: 4716-4846, pUC origin (c): 5229-5902, Ampicillin (b/a) resistance gene (c): 6047-6907, b/a promoter: 6908-7006 (c). (c) = complementary strand.

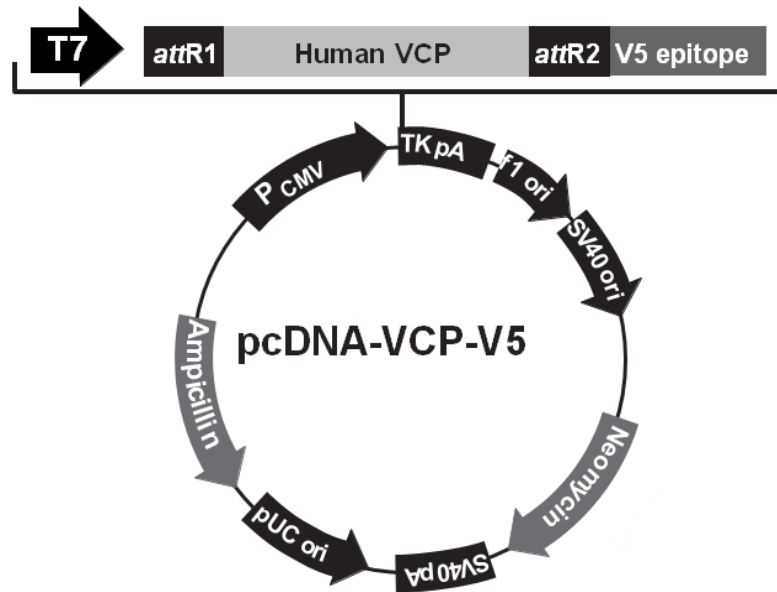


Figure 2.2. *pcDNA3.2-VCP-V5* (8114 nucleotides). Positions of elements in bases: CMV promoter: bases 232-819, T7 promoter/priming site: 863-882, attR1 site: 911-1035; Human VCP ORF no STOP codon: 1036-3453, attR2 site: 3454-3578, V5 epitope: 3604-3645, V5 reverse priming site: 3613-3633, TK polyadenylation signal: 3672-3943, f1 origin: 3979-4407; SV40 early promoter and origin: 4434-4742, Neomycin resistance gene: 4817-5611; SV40 early polyadenylation signal: 5787-5917, pUC origin (c): 6300-6973, Ampicillin (b/a) resistance gene (c): 7118-7978, b/a promoter: 7979-8077 (c). (c) = complementary strand.

Plasmid for *wt* GFP-tagged LC3B was expressed in *pcDNA-DEST53* vector (Fig. 2.3)

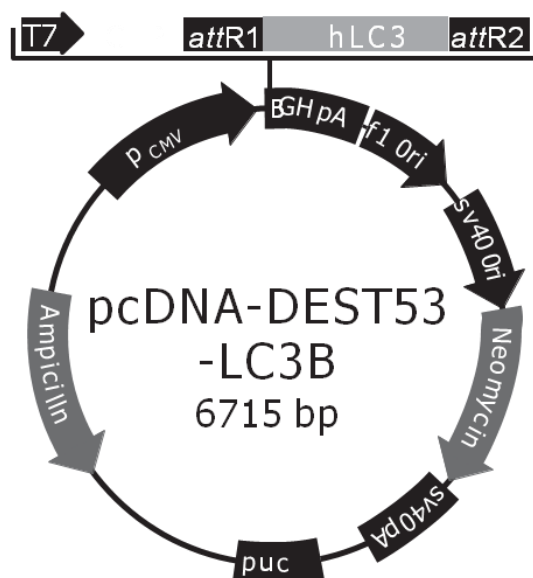


Figure 2.3. *pcDNA-DEST53-LC3B* (6715bp; 7767 nucleotides). Positions of elements in bases: CMV promoter: bases 232-819, T7 promoter: bases 863-882, Cycle 3 GFP (N-terminal): bases 905-1621, attR1 recombination site: bases 1643-1767; Human LC3B ORF with stop codon:

bases 1768-2148, attR2 recombination site: bases 2149-2273, BGH polyadenylation region: bases 2308-2535, f1 origin: bases 2581-3009, SV40 early promoter and origin: bases 3036-3344; Neomycin resistance ORF: bases 3419-4213, SV40 early polyadenylation region: bases 4387-4517, pUC origin: bases 4900-5573, Ampicillin resistance ORF (b/a): bases 5718-6578 (c) b/a promoter: bases 6579-6677 (c). (c) = complementary strand.

Plasmids for HA-tagged poly(Q35) and poly(Q79) were expressed in pCMX vector (Fig. 2.4 and Fig. 2.5 respectively), described in Berke *et al.*, 2004.

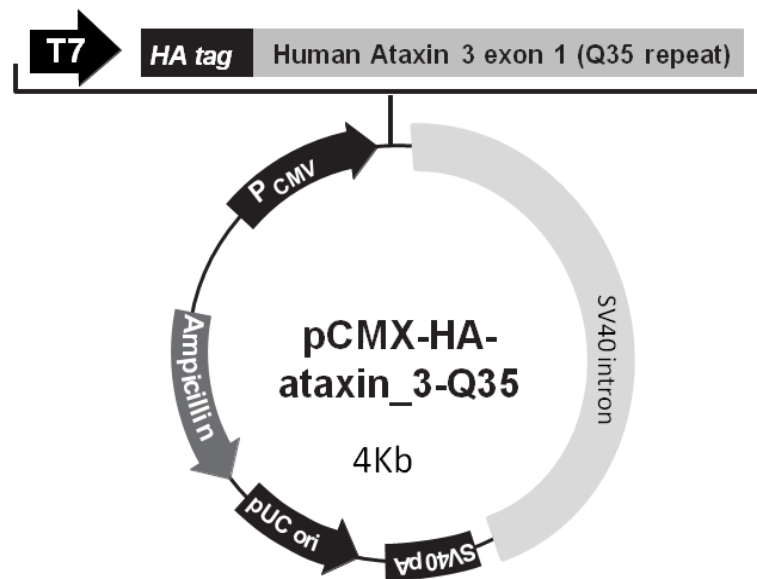


Figure 2.4. *pCMX-HA-ataxin_3-Q35* (4Kb).

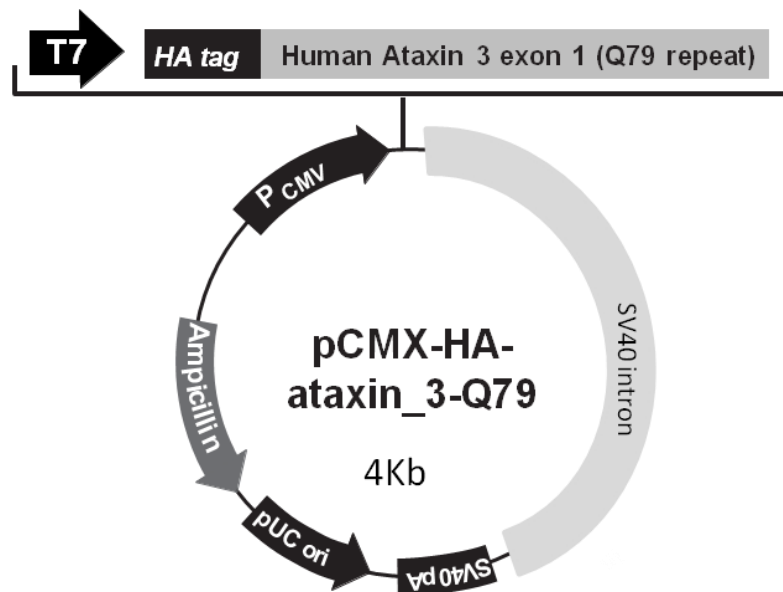


Figure 2.5. *pCMX-HA-ataxin_3-Q79* (4Kb).

Plasmids encoding EGFP-tagged *wt* VCP (Addgene plasmid 23971; **EGFP tag – N- GOI – C –ORF**), EGFP-tagged R155H VCP (Addgene plasmid 23972) and EGFP-tagged DKO (the ATPase-deficient mutant) VCP (Addgene plasmid 23974), were previously described (Tresse *et al.*, 2010) and purchased through the Addgene.org (Appendix, Figure A3-A5; EGFP VCP plasmid maps). Tresse and colleagues constructed the VCP *wt* and mutant plasmids by PCR amplification of the VCP ORFs lacking the stop codons from pcDNA3.1+/VCP-WT, pcDNA3.1+/VCP-R155H, pcDNA3.1+/VCP-A232E, pcDNA3.1+/VCP-DKO, and insertion into the BamHI and HindIII sites of pEGFP-N1 (Clontech) (Tresse *et al.*, 2010).

2.3 Cloning

The cloning procedure covers the steps from the amplification of the source DNA till the preparation of the expression clones.

The materials for cloning were derived from internal sources or from the following companies: Invitrogen, Roche, New England BioLabs (NEB), Fermentas, BioRad, Promega, Sigma Aldrich and Qiagen.

The general practice has been the following: the source gene was amplified by Polymerase Chain Reaction (PCR) using specific primers bearing sequences designed for subsequent insertion into a specific plasmid vectors. The destination vector was amplified with high copy number *E. coli* strains and purified. The PCR products were then purified from solution or from agarose gel. The purified PCR products and the destination vectors were cut with opportune restriction enzymes and treated with T4-polymerase and after with a phosphatase in specific reaction mixtures. The resulting ligation products were used to transform *E. coli* strains (the strains used were: NEB5 α , OmniMAX). The transformed cells were grow in SOC medium (Invitrogen, #15544-034; Composition: 2% tryptone, 0.5% yeast extract, 10 mM NaCl, 2.5 mM KCl, 10 mM MgCl₂, 10 mM MgSO₄, and 20 mM glucose) with agitation and then plated on agar plates containing antibiotics (see below) and incubated overnight. Once obtained the transformants, colonies were selected and checked for the presence of the insert with restriction enzyme digestion followed by Agarose Gel Electrophoresis. The integrity of the cloned gene sequence was then checked by

sequencing, performed by Genome Enterprise limited, John Innes Centre, Norwich. All the desired clones were used to grow minicultures from which glycerol stocks were prepared and kept at -80°C.

2.3.1 Generating pQE9 plasmids encoding His-tagged wt p62 and wt LC3B.

PCR primers for p62-ORF and LC3-ORF were designed using free online primer-design software (<http://www.ncbi.nlm.nih.gov/tools/primer-blast/>), taking particular care of keeping the primer length under 30bp and optimum for the primer melting temperature (T_m). Primers with melting temperatures in the range of 52-58 °C generally produce the best results. Primers with melting temperatures above 65°C have a tendency for secondary annealing (Primer Design Guide, 2012).

The target gene was amplified using basic PCR Protocol (Table 2.1) for the Platinum Taq DNA Polymerase (Invitrogen, #10966). The PCR products were then purified from solution using silica-membrane-based purification employed by the QIAquick PCR Purification Kit (Qiagen #28104).

P62-ORF –F-Sall/ -R-HindIII primers			
<i>Step</i>	<i>T_m</i>	<i>Time</i>	<i>Cycles</i>
Initial denaturation	94°C	2min	1
Denaturation	94°C	15sec	35
Annealing	62°C	15sec	
Extension	68°C	1min	
Incubation	68°C	7min	1
Cycle completion	4°C	∞	1
LC3-ORF –BamHI-F/ -PstI-R primers			
<i>Step</i>	<i>T_m</i>	<i>Time</i>	<i>Cycles</i>
Initial denaturation	94°C	2min	1
Denaturation	94°C	15sec	35
Annealing	64°C	15sec	
Extension	68°C	30sec	
Incubation	68°C	7min	1
Cycle completion	4°C	∞	1

Table 2.1. PCR running conditions for the Platinum Taq DNA Polymerase.

The pQE-9 plasmid DNA (Fig. 2.6) was cut at specific sites within or adjacent to a particular sequence, known as a restriction site. All restriction enzymes used cut the DNA backbone to leave 5' phosphate group, required for subsequent ligation, producing either blunt or sticky ends (with either a 3' or 5' overhang). To cut vector at the specific recognition sequence the following restriction enzymes were used: Sall (Roche #10348783001) and HindIII (Roche #10656313001) for p62-ORF DNA fragment; or PstI (Roche #10621625001) and BamHI (Roche #10220612001) for LC3-ORF DNA fragment. Each restriction enzyme and DNA substrate was mixed with a corresponding Roche buffer. Specifically, for every 1µg of DNA to be digested, 1 Unit of restriction enzyme was used. All restriction digests were carried out at 37°C for 3hrs and enzymes were inactivated at 65°C for 15min.

The pQE-9 digests were next dephosphorylated with Calf intestinal alkaline phosphatase (CIP; NEB #M0290S), to prevent self-ligation and thus increase the success rate of cloning, and purified on a 0.8% agarose gel.

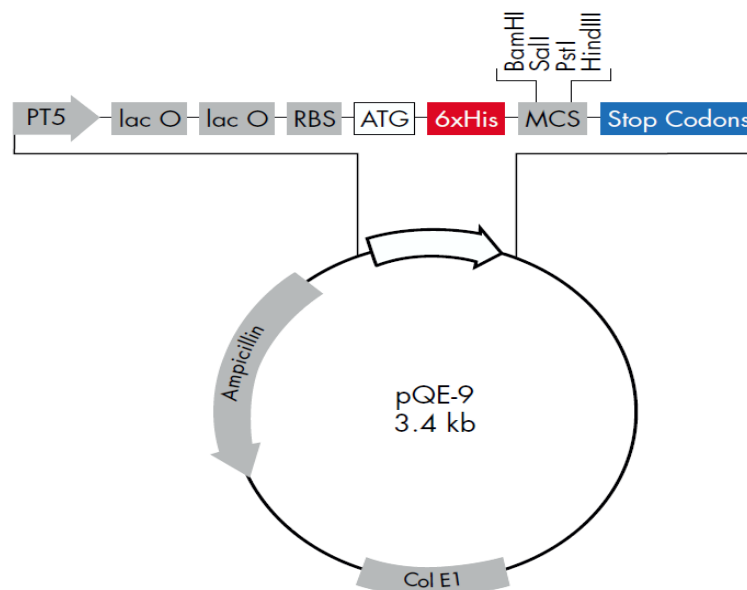


Figure 2.6. *pQE-9 Vector (3439bp)* Quiagen. Positions of elements in bases: 1-6 Start of numbering at XhoI (CTCGAG); 7-87 T5 promoter/lac operator, 61 T5 transcription start; 127-144 6xHis-tag coding sequence; 145-170 Multiple cloning site; 186-280 Lambda t0 transcriptional termination region; 1042-1140 rrnB T1 transcriptional termination region; 1616 ColE1 origin of replication; and 3234-2374 β-lactamase coding sequence.

The amplified DNA products (p62-ORF and LC3-ORF) were next inserted (ligated) into the pQE9 vector/ plasmid using T4 DNA Ligase (Promega #M180A). T4 DNA Ligase catalyzes the joining of two strands of DNA between the 5'-phosphate and the 3'-hydroxyl groups of adjacent nucleotides in either a cohesive-end or blunt-end configuration. The ligation reaction (100ng of vector DNA with 17ng insert DNA and 1µl 10x Ligase Buffer*, plus 0.5µl T4 DNA Ligase) was assembled in a sterile microcentrifuge tube and incubated at room temperature for 3 hours.

* 10X Ligase Reaction Buffer is 300mM Tris-HCl (pH 7.8 at 25°C), 100mM MgCl₂, 100mM DTT and 10mM ATP.

Vectors containing a foreign DNA, pQE-9/p62-ORF or pQE-9/LC3-ORF were thereafter transformed into bacteria - NEB 5-alpha Competent *E.coli* cells (NEB #C2987H). Procedures were carried out according to the high efficiency transformation protocol (NEB #C2987H). The procedure was the following: a tube of competent *E.coli* cells was thawed on ice. Next 1-5µl (containing 1pg-100 ng) of the vector DNA was added to 50µl of cells in a 1.5-ml microfuge tube and incubated on ice for 30 minutes; and heat shocked at 42°C for 30 seconds afterwards. The tubes were then immediately placed back on ice and incubated for further 5 minutes. The transformed cells were then grown in 950µl of SOC medium for 1 hour at 37°C with agitation. 50-100µl of the cell suspension was next plated out on LB agar plates containing ampicillin and incubated overnight at 37°C. The positive control was the transformation of an aliquot of competent cells with a known vector bearing the same resistance. The negative control was an LB-agar plate with not transformed competent cells, which followed the same transformation procedure without the addition of the vector DNA.

Once obtained the transformants, colonies were selected and incubated in LB medium overnight at 37°C. The glycerol stocks were prepared and kept at -80°C. The integrity of the cloned gene sequence was then checked by sequencing.

PCR was carried out accordingly with BIOmix Polymerase (Bioline, BIO-25011) (Table 2.2) and DNA was run on a 1% agarose gel where bands corresponding to either p62 or LC3 DNA were identified**. 6xHis-tagged proteins were purified from *E.coli* under native conditions using QIAexpress Ni-NTA Fast Start protein purification kit and quantified via Bradford assay (Qiagen #30600).

**DNA from pQE9 / clones was sent for sequencing, performed by Genome Enterprise limited, John Innes Centre, Norwich. Following sequencing results NEB 5-alpha Competent E.coli cells containing the sequence-positive plasmids were grown overnight on LB media supplemented with 50 mg/ml ampicillin.

P62-ORF –F-Sall/ -R-HindIII primers			
<i>Step</i>	<i>Tm</i>	<i>Time</i>	<i>Cycles</i>
Initial denaturation	94°C	4min	1
Denaturation	94°C	15sec	35
Annealing	62°C	15sec	
Extension	72°C	1min	
Incubation	72°C	7min	1
Cycle completion	4°C	∞	1
LC3-ORF –BamHI-F/ -PstI-R primers			
<i>Step</i>	<i>Tm</i>	<i>Time</i>	<i>Cycles</i>
Initial denaturation	94°C	4min	1
Denaturation	94°C	15sec	35
Annealing	64°C	15sec	
Extension	72°C	1min	
Incubation	72°C	7min	1
Cycle completion	4°C	∞	1

Table 2.2. PCR running conditions for the Biomix DNA polymerase.

2.3.2 Generating VCP-deletion mutants.

The DNA for full length human protein (Appendix, Fig.A1) was used for creation of VCP-deletion mutants. The DNA has been amplified exploiting specific primers (Table 2.3). The protocol used for PCR amplification can vary in dependence of the annealing and melting temperatures of the primers and of the level of stringency I wanted to reach. In general the protocol has been the following:

Primer	Sequence
AttB dN-VCP-ORF-F	5'- GGGGACAAGTTTGTACAAAAAAGCAGGGCTTCGAA GGAGATAGAA – 3'
AttB ALT-VCP-ORF-F	5'- GGGGACAAGTTTGTACAAAAAAGCAGGGCTTCGAAGGA GATAGAACC – 3'
AttB VCP NOter-ORF-R	5'- GGGGACCACTTTGTACAAGAAAGCTGGGTCGCCATACA GGTCATCATCATT– 3'
AttB dCterm-VCP-ORF-R	5'– GGGGACCACTTTGTACAAGAAAGCTGGGTCTCTGA AGGGTCTGGGC – 3'

Table 2.3. Cloning primers.

Step	Tm	Time	Cycles
Initial denaturation	94°C	2min	1
Denaturation	94°C	30sec	35
Annealing	60°C	30sec	
Extension	72°C	1.5min	
Incubation	72°C	5min	1
Cycle completion	4°C	∞	1

Table 2.4. PCR running conditions.

The C-domain (dC VCP) and both C+N-domains (DKO VCP) deletion PCR products were purified from solution with a QIAquick PCR Purification Kit (Qiagen #28104). The N-domain deletion (dN VCP) PCR product was purified from 0.8% agarose gel using PureLink Quick Gel Extraction Kit (Quiagen #K2100-12).

same resistance. The negative control was an LB-agar plate with not transformed competent cells, which followed the same transformation procedure without the addition of the vector DNA.

Once obtained the transformants, colonies were selected and incubated in LB medium overnight at 37°C. The glycerol stocks were prepared and kept at -80°C.

2.4 Bacterial cell cultures

For extraction of plasmid DNA from Escherichia Coli (E.Coli), bacterial colonies were grown in 5-10mL LB medium supplemented with antibiotics, either 50 mg/ml ampicillin or 50-100 mg/ml kanamycin, at 37°C overnight in a shaker at 180 rpm. The concentration of DNA was measured using nanodrop ND-1000 (Labtech). To prepare high quality plasmid DNA, the QIAprep spin miniprep kit (Qiagen, #27104) was used following the manufacturer instructions. The QIAprep Miniprep Kits use silica-gel-membrane technology to eliminate the cumbersome steps associated with loose resins or slurries. Briefly, the QIAprep miniprep procedure is based on alkaline lysis of bacterial cells followed by adsorption of DNA onto silica in the presence of high salt. Plasmid DNA is eluted in a small volume of Tris buffer (included in each kit) and is immediately ready for use. Once the plasmid DNA has been collected, the nucleic acid concentration was determined using an ultraviolet light spectrophotometer (NanoDrop ND-1000, Labtech).

2.5 Reagents

Majority of reagents was obtained from the following companies: Sigma-Aldrich (UK), Roche (UK), Thermo Scientific (UK) and Invitrogen (UK). Restriction enzymes used for genotyping were purchased from either Roche (UK) or Sigma (UK).

Protein extraction buffers:

- M-PER mammalian protein extraction reagent (Thermo scientific, #78501) - utilises a proprietary detergent in 25mM bicine buffer (pH 7.6);
- T-PER protein extraction reagent (Thermo scientific, #78510) - utilises a proprietary detergent in 25mM bicine, 150mM sodium chloride (pH 7.6);

- Mild NP-40 (from Nonidet-40 detergent) -like lysis buffer (prepared in the lab) - 100mM Tris base, 150mM NaCl and 0.5% Triton X-100 in ddH₂ O;
- Halt™ protease inhibitor cocktail (Thermo scientific, #87786) - contains six potent broad-spectrum protease inhibitors stabilized in dimethylsulfoxide (DMSO) (Table 2.5).

Protease Inhibitor Component	MW	Protease Family Targeted	Inhibitor Type	Concentration in 100X Cocktail
AEBSF•HCl	239.5	Serine proteases	Irreversible	100mM
Aprotinin	6511.5	Serine proteases	Reversible	80μM
Bestatin	308.38	Amino-peptidases	Reversible	5mM
E-64	356.4	Cysteine proteases	Irreversible	1.5mM
Leupeptin	475.6	Serine and cysteine proteases	Reversible	2mM
Pepstatin A	685.9	Aspartic acid proteases	Reversible	1mM

Table 2.5. Formulation and concentration of the Thermo Scientific Halt™ Protease Inhibitor Cocktail (Thermo scientific, #87786 datasheet)

Other ready-made solutions:

Dimethyl sulfoxide (DMSO; Sigma, #D8418), Rapamycin 10nmol (Cell signalling, #9904), Torin1 6mM in DMSO (Axon Medchem, #1833), Wortmannin (Sigma, #W3144-250UL), Bafilomycin A1 (Sigma, #B1793) 0.1mg/ml in DMSO, Lipofectamine 2000 (Invitrogen, #11668), MG132 10mM (Calbiochem, #474791), Cycloheximide 100mg/ml in DMSO (Sigma, #C4859), Tween20 (Sigma, #P1379), Triton X-100 (Sigma, #T8787), Paraformaldehyde 16% (Alfa Aesar, #43368).

2.6 Transfection and Autophagy induction

The culture growth medium was replaced with fresh antibiotic-free DMEM, supplemented with 10% heat-inactivated FCS prior to Transfection. HeLa or MEF cells were transfected with 1.6μg (12-well plate) or 2.5-4μg (6-well plate) plasmid DNA using 2.5-5μl or 5-12 μl Lipofectamine 2000 transfection reagent respectively. The cells were incubated at 37°C for 24-30 hours to allow for protein biosynthesis. In order to induce autophagy, cells were either incubated in HBSS (Hank's Balanced Salt Solution) for 3 hours or treated with 1-1.5μM Torin1 or 200nM Rapamycin for 2-6 hours (as required). Total cell lysates were made using M-PER protein extraction

reagent (Thermo scientific, #78501) with Halt™ protease inhibitor mixture (Thermo scientific, #1861278). Protein expression was then determined by Western blotting. Alternatively, transfected cells were washed with PBS, fixed with 4% paraformaldehyde (PFA) for 20 minutes, blocked and stained for fluorescence microscopy.

2.7 Cycloheximide-chase degradation assay

Cells were grown in culture medium for 24-48 hours prior to the experiment (ready when approximately 80% confluent). Cycloheximide (Sigma, #C4859) was added at 50-100µg/ml and the cells incubated for 0-6 hours. Cells were lysed at the appropriate time point in M-PER protein extraction reagent (Thermo scientific, #78501) with Halt™ protease inhibitor mixture (Thermo scientific, #1861278). Concentration of the total protein extracted was determined using a BCA Protein Assay Kit (Thermo Scientific Pierce, #23227). Equivalent loading and sample stability was determined by Western blotting.

2.8 Co-immunoprecipitation

(Dynabeads Protein G Kit, Invitrogen Cat. no.100.07D)

For Immunoprecipitation experiments, cells were lysed 24 hours after transfection using M-PER protein extraction reagent (Thermo scientific, #78501) with 100 x Halt™ protease inhibitor cocktail (Thermo scientific, #1861278). Protein samples were adjusted to a total concentration of approximately 250µg protein (diluted if necessary), and 50µl of Dynabeads was aliquoted to fresh test tubes. Antibodies diluted in 200µl PBS pH 6.4 containing 0.02% Tween 20 (Sigma, #P1379), were first immobilized on magnetic beads at room temperature for 10-30 minutes. Thereafter clarified cellular lysates were applied to the coupled rabbit (Santa Cruz, #SC-2027) or mouse (Santa Cruz, #SC-2025) IgG- bead complexes, for 10-30 minutes at room temperature, to bind nonspecific proteins (IP:IgG fraction). Small 22µl sample of the pre-cleared protein would be kept as a total protein fraction (Input) to be analysed by protein blotting at the later stage. Pre-cleared lysates were then mixed with specific antibody-bead complexes for 30 minutes – 1 hour to pull down target proteins (bound IP fraction). Following removal of unbound proteins (Unbound fraction) and washing with 1xPBS, the immunoprecipitated proteins were eluted with 20µl Elution

Buffer (50mM Glycine pH2.8) and prepared for analysis by Western blotting (by adding pre-mixed 10µl NuPAGE LDS 4x sample buffer, 4µl NuPAGE 10x reducing agent and 6µl ddH₂O, then heated for 10 minutes at 70°C before loading on a gel).

2.9 Western blot analysis

Total cell lysates were made using M-PER protein extraction reagent (Thermo scientific, #78501) with Halt[™] protease inhibitor mixture (100x; Thermo scientific, #1861278). Concentration of the total protein extracted was determined using a BCA Protein Assay Kit (Thermo Scientific Pierce, #23227) with a set of diluted Albumin (BSA) standards for working range of 20-2000µg/ml concentration. The BCA Working Reagent (WR) (prepared by mixing 50:1 reagent A:B) was added to each test tube containing a sample or a standard in a ratio of 20:1 WR to Sample. Once mixed tubes were incubated at 37°C for 30 minutes and the absorbance of all the samples was measure with the spectrophotometer at 562nm. The average blank-corrected measurement for each BSA standard versus its concentration in µg/ml was plotted generating the standard curve which was then used to determine the protein concentration of each unknown sample.

A 15µg of protein (diluted in the NuPAGE LDS 4x sample buffer (Novex, #NP0007), deionized water and NuPAGE 10x reducing agent (Novex, #NP0004), then heated at 70°C for 10min) and ready-to-use Western Protein standards were loaded on a gel.

The MagicMark[™] XP (Invitrogen, # LC5603) Western Protein Standard with 9 recombinant proteins, each of which contains an IgG binding site, in even increments from 20-220kDa was used for identification of the target proteins over 20kDa in size.

The Precision Plus Protein Dual Color Standards (Bio-Rad, # 161-0374) with 10 bands of 10-250kDa was used for identification of the target proteins below 20kDa in size.

Both Protein Standards were compatible with Western kits for chemiluminescent and fluorescent detection.

For the SDS-PAGE pre-made 4-12% Bis-Tris (Novex, #NP0335BOX) or 3-8% Tris-Acetate (Novex, #EA0375BOX) gels were used. A 1x Running Buffer for the SDS was prepared using:

- 50ml of NuPAGE 20x MES SDS Running Buffer (Novex, #NP0002) in 950ml of deionized water for the Bis-Tris gels.
- 50ml of NuPAGE 20x Tris-Acetate SDS Running Buffer (Novex, #LA0041) in 950ml of deionized water for the Tris-Acetate gels.

For reduced samples the upper buffer chamber of the XCell *SurLock*[®] Mini-Cell gel running tank Module (Invitrogen, EI0002) was filled with 200ml 1x Running Buffer containing 500µl NuPAGE Antioxidant (Novex, #NP0005) and lower buffer chamber was filled with 600ml of 1x Running Buffer (no additives). Gel Electrophoresis was run for either 40 minutes at 200V constant, for the 4-12% Bis-Tris gels, or 1 hour at 150V constant for the 3-8% Tris-Acetate gels. Proteins were transferred from gel on to Nitrocellulose (NC) membrane using XCell II Blot Module (Invitrogen, EI9051). 2x filter pads/filter paper/NC membrane/gel/filter paper/2x filter pads were assembled into a 'sandwich'. A 1x Transfer Buffer was prepared using 50ml of NuPAGE 20x Transfer Buffer (Novex, #NP0006-1), 100ml (for a single gel) or 200ml (for 2 gels) Methanol, 1ml NuPAGE Antioxidant (Novex, #NP0005) and deionized water to 1000ml total volume. Protein bands from the SDS-gel were transferred to the NC membranes at 30 Volts for 1 hour.

2.9.1 Odyssey infrared imaging system (Licor)

The membrane was soaked in 1xPBS for 1 minute to remove residual transfer buffer followed by 1 hour blocking in Odyssey[®] Blocking Buffer (non-mammalian Odyssey blocking reagent in PBS containing 0.1% sodium azide; Licor, #927-40000) or 5% w/v milk in 1xTBS containing 0.01% Tween. The membrane was then incubated with primary antibodies (Table 2.6) in blocking buffer for 1-4 hours at room temperature or overnight at 4°C. After washing 3-5 times for 5min with 1xPBST (1xPBS with 0.01% Tween) or 1xTBST (1xTBS with 0.01% Tween) respectively, the membrane was incubated with secondary antibodies (Table 2.7) in blocking buffer for 30 minutes – 1 hour. The membrane was washed as before and images were acquired and analyzed using the Odyssey CLx infrared imaging system.

Antibody	Company/Code	Reactivity	Concentration	Dilution
Anti-p62	Sigma/P0067	Rabbit	1.2 mg/ml	1/1000
Anti-p62	MBL/M162-3	Mouse	1 mg/ml	1/1000
Anti-LC3	Sigma/L8918	Rabbit	1.2 mg/ml	1/1000
Anti-LC3 B	Sigma/ L7543	Rabbit	1.3 mg/ml	1/1000
Anti-GFP	Invitrogen/A6455	Rabbit	0.2 mg/ml	1/750
Anti-GFP	Abcam/ab1218	Mouse	1.38 mg/ml	1/500-1/2000
Anti-VCP	BD Transduction Lab/ 612183	Mouse	250 µg/ml	1/250-1/1000
Anti-VCP	Cell Signal/2648	Rabbit	100 µg/ml	1/1000
Anti-VCP	Abcam/ab109240	Rabbit	1.0 mg/ml	1/1000-1/5000
Anti-V5	Invitrogen/1038696	Mouse	1.0 mg/ml	1/5000
Anti-V5	Sigma/V8137	Rabbit	4.5 mg/ml	1/3600
Anti-FLAG	Sigma/F7425	Rabbit	0.8 mg/ml	1/320
Anti-FLAG	Sigma/F3165	Mouse	20 µg/ml	1/1000
Anti-actin	Sigma/A3853	Mouse	1.8 mg/ml	1/3000
Anti-FK2	Biomol/PW8810	Mouse	10 mg/ml	1/100-1/1000
Anti-CLC7	Santa Cruz/ sc-28755	Rabbit	200 µg/ml	1/100-1/1000
Anti-SVIP	Sigma/ A3853	Rabbit	0.1 mg/ml	1/200-1/1000
Anti-IκB-α	Cell Signal/9242	Rabbit	100 µg/ml	1/1000
Anti-Ub	Santa Cruz/sc-8017	Mouse	200 µg/ml	1/1000
Anti-Atg5	Sigma/ A0731	Rabbit	1.0 mg/ml	1/500-1/1000
Anti-Atg7	Sigma/ A2856	Rabbit	1.0 mg/ml	1/1000
Anti-LAMP1	Santa Cruz/sc-20011	Rabbit	200 µg/ml	1/1000
Anti-LAMP1	Cell Signal/3243	Rabbit	100 µg/ml	1/1000

Table 2.6. Primary Antibodies

Antibody	Company/Code	Reactivity	Concentration	Dilution
Goat anti-rabbit IRDye 680LT	Licor/926-32221	Rabbit	0.05mg/ml	1/10000
Goat anti-mouse IRDye 680LT	Licor/926-32220	Mouse	0.05mg/ml	1/10000
Goat anti-rabbit IRDye 800CW	Licor/926-32211	Rabbit	0.05mg/ml	1/10000
Goat anti-mouse IRDye 800CW	Licor/926-32210	Mouse	0.05mg/ml	1/10000

Table 2.7. Secondary Infrared Antibodies

2.9.2 WesternBreeze Chemiluminescent Immunodetection (Invitrogen #WB7104 and #WB7106)

Nitrocellulose (NC) membranes were incubated in the appropriate Blocking Solution (For 20ml: 14ml dH₂O, 4ml blocker/diluent part A - concentrated buffered saline solution containing detergent; 2ml blocker/diluents part B - concentrated Hammersten casein solution) for 30 minutes at room temperature (RT). Rinsed with water these were next incubated for 1 hour with Primary Antibody Solution (Primary antibodies in Blocking Solution). After washing 3 times for 5 minutes with diluted Antibody Wash Solution (16x concentrated buffered saline solution containing detergent) provided in the kit, membranes were incubated in Secondary Antibody Solution (ready-to-use solution of alkaline phosphatase-conjugated, affinity purified anti-mouse or anti-rabbit IgG, depending on the origin of the primary antibodies used), also provided in the kit, for 30 minutes. Membranes were then washed as before and rinsed with deionised water. Finally, Chemiluminescent Substrate (ready-to-use solution of CDP-Star chemiluminescent substrate for alkaline phosphatase mixed 80:20 with Chemiluminescent Substrate Enhancer - Nitro-Block-II enhancer for blots on NC membranes) was applied to the surface of the membranes for 5 minutes, followed by preparation of transparency plastic/ membrane sandwich for luminography. Chemiluminescent Immunodetection was used for Western blots of Immunoprecipitation fractions were no further quantification was necessary.

2.9.3 Quantification of Western Blots

All membranes were analysed using the Odyssey CLx infrared imaging system featuring Image Studio Analysis Software Version 4.0 (Licor).

The Odyssey CLx Imager begins image acquisition with the membrane scan were desired channel(s) (700, 800, or both) are selected and AutoScan initiated. When the acquisition is complete, the image appears on the screen where it can be adjusted and processed. In the Analysis tab a rectangle is added around an area of fluorescence (a fluorescent band for desired protein of a known size). The software moves selected shapes to fully enclose areas of fluorescence near the shapes. The Image Studio software assigns a value to all the shapes (bands) based on their relative signal and subtracts the background of the blot (the median value of the pixels in the background segment) from the shapes to obtain consistent data. The

software will not calculate signal for the shapes if a background method is not selected. The signal values assigned to shapes 1, 2 etc. are recorded in the Shapes Table. Data from the Shapes Table can then be copied to an Excel Spreadsheet. The loading control's band (for Actin, unless otherwise stated) with the largest signal is assigned a value of 1 and the signals from each of the other bands in the normalization channel are divided by the largest signal to obtain each band's Normalization Factor. The signal for each band in the other channel is divided by the Normalization Factor of the band in the same lane. Acquired data could then be compared and presented in a graph if required.

2.10 Immunostaining

Following the incubation / treatment period the cells were fixed with 4% PFA solution for 20 minutes followed by several washes with PBS. To block non-specific protein binding, cell slides were incubated with blocking buffer (5-10% FBS in PBS with 0.01% Triton X) for 30 minutes – 1 hour at room temperature (RT), followed by incubation with the primary antibodies (Table 2.8) (diluted at 1/200 - 1/400 in blocking buffer) for either 1 hour at RT or overnight at 4°C on a shaking plate. After washing 3 times for 5-10 minutes with PBS-T (PBS with 0.1% Triton X), the cell slides were incubated in secondary antibodies (Table 2.9) for 30 minutes – 1 hour at RT. Washed with PBS-T slides were mounted with approximately 20µl VectaShield (Vector Laboratories, #H-1000 and #H-1200) mounting media with or without DAPI per slide and covered with glass cover slips.

Antibody	Company/Code	Reactivity	Concentration	Dilution
Anti-p62	Sigma/P0067	Rabbit	1.2 mg/ml	1/400
Anti-p62	MBL/M162-3	Mouse	1 mg/ml	1/400
Anti-LC3	Sigma/L8918	Rabbit	1.2 mg/ml	1/400
Anti-LC3 B	Sigma/ L7543	Rabbit	1.3 mg/ml	1/400
Anti-FK2	Biomol/PW8810	Mouse	10 mg/ml	1/400

Table 2.8. Primary Antibodies used for immunofluorescent staining.

Antibody	Company/Code	Reactivity	Concentration	Dilution
Chicken Alexa Fluor 594	Molec Probe /A-21201	mouse	2 mg/ml	1-10 µg/ml
Chicken Alexa Fluor 594	Molec Probe/ A-21442	rabbit	2 mg/ml	1-10 µg/ml
Chicken Alexa Fluor 488	Molec Probe/ A-21200	mouse	2 mg/ml	1-10 µg/ml
Chicken Alexa Fluor 488	Molec Probe/ A-21441	rabbit	2 mg/ml	1-10 µg/ml
Goat Alexa Fluor 350	Molec Probe/ A-11045	mouse	2 mg/ml	1-10 µg/ml

Table 2.9. Secondary antibodies used for immunofluorescent staining.

2.10 Light Microscopy and imaging

Fluorescence cell imaging was carried out on a Carl Zeiss Axio Imager M2 (with ApoTome attachment) microscope with CCD camera for fluorescence acquisition; using a Plan-APOCHROMAT 40x/1.4 and 63x/1.4 Oil objective lens attached to a high definition camera (AxioCam HRm, Carl Zeiss). Images were processed using Axiovision software version 4.8.

2.11 Imaris analysis

Microscope images were analysed using Imaris software (Bitplane) to count puncta formation and co-localisation by user-defined spot definition parameters. A general diameter of 0.75µm was assumed as the standard for autophagosome size (Mizushima *et al.*, 2010). This allowed the software to locate regions that come close to this measurement in the chosen fluorescent channel and was used for analytical purposes. Puncta generated in each fluorescent channel could be afterwards aligned to determine their co-localisation. The number of puncta per cell and their diameter (ranging from 0.1µm to ≥1µm) was generated and exported to an Excel workbook where the spread of data could be analysed. A mean number of puncta (inclusions) per cell from ≥14 cells examined (from each treatment/ condition) was determined. Statistical analysis was performed using an unpaired two-tailed Student's T-test assuming unequal variance.

2.12 Filter-trap assay

Total cell lysates were made using Mild NP-40-like protein extraction buffer with Halt™ protease inhibitor mixture. Cellular debris was pelleted at 1000 r.p.m. for 10 minutes. Concentration of the total protein extracted was determined using a BCA Protein Assay Kit (Thermo Scientific Pierce, 23227) according to the manufacture guidelines (see above). The extent of aggregation was measured by trapping the aggregated protein on a nitrocellulose membrane (NC), with a 0.2µm pore size and by staining with a specific primary antibody. The efficiency of the NC membrane in capturing and retaining aggregated protein in this assay was tested before (Chang and Kuret, 2008). Interestingly, in terms of precision, the most sensitive detection was found with NC (not cellulose acetate), and by narrowing nitrocellulose porosity to 0.2 µm increased by further 1.7 fold (Chang and Kuret, 2008). Here, the NC membranes were pre-equilibrated by soaking in 1x PBS directly before use. Blotting pads x2 were also soaked before assembling the blotting module. Then, 15µg protein sample diluted in 200µl of Mild NP-40-like buffer was applied onto the membrane, followed by vacuum filtration through a 96-well dot blot apparatus. Afterwards the resultant membrane was blocked in Protein-Free T20 blocking solution (Pierce, #37573; contains a proprietary compound in PBS, pH 6.4 with 0.05% Tween-20 Detergent and Kathon Antimicrobial Agent) for 1 hour, and then incubated with specific primary antibodies (Table 2.2) for another 1 hour. After washing 3 times for 5 minutes with PBST membranes were incubated in horseradish peroxidase (HRP) conjugated Secondary Antibody Solution (Goat anti-mouse or anti-rabbit depending on the origin of the primary antibodies used) for 30 minutes. Membranes were then washed as before and rinsed with deionised water. Finally, Chemiluminescent Substrate was applied to the surface of the membranes for 5 minutes, followed by luminography. Chemiluminescence was recorded on a Fujifilm LAS-3000 Intelligent Dark Box and quantified using the Odyssey CLx Image Studio Analysis Software Version 4.0 (Licor).

2.13 VCP mouse Genotyping

The heterozygous R155H/+ knock-in mice used for protein analysis and primary cell isolation were generated by Dr Watts and colleagues (Badadani *et al.*, 2010) at InGenious Targeting Laboratory, Inc. (Stony Brook, NY) through a Neomycin cassette insertion using 129/SvEv mice.

Briefly, using a FRT-flanked Neomycin cassette insertion, cultured SvEv embryonic stem cells were transgenically modified (Fig. 2.8) to express the pathological *Vcp* R155H/+ mutation and inserted into 129/SvEv blastocysts. The blastocysts were implanted in pseudo pregnant females and the chimeric offspring produced were mated with 129/SvEv mice, resulting in the F1 mutant generation. The expression of mutant VCP was confirmed by RT-PCR using the following primers in the PCR reactions: Forward- 5'-CAC GGT GTT GCT AAA AGG AAA GAA AAG; Reverse- 3'-CTG AAG AAT CTC CAA ACG TCC TGT AGC, after the RT reactions with the reverse primer. These mice were back-crossed with mice of the C57BL/6 strain more than six times, resulting in mice that retained >98% genetic homology with the C57BL/6 strain. The Neomycin cassette was deleted by crossing with the Flp deletion kit mouse model.

VCP R155H Knock-in Targeting Strategy

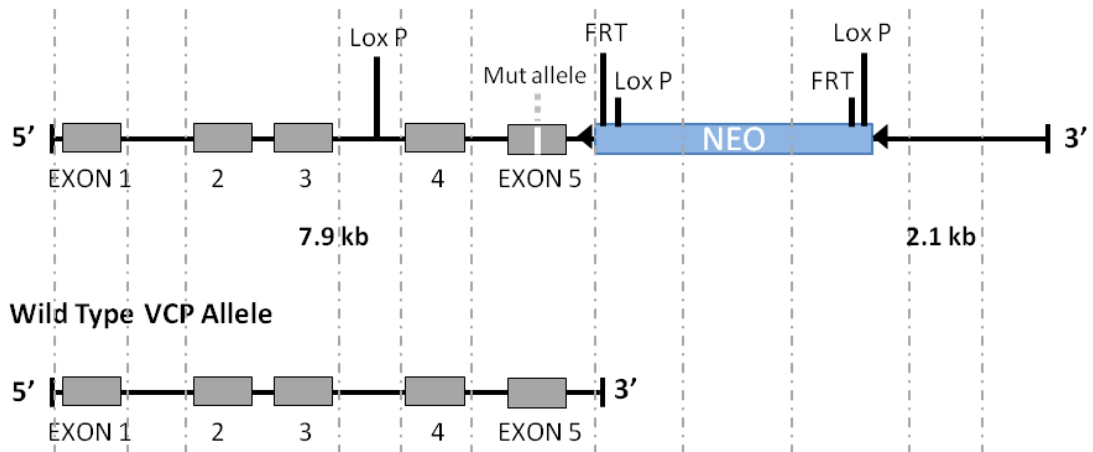


Figure 2.8. Generation of the *VCP*^{R155H/+} knock-in mice. In order to generate a VCP disease mouse model, genomic VCP fragments with 7.9 kb of upstream homology sequence and 2.1 kb of downstream homology sequence were subcloned into a targeting vector. Site-directed mutagenesis using the Quick-Change XL SiteDirected Mutagenesis Kit (Stratagene, La Jolla, CA) was used to introduce the R to H mutation at amino acid position 155 (Badadani *et al.*, 2010). Above is a schematic drawing of R155H targeting strategy of the knock-in allele (top)

and the wild type allele (below). The localizations of the 5' (7.9 kb) and 3' (2.1 kb) targeting sequences are indicated by dashed lines. The exons 1 through 5 are numbered and Neomycin-cassette is marked by Neo. The Neo-cassette is flanked by FTR sites and LoxP restriction sites. Mutation site in exon 5 is indicated.

Mouse DNA was extracted from either a 0.2cm ear punch or tail tip from each young animal. This was initially carried out using Proteinase K (Invitrogen, 25530-049) diluted in ddH₂O and 10xPCR reaction buffer. Tissue was degraded at 65°C for 4-6 hours. Thereafter Proteinase K was inactivated at 95°C for 10-20 minutes. Tissue debris were removed by centrifugation and supernatant, containing mouse DNA, transferred to new sterile Eppendorf tube.

The Proteinase K extraction was later replaced by the "HotSHOT" (hot sodium hydroxide and tris) alkaline lysis method (Truett *et al.*, 2000), proven to be a fast, highly efficient and inexpensive method. Briefly, 75µl of alkaline lysis reagent (25mM NaOH, 0.2mM disodium EDTA in ddH₂O, pH 12) was added to the tissue sample and was heated to 95°C for 30-60 minutes. The tissue sample was checked at 30 minutes and the tubes agitated in order to estimate the degree of lysis. Once lysed, the tissue sample was cooled to 4°C and 75µl of neutralisation buffer (40mM Tris-HCl in ddH₂O, pH 5) was added. The samples were centrifuged at 775g for 3 minutes and the supernatant transferred to another sterile Eppendorf tube.

The VCP region on the genomic DNA template was amplified using 'mus vcp gen-2F' and 'mus vcp gen-2R' primers (Table 2.10). PCR protocol for the 2x BioMix with BIOTAQ DNA polymerase (Bioline, #BIO-25011; Composition: BIOTAQ DNA Polymerase, 2mM dNTPs, 32mM (NH₄)₂SO₄, 125mM Tris-HCl pH8.8, 0.02% Tween, 3mM MgCl₂, Stabiliser) was used, following the manufacture's guidelines. Specifically, for each 25µl reaction a 12.5µl of BioMix was mixed with 2.5µl Template DNA, 1µl of each Primer (2F+2R) and 8µl ddH₂O.

Primer	Sequence
Mus-vcp-gen-2F	5' – TGGAAGGCATCACTGGCAATCTCT – 3'
Mus-vcp-gen-2R	5' – TTAAGGCCATCCAATCTCCAAAAGTA – 3'

Table 2.10. Sequencing primers.

Step	Tm	Time	Cycles
Initial denaturation	94°C	2min	1
Denaturation	94°C	30sec	35
Annealing	60°C	30sec	
Extension	72°C	1.5min	
Incubation	72°C	5min	1
Cycle completion	4°C	∞	1

Table 2.11. PCR running conditions for the sequencing.

Following PCR (Table 2.11), PCR products were digested with either MspI (cuts *wt* allele) or NcoI (cuts mutant allele) restriction enzymes for a 3hours at 37°C and run on a 1% agarose gel at 120V for 1 hour (Appendix Fig. A2). When specifically using NcoI to cut *Vcp* we can identify three fragments corresponding to: a wild-type allele (982bp) and two fragments for mutant allele (700bp and 282bp).

2.14 Primary macrophages culture preparation and *In vitro* osteoclastogenesis

2.14.1 Osteoclast (OCL) differentiation 'monocyte separation protocol'

Primary mouse Bone Marrow Derived Macrophages (BMDMs) and Spleen derived Macrophages (SPLMs) were prepared from >9 week old wild-type and *VCP*^{+/*R155H*} mutant mice. Mouse femurs (also known as the thigh bone) were isolated from adult mice and washed in PBS. Ends of the long bones were cut off in a sterile environment, bone marrow cells were flushed from bones with α -MEM with a sterile 27.5 gauge needle and syringe. Spleens were crushed and washed with α -MEM. Cells were centrifuged at 1500 rpm for 5 minutes and resuspended in α -MEM. Monocytes/macrophages were separated from the rest of the haematopoietic cells on a Ficoll-Paque (GE Healthcare, #17-1440-02) and plated onto a 35mm plate in α -MEM supplemented with 10% heat inactivated FBS and 1% Penicillin-Streptomycin (P/S) antibiotics mix.

After overnight culture the nonadherent cells were counted and split into cell culture plates for osteoclastogenesis. To maintain primary macrophage monolayer (BMDM), cells were grown in α -MEM supplemented with 25ng/ml Macrophage Colony

stimulating factor from mouse (M-CSF; Initially from Sigma, #M9170; R&D Systems, #416-ML-010). To induce osteoclast differentiation BMDMs and SPLMs were maintained with 25ng/ml M-CSF and 50 or 100ng/ml RANK Ligand from mouse (RANKL; Initially from Sigma, #R0525; R&D Systems, #462-TEC-010). Every 2-3 days a $\frac{3}{4}$ of the media was changed with fresh α -MEM media containing M-CSF and RANKL.

2.14.2 OCL differentiation 'quick protocol'

Primary mouse Bone Marrow Derived Macrophages (BMDMs) were prepared from femurs of 3-6 month old wild-type and VCP^{+R155H} mice. Ends of the long bones were cut off in a sterile environment. Bone marrow (BM) cells were flushed from bones with α -MEM (containing 10% HI FCS and 1% P/S) with a sterile 27.5 gauge needle and syringe. Collected cells were then centrifuged at 1400 rpm for 5 minutes and resuspended in fresh media. Whole BM cells were cultured with 10ng/ml M-CSF in α -MEM, on 10cm Tissue Culture dish, for 4 days.

After 4 day culture the nonadherent cells were counted and split into cell culture plates (24-well plate) at 300 000 cells/ well and maintained with 25ng/ml M-CSF for further 3 days. Thereafter, only the adherent fraction was incubated with 25ng/ml M-CSF and 50-100ng/ml RANKL (R&D Systems, #462-TEC-010) for additional 3-6 days. Every 2-3 days a $\frac{3}{4}$ of the media was changed. New media was added to the remaining $\frac{1}{4}$ such that the final concentration of RANKL is 50-100ng/ml and M-CSF is 25ng/ml. OCL-like cells were expected to be present in the next 2-4 days.

2.14.3 OCL differentiation '9-day protocol'

On day 1 femurs were dissected from adult mice and washed in PBS. Whole bone marrow was flushed with α -MEM (containing 10% HI FCS and 1% P/S). Collected cells were then centrifuged at 1500 rpm for 5 minutes and resuspended in 10ml fresh α -MEM containing 5ng/ml M-CSF. On day 2, after overnight culture, the non-attached cell suspension was collected and centrifuged at 1500 rpm. The collected cells were then resuspended in fresh α -MEM containing 30ng/ml M-CSF and maintained in cell culture until day 5. On that day, the non-attached cell suspension was discarded. Whereas the attached cells were washed with PBS, scraped off and resuspended in α -MEM. Cells were counted and split into cell culture plates (96-well plate) at 100 000 -

140 000 cells/well. Those BMDM were maintained in α -MEM growth media supplemented with 25ng/ml M-CSF and 50-100ng/ml RANKL until day 9 (Fig. 2.9).

On day 7 a $\frac{3}{4}$ of the media was changed. New media was added to the remaining $\frac{1}{4}$ such that the final concentration of RANKL is 100ng/ml and M-CSF is 25ng/ml.

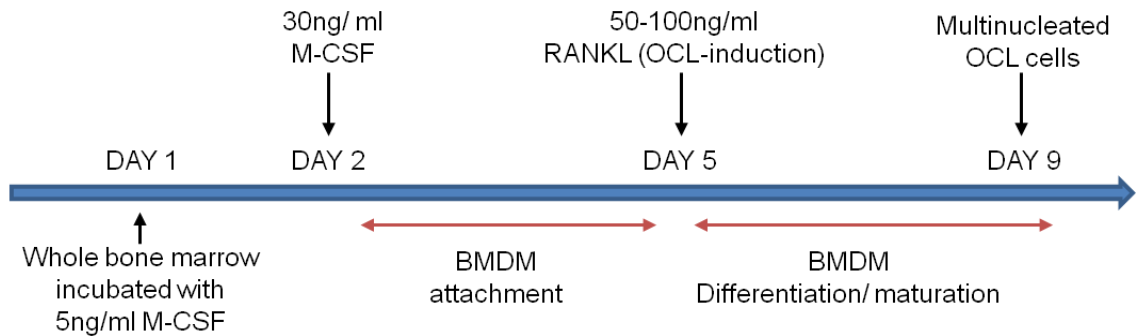


Figure 2.9. 'The 9-day osteoclast differentiation protocol'. The whole bone marrow was collected on day 1 and cultured in the presence of 5ng/ml M-CSF. The nonadherent cells were resuspended in fresh media containing 30ng/ml M-CSF on day 2 and maintained in culture allowing for the BMDM to attach. On day 5 the adherent cells were scraped off and resuspended in fresh α -MEM supplemented with 25ng/ml M-CSF and 50-100ng/ml RANKL. The BMDM were maintained under differentiating conditions until day 9 when multinucleated OCL-like cells could be observed.

2.15 TRAP staining of osteoclasts

To identify osteoclasts, cells grown in the presence of M-CSF and RANKL were fixed with 3.7- 4% paraformaldehyde in PBS, and then stained for tartrate resistant acid phosphatase (TRAP) activity (Sakiyama *et al.*, 2001) with the Acid Phosphatase kit (Sigma, #387A-1KT) following the manufacturer's instructions. Briefly, the fixed cells were first incubated in a solution of Naphthol AS-BI phosphoric acid (12.5mg/ml) and freshly diazotized Fast Garnet GBC (fast garnet GBC base, 7mg/ml, in 0.4mol/l hydrochloric acid with stabilizer mixed with 0.1mmol/l sodium nitrate in a 50:50 ratio). Preparation of the working solution: 1ml diazotized Fast Garnet GBC, 0.5ml Naphthol AS-BI phosphoric acid, 2ml acetate solution (2.5mol/l acetate buffer, pH 5.2) and 1ml of the tartate solution (0.335mol/l L(+)-tartate buffer, pH 4.9) in 45ml ddH₂O. The working solution was mixed by gentle inversion and prewarmed to 37°C before applying to the fixed cells and further incubation for 1 hour at 37°C. After 1

hour incubation, cells were rinsed thoroughly in deionized water and then counterstained for 2 minutes in Hematoxylin Solution (hematoxylin, certified, 6.0 g/l, sodium iodate, 0.6 g/l, aluminum sulfate, 52.8 g/l and stabilizers). Thereafter, cells were rinsed several minutes in alkaline tap water to blue nuclei, allowed to air dry and analysed microscopically.

This procedure employs stable diazonium salts, which form highly insoluble dye deposits. The naphthol AS-BI, released by enzymatic hydrolysis, couples immediately with fast garnet GBC forming insoluble maroon dye deposits at sites of activity (Sigma, #387A-1KT, Procedure No.387). Cells containing tartaric acid-sensitive acid phosphatase are devoid of activity. Those mononuclear cells containing tartaric acid-resistant phosphatase are not affected by such treatment.

2.16 Detection of Active NFκB p65 in the Bone Marrow Derived Macrophages

The Thermo Scientific NFκB p65 transcription Factor Kit (#89859) was used to measure active form of NFκB protein in TNFα or RANKL – activated bone marrow derived macrophages (BMDM).

The BMDM were separated from the whole bone marrow of VCP – mice as described above (2.14 ‘monocyte separation protocol’) and maintained in appropriate growth conditions until reaching at least 70% confluence. To activate NFκB, BMDM were treated with either 50ng/ml recombinant mouse TNFα (stock at 100μg/ml in PBS + 0.1% BSA; R&D Systems, #AA80-235; optimal concentration determined through titration on RAW264.7 cells – Supplementary Fig.S4) or 100ng/ml RANKL for 45 minutes. Thereafter cells were lysed with 100μl M-PER + Halt™ protease inhibitor and the total protein content were demined with BCA protein assay.

The Thermo Scientific NFκB transcription Factor Kit (#89859) contains two streptavidin-coated 96-well plates with bound NFκB biotinylated-consensus sequence. Because only the active form of NFκB binds to the DNA sequence, nonspecific binding is minimized, providing greater signal-to-noise ratios than a traditional enzyme-linked immunosorbent assay (ELISA). The plate was equilibrated to room temperature before opening. A 50μL of Working Buffer (containing ddH₂O,

5x NFκB Binding Buffer and 20x Poly dl-dC) was then added to each well. Either 4μl of Wild Type (prevents NFκB from binding to the sequence attached to the plate) or 4μl of mutant NFκB (does not affect specific NFκB binding) competitor duplex was added to control wells to ensure signal specificity, followed by 2μl of positive control TNFα Activated HeLa Cell Nuclear Extract per well. A 10μg of specific sample extracts was also added to appropriate wells (to a max of 25μl per well). Sealed plate was incubated with mild agitation for 1 hour at room temperature, followed by washes and 1h incubation with the anti-p65 primary antibody (diluted at 1:1000 in Antibody Dilution Buffer). Plate was washed again before incubating with the horseradish peroxidase (HRP) conjugated secondary antibody (diluted at 1:10,000 in Antibody Dilution Buffer) for 1 hour at room temperature. After final washes, a 100μl of chemiluminescent substrate was added to each well. Luminescence was measured using Omega 415-0097 plate reader (BMG LabTech) at 460nm absorbance. Raw data was transferred to the Microsoft Excel workbook for further analysis.

2.17 Statistical Analysis.

When recording difference between two groups the statistical significance was determined using a two-tailed student t-test. A paired t-test was applied when comparing two lots of measurements performed on the same study subject; whereas an unpaired t-test was applied to compare two independent groups. A 95% confidence interval was derived from the differences between the two sets of paired (unpaired) observations (where appropriate). Statistical significance was recorded when the resulting probability (p) value was ≤ 0.05 .

To assess the difference between three or more groups the analysis of Variance (ANOVA) was carried out. When a single independent variable was measured a one-way analysis of variance (ANOVA) was used. When analysing the independent and joint effects of two independent variables a two-way ANOVA was used. In ANOVA the significance of difference between multiple sample means was determined by the F statistics – tests the null hypothesis that the means of several populations are equal – a significant p value ($p \leq 0.05$) was recorded when at least one group mean was significantly different from the others.

For Immunoblotting technical replicates' quantification data are presented as mean \pm SEM (standard error of the means) to indicate the precision of estimated mean of population i.e. how well the sample mean truly represents the entire population mean.

To describe the variability between individual data points within the study sample the data are presented as sample mean with standard deviation (SD) i.e. dispersion of individual observations about the mean - mean (SD).

CHAPTER 3

VCP IN AUTOPHAGY

CHAPTER 3: VCP IN AGGREGATE CLEARANCE

3.1 Introduction

In addition to the relatively well categorised role of VCP in proteasomal degradation, studies of IBMPFD patient tissues suggest the possible involvement of VCP in the autophagy pathway (Watts *et al.*, 2004; Vesa *et al.*, 2009; Ju *et al.*, 2010). A prominent characteristic of the pathology in IBMPFD is the accumulation of ubiquitin conjugates in affected tissues, indicative of a defect in protein degradation. Patients with missense mutations in VCP show degenerating fibres, rimmed vacuoles and ubiquitin- and TDP-43 positive inclusions. In addition, the vacuoles accumulated in IBMPFD patient tissue are enriched in autophagosomal markers p62 and LC3II and are suspected to be representing aberrant autophagosomes (Ju *et al.*, 2009). Such phenotype was reproduced in transgenic mice expressing disease associated mutants of VCP (Badadani *et al.*, 2010; Custer *et al.*, 2010; Nalbandian *et al.*, 2012). The heterozygous (R155H/+) VCP mice demonstrate progressive muscle, bone and brain pathology when compared with their wild-type littermates, with the onset of disease beginning around 6-9 months of age (Nalbandian *et al.*, 2012); and this is accelerated in the homozygote (R155H/R155H) VCP mice that develop prominent ubiquitin-positive aggregates and die by 14-21 days from muscle, spinal cord and cardiac pathology (Nalbandian *et al.*, 2012 2nd). On the cellular level, chemical or genetic inhibition of VCP function, similarly to an IBMPFD mutant VCP expression, leads to the accumulation of non-degradative ubiquitin-containing autophagosomes (Tresse *et al.*, 2010; Chou *et al.*, 2011). Importantly, disease-associated mutations in VCP do not cause detectable impairment in ubiquitin-dependent degradation by the proteasome, further suggesting that defective autophagy contributes to pathological accumulation of ubiquitin conjugates and ubiquitin-positive vacuoles in IBMPFD (Tresse *et al.*, 2010). Furthermore, overexpression of wild-type VCP in a *Drosophila* polyglutamine-disease model mitigates polyglutamine-induced eye degeneration (Koike *et al.*, 2010). Whereas, the VCP^{K524A} mutant inhibits protein degradation, triggering abnormal protein aggregation in the nucleus and cytoplasm and leading to increased cell death (Poksay *et al.*, 2011).

Although previous findings indicate that VCP co-localises with pathological protein aggregates such as expanded polyglutamine aggregates, and is involved in both formation and clearance of these aggregates (Kobayashi *et al.*, 2007; Kakizuka, 2008; Ju *et al.*, 2008), it is not certain which mechanisms are employed in the process. Kobayashi and colleagues observed that VCP recognizes and accumulates onto pre-formed protein aggregates created by proteasome inhibition and proposed that it acts as both aggregate-formase (during the expression of extended polyglutamines (ex-polyQ)) and aggregate-unfoldase (after the ex-polyQ expression becomes low) (Kobayashi *et al.*, 2007). It was also suggested that VCP functions as a carrier of abnormal proteins for collecting them into aggregates and that IBMPFD-mutations in VCP enhance formation of aggregates due to increased ATPase activity (Manno *et al.*, 2010). Interestingly, the yeast VCP – equivalent (Cdc48) was found to be a critical factor for the proteolysis of insoluble misfolded substrates in the nucleus, and the loss of Cdc48 function led to increased inclusion formation *in vivo* (Gallagher *et al.*, 2014). It was also found that VCP interacts with an ubiquitin-binding protein - histone deacetylase 6 (HDAC6), in a ratio which may dictate the fate of misfolded proteins, shuttle them to aggresome or facilitate their autophagic degradation (Ju *et al.*, 2008). Overexpression of HDAC6 in cells expressing disease mutants of VCP partially rescue degradation of ubiquitinated proteins (Ju *et al.*, 2008), suggesting that these two proteins may function in a common biological pathway. Importantly, both HDAC6 and p62 contain ubiquitin- and LC3- binding domains, and interact with the microtubule-associated protein tau, which accumulates in Alzheimer disease brain (Babu *et al.*, 2005; Ding *et al.*, 2008). Interestingly, inhibition of autophagy and also reduction of VCP levels was found to trigger increased levels of tau phosphorylated at Ser^{262/356} in a primary neuronal model (Dolan *et al.*, 2011). Taken together it would appear that VCP interacts with misfolded and aggregated protein and structurally alters them so that they can be trafficked for degradation through either an aggresomal or autophagic fate (Bug and Meyer, 2010; Ju and Weihl, 2010).

Similar to VCP mutants, knock-out of Atg5 or Atg7 (essential for autophagosome formation and in early stages of autophagy) in mice results in intracellular accumulation of ubiquitin-positive protein aggregates in the neuronal cells (Hara *et al.*, 2006) and in the liver (Komatsu *et al.*, 2005). Since the proteasome

activity was not affected by Atg7 knockout it was speculated that the accumulation of those aggregates was a direct result of autophagy deficiency (Hara *et al.*, 2006; Komatsu *et al.*, 2006). It was long thought that inhibition of autophagy would only affect long-lived proteins, but subsequent research has shown the possibility that autophagy inhibition may also impact the flux through the ubiquitin-proteasome system (UPS) and thereby influence clearance of short lived proteins (Korolchuk *et al.*, 2009). After autophagy is inhibited, p62 accumulates, causing impaired delivery of UPS substrates to the proteasome; and knockdown of p62 in autophagy-deficient cells protects against the accumulation of these UPS substrates (Korolchuk *et al.*, 2009). Although a knock-down of p62 normalised levels of UPS substrates it did not affect autophagosome numbers or the autophagic flux (Korolchuk *et al.*, 2009). In addition, overexpression of p62 in normal cells increased levels of ubiquitinated proteins and polyQ aggregation and interestingly this was abrogated by overexpression of VCP (Korolchuk *et al.*, 2009).

Altogether, these findings suggest that degradation of various ubiquitinated substrates on the intersection of autophagy and UPS is coordinated by the interplay of VCP and ubiquitin- and LC3- binding partners. We further propose that VCP is directly involved in the aggregate clearance via autophagy and dysfunction of this pathway (a consequence of deregulating mutations in VCP) results in pathological phenotypes observed in the VCP-associated diseases.

3.2 VCP in autophagy positive cells co-localises not only with Ubiquitin but also with p62 and LC3.

The VCP^{R155H/+} knock-in mice demonstrate muscle weakness starting at approximately 6 months of age, with typical inclusion body Myopathy (IBM) phenotype developing at the mean age of 9 months (Nalbandian *et al.*, 2012). At the cellular level the VCP mice show similar pathology to IBMPFD patients (Badadani *et al.*, 2010; Nalbandian *et al.*, 2012 2nd). The skeleton of these mice is affected by Paget-like lesions with increased bone activity, cortical thickness and osteoclastogenesis (Nalbandian *et al.*, 2013). While it is known that VCP and p62 (both involved in pathogenesis of the PDB) are crucial players in main protein degradation pathways, it is still uncertain if they work together in response to various

aggregated protein challenges. More specifically, p62 is essential for the delivery of ubiquitinated proteins to the autophagy-lysosomal system, is degraded by autophagy and accumulate when this process is impaired (Moscat et al., 2009). Thus, I decided to first observe p62 levels in quadriceps muscle lysates of 6 month and 1 year-old (11–13 month) VCP wild-type (*wt*) or *R155H/+* mice (Fig. 3.1 A) and determine whether autophagy impairment was present in these animals. I examined extracts from 3 animals per age group and per genotype. A significant ~1-fold increase in p62 accumulation was recorded in 1 year-old mutant animals (Fig. 3.1 B) as expected, suggestive of a dysfunction in autophagy pathway and consistent with the findings reported to date (Ju *et al.*, 2009; Nalbandian *et al.*, 2012 2nd).

To elucidate if VCP and p62 have the potential to be working together in clearing ubiquitinated intracellular debris; I then examined the distribution of VCP and p62 in cellular models. Due to the fact that using commercially available primary antibodies to stain for endogenous VCP was unsuccessful, the MEF cells were initially transfected with wild-type (*wt*) VCP-EGFP tagged. The next day cells were treated with either 1.5 μ M Torin 1 (inhibitor of the metabolic regulator mammalian target of rapamycin (mTOR) and activator of autophagy) or 80nM Bafilomycin A1 (inhibitor of late stage autophagy i.e. impairs autophagosome maturation – through acidification, including lysosomal fusion) for 4 hours. I sought to evaluate whether p62 and VCP work cooperatively under different conditions of autophagy induction (not in the basal conditions). Thus the basal level autophagy was up-regulated with Torin1 (increases turnover) and then compared to inhibited autophagy turnover with Bafilomycin (Fig 3.1C). As suspected in both instances *wt* VCP presents mostly in a diffuse staining throughout the cytoplasm and nucleus with few bright vesicles. Significantly more VCP-positive vesicles are formed in cells treated with Torin 1 (Fig3.1D). Whereas, more p62-positive vesicles are observed in Bafilomycin treated cells and this is most likely due to inhibited turnover of p62. Most importantly yellow vesicles –positive for both p62 and VCP- are present in the majority of autophagy active cells (Fig.3.1C). Nevertheless, percentage vesicles positive for both VCP and p62 is roughly the same under both treatment conditions (Fig. 3.3D).

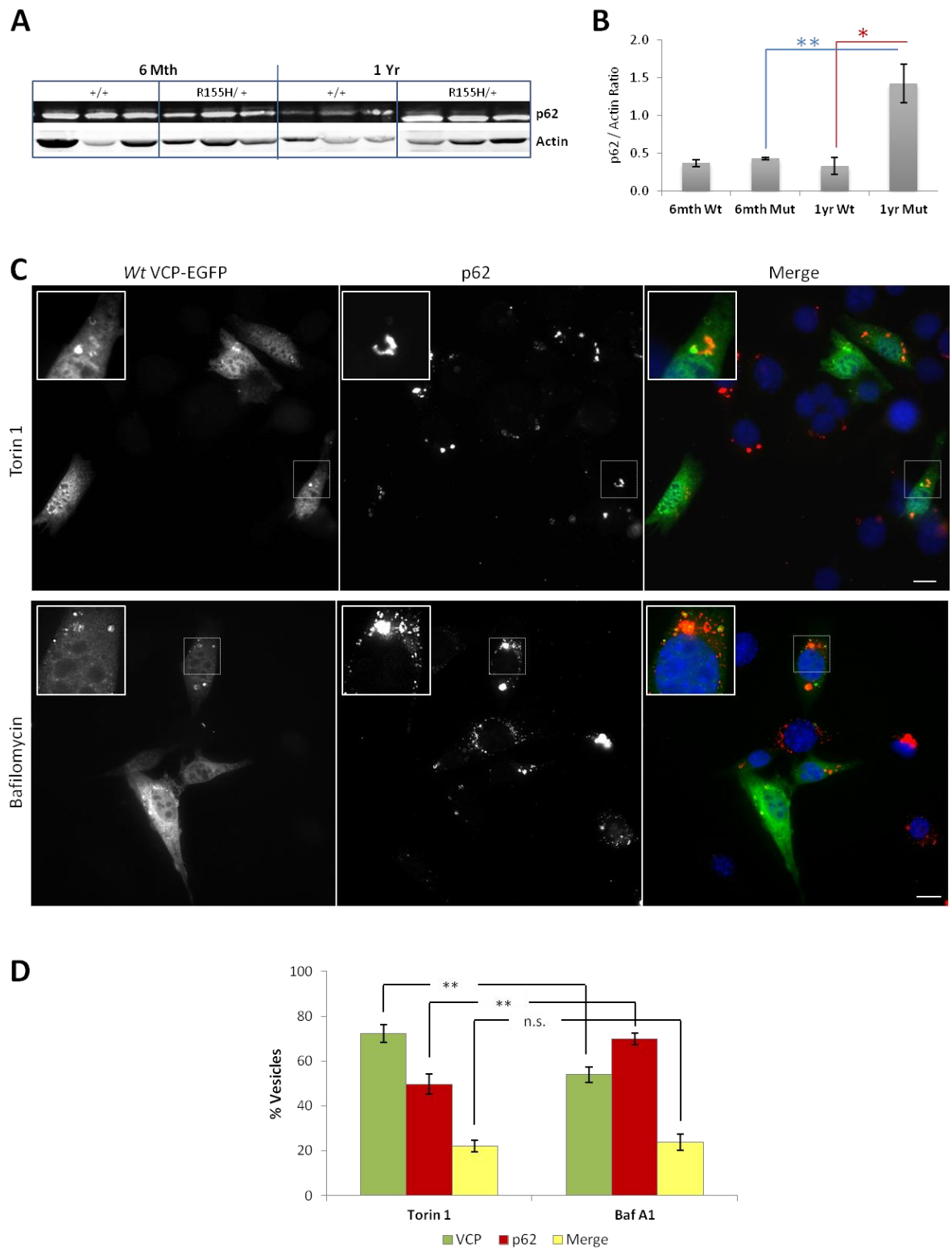


Figure 3.1. VCP R155H mutant mice show accumulation of p62 in muscle. Wild-type VCP localises to p62-positive structures in autophagy active cells. Immunoblot of p62 and actin in 6mth and 1yr-old quadriceps muscle lysates from $VCP^{+/+}$ and $VCP^{R155H/+}$ mice (A) with the bar chart showing the average p62/actin intensity from 3 different animals. Each bar represents the mean with standard deviation from triplicate (* $P < 0.05$, ** $P < 0.01$) (B). MEF cells transfected with wt VCP-EGFP and immunostained for p62 (C) were observed under

induced basal autophagy conditions (upper-Torin 1 treatment), or after Bafilomycin A1 treatment (lower). Enlarged in insets are vesicles positive for either one or both observed proteins. Scale bars equal 10µm. Graph representing the percentage vesicles containing either VCP, p62 or both in cells treated with Torin1 and Bafilomycin A1. Error bars represent standard errors from 15 cells examined for each condition (\pm SEM); ** $p < 0.01$, n.s. Indicates non-significant difference (D)

To verify these results I observed whether wild-type VCP associates with LC3-positive vesicles under conditions of autophagy induction (Fig. 3.2A). The predominant number of small, red LC3 vesicles does not co-localise with VCP vesicles. However, again about a third of vesicles that accumulate in Torin 1 and Bafilomycin treated cells are positive for both VCP and LC3 (Fig. 3.2C). I also observe accumulation of ubiquitin-positive vesicles following Bafilomycin A1 treatment in MEF cells (Fig. 3.2B). Vesicles that accumulate in *wt* VCP-expressing cells are present in both nuclear and cytoplasmic lumen. Importantly, nearly 40% of these vesicles contain ubiquitin-positive material and VCP (Fig. 3.2D). Therefore, I suspect that VCP might be involved in the clearance of some (perhaps larger) ubiquitinated substrates by autophagy.

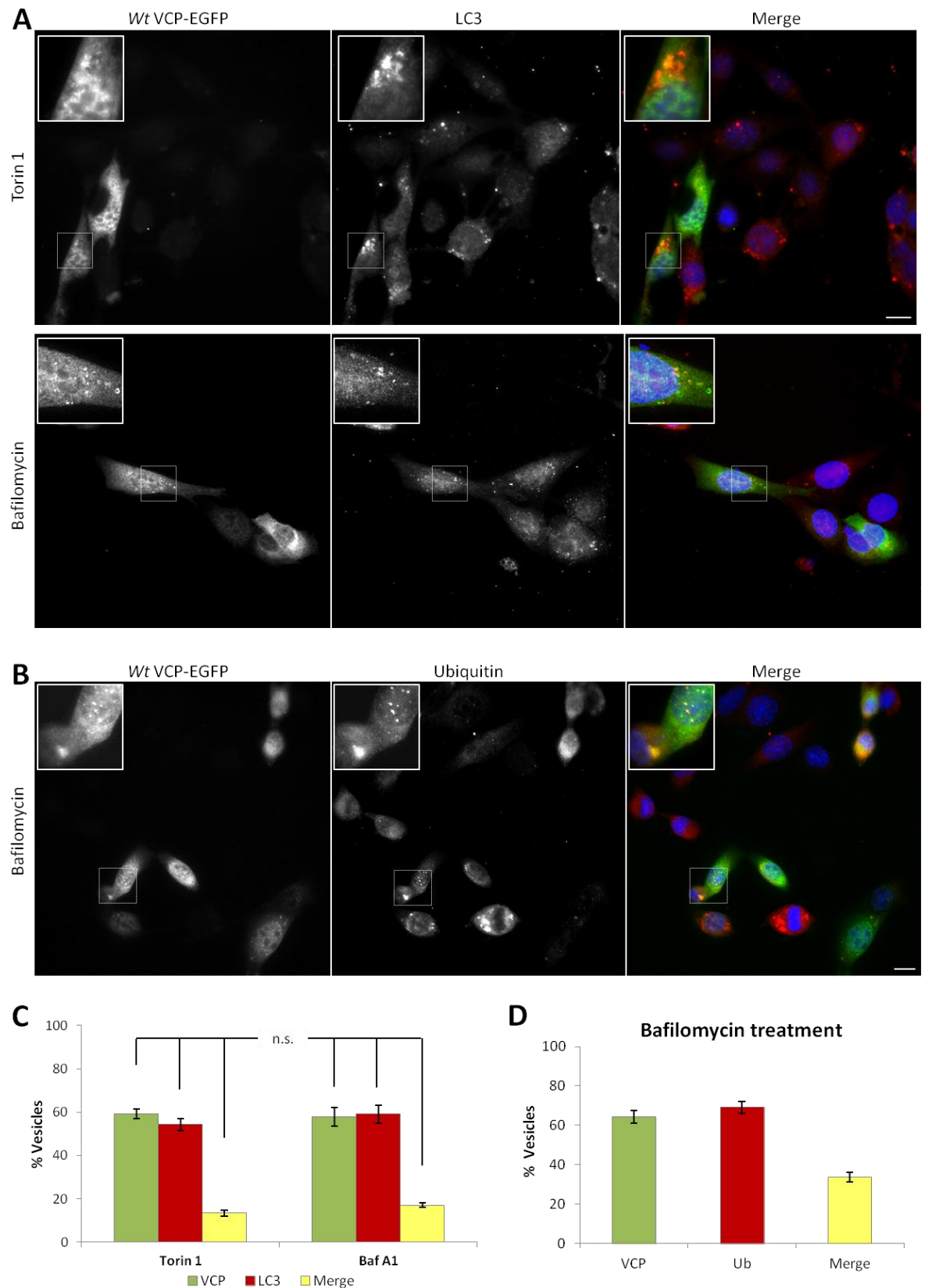


Figure 3.2. Vesicles that accumulate in autophagy active cells are positive for VCP, LC3 and ubiquitin. MEF cells transfected with *wt* VCP-EGFP and immunostained for LC3 (A) or Ubiquitin (Anti-FK2 #PW8810) (B) were observed under induced basal autophagy conditions (upper-Torin 1 treatment), or after Bafilomycin treatment (lower). Enlarged in insets are

vesicles positive for either one or both observed proteins. Scale bars equal 10µm. Graph representing the percentage vesicles containing either VCP, LC3 or both in cells treated with Torin1 and Bafilomycin (BafA1). Error bars represent standard errors from 15 cells examined for each condition (\pm SEM); n.s. Indicates non-significant difference (C). Graph representing the percentage vesicles containing VCP, Ubiquitin (Ub) or both in cells treated with Bafilomycin A1. Error bars indicate standard errors (D).

3.3 VCP co-localises with ubiquitin, p62 and LC3 in cells expressing expanded polyglutamines

To further evaluate if VCP has the potential to work together with p62 in clearing large ubiquitinated substrates I examined the subcellular distribution of VCP and ubiquitin or VCP and p62 in the presence of either a pathogenic glutamine repeat (Q79), which is used as an autophagic substrate, or a non-pathogenic control glutamine repeat (Q35) (UPS substrate). The wt VCP-EGFP was co-expressed with either HA-tagged Q79 or Q35 polyglutamines in MEF cells for 24 hours (Fig 3.3). Cells expressing Q35 polyglutamines show diffuse green staining throughout with VCP-positive ubiquitinated perinuclear aggregates (Fig 3.3A top panel). These aggregates appear smaller but concentrated. In cells co-transfected with Q79 polyglutamines both VCP and ubiquitin surround larger, cytoplasmic inclusion bodies (Fig. 3.3A bottom panel). Also, as shown in Fig. 3.3B (bottom panel), cells expressing expanded 79-residue glutamine repeat displayed aggregates that co-localised with both VCP and p62, suggesting a role for VCP in the clearance of this substrate via autophagy. Whereas cells expressing expanded 35-residue glutamine repeat show small p62-positive punctuate structures and a few VCP-positive perinuclear vesicles (Fig 3.3B top panel), majority of which do not co-localise with p62.

To determine whether VCP is involved in clearance of pathogenic substrates by autophagy I immunostained cells co-transfected with polyglutamines and wt VCP-EGFP for LC3 - membrane associated marker of autophagic vesicles (Fig. 3.4A). In cells expressing a shorter polyglutamine (Q35) LC3 did not associate with VCP-positive perinuclear aggregates (Fig. 3.4A top panel). Only some cells show small LC3-punctate structure.

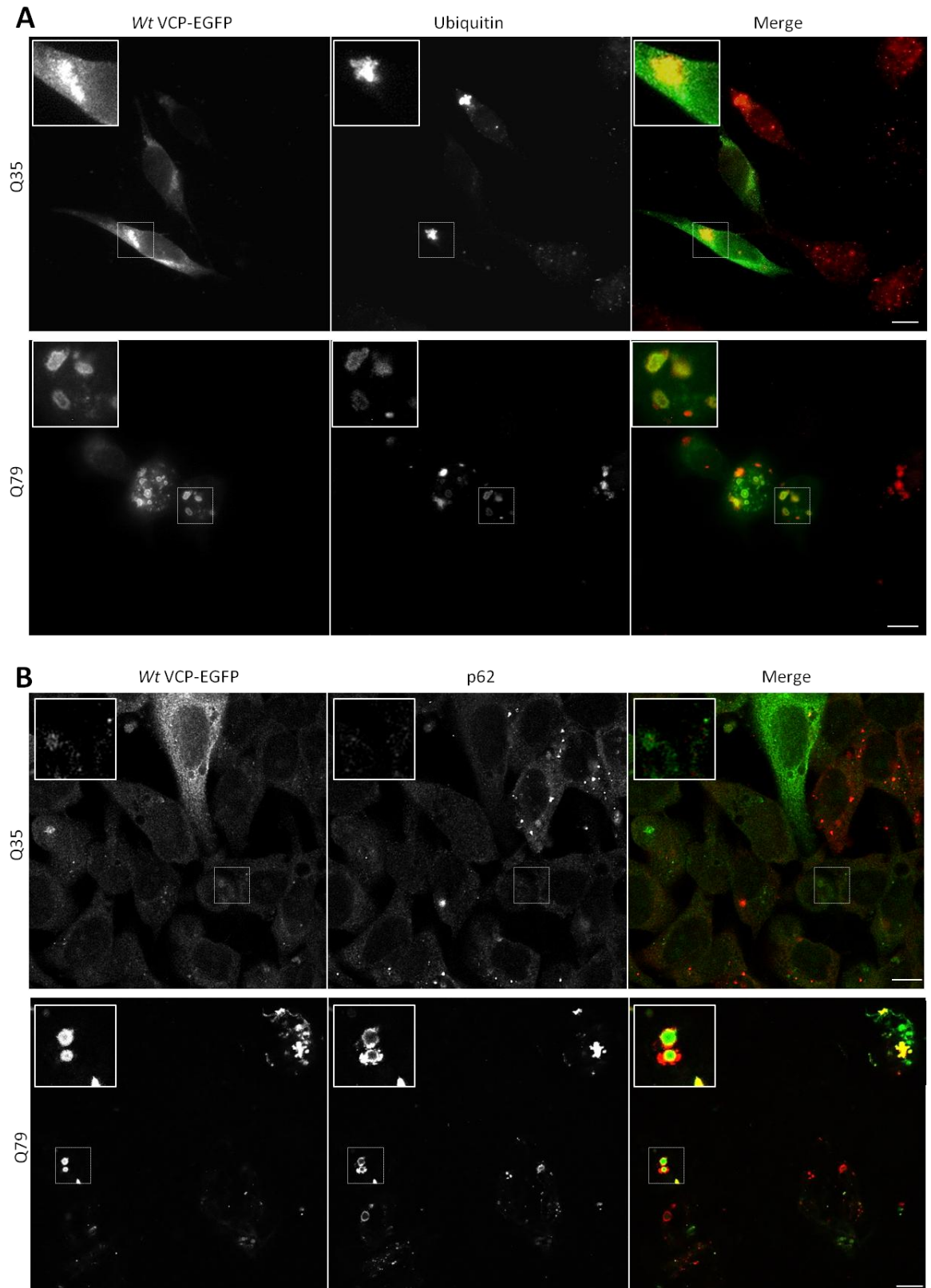


Figure 3.3. Large vesicles accumulating in polyglutamine expressing cells are positive for VCP, ubiquitin and p62. MEF cells were co-transfected with wt VCP-EGFP and either Q35 or Q79 glutamine repeats. Later immunostained for Ubiquitin (A) or p62 (B). Enlarged in insets are aggregated structures positive for either one or both observed proteins. Scale bars equal 10 μ m.

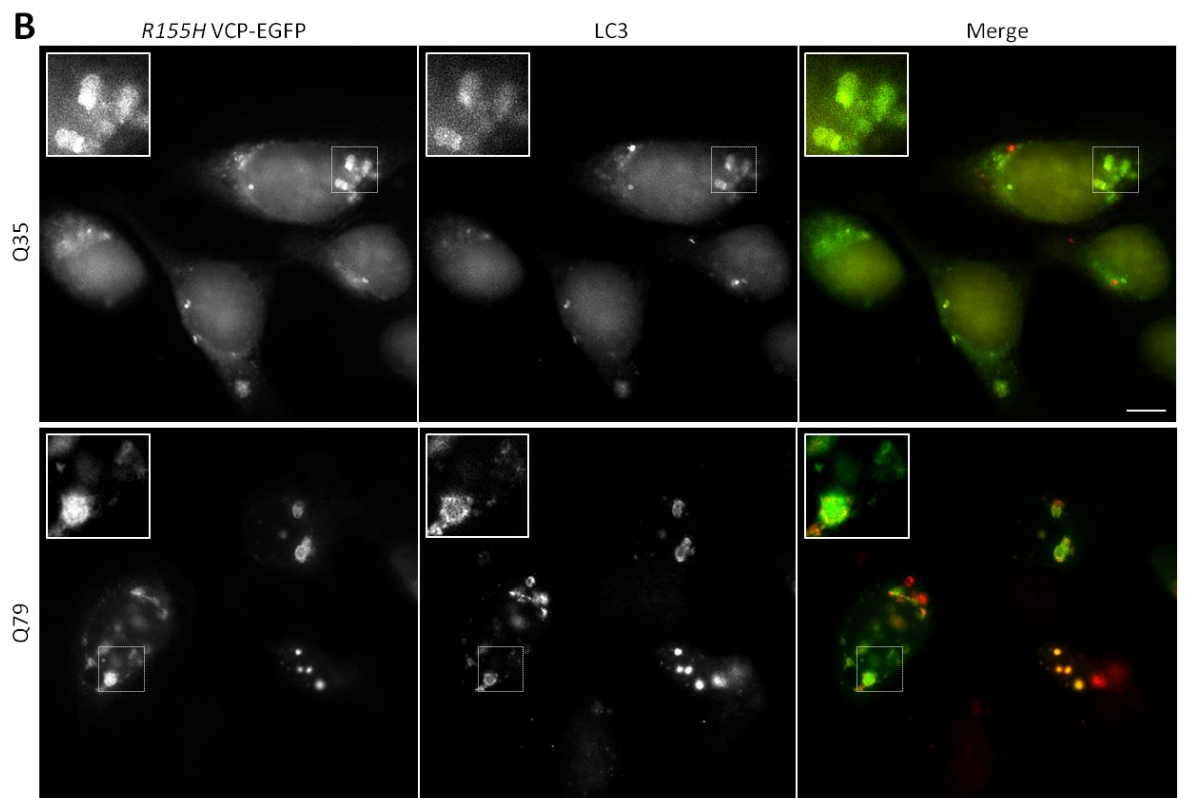
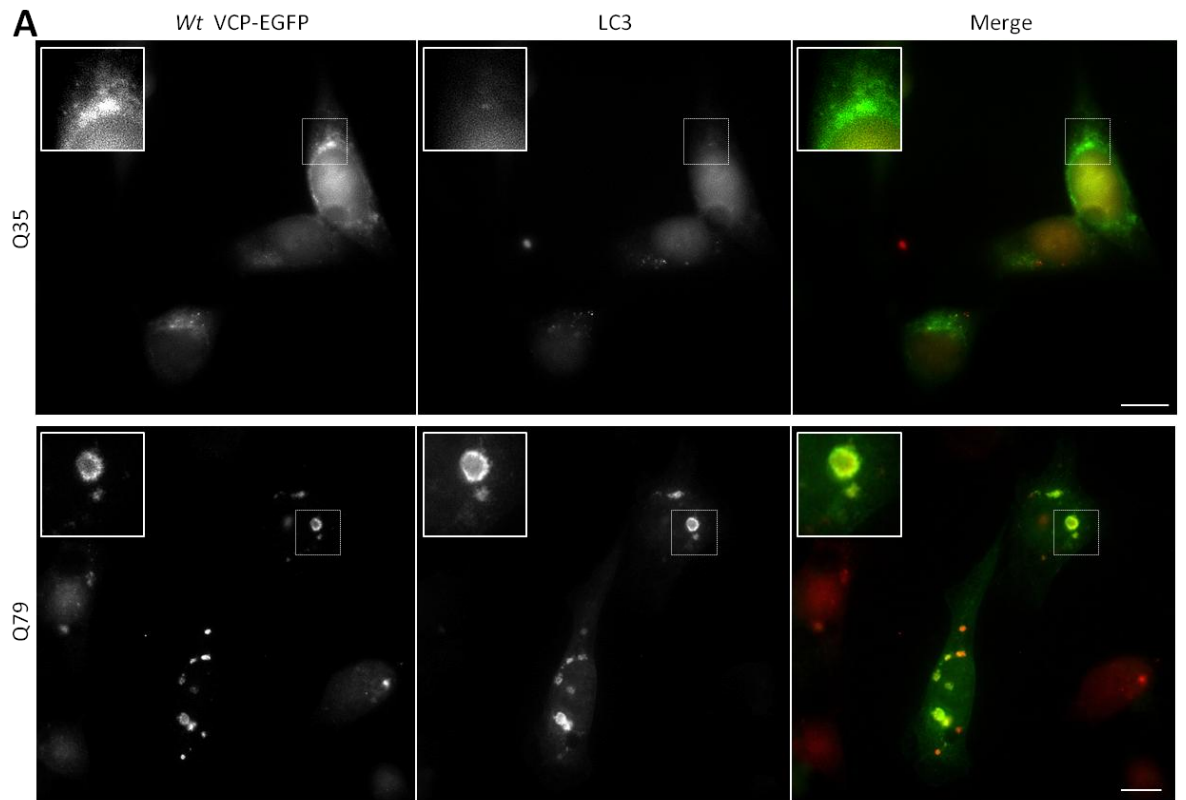
In contrast, cells expressing a pathogenic polyglutamine (Q79) displayed large doughnut-like shaped vesicles (inclusions), positive for both VCP and LC3 (Fig 3.3A bottom panel). Both VCP and LC3 formed a darker ring around lighter lumen of the vesicle. It is possible that VCP might associate with autophagosome membranes transiently or at some low level (maybe via binding to LC3) in a way that is functionally significant. Especially, since VCP is known to functionally associate with membranes of the nuclear envelope, endoplasmic reticulum and the Golgi apparatus (Roy *et al.*, 2000; Halawani *et al.*, 2009; Manno *et al.*, 2010). Altogether, I conclude that because VCP co-localises with p62 and LC3, it could be directly involved in the autophagic clearance of ubiquitinated polyglutamine substrates and aggregates.

3.4 Cells expressing VCP mutants are more sensitive to protein aggregation

The experiments described above show that VCP co-localises with p62 and LC3 in poly-ubiquitinated protein aggregates. Whilst previous reports imply a defect in protein turnover resulting in increased aggregation in tissues of IBMPFD patients (Mizuno *et al.*, 2003; Ju *et al.*, 2009) and in animal models (Nalbandian *et al.*, 2012) of the VCP disease-mutants. Therefore, combined with the preceding data, these findings strongly suggest that VCP is involved in the clearance of poly-ubiquitinated substrates. To gain further evidence for the role of VCP in autophagy I then examined the ability of cells containing mutant VCP to remove non-pathogenic glutamine repeats. Co-expression of R155H VCP-EGFP mutant with Q35 polyglutamine in cell culture resulted in accumulation of large aggregates, co-stained for both VCP and LC3 (Fig. 3.4B top panel). Similarly, co-expression of mutant VCP with extended pathogenic polyglutamines (Q79) in MEF cells also resulted in VCP-positive, doughnut-like shaped vesicles (inclusions) co-localised with LC3 (Fig. 3.4B bottom panel).

The appearance of abnormal, large vesicles in cells expressing non-pathogenic polyglutamines suggests that mutant VCP increases cell's sensitivity to protein aggregation. To confirm this suspicion, I used the 'Imaris' software analysis to determine the number of vesicles (aggregates, inclusion) per cell in poly(Q35) and wild-type (*wt*) or mutant VCP expressing cells. Cells expressing R155H VCP-EGFP in

conjunction with the Q35 repeat formed significantly more aggregates per cell than cells expressing *wt* VCP (Fig. 3.4C). In addition, looking at the co-localisation of VCP puncta with the LC3 puncta in Q35-containing MEF cells, I found that there was significantly more VCP and LC3 co-stained aggregates (autophagosomes) in R155H VCP mutant-expressing cells. More than 50% of R155H VCP puncta co-localised with LC3 puncta, whereas only about 20% of all aggregates was positive for *wt* VCP and LC3 in Q35 expressing cells (Fig. 3.4D). Next, I utilised 'Imaris' to analyse aggregate formation in cells expressing pathogenic Q79 polyglutamines. I found that cells expressing R155H VCP in conjunction with the Q79 repeats formed significantly more aggregates per cell than cells expressing *wt* VCP (Fig. 3.4C). I also observed that the overall number of VCP-positive aggregates formed in cells expressing R155H VCP in conjunction with the Q35 repeat is similar to the number of aggregates formed in cells expressing *wt* VCP in conjunction with pathogenic Q79 repeat (Fig. 3.4C). Nevertheless in cells expressing Q79 polyglutamine both *wt* and mutant VCP positive aggregates were more likely to co-localise with the LC3 puncta (autophagosomes) than in cells expressing Q35 polyglutamine (Fig. 3.4D). Nearly 75% and more than 80% of all cellular aggregates were positive for VCP and LC3 in cells co-expressing Q79 and *wt* VCP or Q79 and R155H VCP respectively. Thus, I suspect that IBMPFD mutations in VCP make cells more sensitive to protein aggregation resulting in activation of the autophagy pathway (dictated by the increased number of LC3-positive inclusions).



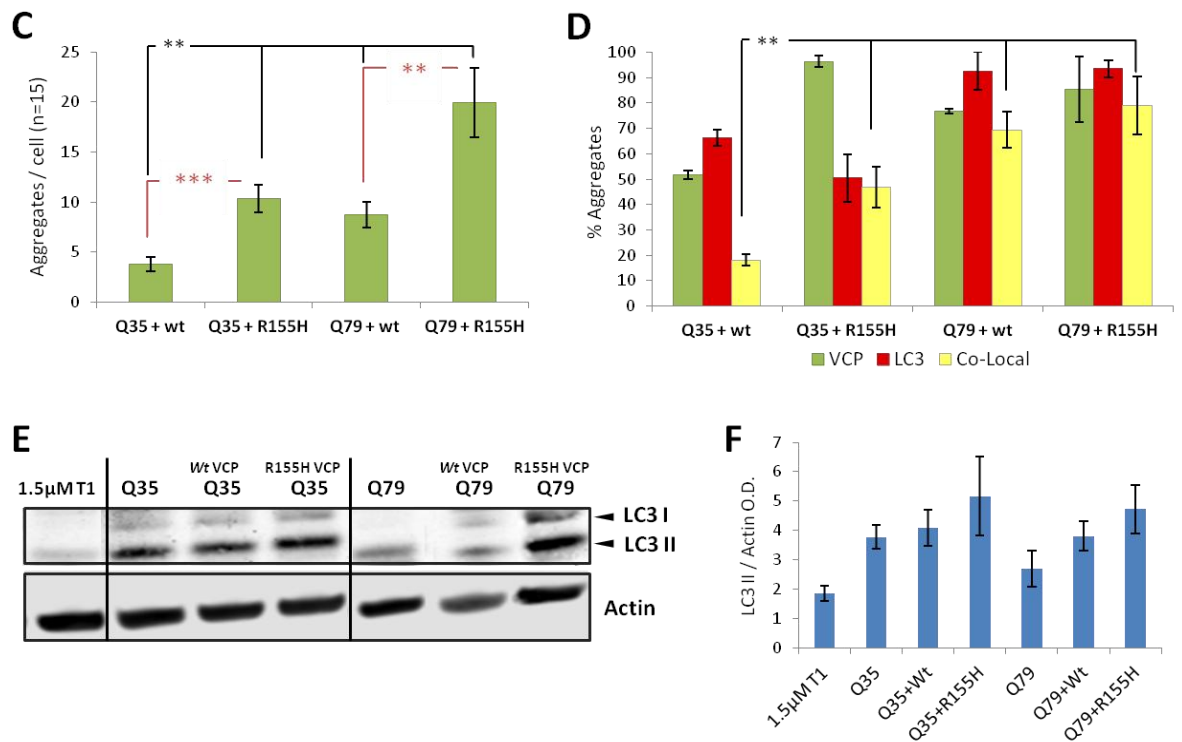


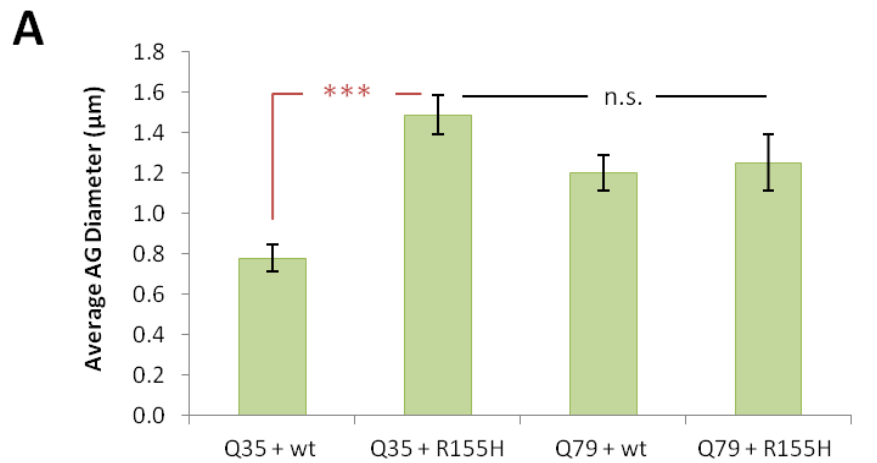
Figure 3.4. Large LC3-positive aggregates accumulate in cells expressing polyglutamines and mutant VCP. MEF cells were co-transfected with either Q35 or Q79 glutamine repeats and wt VCP-EGFP (A) or R155H VCP-EGFP (B). Enlarged in insets are aggregated structures positive for VCP and/or LC3. Note co-aggregation of mutant VCP and LC3 with short poly(Q)-35 repeats. Scale bars equal 10μm. Graphs showing the average number of VCP-positive aggregates per cell (C) and the percentage VCP, LC3-containing aggregates and autophagosomes i.e. aggregates positive for both LC3 and VCP (D) in 15 cells examined for each condition. Each bar represents the mean number of aggregates per cell ±SEM, (One Way ANOVA followed by t-test with **P<0.01, ***P<0.001). Immunoblot against LC3 and actin in MEF cells either treated with 1.5μM Torin 1 (control) or transfected with wt or R155H mutant VCP-EGFP and/or polyglutamines (E). Quantification of LC3II normalized against actin in drug-exposed/ transfected MEF cells (F). Error bars indicate standard deviation from triplicate samples.

I then used the 'Imaris' software to determine the size of aggregates in cells expressing either non-pathogenic or pathogenic polyglutamines, assuming a general diameter of 0.75μm as the average for autophagosome size. The software located regions that come close to this measurement in the chosen fluorescent channel allowing calculations of changes in puncta diameter. The average diameter of VCP-positive aggregates in cells co-expressing mutant VCP and Q35 is significantly larger than in cells co-expressing Q35 and wt VCP (Fig. 3.5A). In contrast, there was no

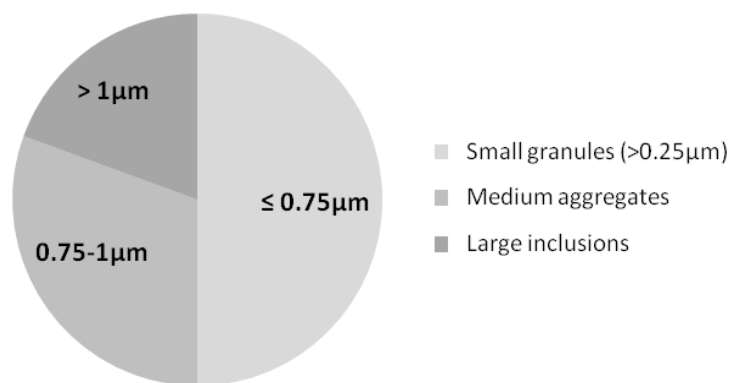
apparent difference in average diameter of VCP-positive aggregates in cells expressing Q79 polyglutamines in conjunction with either *wt* or R155H mutant VCP (Fig. 3.5A). Furthermore, when looking at the size distribution of aggregates in cells expressing non-pathogenic Q35 repeats, it became apparent that the majority of aggregates (~85%) that accumulate in R155H VCP mutant were over 0.75 μ m diameter in size (Fig. 3.5C). Whereas, less than 15% of all aggregates found in mutant VCP expressing cells were smaller than 0.75 μ m diameter. Conversely, cells expressing *wt* VCP not only displayed much less aggregates than cells expressing mutant VCP, but 50% of these were under 0.75 μ m diameter in size (Fig. 3.5B).

I next went on to determine expression levels of LC3 in the poly(Q) and EGFP-VCP (wild-type and mutant) - transfected MEF cells (Fig. 3.4E). Lysates from MEF cells treated with 1.5 μ M Torin1 for 5 hours were used to show LC3 flux in cells with induced autophagy signaling. It is evident that cells co-transfected with either Q35 or Q79 and R155H VCP accumulated more lipidated, membrane bound LC3II levels when compared to cells expressing *wt* VCP and either polyglutamines or cells treated with Torin 1 (Fig. 3.4E and F). Although not significant, elevated LC3II in cells expressing mutant VCP might indicate aberrant clearance of large, polyubiquitinated inclusions and accumulation of non-degradable aggregates in the cell.

Collectively, these data provide more detailed information on effects of the mutant VCP on the formation of protein aggregates in the cell, namely that it makes cell more sensitive to protein aggregation. Moreover, my findings suggest that the aberrant aggregation of both pathogenic and no-pathogenic substrates observed in IBMPFD mutants is likely to result from defects in autophagy rather than in the UPS, due to observed accumulation of not only ubiquitinated substrates but also autophagy markers – p62 and LC3.



B Size distribution (%) of AG in Q35 + wt VCP (n=15)



C Size distribution (%) of AG in Q35 + R155H VCP (n=15)

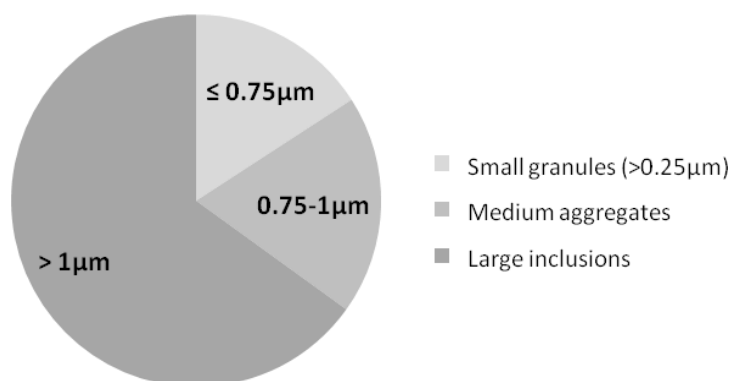


Figure 3.5. More of large aggregates is formed in cells expressing mutant VCP. MEF cells were co-transfected with either Q35 or Q79 glutamine repeats and wt or R155H VCP-EGFP. Graph showing the average diameter of VCP-positive aggregates (AG) in cells expressing wt or mutant forms of VCP (A). Analysis of variance (ANOVA) was followed by a comparison t-tests to assess the differences between the samples. Size is estimated in µm. Each bar

represents the mean \pm SEM, (***) $P < 0.001$, n.s. non-significant difference). Pie charts describing size distribution of aggregates in cells transfected with Q35 glutamines and either wt VCP (B) or R155H VCP (C). Diameter of each granule/aggregate was determined via Imaris analysis of Z-stacked immunofluorescent images, presented as a percentage of the total number of aggregates $> 0.25\mu\text{m}$ in 15 cells examined for each condition.

3.5 Overexpression of wt VCP in the cell culture increases clearance of poly-ubiquitinated substrates.

When autophagy is inhibited aggregates and ubiquitinated proteins accumulate in cells and tissues (Komatsu *et al.*, 2006; Yang and Kilonsky 2010). The pathology of IBMPFD is characterised by accumulation of ubiquitin conjugates indicative of a defect in protein degradation, and my observations suggest that disease-associated mutations in VCP make cells more prone to protein aggregation. To further validate these findings, I next sought to determine the ability of cells containing mutant VCP to remove nonpathogenic poly-glutamine repeats. Again MEF cells were co-transfected with both Q35 or Q79 polyglutamines and wt, R155H or DKO (a catalytically dead, D1 and D2 ATPase mutant; functions as dominant negative when expressed exogenously) VCP-EGFP. The levels of accumulated ubiquitinated protein aggregates were then analysed by a filter-trap assay with anti-FK2 (Ubiquitin) antibody (Fig. 3.6A). As shown in Figure 3.6B, ubiquitinated aggregates accumulated largely in VCP mutant expressing cells when compared with that in non-transfected control (Null). Furthermore, the IBMPFD-specific mutant VCP (R155H) sequester non-pathogenic poly(Q)-35 repeat into inclusion bodies, indicated by nearly 3 fold increase in ubiquitinated aggregates when compared to that in wt VCP-EGFP expressing MEFs (Fig. 3.6B middle graph). As expected pathogenic poly(Q)-79 repeats are also sequestered into large non-soluble aggregates in VCP mutant expressing cells (Fig. 3.6B bottom graph). In contrast overexpression of wt VCP reduces aggregation, possibly promoting clearance of poly-ubiquitinated aggregates. This experiment was repeated on three separate occasions, concentrating on the IBMPFD-mutant and wt VCP. Combined results revealed a significantly higher insoluble aggregate content in cells expressing mutant protein (Fig. 3.6C). Conversely, a sole over-expression of wt VCP significantly reduced insoluble aggregate generation when compared to that in mutant VCP transfected cells.

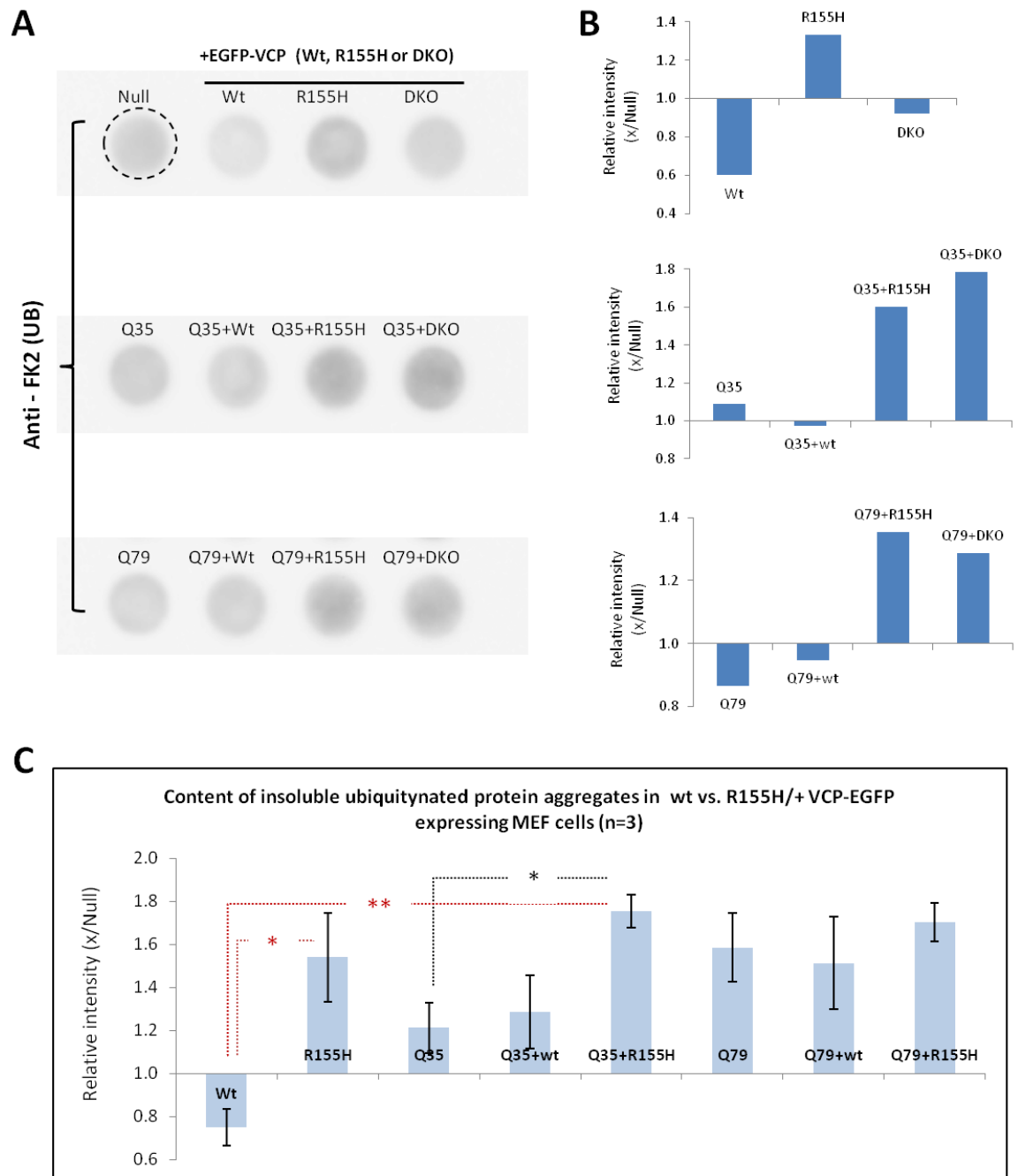


Figure 3.6. Cells expressing VCP mutants are defective in aggregate clearance. Filter-trap analysis immunoblots of SDS-insoluble ubiquitinated aggregates generated in cells co-transfected with either Q35 or Q79 glutamine repeats and *wt*, R155H or Double ATPase domain mutant (DKO) VCP-EGFP as indicated (A). The signal intensity from the ubiquitin immunoblots was quantified and presented as relative percentage values of the non-transfected control (Null) (B). The average intensity from 3 separate experiments is shown in (C), error bars indicate standard deviation from triplicates. Note the measurable accumulation of ubiquitin-positive aggregates in R155H/+ VCP expressing cells and in cells co-transfected with mutant VCPs and poly(Q)'s; (* $P < 0.05$, ** $P < 0.01$).

There was no significant difference in the concentration of insoluble, ubiquitinated aggregates in cells expressing pathogenic Q79 polyglutamines. Collectively, these findings suggest that *wt* VCP is not only essential in clearing ubiquitinated protein substrates but also, when over-expressed, can increase the clearance of protein aggregates. With the preceding results in mind I can postulate that VCP is likely to participate in the autophagic degradation of ubiquitinated protein cargo in a similar way to p62. I therefore propose that VCP interacts with the autophagic machinery and decide to investigate further whether VCP binds directly to p62.

3.6 Discussion

In this chapter I wanted to further characterise the role of VCP and p62 in the cell, especially during autophagy. I investigated the subcellular localisation of VCP and p62 by inducing autophagy by either Torin 1 treatment or expression of expanded polyglutamine repeat (aggregate-prone proteins with polyglutamine and polyalanine expansions which are degraded by autophagy) (Ravikumar *et al.*, 2002). The most striking observation was that in cells expressing a pathologic expanded polyglutamine repeat VCP, p62 and LC3 (a binding partner of p62) all co-localised to the outside of the ubiquitin-positive inclusion body (aggregated polyglutamine). This was not surprising, as the expression of the expanded pathogenic polyglutamine does produce cellular pathology seen in the disease state. Thus, this was the first indication that VCP and p62 may interact directly and that VCP may have a defined role in the early autophagic process, like p62. Further to this, when autophagy was induced by Torin 1 treatment or inhibited at late stage with Bafilomycin A1, again there was co-localisation of VCP and p62 as well as VCP and LC3 (although it was less pronounced). To examine this in physiological conditions I looked at the levels of p62 in muscle (quadriceps) from aged wild type and heterozygous VCP^{R155H/+} mice. I compared samples from six month and one year old mice, where we have previously shown that muscle from these animals develop similar inclusion body pathology to that seen in the human disease, in an age dependant manner (Nalbandian *et al.*, 2012). Nevertheless, in the mouse there is no apparent inclusion body histopathology before they reach approximately one year of age and at six months of age there is no difference in the histology of wild type and heterozygous muscle (Badadani *et al.*,

2010; Nalbandian *et al.*, 2012). In accordance with these findings I observed an age dependant significant increase in the levels of p62 in only the one year old heterozygous muscle (Fig. 3.1B).

Although previous findings indicate that VCP co-localises with expanded polyglutamine aggregates and is involved in both formation and clearance of these aggregates (Kobayashi *et al.*, 2007; Kakizuka, 2008; Ju *et al.*, 2008), it is not certain which mechanisms are employed in the process. One suggestion is that histone deacetylase 6 (HDAC6), an ubiquitin-binding protein, interacts with VCP in a ratio which dictates the fate of misfolded proteins shuttles them to aggresome and facilitates their autophagic degradation (Ju *et al.*, 2008). Interestingly, both HDAC6 and p62 contain ubiquitin- and LC3- binding domains, and interact with the microtubule-associated protein tau, which accumulates in Alzheimer disease brain - where VCP was also implicated (Babu *et al.*, 2005; Ding *et al.*, 2008). It is also believed that VCP actually protects against the toxic effects of insoluble polyglutamine aggregates with previous studies showing that increased expression of *wt* VCP reduces polyglutamine inclusion bodies in the *Drosophila* model (Koike *et al.*, 2010). Results of this chapter further demonstrate that VCP plays an important role in the degradation of expanded polyglutamine repeats. While the mutant VCP seemed to co-localise in a similar pattern as the *wt* VCP around the pathogenic Q79 polyglutamine inclusions, I have also observed inclusions in cells expressing the control non-pathogenic polyglutamine repeat and mutant R155H VCP. I found that the co-expression of mutant VCP and the Q35 (non-pathogenic polyglutamine repeat) leads to an increased number of inclusions that were not seen in cells co-expressing both the *wt* VCP and Q35 vectors (Fig. 3.3B and 3.4). Although, the Q35 construct is larger than the normal number of repeats seen in the general population (Chen *et al.*, 2002) it is still considered non-pathogenic. This would be consistent with the lack of inclusion bodies seen in cells co-expressing both the *wt* VCP and Q35 vectors. The Q35 polyglutamine repeat should normally show a more diffuse distribution (Fig 3.3) and be degraded by the 26S proteasome. Therefore aggregates that accumulate in cells co-expressing mutant VCP and the Q35 would indicate that the R155H mutation in VCP increases the cell's sensitivity to potentially aggresome prone proteins, like the larger 'normal' polyglutamine repeat (Q35). These findings were additionally

confirmed by the Imaris analysis of co-transfected cells (Fig. 3.4C and D), showing a significantly higher aggregate formation in VCP mutant expressing cells. The Q35 inclusions (in R155H VCP expressing cells) like the pathogenic Q79 repeats, are surrounded by co-localised VCP, p62 and LC3, suggesting that these are pathological inclusion bodies containing the Q35 polyglutamine repeat. In addition, expression of R155H VCP in Q35-containing cells resulted in accumulation of numerous large aggregates over 1µm in diameter that were rarely observed in wild-type VCP. There are three scenarios that could potentially lead to this outcome:

1. The Q35 protein can no longer be degraded by the proteasome because VCP has lost its segregate/unfoldase activity that 'untangles' aggregates prone proteins.
2. The polyubiquitinated Q35 substrate is misdirected or inappropriately directed to the autophagy pathway.
3. That VCP has lost its ability to recognise and/or bind the polyubiquitinated Q35 substrate, so it is not being degraded by the proteasome.

I further explored the effects of mutant VCP on autophagy in immortalised primary cells (mouse embryonic fibroblasts, MEFs) by western blotting (WB) using antibodies to LC3 (Fig. 3.4E and F). The expression of the Q79 expanded glutamine repeat led to an increase in the levels of LC3II (a marker for activated autophagy) in cells expressing either *wt* or mutant VCP when compared to cells just expressing the Q79 repeat. This suggests that the overexpression of either the mutant or *wt* VCP does indeed increase autophagy and potentially enhance the clearance of the pathogenic inclusion bodies. Contrary, the expression of the non-pathogenic Q35 polyglutamine repeat increased the levels of LC3II in all cells (expressing Q35 only, or Q35 with either *wt* or mutant VCP). Intriguingly, for cells just expressing the Q35 repeat the increased late stage autophagy response was far greater than the one elicited by the Q79 repeat. Nevertheless, the co-expression of *wt* VCP with the Q35 repeat had very similar levels of LC3II as the cells just expressing the Q35 repeat. These observations are potentially very significant for three reasons:

1. The Q35 repeat induces autophagy, so potentially is not normally degraded by the proteasome.

2. Cells can normally cope with the autophagy clearance of the Q35 repeat and it is non-pathogenic.
3. The overexpression of *wt* VCP does not further enhance the autophagy response to Q35 repeats compared to the cells normal response (not the case for the pathogenic Q79 response). Suggesting that VCP plays a differential regulatory role in the cells response to clearing pathogenic inclusion bodies.

The co-expression of the Q35 repeat with mutant VCP shown a slight increase in LC3II levels, but this was not significant. Nevertheless, as it is shown by the Imaris image analysis in Figure 3.4(C and D) there was a significant increase in the number of pathogenic inclusion bodies in cells co-expressing Q35 and mutant VCP. To corroborate this aggregate-clearance defect, I also examined the insoluble aggregated fraction, by a filter trap assay, in cells expressing Q35 or Q79 glutamine repeats in conjunction with either *wt*-VCP, R155H-VCP or DKO-VCP (which has mutations in both ATPase domains creating a dominant negative effect). The functional feature of the filter trap analysis is the combination of porous membrane which allows small insoluble proteins to pass through and immunoblotting for a specific aggregate's content. Only large aggregates are immobilised on the membrane, which can be then immuno-probed with a conjugated ubiquitin antibody in a manner similar to Western Blotting. In MEFs transfected with just *wt*-VCP, R155H-VCP or DKO-VCP, there was a significant increase in polyubiquitinated aggregates in cells expressing the R155H mutant VCP (Fig. 3.6B). By contrast, the inactive DKO mutant did not show increased aggregation. Similarly, in cells co-transfected with Q35 and VCP vectors, there was again a dramatic increase in polyubiquitinated aggregates for those cells expressing either R155H-VCP or DKO-VCP, but not in *wt*-VCP or just Q35 expressing cells. These observations were similar to the results from experiments using the Q79 repeats, where again just the R155H and DKO expressing cells showed an increase in polyubiquitinated aggregates (Fig. 3.6B). If Q35 is indeed an autophagy substrate then the inclusion bodies seen in the mutant VCP expressing cells suggests that the mutations in VCP reduce autophagic efficiency in degradation of normal aggregate-prone (autophagy) substrates. This would be consistent with the current thought that IBMPFD mutations in VCP cause a block in late stage autophagy (Ju *et al.*, 2009).

It was also interesting to note that wild-type VCP co-localised to a fair extent with p62 positive vesicles in normal cells under different conditions of autophagy induction (Fig. 3.1). Furthermore, it was previously shown that overexpression of wild-type VCP increases the clearance of ubiquitinated substrates in the cell and that p62 and VCP compete for these substrates for degradation by either autophagy or the proteasome, respectively (Korolchuk *et al.*, 2009). Importantly, disease-associated mutations in VCP also lead to p62 accumulation in adult VCP^{R155H/+} mice muscle, likely due to impaired VCP function. Combined with the preceding data these observations suggest that these two proteins may function in a common biological pathway. The evidence suggests the pathology of IBMPFD is due to a defect in autophagy with a lack of any impairment in the UPS (including the ERAD and UFD pathways) (Tresse *et al.*, 2010). My findings further indicate that VCP, in the similar way to p62, is essential for clearance of ubiquitinated proteins. Therefore, I propose that an impairment of autophagy-dependent protein aggregates degradation is likely to be the direct result of VCP mutations.

CHAPTER 4

VCP FORMS A COMPLEX WITH P62

CHAPTER 4: VCP FORMS A COMPLEX WITH p62

4.1 Introduction

VCP is one of the most abundantly existing intracellular protein and acts in various cellular functions, including protein degradation, membrane fusion and cell cycle control (Chapman *et al.* 2011; Bug and Mayer, 2012). The multifunction suggests the presence of multi-partners and/or multi-localisation of VCP itself. Indeed, VCP has been proposed to use its co-factors differentially to carry out this diversity of activity (Table 4.1). The N-domain and the C-terminus on VCP are mainly responsible for the interactions with those various binding partners (Fig. 4.1). The N-terminal binding site was described a general site of interactions for many cofactors with the ubiquitin regulatory X (UBX) and ubiquitin D (UBD) domain-containing protein cofactors, such as Ubx2 and Ufd1/Npl4 respectively (Chapman *et al.* 2011). The p47 for example, required in membrane fusion in post-mitotic reassembly of Golgi apparatus and transitional ER, binds to the N-domain on VCP via its UBX domain (consensus sequence R...FPR; dots indicate separation in primary sequence) as a trimmer, blocking other cofactors from binding (Mayer *et al.*, 1998). Interestingly, Ufd1/Npl4 complex, involved in the ER-associated protein degradation, binds to a single subunit of VCP in a p47 excluding manner (Yeung *et al.*, 2008). Other cofactors interact with the N-domain of VCP via small peptide motifs including binding site 1 (BS1), VCP-binding (VBM) and VCP-interacting (VIM) motifs (Yeung *et al.*, 2008; Dargemont *et al.*, 2012). The BS1 motif (consensus sequence FxGxGQRn; x – any amino acid, n - nonpolar) resides in p47 and Ufd1 and is a short hydrophobic peptide stretch which may be responsible for positioning the adapter in the right orientation with respect to VCP and its movements, facilitating general recruitment to the UBD domain (Bruderer *et al.*, 2004). The VBM motif (consensus sequence E(I/L)RRRR) was found in ubiquitin-related enzymes, including deubiquitinase ataxin-3 (Atx3) (Boeddich *et al.*, 2006) and ubiquitin ligase HRD1 (Kikkert *et al.*, 2004). The VIM motif (consensus sequence (K/R)RxxLxAAERRxQ) was identified in a small VCP-interacting protein (SVIP) - an inhibitor of ERAD pathway (Nagahama *et al.*, 2003) and in gp78 (an ubiquitin ligase for ER-associated degradation, also called AMFR-Autocrine motility receptor) (Ballar *et al.*, 2006). The VBM and VIM motifs both contain at least four

conserved basic arginine (Arg) and lysine (Lys) residues in their sequences (Liu *et al.*, 2013). These Arg/Lys-rich motifs are localised on α -helices and form a positively charged patch on the helical surface, which may be beneficial to VCP binding (Liu *et al.*, 2013). Indeed, VIM motif of SVIP has more positive charges concentrated on an area of the helical structure than VBM motif of HRD1 and exhibits a stronger binding affinity for VCP (Liu *et al.*, 2013). Structurally, the Arg/Lys residues in VIM are separated into two regions by several residues in sequence, producing a more extended binding interface, whereas the binding interface of the VBM localises to a single cluster region (Hanzelmann *et al.*, 2011; Liu *et al.*, 2013). Interestingly, almost all proteins containing the arginine/lysine-rich peptide motifs are involved in ubiquitin-related protein degradation (Boeddich *et al.*, 2006; Ballar *et al.*, 2006; Hanzelmann *et al.*, 2011) hence VIM/VBM motifs should be considered when indentifying novel VCP binding partners in the future.

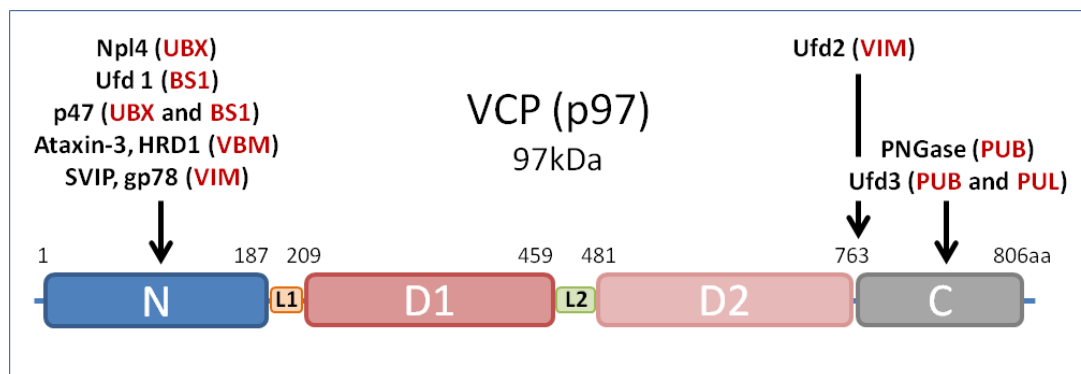


Figure 4.1. Schematic diagram showing VCP protein structure. Each subunit of a VCP protein consists of N-terminal domain (1-187) (blue), the two AAA ATPase domains: D1 (209-460) (crimson) and D2 (481-761) (blush), and a C-terminal tail (762-806) (grey). There are two linker domains in the protein: N-D1 linker (orange) and flexible D1-D2 linker (green). Known VCP cofactors bind by specific VCP-interaction domains (UBX, PUB or PUL domains) or linear motifs (VIM, VBM). Some cofactors act as ubiquitin adaptors through different ubiquitin-interaction domains (Npl4, Ufd1, p47).

Recent studies demonstrate that the amino –terminal region on VCP (amino acids 1-199) is not only critical but also sufficient for the association with the carboxyl terminus of gp78 *in vitro* (Grelle *et al.*, 2006). Intriguingly, mutations within the N-domain that result in either R93C, R95G or R155H amino acid changes did not affect

the binding of cofactors in an *in vitro* protein binding assay (Huberts *et al.*, 2007; Fernandez-Saiz and Buchberger 2010). In fact, it was reported that R95G and R155H mutants have elevated binding affinities for p47 and UFD1-Npl4 complex *in vivo* (Fernandez-Saiz and Buchberger 2010). In contrast, the P137L mutation completely abolishes VCP interactions with Ufd1, Npl4 and p47, while conserving its gp78 binding (Erzurumlu *et al.*, 2013). Such binding differences could be due to some alterations occurring in the short loop that follows P137L change, residues 140-144 (Erzurumlu *et al.*, 2013).

Co-factors that bind to the VCP C-domain include Ufd3 (functions in the endosomal sorting by its association with Hse1, a component of endosomal sorting complex required for transport (ESCRT) system) and PNGase (peptide:N-glycanase; functions in the post-translational modifications of substrates), which associate via the PNGase/ubiquitin-associated (PUB) domain (Madsen *et al.*, 2009; Han *et al.*, 2014). The Ufd2, an E4 enzyme involved in extending ubiquitin chains, is an interesting VCP binding partner as it does not bind to the N- or C-domain, but somewhere in D2 or C-domain region (Chapman *et al.* 2011). Notably, despite Ufd2 lacking the PUB domain (instead binds via the VIM motif), binding of Ufd2 and Ufd3 to VCP is mutually exclusive (Rumpf and Jentsch, 2006; Jentsch and Rumpf, 2007). This effect could be caused by either phosphorylation of Tyr805 near the C-terminus of VCP, which has been shown to block binding of PUB domain containing proteins *in vitro* (Ewens *et al.*, 2010) or by the combination of upregulated Ufd2, due to the stress conditions, versus tighter binding of Ufd3 to the VCP (Rumpf and Jentsch, 2006; Yeung *et al.*, 2008).

Currently, the proposed binding partners of VCP seem to serve one of two roles:

- 1) Regulate VCP at the level of substrate interaction and/or ATP turnover
- 2) Modify the substrates engaged by VCP and in turn dictate the fate of these substrates - degradation or release for reuse.

This versatility of VCP in adaptor binding also highlights the need to discover missing VCP cofactors and substrates involved in the more poorly defined pathways.

		Interacting domain/ motif	Cofactor	Function	
VCP interaction	N-terminus binding	UBX	p47, Ufd1-Npl4	Membrane fusion, transcription factor regulation	
		VBM	Ataxin-3	De-Ub enzyme, retrotranslocation	
	C-terminus binding	PUB (or PUG)	PNGase, Ufd3	Deglycolisation, ERAD; Control of Ub in cell	
		PUL	Doa1, Ufd3	Cell division in yeast; ERAD	
	Other	C, ND1	VIM	Ufd2, gp78, SVIP	E4 enzyme; membrane associated E3; ERAD inhibitor
		NC	SHIP box	Dfm1p	ERAD in yeast

Table 4.1. Proposed VCP-interacting motifs and identified to date cofactors.

Recent studies suggest that p62 (SQSTM1) protein, via its interaction with LC3, mediates degradation of ubiquitinated substrates through autophagy (Bjorkoy *et al.*, 2005; Pankiv *et al.*, 2007). The p62 is a 440 residue long adaptor protein. Structurally the p62 protein consists of a PB1 (Phox and Bem1p) domain that binds the atypical PKC (aPKC) and is responsible for self-oligomerisation of p62, a ZZ finger - a binding site for the ring-finger protein tumour necrosis factor (TNF) receptor-associated factor 6 (TRAF6), two PEST sequences (rich in proline, glutamic acid, serine and threonine) associated with proteins that have a short intracellular half-life (Rechsteiner and Rogers, 1996), and a ubiquitin (Ub)-associated (UBA) domain (Fig. 4.2) (Geetha and Wooten, 2002; Seibenhener *et al.*, 2007). The UBA domain, found at the p62 C-terminus, contains the Isoleucine (Ile⁴⁴)/ Valine (Val⁷⁰) Ub-binding-specificity hydrophobic patch on its β -sheet surface (Long *et al.*, 2008). The unique feature of the p62 UBA domain is however its ability to form a highly stable dimer, where the same interface is used for dimerisation as for Ub binding (Long *et al.*, 2010; Searle *et al.*, 2012). This means that UBA dimerisation strongly represses the binding of mono-Ub, whereas multiple Ub interactions from a polyUb chain result in high-affinity binding due to the avidity effect from the polyUb chain (Searle *et al.*, 2012). Nevertheless, the p62 not only binds directly to poly- and mono-ubiquitin through its

C-terminal UBA domain but also binds directly to the the autophagy effector protein LC3 and to the related GABARAP and GABARAP-like proteins (Pankiv *et al.*, 2007). The region responsible for this interaction is a short 22-amino acid long peptide sequence located N-terminally to the UBA domain, named the LC3 interacting region (LIR) of p62 (Pankiv *et al.*, 2007). The LIR is an acidic peptide sequence containing three glutamate and four aspartate residues and mutation of the C-terminal aspartate residue (DDD motif) abates binding to LC3B (Pankiv *et al.*, 2007).

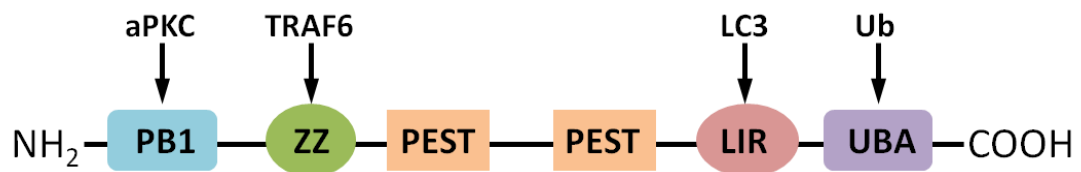


Figure 4.2. Schematic diagram showing p62 protein structure. The p62 protein consists of PB1 (Phox and Bem1p) domain, ZZ (Zinc finger) domain, 2 PEST (Proline, Glutamic acid, Serine and Threonine) domains LIR (LC3-binding) domain and UBA Ub-associated) domain. The general structure is common to all p62 homologues except for ZIP2, which lacks TRAF6 binding region (Geetha and Wooten, 2002)

The LC3 belongs to the family of microtubule-associated proteins (MAPs) and is cleaved by a cysteine protease to produce LC3I which is located in cytosolic fraction, that in turn is converted to LC3II which is then covalently attached to phosphatidylethanolamine (PE) on its C terminus and bound to autophagosome membranes (Kouno *et al.*, 2005). The cytosolic LC3I is a small protein with a molecular mass of approximately 18kDa and is structurally divided into N-terminal sub domains (residues 1–29) with two α -helices and C-terminal sub domains (residues 30-120) that adopt an ubiquitin fold (Kuno *et al.*, 2005). Interestingly, only full-length LC3B interacts with p62, whereas the p62 LIR alone is sufficient for binding to all LC3 and GABARAP family proteins (Pankiv *et al.*, 2007).

While p62 has many motifs and binding domains it is unknown if it contains any motifs or domains that have been identified in other proteins that bind to VCP. Currently there are three motifs that have been identified for binding to VCP (Yeung *et al.*, 2008 and Stepf *et al.*, 2011). The SHP box first defined in the Derlin-1 yeast homologue, Dfm1p with CDC48 and consists of an 8 residue motif (FxGxGQRU, where x is any amino acid and u is a non-polar residue). This motif was also identified in the

p47 yeast homologue Shp1p, from which this motif gets its SHP name. The VCP-interacting motif (VIM) has been identified in VCP interacting proteins including the small VCP-interacting protein (SVIP), glycoprotein 78 (gp78) and the membrane-spanning ubiquitin E3 ligase Hrd1. The VIM consists of 38 residue semi-conserved motif with a core 11 residue motif of Rx₅AAx₂R. The final motif is the VCP-binding motif (VBM), originally identified in the poly-glutamine tract containing protein Atx3 and recently the VBM was also identified in Hrd1 (which also contains VIM). The VBM is a bipartite motif of 11 residues (ELRRRRx₃FE). I used the scan prosite bioinformatics tool (<http://prosite.expasy.org/scanprosite/>) to screen various motif (pattern) strings against the peptide sequences of the three known SQSTM1 protein sequences (NP_003891 p62 variant 1, NP_001135770 p62 variant 2 and NP_001135771 p62 variant 3). The degenerate search patterns were utilised to increase the likelihood of identifying any potential motifs, such as F-x-G-x-G-x-R for the SHP box, E-L-R-x-R-R-x(4)-E for the VBM and R-x(5)-A-A-x(2)-R for VIM. These search terms did not identify any known VCP binding motifs/domains in p62. Nevertheless, given the large number of proteins that are known to interact/bind to VCP but do not contain any of these known motifs, does not rule out the potential of p62 to bind directly or indirectly.

My initial immunostaining experiments showed that VCP, p62 and LC3 co-localised to inclusion bodies and sites of aggregated protein, thus I suspect that VCP, p62 and LC3 could potentially be directly or indirectly interacting with each other.

4.2 VCP directly interacts with p62 in the mTOR/ autophagy dependant manner.

It has been established that p62 is involved in the autophagy pathway and that it directly interacts with LC3 (Bjorkoy et al, 2005; Pankiv et al, 2007). I observed that in cells expressing a pathologic expanded polyglutamine repeat, VCP, ubiquitin, p62 and LC3 all co-localised to the outside of the large vesicles (aggregated polyglutamine; Chapter 3, Fig. 3.3 – 3.4). I have also seen co-localisation of VCP and p62 when autophagy was induced by Torin 1 treatment and when autophagosome maturation was inhibited with Bafilomycin A1 (Chapter 3, Fig. 3.1). This potentially indicates that VCP and p62 may interact directly and that VCP may have a defined

role in the early autophagy process, like p62. Therefore I suspect that VCP binds p62 and promotes autophagy in the presence of protein aggregates.

I first examined if p62 and LC3 or p62 and VCP co-immunoprecipitated (co-IP'd) in the following conditions: fed (normal conditions), starved (incubated in the nutrient deprived media - HBSS) and autophagy induced (treated with Rapamycin). For each IP experiment a pre-cleared total protein fraction was used as a positive control (Input) for the pull down target protein (bound IP fraction). For the negative control I referred to a peptide fraction eluted from Immunoglobulin (IgG, rabbit or mouse) coated beads. This approach helps detect co-immunoprecipitated proteins and eliminates false-positive results.

To begin evaluating if VCP interacts with p62, I over-expressed either wild-type (*wt*) p62-FLAG or wild-type (*wt*) VCP-V5 in HeLa cells for 24 hours in fed conditions. Thereafter the transfected cells were either maintained in nutrient-rich conditions or starved in HBSS (Hanks balanced salt solution; to activate starvation-induced autophagy) for 3 hours or treated with 100nM rapamycin for further 2 hours (to inhibit mTOR signalling and activate autophagy). Then, either *wt* p62-FLAG or *wt* VCP-V5 was immunoprecipitated (IP) from total cellular extracts using anti-FLAG (Sigma/F7425) or anti-V5 (Sigma/V8137) antibody respectively and precipitated fractions were analysed by Western blotting. There was no apparent association of endogenous VCP with p62 in cells maintained under fed conditions (Fig. 4.3 A (i) and Fig. 4.3B) or in cells treated with rapamycin (Fig. 4.3B). On the other hand the results for co-IP of LC3 with p62 were neither convincing (although a faint band at 16kDa size was recorded (Fig. 4.3 A (ii))).

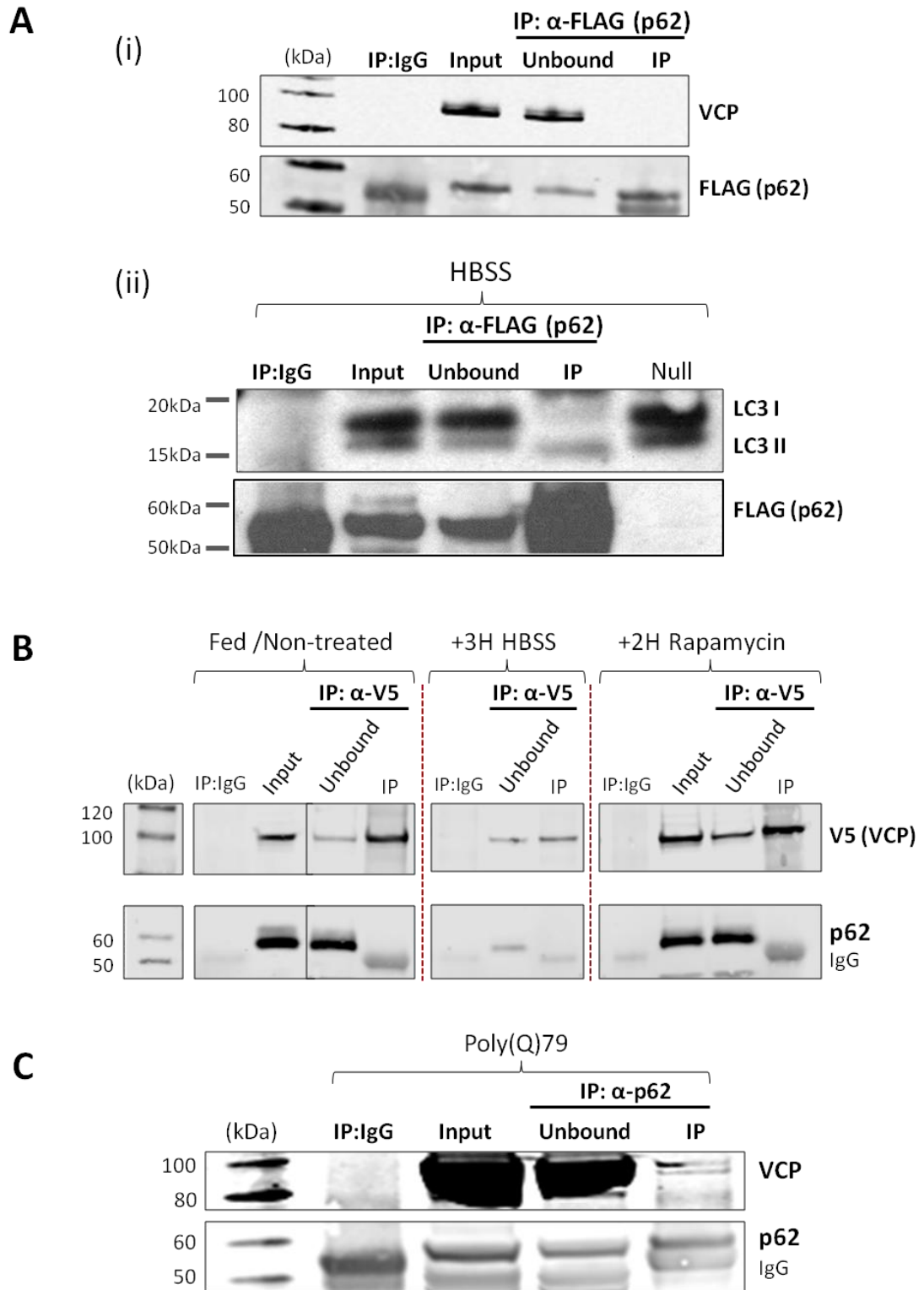


Figure 4.3. Immunoprecipitation (IP) of the VCP and autophagy markers LC3 and p62. HeLa cells were transfected with p62-FLAG and after 24h were either maintained in nutrient-rich conditions (A (i)) or in HBSS for further 3h (A (ii)). Alternatively HeLa cells were transfected with a V5-tagged *wt* VCP for 24h (B) and maintained in either fed conditions or starved in HBSS for the last 3h of incubation; or treated with 100nM rapamycin for further 2h. Cell lysates were then subject to Immunoprecipitation (IP) by anti-FLAG antibody (Sigma/F7425)

(A) or anti-V5 antibody (Sigma/V8137) (B). Pathogenic poly-(Q) 79 glutamines were expressed in MEF cells for 24h and analysed for co-IP of VCP with p62 using anti-p62 antibody (C). Presence of pulled down proteins was determined by Western blotting with anti-FLAG and anti-LC3 (A), anti-V5 and anti-p62 (B) or with anti-p62 and anti-VCP (C) antibodies.

In order to optimise IP conditions and eliminate the inconsistency of the results, I systematically varied transfection methodologies and materials used. The main areas which I addressed were: plasmid DNA used for cell transfection and its concentration, amount of the transfection reagent used, number of plasmids used, timeline of transfection (in hours), additional exposure to stress-inducing reagents and cell line exposed (Table 4.2). I initially observed no co-immunoprecipitation of VCP with p62 regardless of the transfection variables. This was also the case in the reverse experiments where *wt* VCP-V5 bound to beads did not pull down p62. However, similarly co-IP of LC3 with p62 did not establish a strong interaction, thus I was not convinced that there was no interaction between p62 and VCP.

No.	Transfection variants					Cell line	Abs for IP	Western Abs	Results
	Plasmid	DNA per well	L 2000	Additional reagents	Time				
1	<i>wt</i> p62-FLAG	4µg	5µl	none	30 hrs	HeLa	α-FLAG (F7425)	α-FLAG α-LC3 α-VCP	Neither LC3 nor VCP co-purified with p62-FLAG
2	<i>wt</i> p62-FLAG	4µg	9µl	HBSS	24h+3h	HeLa	α-FLAG	α-FLAG α-LC3	LC3 co-purification not
3	<i>wt</i> p62-FLAG	4µg	10µl	HBSS	24h+3h	HeLa	α-FLAG	α-FLAG α-LC3	LC3 II co-purified, Fig 5A - 2nd
4	<i>wt</i> vcp-V5	4µg	9µl	HBSS or None	24h+3h	HeLa	α-V5 (V8137)	α-V5 α-p62	p62 did not co-IP with <i>wt</i> vcp-V5
5	<i>wt</i> vcp-V5	4µg	9µl	HBSS	21h+3h	HeLa	α-V5	α-V5 α-LC3	LC3 unbound
6	<i>wt</i> p62-FLAG and <i>wt</i> vcp-V5	2µg+2µg	8µl	HBSS	24h+2h	HeLa	α-FLAG	α-FLAG α-vcp	No vcp co-purified
7	<i>wt</i> p62-FLAG and <i>wt</i> vcp-V5	2µg+2µg	8µl	none	24hrs	HEK293	α-V5	α-FLAG α-V5	no V5 precipitated
8	<i>wt</i> p62-FLAG	4µg	7µl	none	24hrs	HeLa	α-FLAG	α-FLAG α-LC3	unclear/ faint bands
9	<i>wt</i> vcp-V5	4µg	7µl	none	24hrs	HeLa	α-V5	α-V5 α-LC3	unclear bands
10	EGFP-LC3	4µg	7µl	none	24hrs	HeLa	α-GFP (ab1218)	α-p62 α-GFP (ab1218)	No GFP-LC3 precipitated; p62 unbound
11	EGFP-LC3 and <i>wt</i> p62-FLAG	2µg+2µg	7µl	none	24hrs	HeLa	α-FLAG	α-FLAG α-VCP α-LC3 or α-	Neither GFP-LC3/ LC3 nor VCP co-purified
12	<i>wt</i> vcp-V5	4µg	7.5µl	200ng/ml rapamycin	24h+2h	HeLa	α-V5	α-V5 α-p62	High background noise/ non-specific binding at around 60kDa
13	<i>wt</i> p53-hLC3	4µg	7µl	200ng/ml rapamycin	22h+2h	HeLa	α-p62 (P0067)	α-p62 α-GFP (ab1218)	No co-purification
14	HA-poly(Q)79	N/A	8µl	none	24h	MEF	α-p62	α-p62	VCP co-IP with p62

Table 4.2. Experimental variables for optimizing IP results. Areas addressed were: plasmid/s DNA used for the cell transfection, amount of the Lipofectamine2000 (L2000) - transfection

reagent - used, timeline of transfection (in hours) and cell line exposed. Additional reagents, such as Rapamycin, were used to directly activate autophagy in treated cultures. Starvation-induced-autophagy response was achieved through 2-3hrs incubation in Hanks Balanced Salt Solution (HBSS).

Results outlined in this table correspond with Figure A6 (No. 4 -13) in APPENDIX (Fig. A6).

Since I have observed that p62 and VCP co-localise to pathogenic polyglutamines I next decided to determine if I can see VCP and p62 co-precipitate in cells expressing Q79 polyglutamines. I expressed pathogenic Q79 polyglutamines in MEF cells as described before and used standard Dynabeds' IP protocol with antibody against p62 (Sigma/P0067) and recorded co-precipitation of endogenous wild type VCP with p62 (Fig. 4.3C; Appendix Fig. A7). This result potentially supports my findings from the immunostaining studies, suggesting that both VCP and p62 are involved in the clearance of large poly-ubiquitinated substrates. Although this interaction is suggestive of autophagy, the exact mechanisms of pathway activation remained to be fully delineated. I therefore continued with various treatments to directly induce autophagy in cell culture.

I found that the optimal conditions were to co-transfect HeLa cells with *wt* p62-FLAG and *wt* VCP-V5 for 24 hours and treating them with either Torin1 (inducer of autophagy), HBSS starvation (inducer of autophagy) or Bafilomycin A1 (late stage inhibitor of autophagy), I determined that co-IP of VCP with p62 is mTOR dependant (Fig. 4.4). In detail, cells were treated at 20 hours post-transfection with either 1 μ M Torin1 or 50nM Bafilomycin A1 for further 4 hours, or incubated in the HBSS starvation media for 3 hours. Thereafter a *wt* p62-FLAG was immunoprecipitated from total cellular extracts using rabbit anti-FLAG antibody (Sigma/F7425) and precipitated fractions were analysed by Western blotting. I observed that endogenous wild type VCP precipitated with *wt* p62-FLAG only when autophagy was induced with a potent mTOR activity inhibitor (Fig. 4.4 B-C). Interestingly, VCP did not form a complex with p62 when autophagy was induced through starvation (Fig. 4.4A), neither when the protein degradation was inhibited through suppression of autophagosome acidification (Fig. 4.4B). Those findings were further validated by additional co-IP of VCP and p62 in cells treated with 1 μ M Torin1 as described above

(Appendix Fig.A8). The above results indicate that in my hands VCP interacts with p62 in an mTOR dependant manner, where inhibition of mTOR signalling results in activation of p62/VCP complex formation and clearance of ubiquitinated substrates via autophagy (Fig 4.4C).

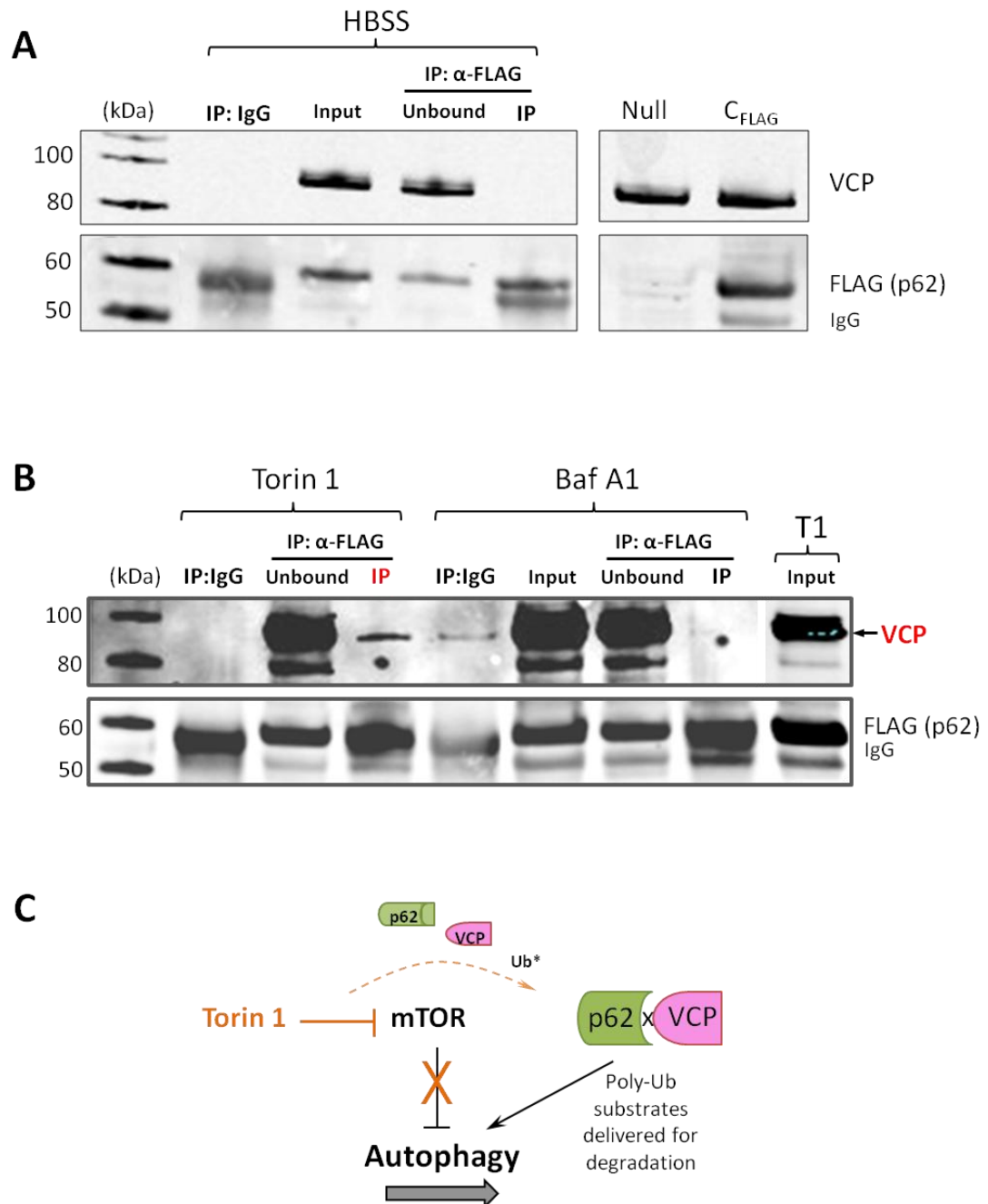


Figure 4.4. Wt VCP Immunoprecipitates (IP) with wt p62 in the mTOR-dependant manner. HeLa cells were co-transfected with wt p62-FLAG and wt VCP-V5 and after 24h incubated in HBSS for further 3h (A). Alternatively 20h – post transfection cells were treated with either 1µM Torin1 or Bafilomycin A1 for further 4h (B). Cell lysates were then subject to Immunoprecipitation by anti-FLAG antibody (Sigma/F7425). Pulled down proteins were

analyzed by Western blotting with anti-FLAG and anti-VCP antibodies. The mTOR inhibition is essential for the clearance of polyubiquitinated substrates by interacting VCP and p62 (C).

Next to determine the effects of mutations in VCP on complex formation with *wt* p62, I co-transfected HeLa cells with GFP-tagged VCP mutants i.e. R155H VCP-EGFP or DKO VCP-EGFP (Fig. 4.5). In addition to that, cells were treated with 100nM rapamycin in 75%HBSS + 25% DMEM media mixture for further 3 hours to induce autophagy. A *wt* p62 was immunoprecipitated with anti-p62 antibody followed by Western blotting with anti-GFP rabbit and anti-VCP mouse (Fig. 4.5A) to observe for interaction. In Figure 4.5 A and B, it would appear that both R155H VCP and DKO VCP might still be able to form complexes with p62 although a nonspecific binding is also observed. Therefore, I can only speculate that mutations in the N-terminal region of VCP do not halt its affinity for binding to p62.

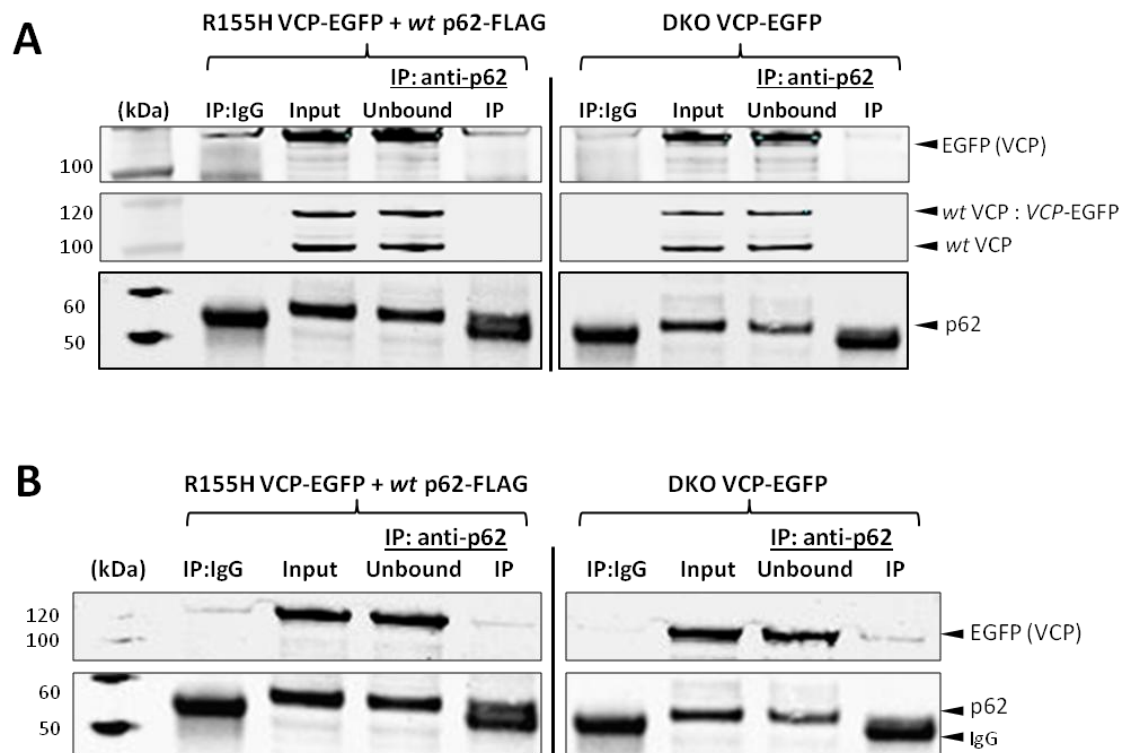


Figure 4.5. Co-immunoprecipitation (IP) of mutant VCP with *wt* p62. HeLa cells were co-transfected with R155H VCP-EGFP and *wt* p62-FLAG or with DKO VCP-EGFP alone. After 24h cells were incubated in 75%HBSS + 25% DMEM with 100nM rapamycin for further 3 hours. Binding was determined by IP with anti-p62 antibody and Western blot with anti-GFP rabbit (A and B) and anti-VCP mouse antibodies (A). Blots in A and B are from two independent experiments.

Nevertheless, collectively all of the above investigations have identified a previously unknown function of VCP that is not only involved in the autophagy pathway but also directly interacts with p62. Crucially, complex formation with the IBMPFD-mutant VCP further supports our proposed disease model for IBMPFD, where a defect in basal autophagy leads to the observed cellular pathology in affected tissues.

Based on these observations, I then decided to determine which VCP regions/domains are involved in the binding of p62 and LC3. To test whether there is a direct or indirect association between VCP and p62 bacterial plasmids expressing His-tagged wt-p62, wt-LC3 and wt-VCP (Chapter 2; 2.4) and plasmids expressing truncated versions of VCP were constructed. Since VCP binds other known adaptor proteins via the binding sites primarily located on the N- and C-domains I have designed VCP deletion constructs of the N- and C- domain deletions (Fig. 4.6 B and C). The oligonucleotides for PCR reactions (Fig. 4.6A) were purchased from Sigma. The domain mutants (deletions) were cloned in pDONR221 plasmid (Chapter 2, Fig. 2.7) according to the Gateway BP recombination reaction as described in the Gateway technology instruction manual (Invitrogen) (Chapter 2; 2.3). Due to the time constrains I was unable to pursuit further work and all these plasmids are currently stored at -80° and if sequenced can be translated *in vitro* and subjected to pull-down experiments.

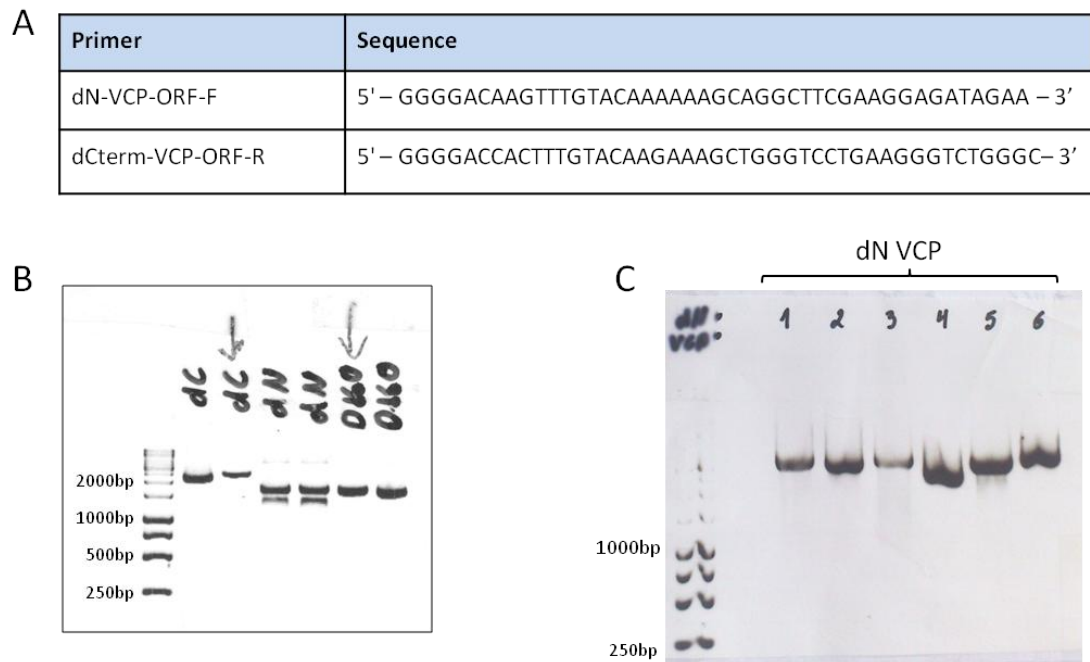


Figure 4.6. Design of the VCP deletion constructs. Primers for generating truncated VCP protein (A) were used to amplify the desired regions on a full length human protein (Appendix, Fig. A1) and PCR products were run on a 1% agarose gel at 120V for 1 h (B). The N-domain deletion VCP was gel purified using a PureLink Quick Gel Extraction kit (Invitrogen #K2100-12), amplified and validated via gel electrophoresis (C).

4.3 Discussion

To determine if the co-localisation of VCP and p62 is a physical interaction of some description I examined if p62 co-immunoprecipitated with VCP. These experiments took a lot of optimisation as initially the co-immunoprecipitation of VCP with p62 was very inconsistent. I found that the key to making the initial finding reproducible was determining that the interaction was in fact autophagy dependent. This enabled me to show that both wild type VCP and mutant R155H VCP bind p62. These findings are significant as they directly link VCP with components of the autophagy pathway and lead me to hypothesise that VCP plays a role in the early stages of autophagy (Fig.4.7) by interacting with p62. I speculate that p62 is a binding partner for VCP and that either VCP, p62 or both (perhaps with an unknown secondary binding partner) identify and bind polyubiquitinated substrates. It is highly likely that p62 then binds LC3 via its LIR (LC3 Interacting Region) domain and thus delivers the polyubiquitinated substrate to the autophagosome. This would be

consistent with what is known on how VCP carries out its many different functions within the cell (Yeung *et al.*, 2008; Meyer *et al.*, 2012).

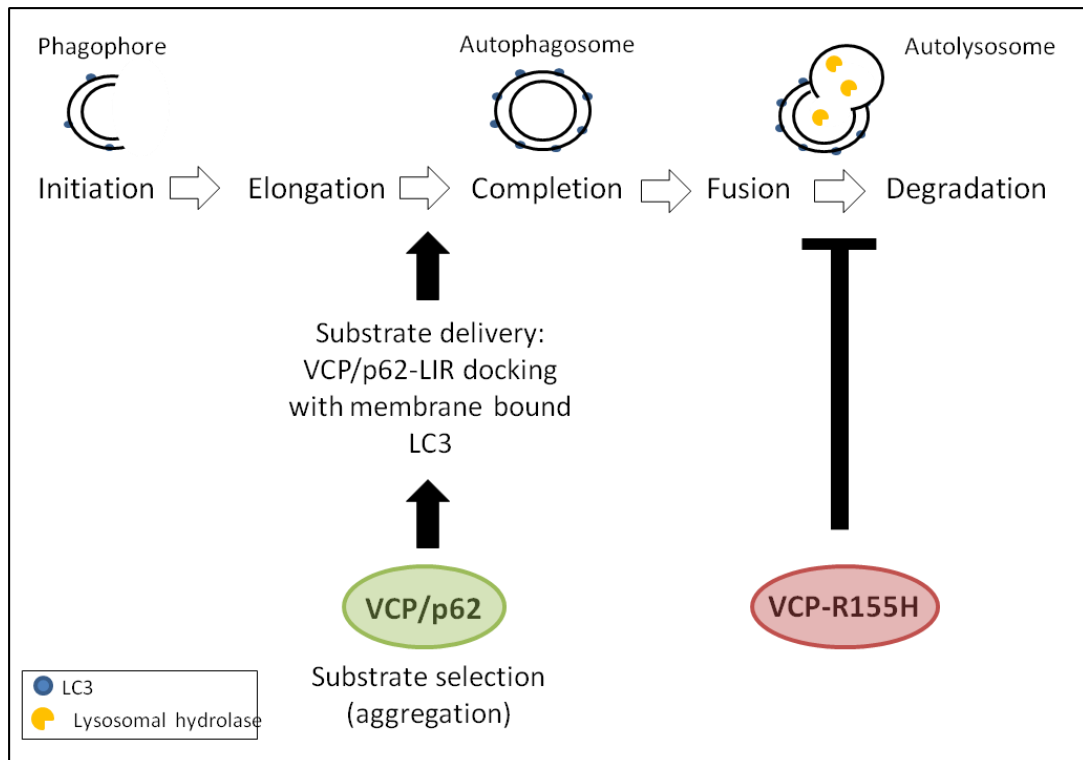


Figure 4.7. Model showing how the VCP/p62 interaction potentially is used for substrate selection and delivery to the macroautophagy pathway. Here, p62 acts as a VCP binding partner, with either p62, VCP or both bind to polyubiquitinated substrates; and the LIR domain of p62 is used to target the complex to the lipid bound LC3 in the nascent autophagosome. It is currently thought that the IBMPFD mutations in VCP inhibit late stage autophagy by some not fully defined mechanism (Ju *et al.*, 2009; Tresse *et al.*, 2010).

While there are many known VCP binding partners the most commonly used ones (Table 4.3) all have various ubiquitin associated functions. These include E3 and E4 ubiquitin ligases, deubiquitinating enzymes and ubiquitin binding proteins. Furthermore, all of VCP actions are conducted through ubiquitin based interactions. I have therefore shown that VCP uses these interactions as part of the early autophagy pathway. Interestingly, the molecular lesions, caused by VCP mutations, seem to affect late autophagy suggesting another, as yet unidentified, autophagy based role (Fig.4.7).

Protein	Activity	Ub Link
Atx3	E3/DUB	K48
BRCA1	E3	K6
CHIP	E3/E4	K48/K63
Dorfin	E3	K63
Ufd1	E3	K48
Ufd2a	E3/E4	K29/K48
Ufd3	E3	K29
Ufd4	E3	K29
HDAC6	Binds Ub	K48/K63
Npl4	Binds Ub	K63
p47	Binds Ub	48
p62	Binds Ub	K63
Rad23a	Binds Ub	K48
SAK1	Binds Ub	K48

Table 4.3. Common binding partners for VCP.

Such data support the hypothesis that p62 either is a VCP binding partner or at least forms a complex with VCP and that VCP has an active role in the degradation of ubiquitinated substrates by autophagy. With this knowledge, I then decided to determine which VCP regions/domains are involved in the binding of p62 and LC3, and if interaction of VCP with LC3 II in the autophagic membranes depends solely on the p62 binding. To address this question I have constructed bacterial plasmids expressing His-tagged *wt* p62, *wt* LC3 (Chapter 2, 2.3.1) or truncated versions of VCP (Chapter 2, 2.3.2; Fig.4.6). I planned to use the purified recombinant proteins in pull-down experiments to locate p62 binding sites, although, due to the time constrains I was not able (as yet) to translate those plasmids *in vitro* and subject to pull down experiments.

CHAPTER 5

STABILITY AND DEGRADATION OF VCP

CHAPTER 5: STABILITY AND DEGRADATION OF VCP

5.1 Introduction

In association with the ubiquitin-proteasome system (UPS), VCP acts as a molecular segregase and mediates ubiquitin-dependent extraction of substrates from multiprotein complexes for recycling or degradation by the 26S proteasome (Meyer *et al.*, 2012). It has been shown that the N-terminal domain of VCP can bind ubiquitin directly, with a preference for polyubiquitin chains (Ye *et al.*, 2003), VCP usually requires interaction with a diverse group of adapter proteins that enable it to target specific substrates for degradation (Ju and Wehl, 2010). Ufd1 and Npl4 are the main binding partners that mediate the proteasome-related activities of VCP. Although, VCP can also interact with substrates that have not been modified by a poly-ubiquitin chain, Ye and colleagues proposed the dual recognition model for selection of specific substrates for degradation (Ye *et al.*, 2003). In summary, the unfolded segment of substrate is initially recognised by VCP then, after a polyubiquitin chain has been attached to the substrate, the VCP-Ufd1-Npl4 complex binds to the ubiquitinated substrate, what in turn activates the ATPase to extract the polypeptide chains out of the membrane (Ye *et al.*, 2003). Importantly, the ATP hydrolysing ability of VCP is indispensable for its function and is also influenced by many factors. For instance, binding of the adaptor protein p47 (in p97/p47-mediated membrane fusion of Golgi and ER) to the N-domain of VCP has an inhibitory effect on the ATPase activity (Meyer *et al.*, 1998). Notably, VCP mutants that lacked ATPase activities show no membrane fusion activities in the *in vitro* reassembly assay (Uchiyama *et al.*, 2002). In addition to the binding of adaptor proteins, VCP ATPase activities are modified by phosphorylation and acetylation throughout the protein, especially in the D2 α -domain (Mori-Konya *et al.*, 2009). Collectively, these multilevel regulatory mechanisms may explain the multiple functions of VCP observed in different cell conditions. With the evidence for VCP playing a role in autophagy coming from studies on the pathogenesis of IBMPFD and the vast evidence linking VCP to the UPS one unresolved fundamental question remains: how is VCP itself turned over?

5.2 VCP stability is linked to p62 instability in cells.

Through its ability to structurally remodel and edit ubiquitinated substrates, with the help of associated cofactors, VCP governs many critical cellular pathways. I have shown that it interacts directly with key components of the autophagy pathway, so my next step was to determine how VCP is degraded in the cell. The p62 protein is an ubiquitin binding protein and as I have found, a binding partner of VCP, delivers ubiquitinated proteins to autophagic machinery and is known to be degraded by autophagy (Bjorkoy *et al.*, 2005; Bjorkoy *et al.*, 2009). It has been shown that the half-life of p62 is 6 hours which makes it a useful control for monitoring autophagy-mediated degradation (Bjorkoy *et al.*, 2005).

First of all, I wanted to confirm the rate of turn-over for p62 and determine the general stability of VCP in differentiated cells (i.e. not autophagy or proteasome dependent). I performed a cycloheximide (CHX) chase assay in cell culture (Fig. 5.1, Fig 5.2; Appendix Fig.A9 and A10). Here, MEF cells were treated with 100µg/ml of CHX and the soluble fraction of the lysates was analysed by Western blotting at 0, 2, 4 and 6 hours after CHX treatment (Fig. 5.1A). As shown in Figure 5.1B, the levels of p62 do consistently decrease over time and are lowest at 6 hours post treatment. Interestingly VCP seemed to be more stable with a consistent slight increase in protein levels at 4 hours post treatment before beginning to drop at 6 hours post treatment (Fig. 5.1 B and C) suggesting unusual protein cycling pattern.

With those observations in mind I next wanted to evaluate if p62 was playing a role in the turnover of VCP. Here, I exposed both p62-expressing (*wt*) MEFs (MEF +/+) and p62-knockout (p62-KO) MEFs to 100µg/ml of CHX for 0-6 hours. As before I then assessed the levels of p62 and VCP at each time-point via immunoblotting (Fig. 5.2A). VCP remained stable in both *wt* and p62-KO cells up to 4 hours of the chase (Fig. 5.2B and C) but whereas VCP levels begin to decrease in the *wt* cells at 6 hours, it continued to increase in the p62-KO cells. As expected there is none to very low detectable expression of the endogenous p62 protein in the p62-KO cells, but the levels of VCP are seemingly increased despite the lack of new protein synthesis (Fig. 5.2C).

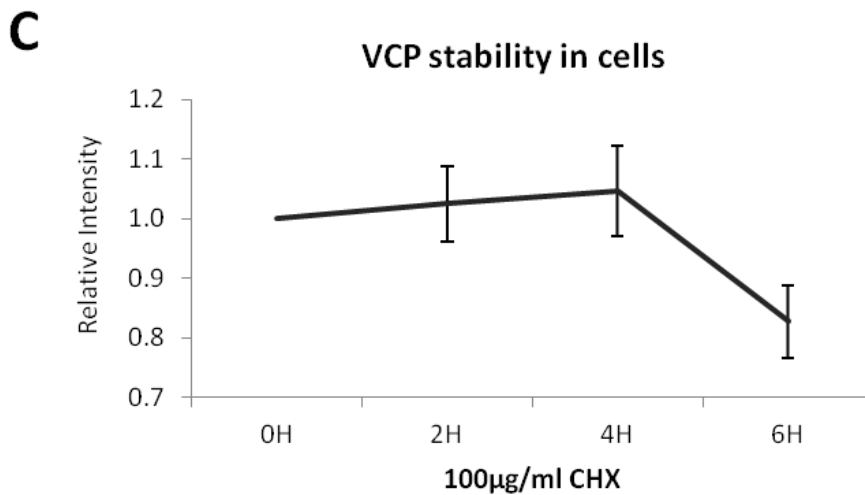
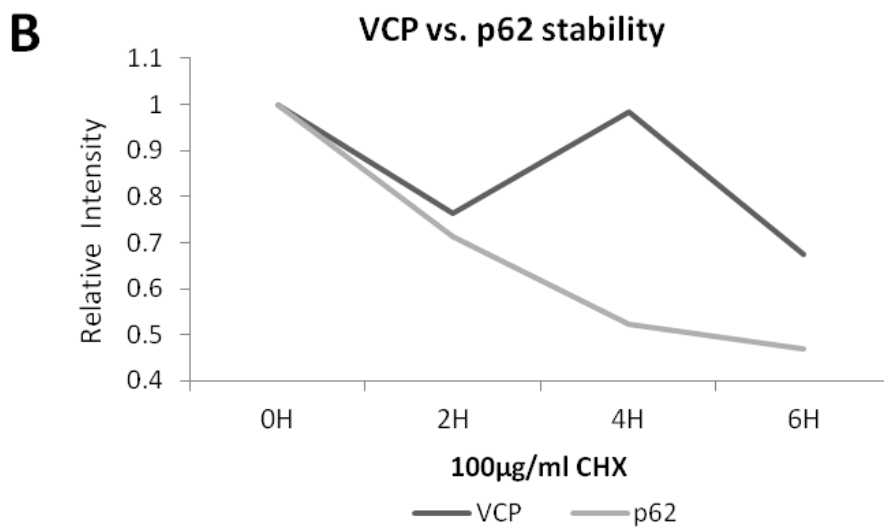
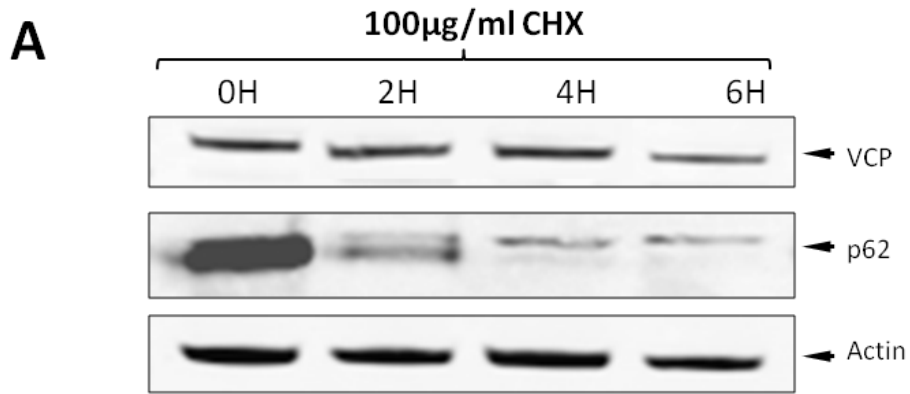


Figure 5.1. p62 and VCP stability in cells. Immunoblot for VCP, p62 and actin from cellular extracts of MEF cells incubated with 100µg/ml Cycloheximide (CHX) for 0-6hrs (A). Densitometry analysis of normalized to actin p62 and VCP expression in MEF cells from the immunoblot shown in A; results presented as a relative intensity values of an intensity at 0H (0H=1.0); data obtained from a single experiment (B). The signal intensity from the VCP

immunoblots from four independent experiments was quantified and presented as relative intensity values of the VCP at 0 hours exposure to 100 μ g/ml CHX (OH=1.0); Line chart shows mean intensity \pm SEM (precision for an estimated population mean) for normalized replicates at each time point.

To further explore this outcome I assessed the amount of VCP present in the insoluble fractions of the cellular lysate at each time point of CHX-chase using a filter trap assay. Here, the insoluble fractions are captured on a nitrocellulose membrane, such that only the large aggregated insoluble complexes are captured and small insoluble complexes will pass through the membrane (Fig. 5.2D). In p62-positive (*wt*) MEFs (MEF +/+) the levels of insoluble aggregated VCP remained relatively constant throughout the chase, whereas in p62-KO cells it increases from the 2 hour time point to peak at 4 hours followed by a rapid decrease by 6 hours (Fig. 5.2E) (See Appendix: Fig.A11 for the levels of insoluble aggregated p62 and ubiquitinated-protein aggregates generated in the wild-type and p62-KO MEFs).

It is apparent that the filter-trap assay's results correlate with the results obtained from the soluble protein fractions of cells exposed to 100 μ g/ml of CHX for 0-6 hours (Fig. 5.2C). Namely, where VCP aggregated rapidly decreased in the insoluble fraction of the p62-KO cells between 4 and 6 hours time point (Fig. 5.2E), it continued to increase in the soluble fraction of those cells by 6 hours (Fig. 5.2C).

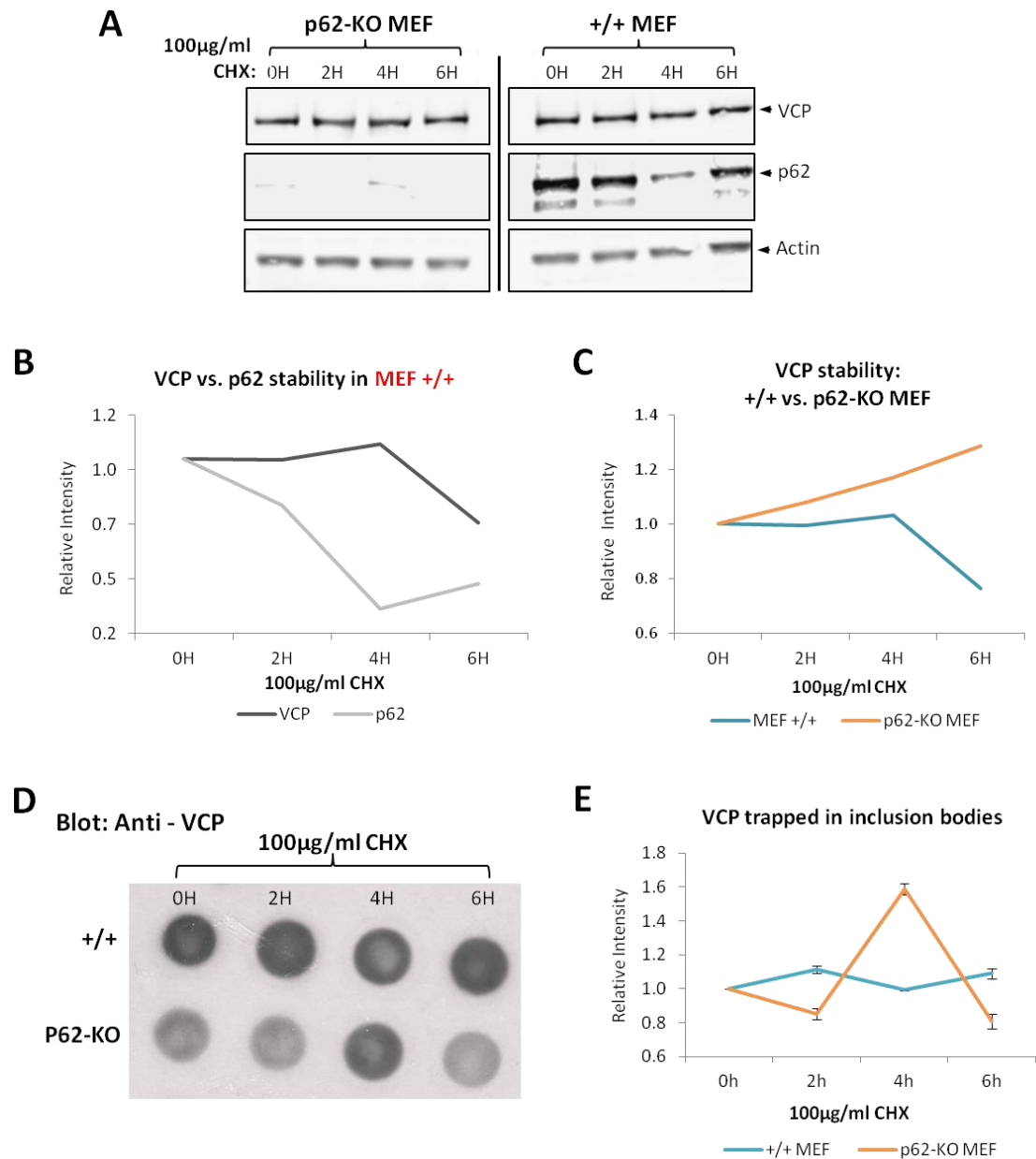


Figure 5.2. VCP stability increases in cells lacking p62. Immunoblot from cellular extracts of p62-expressing (MEF +/+) and p62-knockout (p62-KO MEF) MEFs exposed to 100µg/ml Cycloheximide (CHX) for 0-6hrs (A). Densitometry analysis of normalized to actin p62 and VCP expression in MEF +/+ cells (B), and comparison of normalized to actin VCP expression in p62-KO versus VCP expression in p62-expressing (MEF +/+) MEF cells (C). Figures presented in B and C show the relative intensity readings (with intensity at 0H=1.0) calculated from arbitrary optical density results normalized to loading control-actin from immunoblots shown in A. Results obtained in this experiment were reproducible in an independent duplicate experiment and are presented in Appendix Fig.A9. Filter-trap analysis of the VCP content of SDS-insoluble protein aggregates in p62-expressing (+/+) and p62-knockout (p62-KO) MEFs exposed to 100µg/ml Cycloheximide (CHX) for 0-6hrs (D). The signal intensity from the VCP filter-trap immunoblots from three independent experiments was quantified and presented

as relative intensity values of the VCP control at 0 hours exposure to the CHX treatment (OH=1.0); Line charts show mean intensity \pm SEM (precision for an estimated population mean) for normalized replicates at each time point (E).

Thereafter, to test whether stability of VCP is affected by autophagy, I used two methods to up-regulate activation of autophagy, either by starvation in HBSS media or inhibition of mTOR by Torin 1 treatment (Fig. 5.3 A-D). To initiate autophagy by starvation, HeLa cells were incubated in HBSS starvation media in addition to exposure to 100 μ g/ml CHX for 0-6 hours. As expected decreased p62 levels (increased turnover) can be observed when autophagy is induced, with the lowest levels of p62 at 6 hours (Fig. 5.3A and B). As observed previously VCP levels increase, this time they rise at 2 to 4 hours after autophagy induction and return to normal at 6 hours (Fig. 5.3C). Almost identical response in VCP levels was noted when MEF cells were treated with Torin 1 (6 μ M for 5 hours) to induce autophagy (Fig. 5.3D and E) with a subsequent exposure to 100 μ g/ml CHX for 0-5 hours. Again, VCP expression increases in those cells at approximately 2 hours and return to basal levels at 5 hours (Fig. 5.3E). Unmistakably these results show a uniform VCP stability pattern in both cell types (normal murine MEF and cancer-derived human HeLa cells) in response to autophagy induction.

Next I wanted to determine if VCP is a substrate for degradation via the proteasome. Here, I treated MEF cells with the proteasome inhibitor MG132 at 25 μ M concentration for 6 hours. Following proteasome inhibition the protein synthesis was then inhibited for 0-6 hours with cycloheximide (CHX) treatment. Initially decreasing levels of both p62 and VCP were noted in the presence of MG132 (Fig. 5.3F). Although, densitometry analysis reveals that VCP expression (normalised to actin) decreases from 0 to 4 hours and plateaus from 4 to approximately 6 hours, while p62 levels decrease steadily (Fig. 5.3G). Those results alone might imply that even if the ubiquitin-proteasome system (UPS) is not necessarily solely responsible for degrading VCP it is a functional component a multiple-pathway/adaptor coupled mechanism involved in regulating stability of the VCP (Fig. 5.4D).

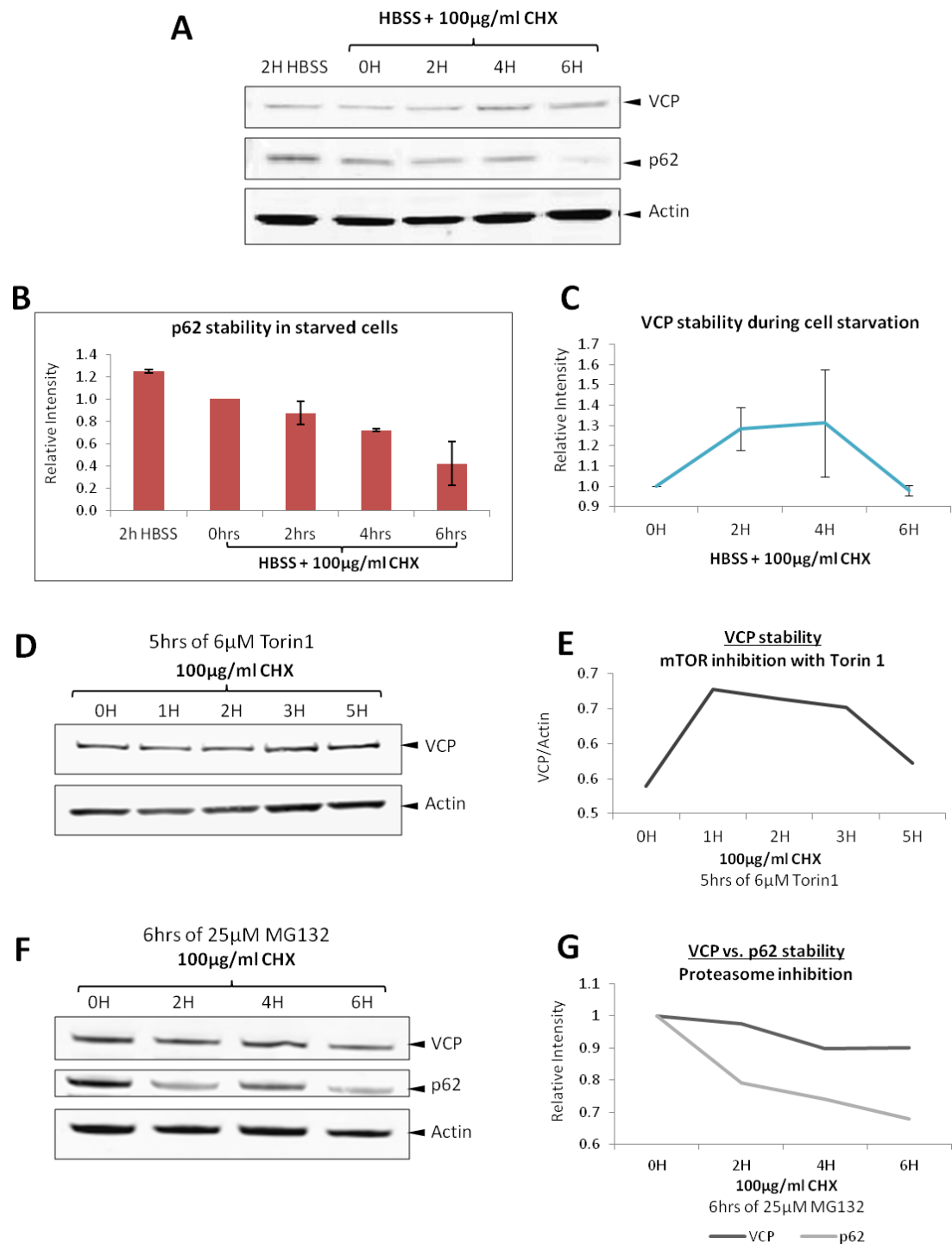


Figure 5.3. Autophagy regulates VCP protein levels. Immunoblot for VCP, p62 and actin from cellular extracts of HeLa cells incubated in HBSS media containing 100µg/ml CHX for 0-6hrs (A). Densitometry analysis of normalized to actin p62 (B) and VCP (C) expression in starved cells. Figures shown in B and C represent the average intensity from 3 independent experiments; presented as relative intensity values of the non-treated controls at 0hrs (0H= 1.0). Each time point represents the normalized mean intensity \pm SEM (indicate the precision for an estimated population mean). Lysates from MEF cells treated for 5hrs with 6µM Torin1 prior to the exposure to 100µg/ml CHX for 0-5hrs were immunoblotted (D) and analysed for

VCP levels by densitometry (E). Western blot (F) and comparison of normalized to actin endogenous VCP and p62 expression in MEF cells treated with 25 μ M MG132 for 6 hours followed by 0-6hrs exposure to 100 μ g/ml CHX (G). Data shown in figures D-G are from single experiments and are yet to be replicated.

Finally, I wanted to determine if the IBMPFD mutations in VCP affect the protein stability in differentiated cells. I expressed R155H mutant VCP (R155H VCP-V5) and wild type VCP (*wt* VCP-V5), both V5-tagged, in Hela cells for 20-22 hours prior to the CHX-treatment. Thereafter, cellular extracts at 0-6 hours were analysed by Western blotting with antibodies for V5-tagged (*wt* and mutant) VCP and endogenous p62 (Fig. 5.4A). The average VCP expression from three independent experiments plotted in a linear graph in figure 5.4 B shows that *wt* VCP is more stable than the R155H mutant VCP, suggesting that the mutant protein may be preferentially degraded. The degradation of p62 in VCP-mutant expressing cells is unaffected (Fig. 5.4 A and C), whereas overexpression of the wild type VCP appears to be stabilizing endogenous p62 expression, possibly halting its degradation (Fig. 5.4C). Consistently with my earlier results, the decrease in VCP levels is not linear; initially dropping then peaking at 4 hours and again reducing at 6 hours.

In summary to this results chapter, I have shown that stability of VCP is directly linked to p62 instability since endogenous VCP continues to increase in the soluble fraction of the p62-knockout cells, despite the lack of new protein synthesis. I have also noted that overexpression of *wt* VCP in cells halts degradation of p62, whilst it is still being recycled itself. Last but not least, I have shown that R155H mutant VCP is less stable than wild type VCP as it appears to be less efficiently recycled and quicker degraded.

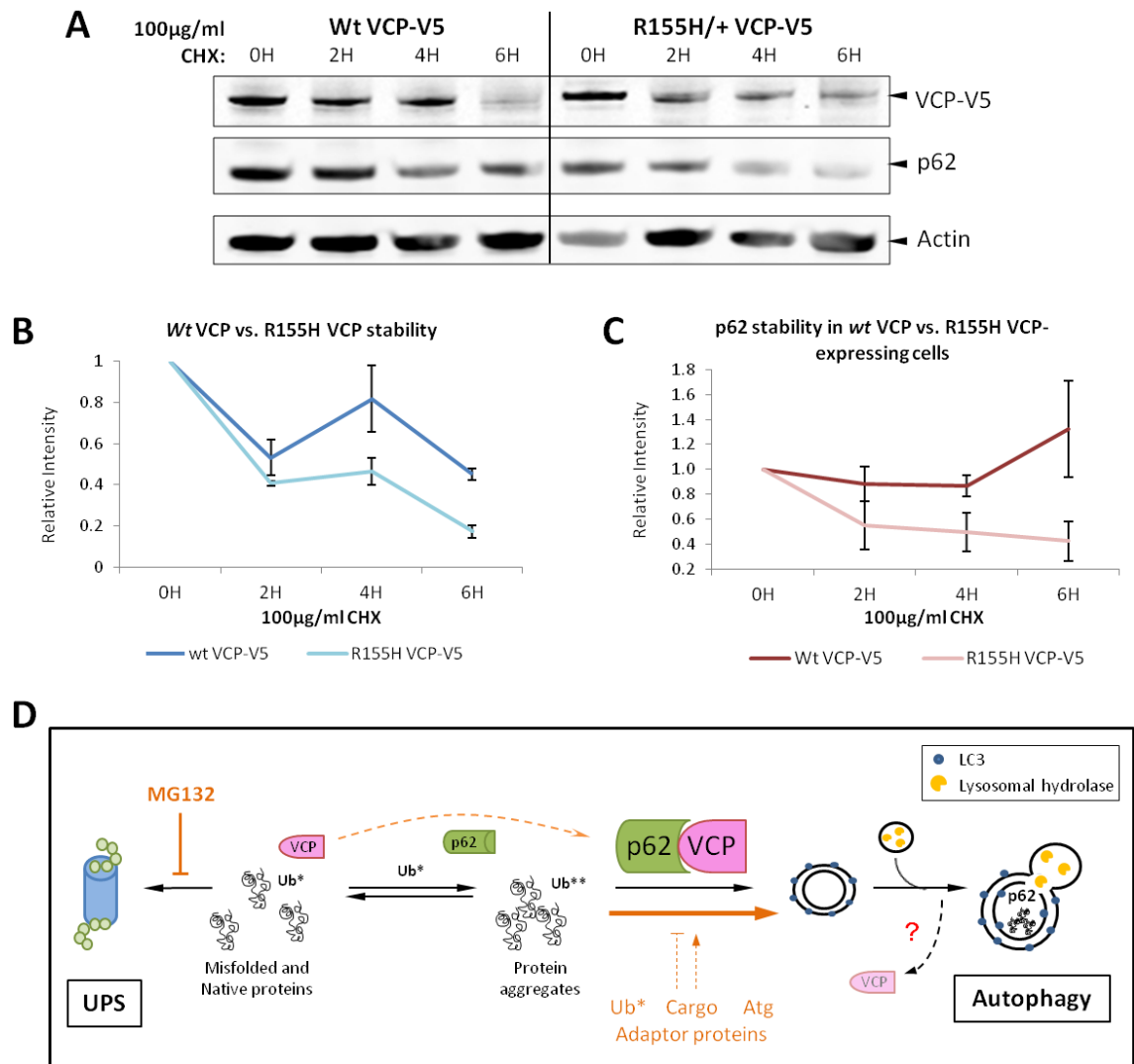


Figure 5.4. Overexpression of wt VCP increases stability of the endogenous p62. Immunoblot from cellular extracts of MEF cells, transfected with either wt VCP-V5 or R155H VCP-V5, exposed to 100µg/ml Cycloheximide (CHX) for 0-6hrs (A). Comparison of normalized to actin densitometric levels of wt and R155H VCP-V5 expression (B) and endogenous p62 expression (C) in transfected MEF cells. Figures shown in B and C represent the average intensity from 3 independent experiments, presented as relative values of the non-treated controls at 0hrs (0H=1.0). Line charts show mean intensity \pm SEM (precision for an estimated population mean) for normalized replicates at each time point. Diagram summarizing hypothetical routes for the VCPs participation in cellular degradation pathways (D). VCP is critical for the coordination between the UPS and Autophagy pathway. Misfolded proteins and unneeded native proteins are degraded by the UPS in 26S Proteasome. Protein aggregates formed by misfolded proteins that have escaped UPS are removed by Autophagy. It is likely that p62 and other putative regulators influence the stability of VCP in cells; either promoting or preventing its multi-ubiquitination and consequent degradation.

5.3 Discussion

While VCP is the main shuttle protein taking polyubiquitinated substrates to the proteasome it is not known by which route VCP itself is degraded. It has been shown that p62 is important in targeting polyubiquitinated substrates to the autophagosome and it is itself degraded by autophagy (Pankiv *et al.*, 2007; Bjorkoy *et al.*, 2009). Using p62 as a control for degradation by autophagy I initially just inhibited protein synthesis with cycloheximide (CHX) and measured both VCP and p62 levels over 6 hours. As expected, p62 level decreased with time, with a half-life of 6 hours as previously reported (Bjorkoy *et al.*, 2005). Interestingly, VCP levels seemed to increase until about 4 hours, and then it started to go down. Obviously this increase is unlikely to be due to protein synthesis, so it must be controlled via another mechanism. Since I have shown that VCP is involved in the autophagy pathway and that it binds p62 in an autophagy dependent manner, I went on to see if p62 was needed for VCP degradation. In that set of investigations I used normal, p62 expressing (*wt*) and p62 knockout (p62-KO) MEF cell lines. Importantly, the p62-KO cell line is not autophagy negative, is just deficient in p62 protein (Komatsu *et al.*, 2007). In p62-KO cells, VCP levels continued to increase over time and did not seem to be degraded. As any increase in protein level after cycloheximide treatment can only be due to changes in protein solubility, I used a filter trap assay to analyse the levels of VCP contained in insoluble aggregates after cycloheximide treatment. I found that in the *wt* MEFs the level of insoluble VCP was relatively stable over the 6 hour time period. Conversely, in the p62-KO MEFs the level of insoluble aggregated VCP peaked at 4 hours then returned to its starting level. Therefore it would appear that the solubility of VCP in cell is regulated in a p62 dependent manner. In that case, the spike of insoluble aggregated VCP I see at 4 hours post cycloheximide treatment in p62-KO MEFs, could be the result of VCP collecting and aggregating polyubiquitinated substrates to be degraded by autophagy in the absence of p62.

I have also induced autophagy by starvation and again, after cycloheximide treatment, measured VCP and p62 levels. Here I have found that, as expected p62 was degraded steadily over the time course (Fig.5.3B), although VCP levels increased faster than with no autophagy induction and peaked at 2 hours before returning to

basal levels at 6 hours. Similarly, when autophagy was induced by Torin1 treatment, VCP levels increases rapidly, peaking at 1 hour, before returning towards initial levels at the end of the time course. To elucidate if VCP might be a substrate for the UPS degradation I inhibited the proteasome with MG132, in conjunction with cycloheximide treatment. As predicted the proteasome inhibition did not affect the degradation of p62 over the time course, which is consistent with p62 being degraded by autophagy. This did however have an effect on the degradation of VCP, resulting in a consistent decrease in the VCP levels (with no peaks half-way through the CHX-chase), suggesting that proteasome inhibition might increase the efficiency of soluble VCP degradation and stop the release of the insoluble pool of VCP. Therefore, the likely hypothesis is that soluble pool of VCP is either being degraded by autophagy (and not the proteasome) or it is being sequestered to the growing (insoluble) aggresome resulting from the proteasomal inhibition.

I have then looked at the stability of the mutant form of VCP by transiently expressing *wt* or R155H mutant VCP in cell lines, which were then treated with cycloheximide. The levels of VCP decreased over the time course and the characteristic peaking at 4 hours was still evident for *wt* VCP, although it was less pronounced in the mutant VCP (Fig. 5.4B), implying that mutant VCP is less likely to be released from the insoluble aggregate pool. Furthermore, the levels of the R155H VCP also seemed to decrease faster than those of *wt* VCP, suggesting that the mutant protomers are less stable than the wild-type protein. Interestingly, the overexpression of *wt* VCP stabilised the levels of endogenous p62, while the overexpression of mutant VCP did not increase p62 stability, allowing for normal degradation.

These experiments have highlighted the complexity of the cellular processes involved in protein turnover. In summary, I have found that:

1. VCP is in two states in the cell, one where it is soluble and the other where it is insoluble and aggregated.
2. VCP can be released from the insoluble aggregated fraction and recycled to the soluble fraction of VCP (unlike p62 which does seem to be degraded but not recycled).

3. In the absence of p62 in the cell, VCP is sequestered into insoluble aggregates which peak around 4 hours after inhibition of protein synthesis, and then VCP is released back to the soluble fraction. This would suggest that perhaps VCP is compensating for the loss of p62 by shuttling substrates to the proteasome for degradation.
4. Mutant VCP seems to be less stable than wild type VCP, suggesting that the mutant VCP is not recycled efficiently and is being degraded (potentially by autophagy as p62 is degraded faster in cells expressing R155H-VCP). This could be because the mutant VCP is unable to release its substrates and is being aggregated as a result.

CHAPTER 6

AUTOPHAGY AND OSTEOCLASTOGENESIS

CHAPTER 6: AUTOPHAGY AND OSTEOCLASTOGENESIS

6.1 Introduction

The skeleton is a dynamic tissue that undergoes continuous remodelling to sustain calcium homeostasis, repair microfractures and respond to mechanical load. The bone remodelling process is complex and relies on coupling between bone formation and resorption that involves osteoblasts (bone forming cells), osteocytes (mature, embedded bone forming cells) and osteoclasts (bone resorbing cells).

One of many important cellular events in bone remodelling is bone resorption by osteoclasts, which is preceded by osteoclastogenesis and followed by apoptosis. Osteoclasts are multinucleated and non-dividing principal resorptive cells of bone, formed by fusion of mononuclear progenitors of monocyte-macrophage lineage. These mature polykaryons play a central role in the formation and turnover of the skeleton thus regulating its mass. Osteoclast differentiation entails binding of RANK ligand (RANKL, originally identified as TRANCE - TNF-related activation-induced cytokine) to its cognate receptor (RANK) on myeloid progenitor cells and subsequent activation of multiple intracellular pathways including AKT/PI3K, MAP kinase, and NF κ B (Otero *et al.*, 2012; Khosla, 2001). A ubiquitous NF κ B pathway is activated by diverse immunological and inflammatory stimuli including inflammatory cytokines such as TNF α and IL-1, T-cell activation signals, growth factors and stress inducers (Abu-Amer *et al.*, 2008; Baldwin, 2001). These proteins have been classified into canonical and non-canonical NF κ B pathways (Fig 6.1). The canonical pathway which is activated by RANKL as well as by inflammatory stimuli including TNF α and IL-1 β , is regulated by the I κ B kinase (IKK) complex dominated by IKK β and IKK γ /NEMO leading to phosphorylation of I κ B and activation of p50, p65 (RelA), cRel transcriptional complexes (Otero *et al.*, 2012; Abu-Amer *et al.*, 2008). On the contrary, the non-canonical NF κ B pathway is regulated by NF κ B-inducing kinase (NIK) which in turn activates IKK α leading to proteolytic processing of the inhibitory protein p100, in osteoclast precursors, and releasing p52 and RelB, the downstream effectors of this pathway (Novack *et al.*, 2003). Unlike stable IKK complex, NIK is constitutively degraded due to its interaction with TRAF3 (Yao *et al.*, 2009).

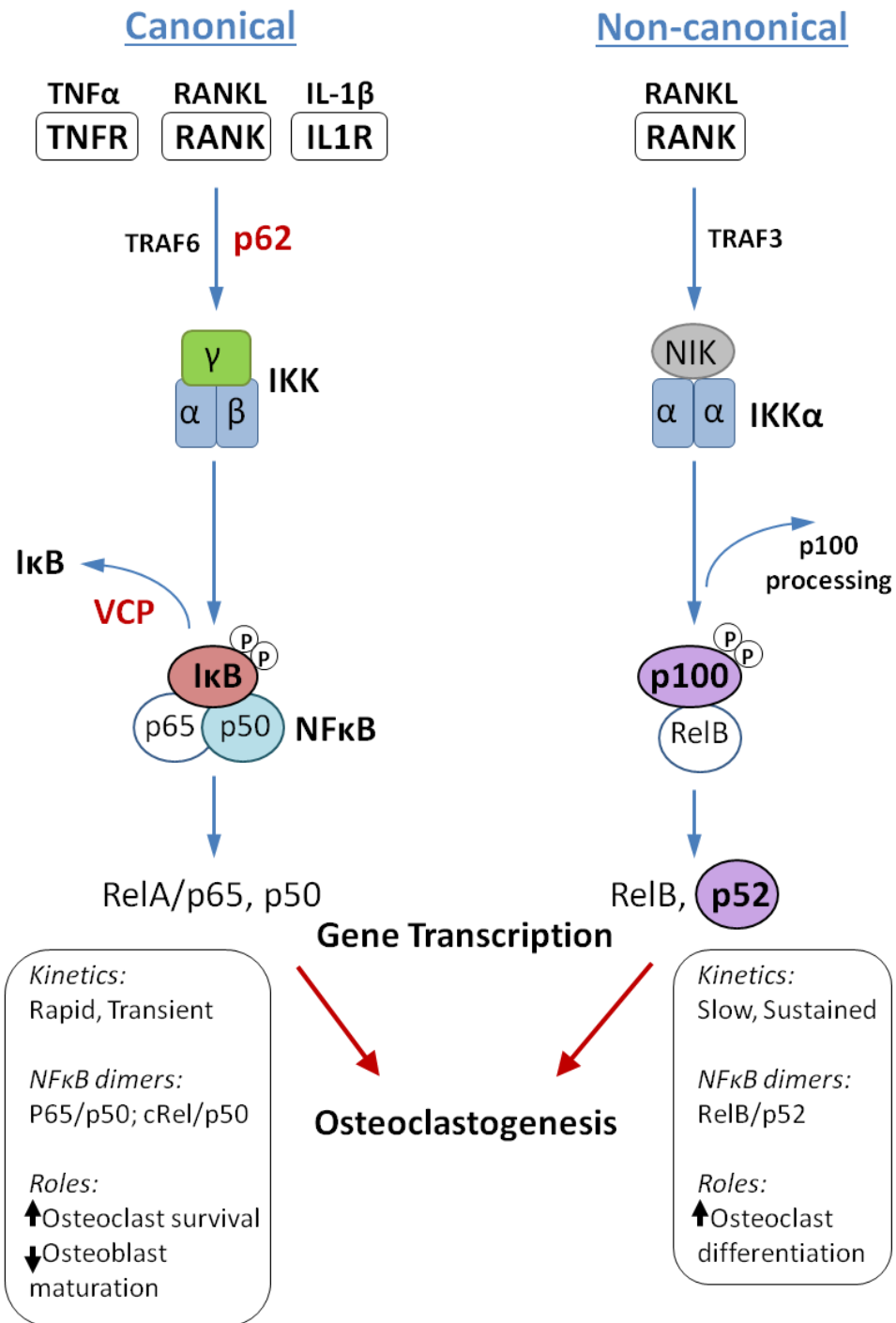


Figure 6.1. Canonical and non-canonical NF- κ B signalling pathways. Canonical pathway is triggered by numerous signals, including RANKL, TNF α and other inflammatory mediators. It involves activation of I κ B kinase (IKK) complex (regulated via p62/TRAF6/aPKC complex), IKK-mediated I κ B α phosphorylation and subsequent degradation (mediated by the VCP), resulting in rapid and transient nuclear translocation of the NF κ B, predominantly p65/p50 heterodimers. Non-canonical NF κ B pathway relies on phosphorylation-induced processing of p100 to p52 via the proteasome. This is triggered by signalling from a subset of TNFR members, although, in the skeletal cells, the only established activator of this pathway is

RANKL. RANKL activates the non-canonical pathway NF κ B pathway by blocking TRAF3-mediated NIK degradation. This pathway is dependent on NIK and IKK α , but not on the trimeric IKK complex, and mediates the persistent activation of RelB/p52 complex.

Upon specific stimulation, TRAF3 binds to the cytokine receptor and NIK protein is stabilized. NIK-induced processing of p100 is associated with site-specific phosphorylation and subsequent ubiquitination, generating the mature p52 and inducing nuclear translocation of the RelB/p52 heterodimers. The C-terminal region of p100 contains two serine residues, S866 and S870, which resemble the phosphorylation site of I κ B α (Sun 2011; Xiao *et al.*, 2001). A lysine residue K856, located upstream of the phosphorylation site of p100, serves as the ubiquitin acceptor site and is analogous to the ubiquitination site (K22) of I κ B α (Novack, 2011; Novack *et al.*, 2003). Only a subset of TNF family cytokines, including RANKL but not TNF α , can activate the non-canonical pathway due to the ability of their corresponding receptors to bind TRAF3 (Hauer *et al.*, 2005).

Ultimately, RANK ligand is considered to be a master regulator of physiologic osteoclastogenesis and many factors that stimulate its expression have been identified. Briefly, para-thyroid hormone, prostaglandin E2, dexamethason, inflammatory cytokines such as interleukin-1 (IL-1) and tumour necrosis factor alpha (TNF α), or 1,25 dihydroxy-vitamin D3 can stimulate RANKL expression (Wada *et al.*, 2006). By contrast, estrogen or transforming growth factor β (TGF β) attenuates RANKL expression (Kasagi and Chen 2013; Weitzmann and Pacifici 2006). RANK receptor has a long cytoplasmic domain without kinase activity that bears several TRAF-binding domains. Binding and autoubiquitination of TRAF6, and interaction between aPKC and p62 are required for sustained activation of the canonical NF κ B pathway (Novack 2011; Lamothe *et al.*, 2007).

TNF α is a potent activator of classical NF κ B and there is a strong consensus that TNF α and RANKL can act synergistically to induce osteoclastogenesis (Zou *et al.*, 2001). RANKL stimulates TNF α release from osteoclast progenitors promoting their differentiation. Furthermore, TNF α , aside from its RANKL-costimulatory osteoclastogenic function, was also shown to induce osteoclast formation in

RANK/RANKL-deficient mice, in vivo, despite the fact that these mice also lacked NF κ B p100 subunit (Yao *et al.*, 2009).

The etiology of Paget's disease (PDB) is complicated and various genetic and environmental factors have been implicated in the pathophysiology of this disease. The most common genetic contribution comes from mutations in the coding region of gene encoding the p62 protein. Those mutations result in loss of function of the C-terminal ubiquitin association (UBA) domain and lead to elevated cytokine activation of NF κ B. Other genes involved in PDB are *TNFRSF11A* (encodes for RANK), *TNFRSF11B* (encodes for osteoprotegerin – OPG, a decoy receptor for RANKL) and *VCP/p97* (encodes for VCP) (Sabharwal *et al.*, 2014; Galson and Roodman 2014). The exact functional malfunction caused by mutations in *VCP* gene is less defined. VCP regulates the degradation of I κ B, releasing NF κ B to be activated by phosphorylation and then translocated to the nucleus. Knockdown of VCP results in accumulation of I κ B and decreased activation of NF κ B (Vandermoere *et al.*, 2006). Therefore the pathogenic mechanism of VCP mutations may involve increased clearance of I κ B and consequently increased downstream activation of NF κ B with pathological consequences. Interestingly, recent report proposes that although a short term activation of NF κ B is mediated by the proteasomal degradation of I κ B α , persistently activated NF κ B state is achieved via the induction of autophagy at later phases, following stimulation with TNF α (Colleran *et al.*, 2011).

On the other hand, a main characteristic of pagetic osteoclast precursors is that they are sensitive to lower levels of osteotropic factors than normal precursors. Interestingly, both p62 and VCP mutations make osteoclast precursors more responsive to RANKL, TNF α and 1,25-dihydroxyvitamin D3 (Chung *et al.*, 2011; Hiruma *et al.*, 2008). Furthermore, osteoclast precursors from mice with a P394L p62 mutation (equivalent to P392L mutation in humans) were noted to be not only over-sensitive to RANKL but also show an increased expression of autophagy-related genes, *atg5* and *lc3* (Daroszewszka *et al.*, 2011). This would imply that regulation of NF κ B pathway by p62, VCP and other regulatory proteins is more sophisticated and does not only involve the ubiquitin-dependent degradation of key modulators of the pathway.

Unmistakably, osteoclasts are the primary cells affected by PDB and show both physiological and morphological abnormalities. They are increased in both number and size and contain up to 100 nuclei, in contrast to 3-20 nuclei in normal osteoclasts (Sabharwal *et al.*, 2014; Ralston 2008). Another feature of pagetic osteoclasts is the characteristic ubiquitinated nuclear and cytoplasmic inclusions (Badadani *et al.*, 2010; Kimonis *et al.*, 2008). These features suggest that a degradation pathway(s) is likely to be disrupted in those cells.

There are two main degradation pathways that are important for intracellular protein homeostasis; these are ubiquitin-proteasome system (UPS) and autophagy pathway. Crucially, both VCP and p62 are placed at a unique position within these protein degradation pathways. In settings of impaired autophagy, the accumulation of p62 results in a sequestration of UPS substrates; and this can be overcome by the overexpression of VCP (Korolchuk *et al.*, 2009). Autophagy is particularly important in the event of undernourishment and of oxidative stress, where it is induced to degrade long lived proteins and damaged organelles to generate amino acids for biosynthetic processes. Moreover, in addition to turnover of cellular components and homeostasis maintenance, autophagy is also implemented in development and differentiation of multiple cell types, such as adipocyte and chondrocyte (Singh *et al.*, 2009; Srinivas *et al.*, 2009). Interestingly, it has been recently reported that autophagy has an essential regulatory role in the hypoxia-induced osteoclastogenesis (Zhao *et al.*, 2012). Zhao and colleagues observed an increase in osteoclast formation due to hypoxia-induced autophagy and determined it to be regulated via the HIF-1 α /BNIP3 dependent pathway (Zhao *et al.*, 2012). Stimulatory effects of autophagy on osteoclastogenesis were also reported in patients with rheumatoid arthritis (RA) (Lin *et al.*, 2013). The key player in the pathogenesis of RA - TNF α increased expression of Atg7 and LC3II in murine osteoclasts, whereas inhibition of autophagy either by knockdown of ATG7 or by treatment with Bafilomycin A1, strongly impaired osteoclast differentiation and expression of osteoclast-associated genes (Lin *et al.*, 2013). Furthermore, microgravity stimulation induced autophagy in preosteoclast cells, identified by elevated expression of Atg5, LC3 and Atg16 mRNA and protein levels, resulting in enhanced osteoclast differentiation (Sambandam *et al.*, 2014). Others also found that several key autophagy-related markers, including p62 were

significantly altered during RANKL-induced osteoclast differentiation (Li et al., 2014; Daroszewska *et al.*, 2010). Contrarily, the knockdown of p62 attenuated RANKL-induced expression of autophagy- and osteoclastogenesis- related genes, accumulation of LC3 and formation of TRAP-positive multinuclear cells (Li et al., 2014).

On the other hand, since osteoclasts are highly specialised and terminally differentiated, they may be particularly sensitive to the accumulation of aggregated proteins and depend on autophagy for survival. Indeed, formation of large cytoplasmic aggregates, which contained functionally coupled p62 and autophagy-linked FYVE domain containing protein (ALFY/ WDFY3) was noted in mature osteoclasts under conditions of nutrient deprivation (Hocking et al., 2010). Furthermore, treatment with inhibitor of autophagy – Bafilomycin A1 increased LC3 II protein levels in osteoclasts from P394L p62 mutant mice, compared with wild type osteoclasts, suggesting dysregulation of autophagy and enhanced autophagosome formation (Daroszewska *et al.*, 2011).

Although the precise mechanisms are still unclear it becomes apparent that autophagy has a role to play in regulating osteoclast formation and function. Having proposed a role for VCP in the autophagy pathway, it is next in line to study how the R155H mutation in VCP disrupts this process in the osteoclast. Finally, gaining a better understanding of the autophagy pathway in bone could potentially highlight new targets for development of therapeutic agents for osteolytic diseases.

6.2 Inhibition of the mTOR signalling suppresses both early and late stages of osteoclast differentiation

Mutations in the p62/SQSTM1 gene result in a classic form of PDB, which shows similar cellular pathology to that seen in PDB caused by VCP mutations (i.e. accumulation of protein inclusion bodies) (Chung *et al.*, 2011). Furthermore, both p62 and VCP are integral to ubiquitin-based protein degradation pathways and my earlier investigations suggest that they directly interact with each other in an autophagy-specific manner. Although, the mammalian target of rapamycin (mTOR) kinase is involved in the promotion of osteoclast formation, it is also a major switch between anabolic and catabolic processes (Glantschnig *et al.*, 2003), including regulation of autophagy. Therefore it is not a surprise that inhibition of mTOR activity increases cell death rate of mature osteoclasts, and significantly reduces bone resorption (Glantsching *et al.*, 2003).

To determine the importance of autophagy during osteoclastogenesis I examined the effects of inhibiting mTOR activity at different stages of osteoclast progenitor cells differentiation. For those experiments I used a murine monocytic cell line RAW264.7 – a useful cell model for differentiating osteoclast-like cells. I established that the optimal conditions for differentiation were to seed RAW264.7 cells at 300 000 – 600 000 cells per well (in a 12-well plate) and culture them in the presence of 100ng/ml RANKL for 6 days, following on large osteoclast-like (OCL) cells were observed (Fig. 6.2 B and D).

First, I examined the effects of rapamycin, known to modulate mTOR signalling, on RAW264.7 differentiation. The choice of inhibitor was prompted by interesting findings from recent studies, which suggested that rapamycin might play a role in regulation of osteoclast differentiation and activity (Smink *et al.*, 2012; Kim *et al.*, 2012). Smink and colleagues proposed that mTOR signalling controls transcription factor CCAAT/enhancer binding protein β (C/EBP β) isoform ratio that mediates the expression level of the monocytic transcription factor MafB, which then directs macrophage versus osteoclast differentiation (Smink *et al.*, 2009; Smink *et al.*, 2012; Kim *et al.*, 2012). Briefly, the investigators suggested that inactivation of the mTOR

pathway with rapamycin results in a translational shift of the C/EBP β toward LAP isoform that in turn restricts osteoclast formation (Smink *et al.*, 2009).

RAW264.7 cells cultured under differentiating conditions, as described above, were left untreated or were exposed to 220nM rapamycin on day 1, both day 1 and day 4, or day 4 of the cell culture. Significantly large reduction in the number of mature osteoclast-like (OCL) cells was noted in cultures treated with this drug on day 1. Nevertheless, an approximately 2-fold reduction (statistically significant – determined with a t-test) was also observed on day 4 and day 1 plus day 4 (Fig. 6.1E) when compared to a non-treated control.

In an independent experiment differentiating cultures were also treated with a vacuolar ATPase (V-ATPase) inhibitor bafilomycin A1, known to not only block the acidification of autophagosomes and thus inhibit degradation of proteinous inclusions, but also effectively inhibit bone resorption (Xu *et al.*, 2003; Quin *et al.*, 2012). RAW264.7 cells exposed to 100nM Bafilomycin A1 for over 24 hours exhibited apoptosis (over 90% cells detached, results not documented). These results were not unexpected since it has previously been shown that Bafilomycin A1 induces apoptosis of both RAW cells and osteoclasts in a dose dependent manner (Xu *et al.*, 2003). In contrast to Bafilomycin A1 treatment with Rapamycin did not affect cell viability during the period of the experiment.

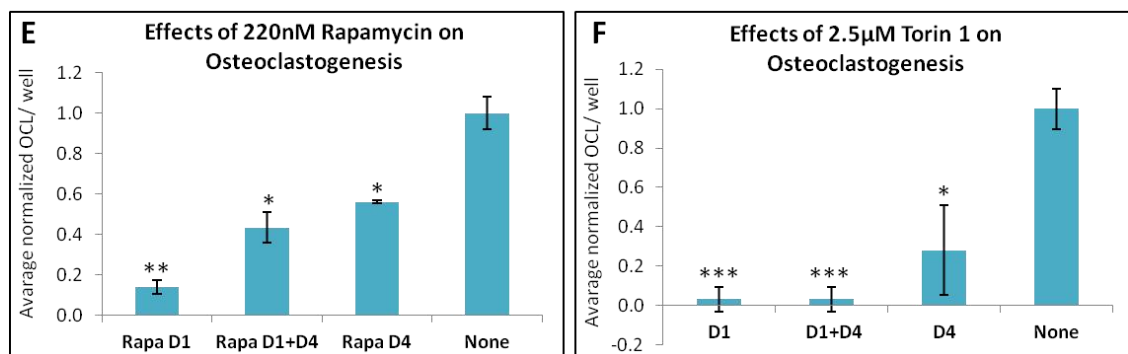
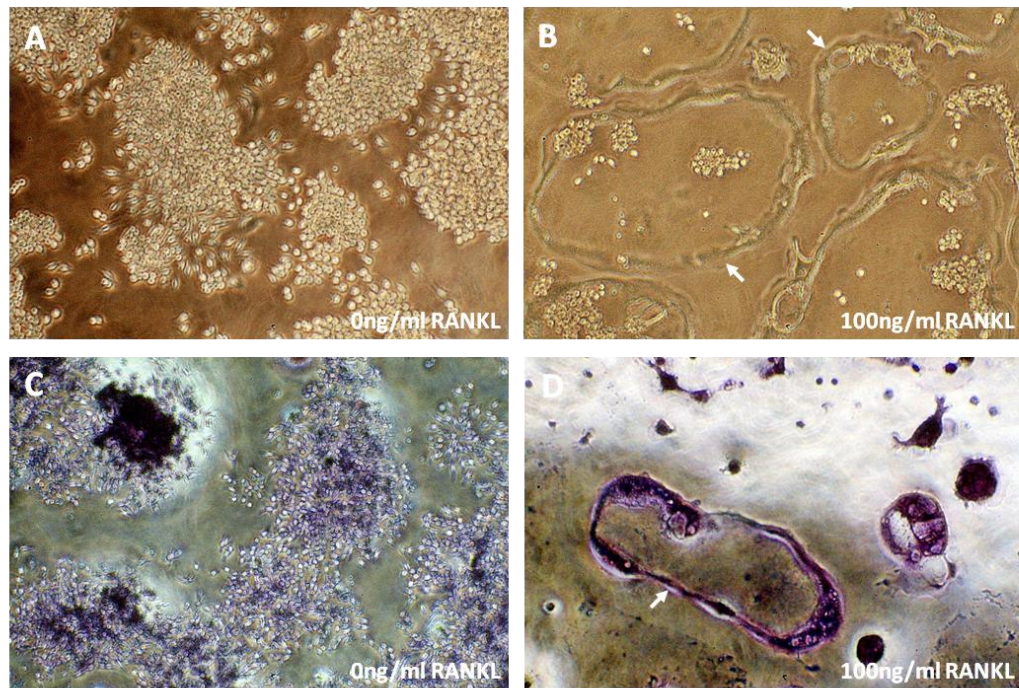


Figure 6.2. Inhibition of the mTOR signalling suppresses both early and late stages of osteoclast differentiation. RAW264.7 cells were cultured in the presence of 100ng/ml RANKL (R&D Systems) for 6 days, with ¼ of the media changed on day 3. Light microscopy images of non-differentiated macrophages/monocytes are shown in A and C and osteoclast-like (OCL) cells are captured in B and D (indicated by white arrows). In images C and D cells were stained for TRAP activity. Magnification is 400x.

Differentiating RAW264.7 cultures were treated with mTOR signalling inhibitors (Rapamycin or Torin 1) on either day 1, day 4 or both day 1 and day 4 (E, F). Cells were then fixed, stained for TRAP activity and scored for osteoclast-like cells (OCL) per well. In both graphs, data are shown as normalized Mean (SD) of OCL cells per well from independent experiments performed in four samples. None-treated cells were used as a positive control. Number of OCL per treatment sample was normalized to none-treated control. Unpaired t-test: *P<0.05, **P<0.01, ***P<0.001

Next I examined a more potent and selective ATP-competitive inhibitor of the mTOR serine/threonine kinase – Torin 1. When preparing for the experiment with Torin 1 I had to consider the effect that prolonged exposure to this drug will have on a regulatory feedback loop between mTOR catalytic complexes and phosphoinositide 3-kinase (PI3K). When mTORC1 (mTOR- complex 1) is inhibited for a prolonged period of times (over 5 hours), PI3K becomes hyper-activated and in turn promotes mTOR signalling cascade (Zhou *et al.*, 2010). Therefore to avoid such complication it is recommended to use this drug at a concentration of at least 250nM for long term experiments (Axon Medchem, #1833 Datasheet).

In this investigation RAW264.7 cells were maintained in the presence of 100ng/ml RANKL for 6 days, and were either left untreated or were additionally exposed to 1.67 μ M (Appendix, Fig A13) or to 2.5 μ M Torin 1 (Fig 6.2F) on day 1, both day 1 and day 4, or day 4 of the experiment. Such high concentration of the drug should ensure successful inactivation of the mTOR signalling cascade and enable accurate observation of the exhibited cell response. Indeed, a nearly complete inhibition of osteoclastogenesis was observed when differentiating RAW264.7 cells were treated with Torin 1 on day 1 as well as on both day 1 plus day 4 (Fig. 6.2F) and also a significant 3.5-fold reduction in OCL cell number was noted when treated on day 4 alone.

Together, these results indicate that inhibition of mTOR activity with either rapamycin or Torin 1 causes marked reduction in RANKL – dependent osteoclast formation of murine monocytic cell line RAW264.7 regardless of the treatment time. This further emphasizes the importance of mTOR signalling for osteoclast formation and survival but sheds little light on determining if activation of autophagy is the pathway responsible for this response.

6.3 Osteoclast differentiation from the primary Bone marrow derived macrophages.

Ultimately I wanted to elucidate to what extent does the disruption of autophagy pathway affect differentiation of Pagetic osteoclasts. I planned to isolate osteoclasts from VCP^{R155H/+} and VCP^{+/+} mice and test their sensitivity to various cellular and chemical factors, such as mTOR signalling or autophagy inhibitors.

At first, I have isolated bone marrow derived macrophages (BMDM) and spleen derived macrophages (SPLM) from 3- 6 month old mice as described in the Materials and Methods (Chapter 2; 2.14 'monocyte separation protocol'). Primary macrophages were plated at 5×10^5 cells per well in 6-well plates (well diameter of 34.8mm) and incubated with 25ng/ml M-CSF (Sigma, #M9170) and either 50 or 100ng/ml RANKL (Sigma, #R0525) for 5 days. No characteristically large osteoclast-like (OCL) cells were found in the culture plates on day 5. Moreover, on the 4th day of the culture many cells had detached exhibiting increased rates of cell death, thus emphasising that other factors could have been upsetting the growth conditions. Next, since monocyte-macrophage derived cells are more likely to successfully fuse into multinucleated osteoclasts when cultured at high cell density, I increased number of cells plated per area of a well. This time, BMDMs were plated at 1.5×10^5 cells per well and SPLMs at 2×10^5 per well in 96-well plates (well diameter of 5.4mm) and incubated in the presence of 25ng/ml M-CSF and 100ng/ml RANKL for 5-6 days. Nevertheless, yet again there were no OCL cells present in either of the macrophage cultures.

In order to trouble shoot the lack of differentiated cells and optimise the culture conditions I decided to further vary the plating cell number (BMDM at 1.5×10^5 to 3×10^5 and SPLM at 2×10^5 to 5×10^5 , in 96-well plates). Unfortunately, increasing the plating cell number had little to no effect on anticipated differentiation. Since the exhibited viability of the monocyte-macrophage derived primary cells was also in doubt, another factor I found in need of adjusting was foetal calf serum source and its preparation for the cell culture. It was discovered that serum (which came from the communal lab stocks) used so far had not been heat inactivated prior to being labelled as fit for the cell culture use and other users (members of adjacent labs) also

encountered some issues with the viability of their sensitive cell lines. At this point, I purchased calf serum from other outside sources (HyClone Europe and HyClone South America) heat inactivated it and tested on our sensitive primary cell lines. The HyClone calf serum from South America was the most effective in sustaining viability of these cells for over 6 days. Although, an early cell death of the primary macrophages was no longer an issue, cell differentiation was still not happening. Therefore I then decided to test the potency of the RANKL cytokine on the murine monocytic cell line RAW264.7. RAW264.7 cells were cultured in the presence of 25ng/ml, 50ng/ml or 100ng/ml RANKL (Sigma, #R0525) for 6 days, following on large osteoclast-like cells were observed only in cultures treated with 100ng/ml RANKL (Data not included). Given that commercially available RANKL is very unstable and last for approximately 3 months after reconstitution, a new recombinant mouse RANKL was ordered from the R&D Systems (#462-TEC-010). After testing the new cytokine on RAW264.7 cells I observed that as low as 5ng/ml of RANKL was sufficient to induce OCL cells formation in this cell line (Fig. 6.3 A-C).

Nevertheless, using new more potent stocks of RANKL on the primary cells was not as straight forward as on the RAW264.7 cells. I had to vary the method of isolating primary macrophages from the whole bone marrow (Chapter 2; 2.14) and eventually by adjusting the original protocol to incubating BMDM with M-CSF alone for the first 3 days (Chapter 2; 2.14 'The IUPS protocol') prior to exposure to RANKL I observed differentiation to OCL cells. Differentiated/ mature osteoclasts were present on day 7 of the differentiation stage (Day 1 when RANKL was first added) (Fig. 6.3 D-F). Importantly, primary macrophages were only able to differentiate in the presence of at least 10ng/ml of RANKL. Cells incubated with 5ng/ml RANKL did not differentiate (Fig. 6.3C).

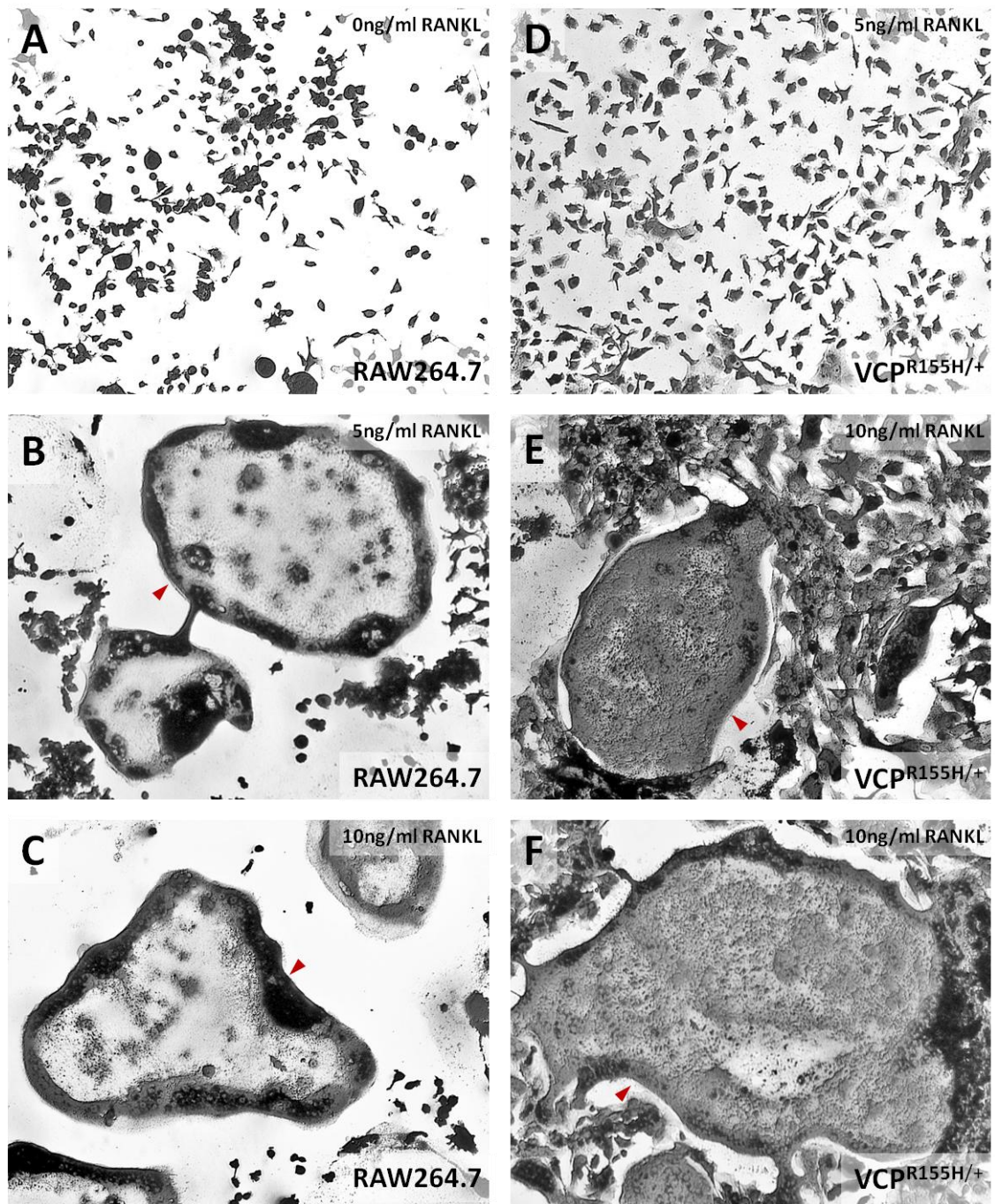


Figure 6.3. Differentiating osteoclasts from RAW264.7 cells and Bone marrow derived macrophages (BMDM). RAW264.7 (A-C) and primary BMDM from VCP^{R155H/+} mouse (D-F) were cultured in α -MEM alone (A) or in the presence of either 25ng/ml M-CSF and 5ng/ml RANKL (B, D) or 25ng/ml M-CSF and 10ng/ml RANKL (C and E-F). Light microscopy images of cells fixed and stained for TRAP activity on day 7 of differentiation show non-differentiated macrophages in A and D and osteoclast-like (OCL) cells in B, C, E and F (indicated by red arrowheads).

Although, initially successful I was unable to repeatedly and consistently differentiate OCLs from the macrophages of VCP mice in the following weeks. Therefore I decided to test the 'IUPS protocol' and RANKL (R&D Systems #462-TEC-010) on BMDM from mice with different genetic make-up. I repeated, but also varied, the differentiation protocol (plating cell number, cytokine concentrations) using BMDM from 14 week-old Balb/c female and 24 week-old CD-1 male; and continued with BMDM from >9 week-old VCP mice. With media changed every 2-4 days, I extended culture time to up to 10 days, but still there was no consistency with OCL cells observed.

Due to the time constraints and lack of success with the primary cells I have abandoned optimising osteoclast differentiation experiments in the favour of OCL-progenitor cells and concentrated on their responses to cell stress that challenges the UPS and Autophagy pathways.

6.4 Inducers of protein aggregation lead to increased NFκB activation and p65 nuclear translocation in the primary BMDM.

The Nuclear Factor kappa B (NFκB) family of transcription factors is implicated in the regulation of genes involved in various developmental processes, including promotion of osteoclastogenesis. The NFκB proteins are structurally related and form a variety of homo- and heterodimers, with the p50/p65 heterodimers being the most common (Soyza *et al.*, 2012). VCP has been identified as an important component of the NFκB pathway, as it binds ubiquitinated IκBα and shuttles it to the 26S proteasome for degradation (Daroszewska and Ralston, 2005). This in turn, allows NFκB for translocation to the nucleus and subsequently activation of various response genes involved in that particular NFκB pathway. Since one of the phenotypes of IBMPFD is Paget disease of the bone, it had been proposed that deregulation of the RANKL-NFκB pathway is the main cause for the observed bone phenotype (Ralston, 2008). As shown in Figure 6.4, this pathway contains both VCP and p62 at separate steps in the pathway. Nevertheless, I have shown that VCP and p62 interact either directly or indirectly as a complex during autophagy. In the case of IBMPFD this could mean that the disruption of a non-canonical autophagy based

pathway could lead to deregulation of NFκB signalling. Similar to the pathology seen in muscle and the brain, pagetic osteoclasts show nuclear accumulation of ubiquitin positive protein aggregates (Kimonis *et al.*, 2008: 2nd) suggesting that disruption of autophagy could be the underlying molecular lesion that gives rise to PDB.

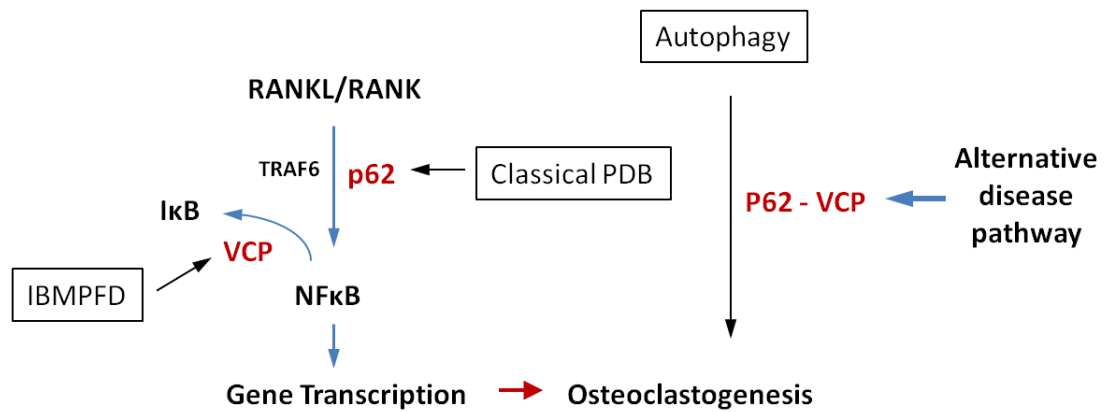


Figure 6.4. Disrupted regulatory pathways lead to over-activation of the NFκB signalling cascade and increased osteoclastogenesis. The RANKL cytokine binds to the RANK receptor and in the absence of inhibitors, downstream TRAF6 associates with RANK and p62 adapter protein. p62 stimulates downstream signalling that results in activation of target gene expression and initiation of osteoclast formation. VCP binds ubiquitinated IκB and shuttles it to the 26S proteasome for degradation. This in turn, allows NFκB for translocation to the nucleus and subsequently activation of various response genes involved in osteoclastogenesis. Mutations in *p62* gene result in a Classical PDB and mutations in *VCP* result in the IBMPFD-associated PDB. Alternatively VCP and p62 may interact directly in a different pathway (autophagy-linked) that leads to PDB when either is mutated.

Abnormal bone remodelling and cellular pathology in IBMPFD patients are suggestive of impairment at early stages of osteoclastogenesis. Delicate balance between signalling for cell survival or cell differentiation, with VCP responsible for keeping it in check, would be thus disrupted in osteoclast progenitor cells of IBMPFD-mutants. Importantly, precursor osteoclasts from PDB patients (Menaar *et al.*, 2000) and from the transgenic mice with the P392L p62 mutation (Hiruma *et al.*, 2008) have previously been reported to be hypersensitive to TNFα, RANKL and M-CSF. Notably, it has also been determined that PDB associated mutations in p62 cause increased NFκB signalling (Rea *et al.*, 2009).

To elucidate if IBMPFD mutations in VCP affect RANKL and TNF α stimulated NF κ B signalling in a similar manner to p62, I used bone marrow derived macrophages (BMDM) from wild type (*VCP^{+/+}*) and mutant (*VCP^{R155H/+}*) 3 month (11-15 weeks) old mice, which were cultured in the presence of 25ng/ml M-CSF, with media changed every 2-3 days. Once the cells were approximately 70-80% confluent, they were exposed to either 50ng/ml TNF α (Appendix, Fig A14) or 100ng/ml RANKL for 45 minutes to activate NF κ B signalling cascade. NF κ B measurements were obtained using an NF κ B p65 transcription factor ELISA assay that specifically detects active NF κ B in both the primary antibody p65 and a secondary horseradish peroxidase (HRP) conjugated antibody. I found that activation of NF κ B p65 was higher in *VCP^{R155H/+}* cells than in the wild type macrophages, induced by both TNF α and RANKL pathway activators, although the increase was only significantly different for TNF α (unpaired t-test, $p < 0.01$) (Fig. 6.5 A and B). At this point it is not known if this was a result of an impairment of autophagy or an upregulation of I κ B α degradation.

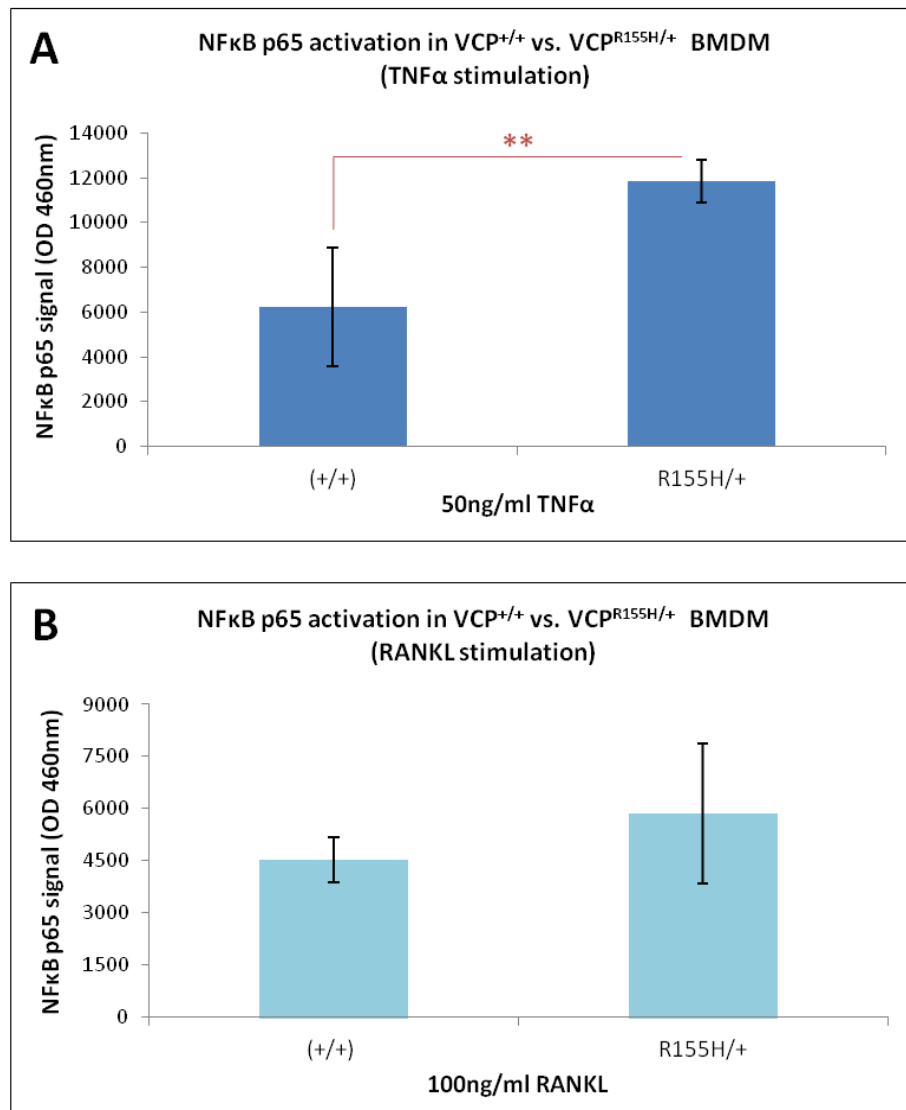


Figure 6.5. VCP mutant increases NFκB activation in BMDM. BMDM were separated from whole marrow cells of VCP^{+/+} and VCP^{R155H/+} mice and maintained in αMEM, supplemented with 25ng/ml M-CSF for required period of time, with media changed every 2-3 days. Once reaching 70-80% confluence the BMDM were exposed to either TNFα at 50ng/ml concentration (A) or 100ng/ml RANKL (B) for 45min to induce NFκB signalling cascade. Active NFκB p65 was measured using an NFκB transcription factor assay (Thermo Scientific #89859). The colour development was read at an absorbance (OD) level of 460nm. Each bar in (A) represents the mean (SD) for three different samples performed in triplicate; Unpaired t-test, **P<0.01. RANKL activation was tested on two different samples performed in triplicate; Mean (SD) (B).

Therefore, I next examined the effects of autophagy inhibition and induction on the TNFα-induced NFκB pathway. Here, BMDM from VCP^{+/+} and VCP^{R155H/+} mice were grown as described before and were either left untreated or treated with

1.5 μ M Torin1 (inducer of autophagy), 80nM Bafilomycin A1 (late stage inhibitor of autophagy) for 4 hours, or 100nM Wortmannin (early stage inhibitor of autophagy) for 3 hours (Fig. 6.6A). Thereafter, active NF κ B p65 measurements were obtained using an NF κ B transcription factor ELISA with absorbance read at 460nm.

A two-way analysis of variance determined that a type of treatment inflicted on BMDM had significant effect on the activation of NF κ B p65 ($F=19.92$, $p<0.001$). There was also a significant difference in TNF α induced activation of NF κ B between wild type (VCP^{+/+}) and mutant (VCP^{R155H/+}) macrophages ($F=17.82$, $p<0.001$). It was apparent that induction of autophagy through mTOR inhibition had little effect on NF κ B activation in both mutant and wild type macrophages (Fig. 6.6 B-C). Conversely, inhibition of the late phase of autophagy with Bafilomycin A1 dramatically increased NF κ B activation in osteoclast progenitor cells from VCP^{+/+} mice (Fig. 6.6B) and had significant effect on VCP^{R155H/+} BMDM (Fig. 6.6C). Wortmannin also significantly increased activation of NF κ B signalling in wild type macrophages (Fig. 6.6B). Interestingly, this treatment had little to none effect on mutant macrophages (Fig. 6.6C). Hence, it would appear that inhibition of autophagy in osteoclast progenitor cells results in increased NF κ B activation. Statistically observed influence of treatment type on the NF κ B p65 activation did not depend on whether the BMDM were wild type nor had the R155H mutation in VCP (ANOVA, $F=1.56$, $p=2.77$). Nevertheless, it would seem that the R155H mutation in VCP alone efficiently induces NF κ B activation, likely due to disruption of the basal macroautophagy pathway, although the exact mechanism remains to be elucidated.

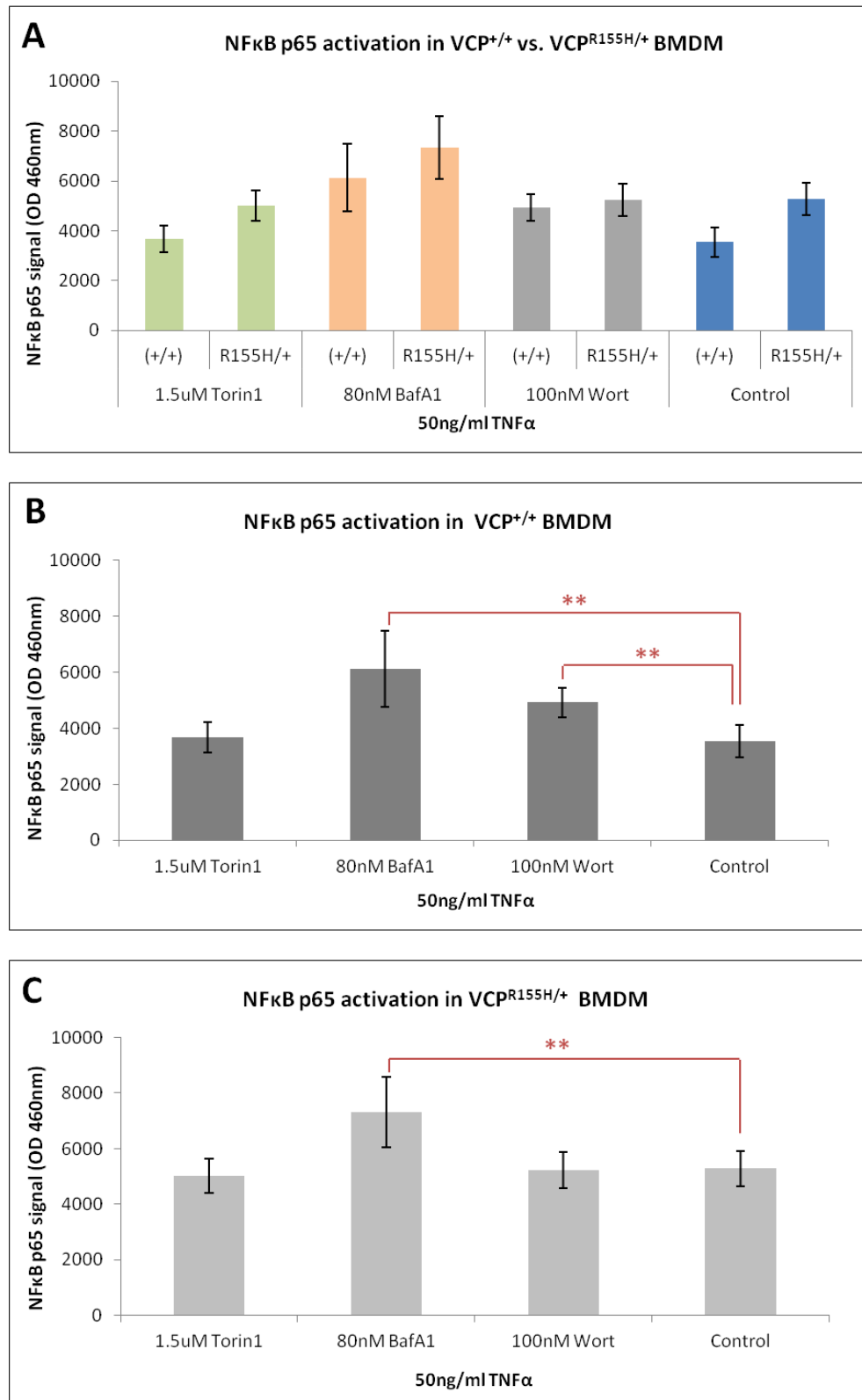


Figure 6.6. Autophagy inhibitors, Bafilomycin A1 and Wortmannin, increase NFκB activation in BMDM. BMDM were separated from whole marrow cells of VCP^{+/+} and VCP^{R155H/+} mice and maintained in αMEM supplemented with 25ng/ml M-CSF for required period of time, with media changed every 2-3days. On the day of experiment BMDM were either left untreated (Control) or treated with Bafilomycin A1 (Baf A1) or Torin1 for 4h, or

Wortmannin (Wort) for 3h at indicated concentrations. Control samples were incubated in medium alone supplemented with 25ng/ml M-CSF. For the last 45min of each treatment cells were exposed to TNF α at 50ng/ml concentration to induce NF κ B signalling cascade (A-C). Active NF κ B p65 was measured using an NF κ B transcription factor assay (Thermo Scientific #89859). The colour development was read at an absorbance (OD) level of 460nm. Each bar represents the mean (SD) from three different samples with triplicate. Significance was measured using two-way ANOVA, recording significant effect for genotype F(1,56)=17.82, p<0.001 and effect for treatment F(3,56)=14.92, p<0.001 (A). Analysis of variance was followed by comparison t-tests to assess the differences between the nontreated control in VCP^{+/+} (B) and VCP^{R155H/+} (C) cells exposed to described treatments, **P<0.01.

Having established that activation of NF κ B increases in BMDM treated with autophagy inhibitors, I was further interested in determining cellular levels of autophagosomal markers in those cells. From the BMDM extracts of 3 month-old VCP^{+/+} and VCP^{R155H} mice examined for the TNF α induced NF κ B activation I have immunoblotted a single representative sample from each Control, 1.5 μ M Torin1 and 80nM Bafilomycin A1 treatments (Fig. 6.7A). Due to low sample volume I was unable to analyse equal number of replicate samples for each treatment. Nevertheless, as seen in Figure 6.7 (A and C) macrophages from mutant mice appear more sensitive to Bafilomycin A1 treatment, accumulating more lipidated LC3II than wild type cells. The assembly of the essential for autophagosome formation Atg5-Atg12 (/Atg16) complex is also elevated in mutant cells, suggesting up-regulated early autophagy signalling (Fig. 6.7B). Contrary to expected, the autophagy flux appears normal in both VCP^{+/+} and VCP^{R155H} BMDM, incubated with the mTOR inhibitor (Fig. 6.7 A and B). In contrast, non-treated, TNF α activated wild type Control displays elevated expression of both LC3II and Atg5-Atg12 initiation complex, implying that those particular representative cells had increased signalling for autophagy at the time of experiment. To determine whether it was a treatment or a single sample specific response further replicates would need to be analysed and statistical significance recorded.

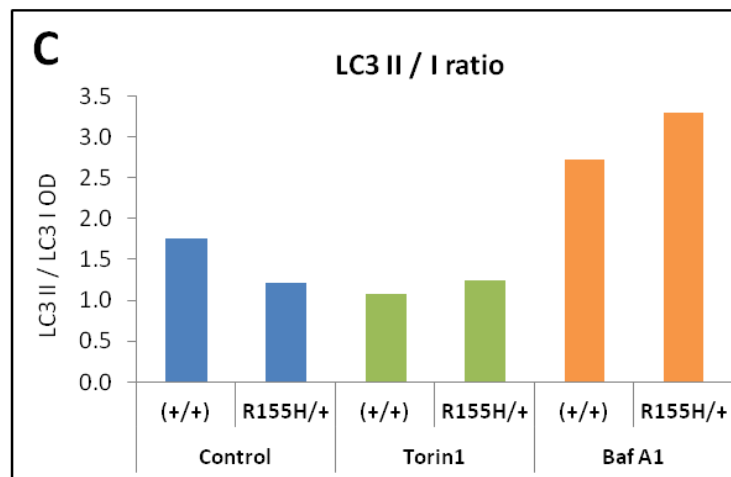
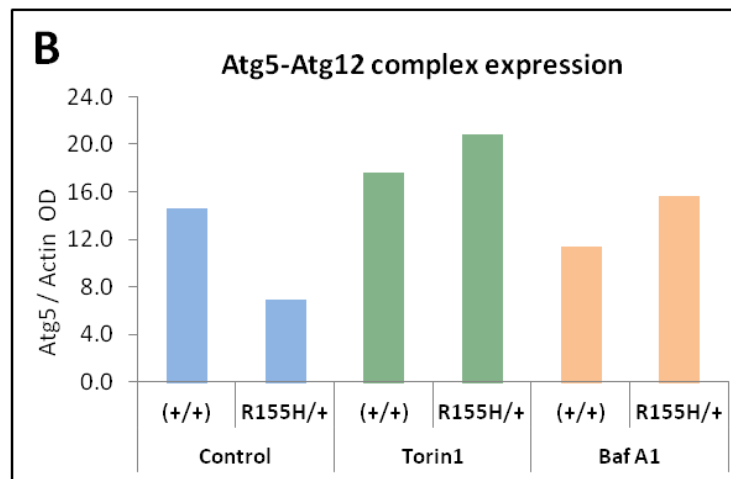
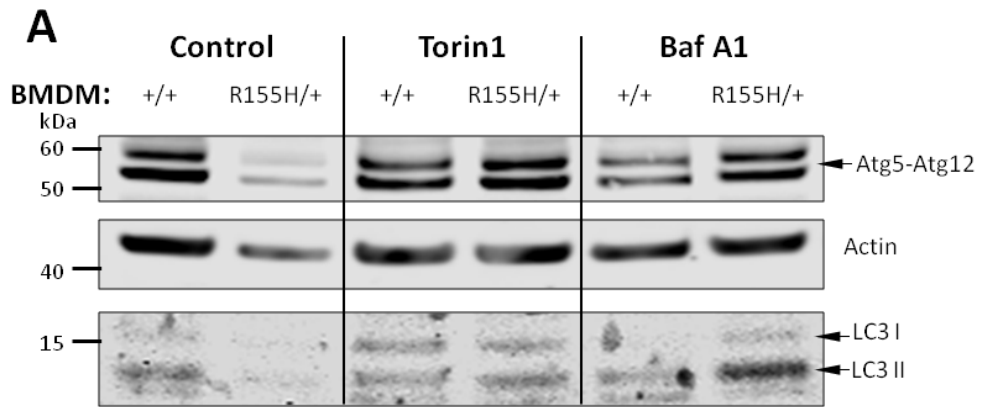


Figure 6.7. Autophagy inhibition leads to accumulation of LC3II-positive inclusions in BMDM. BMDM separated from whole marrow cells of VCP^{+/+} and VCP^{R155H/+} mice and maintained in α MEM with 25ng/ml M-CSF for required period of time, were either left untreated (Control) or treated with 80nM Bafilomycin A1 (Baf A1) or 1.5 μ M Torin1 for 4h. Control samples were incubated in medium alone supplemented with 25ng/ml M-CSF. For the last 45min of each treatment cells were exposed to 50ng/ml TNF α to induce NF κ B signalling cascade. Cell lysates were immunoblotted for LC3 and Atg5 (Atg5-Atg12 complex)

(A). Bar charts show Atg5/Actin (B) and LC3II/LC3I (C) optical density (OD) ratios in drug exposed, TNF α -activated macrophages. Presented data come from a single experiment with no replicates.

Collectively the above data suggest that increased accumulation of protein aggregates in osteoclast precursor cells has stimulating effect on the activation of NF κ B signalling cascade. This in turn results in enhanced osteoclastogenic potential of the BMDM, clearly observed in the IBMPFD cases. Therefore this would imply that mutations in VCP, resulting in disruption of autophagic processes, cause an increase in osteoclast differentiation as a direct effect of an overactive NF κ B. Interestingly, while inhibition of autophagy induces NF κ B activation, stimulation of this degradation pathway has little to no effect on the osteoclastogenic signalling cascade.

6.5 Discussion

Previously I have shown that VCP and p62 interact directly in early autophagy and there is a complex relationship between the stability/aggregate status of VCP and the autophagy/proteasome axis. Further to this I have found significant differences in how the R155H mutation effects the action of VCP in these new functions. Overall, this has led me to consider the possibility that the NF κ B pathway may not be the molecular lesion in PDB and that the cause could be the result of a defect in actions of the VCP/p62 complex, leading to deregulation of autophagy and ultimately PDB pathology. Therefore, to determine the importance of autophagy during osteoclastogenesis, I first decided to examine the effects of inhibiting mTOR activity at different stages of osteoclast progenitor cells differentiation. I observed the rate of differentiation of RAW264.7 cells cultured with either rapamycin or Torin1 on various days of the cell culture and found that the induction of autophagy at any stage of osteoclastogenesis has an inhibitory effect. Those results were not that surprising since other observations reported in the field suggest that modulation of mTOR signalling has a major effect on the development and function of osteoclasts.

Suppression of the m-TOR pathway is a requirement for osteoprotegerin (OPG)/ osteoclastogenesis inhibitory factor production in bone marrow stromal cells

(Mogi and Kondo, 2009). Therefore, it is not surprising that inhibition of mTOR activity results in increased cell death rate of mature osteoclasts, and significantly reduced bone resorption (Glantsching *et al.*, 2003; Indo *et al.*, 2013). Recent studies also show that mTOR signalling controls transcription factor CCAAT/enhancer binding protein β (C/EBP β) isoform ratio, which is responsible for regulating osteoclast differentiation and bone homeostasis (Smink *et al.*, 2009; Smink and Leutz, 2010). C/EBP β was found to be expressed as two different protein isoforms of variable amino terminal length, termed LAP and LIP. Switch between C/EBP β isoforms mediates the expression level of the monocytic transcription factor MafB, which directs macrophage versus osteoclast differentiation (Kim *et al.*, 2007; Smink *et al.*, 2009) (Fig. 6.8). Inactivation of the mTOR pathway with rapamycin results in a translational shift of the C/EBP β toward LAP isoform that in turn restricts osteoclast formation. Rapamycin is therefore believed to be a promising therapeutic agent for treating osteolytic bone diseases. Besides, rapamycin and its derivatives have already proven to effectively decrease tumour cell proliferation when tested in clinical trials for treatment of different types of cancer (Chan *et al.*, 2005; Berenson and Yellin, 2008; Lee *et al.*, 2014).

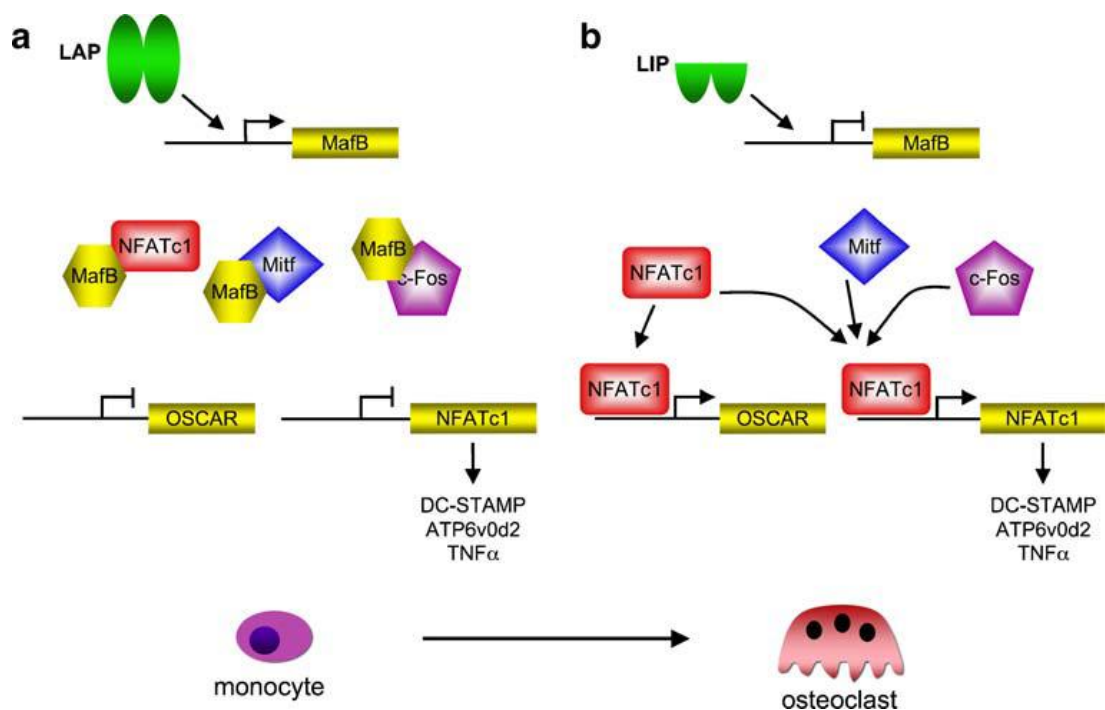


Figure 6.8. *C/EBP β is a master switch in osteoclast differentiation.* **a)** The LAP isoform induces expression of MafB, which binds to and inactivates NFATc1, Mitf and c-Fos

transcription factors. This in turn, prevents osteoclast differentiation. **b)** The LIP isoform inhibits MafB expression. This allows for the osteoclast transcription factors to activate target genes (OSCAR and NFATc1) and osteoclast differentiation. (Smink and Leutz, 2010)

Interestingly, rapamycin, alone or in synergy with TGF β , was also shown to induce osteoclastogenesis of RAW264.7 cells in the presence of RANKL (Shui *et al.*, 2002). Moreover, preceding study proposed that rapamycin decreases protein levels of osteoprotegerin (OPG), a decoy receptor for RANKL, but increases RANKL production in bone marrow stromal cells (Hofbauer *et al.*, 2001). These findings suggest that immunosuppressants have direct effect on osteoclast progenitor cells, but contrast with observations of the more recent studies (Kim *et al.*, 2007; Smink *et al.*, 2012). Therefore it is likely that action of rapamycin (and other mTOR inhibitors) varies in early and late stages of osteoclast differentiation.

Although not examined in my investigations, proteasome inhibitors such as MG132 were shown to directly impair osteoclast formation and function through the disruption of key RANKL-mediated signalling cascades (Ang *et al.*, 2009). Namely, altered the subcellular targeting and distribution of p62 and TRAF6, resulting in the accumulation of p62 in osteoclast like-cells. Additionally, proteasomal inhibition also blocked RANKL-induced NF κ B activation by preventing I κ B degradation and nuclear translocation of p65 (Ang *et al.*, 2009). Notably, there appears to be a mechanistic link between protein degradation pathways and osteoclast formation. Further examination of both autophagy and proteasome regulators, including the use of animal models, will be required to fully elucidate their overall effect.

NF κ B is activated by RANKL both in RAW264.7 cells and in monocytes (Hsu *et al.*, 1999) and is required for osteoclast formation *in vivo*. Although, the extended aim of this project was to study osteoclastogenesis in the IBMPFD mouse model and the sensitivity of osteoclast precursors to protein degradation pathways modulators, I encountered some difficulties with optimising the differentiation protocol for the primary bone marrow derived macrophages (BMDM). Keeping in mind that primary BMDM are known to be quite temperamental and difficult to differentiate under basal cell culture conditions, I tested a few standard protocols, which had been successfully applied in many key publications in the field (Chapter 2, 2.14). In addition

to this, I have changed growth media and ordered new foetal calf serum stocks; I have also tested RANKL cytokines from different suppliers, recommended by other scientists in the field. In addition, I have tested all of the above on BMDM from mice with different genetic make-up, such as Balb/c (~3mth/14wks-old female) and CD-1 (6mth/24wks-old male). Nevertheless, due to the time constraints and lack of success with the primary cells I was neither able to further examine the effects of inhibiting mTOR activity at different stages of osteoclast progenitor cells differentiation nor prepared to determine how osteoclasts respond to cell stress that challenges the UPS and macroautophagy pathways.

Given the difficulties getting primary BMDM to undergo osteoclastogenesis, I have instead concentrated on non-differentiated macrophages from the wild type (VCP^{+/+}) and heterozygous VCP^{R155H/+} mice. I used those cells to determine if there was any difference in the NFκB pathway activation in response to either RANKL or TNFα. I found an increased activation of NFκB in response to both RANKL and TNFα in mutant cells, although only the TNFα response was significantly increased. Seeing that the TNFα response was the most robust, I then examined the effects of either inducing or inhibiting autophagy on the TNFα activation of NFκB. Interestingly, the induction of autophagy by Torin1 increased the level of NFκB activation in wild type cells (compared to non-Torin1 treated wild type cells) but did not further increase the activation in the mutant cells. As a result there was no significant difference in the NFκB activation between wild type and mutant cells after Torin1 treatment. On the other hand, in wild type cells the inhibition of early autophagy with Wortmannin or late autophagy by Bafilomycin A1 treatments significantly increased NFκB activation. While in mutant cells only Bafilomycin A1 treatment significantly increased NFκB activation, and similar to Torin1 treatment, Wortmannin treatment did not further increase NFκB activation. These observations demonstrate that selective inhibition potentially attenuate osteoclastogenesis activation in wild type cells but also to certain extent in mutant cells.

Furthermore, my initial examination of early (Atg5) and late (LC3II) autophagy markers in BMDM, in response to TNFα stimulation and autophagy induction or inhibition, suggests that VCP mutation causes a blunted response to TNFα induced

autophagy. In cells just treated with TNF α the levels of Atg5 and LC3II were lower in the VCP mutant than those of wild type cells. Conversely, when autophagy was inhibited by Bafilomycin A1, the Atg5 and LC3II levels were higher in mutant than those in wild type cells. This would fit with the earlier NF κ B data that show no effect on NF κ B activation in mutant cells when early autophagy is inhibited with Wortmannin.

Nevertheless, the increased sensitivity of mutant macrophages to either TNF α or RANKL seems to be a defect in early autophagy (potentially a new role for VCP identified in Chapters 3 to 5) implied by the lack of autophagy induction in mutant cells after cytokine treatment. This would also fit with the potential role of p62 in PDB and that both p62 and VCP mutations cause the same molecular defect in cytokine induced activation of autophagy. In light of these findings it is tempting to speculate that the possible disease mechanism could be decreased RANK receptor recycling, due to impairment of autophagy, which in turn would lead to increased downstream signalling. This is not that unlikely since VCP has been previously shown to regulate the recycling of dNRAMP receptor, facilitating the SINV infection of Human cells (Panda *et al.*, 2013).

In summary, the results presented in this study further substantiate the implications of a likely cross-talk between degradation pathways and RANK-mediated signalling in osteolytic bone disease.

CHAPTER 7

DISCUSSION

CHAPTER 7: DISCUSSION

7.1 The VCP binds to p62 and is involved in the clearance of ubiquitinated protein aggregates by autophagy

Mutations in the VCP gene lead to the autosomal dominant, multisystem disorder named IBMPFD, characterised by an Inclusion Body Myopathy (IBM), Paget disease of the bone (PDB) and Frontotemporal dementia (FTD) (Watts *et al.*, 2004). Cellular degeneration and ubiquitinated protein inclusions, that are also positive for p62 and LC3 (Tresse *et al.*, 2010), unify the pathologies of three disparate tissues (muscle, bone and brain) in IBMPFD. Unlike other inclusion body disorders, like the expanded polyglutamine diseases, mutant VCP does not make up the major component of the accumulated protein in IBMPFD (Higashiyama *et al.*, 2002; Schroder *et al.*, 2005). VCP is also found in other inclusion diseases but only in small concentrations (Mori *et al.*, 2012) and is not used as a major diagnostic marker in the histopathology of these disorders. Interestingly, mutations in p62 can lead to an inherited form of PDB (26.5% of familiar PDB in Caucasian patients) and is associated with 8.9% of sporadic incidences in the UK (Hocking *et al.*, 2002), which phenotypically is almost identical to the PDB resulting from VCP mutations. At the molecular level both mutant VCP and p62 based PDB have ubiquitin-positive inclusions within the nuclei of pagetic osteoclasts (Leach *et al.*, 2006; Kimonis *et al.*, 2008). In other inclusion body disorders, p62 is used as a histopathology marker, particularly for neurodegenerative disorders (Homma *et al.*, 2014; Nakano *et al.*, 2004; Nakaso *et al.*, 2004), although in these disorders p62 is normal and not mutated. This would suggest that p62 has an important role in the pathways that are deregulated as a result of mutations in those particular disease genes for the Alzheimer's, Parkinson's or Huntington's disease. The function of p62 has been an area of intense study in recent years and now it has been shown that p62 plays an important role in early autophagy (Itakura and Mizushima, 2011). Further to this, it has been shown that VCP and p62 both play an important role in the equilibrium of protein homeostasis by the proteasome and autophagy (Korolchuk *et al.*, 2009), although the exact mechanism of this interaction has not been yet elucidated.

In Chapter 3 I have shown that wild-type VCP co-localises with numerous p62 and LC3 (a binding partner of p62) - positive vesicles that accumulate following Bafilomycin A1 treatment. I have also observed a similar association in cells exposed to the autophagy inducer – Torin 1. These observations contrast with previously reported findings, where researchers found neither wild-type nor mutant VCP to associate with LC3-positive vesicles (Tresse *et al.*, 2010). However, their experiments were performed in basal conditions, whereas I noted the described association of VCP with p62 and LC3 under different conditions of autophagy induction. Tresse and colleagues recorded a nearly 3.5 fold accumulation of p62 protein and accumulation of large autophagic vesicles in MEFs following the RNAi-mediated VCP knockdown (Tresse *et al.*, 2010). Expression of disease-associated VCP mutants (R155H and A232E) also caused this autophagy defect (Ju *et al.*, 2009; Tresse *et al.*, 2010). Similarly, I found a significant increase in polyubiquitinated aggregates in normal cells expressing the R155H mutant VCP, but not in cells expressing a catalytically inactive DKO mutant VCP. However, cells expressing aggregate-prone expanded polyglutamines both R155H and DKO mutant VCP show increased aggregation of ubiquitinated substrates. These observations suggest that mutations in VCP reduce efficiency in degradation of aggregate-prone polypeptides, which partially explains cellular pathology seen in the IBMPFD patients. I also recorded a significant accumulation of p62 in muscle tissue from adult VCP^{R155H/+} mice (the IBMPFD mouse model) but not in the wild-type litter mates. I observed that p62 co-localises with wild-type VCP to large aggregates that formed in cells expressing expanded, pathogenic glutamine repeats (Q79, degraded via autophagy) but not in cells expressing control polyglutamines (Q35). These data support the previously published results where wild-type VCP-GFP co-localised with FLAG-tagged Q79 aggregates but not with Q35 (Manno *et al.*, 2010). Further to this, I show accumulation of large (over 1µm in diameter) LC3-positive aggregates in cells expressing mutant VCP and polyglutamines (in both Q35 and Q79 – expressing cells) and thus speculate these to be autophagosomes (degraded via autophagy). The autophagosomes that accumulate due to impaired VCP function contain ubiquitin-positive contents (Tresse *et al.*, 2010), which the authors attribute to defective autophagy maturation (processes that occur after autophagosome formation).

Interestingly, the structural alteration of the N domain of VCP was reported to induce impaired maturation of autophagosome (Yamanaka *et al.*, 2012). Likewise, a xanthohumol (XN, a prenylated chalcone present in hops and beer) has been found to directly bind to the N-domain of VCP, resulting in increased LC3-II and p62 accumulation, a consequence of a block of autophagosome maturation (Sasazawa *et al.*, 2012). In contrast, IBMPFD – associated mutations (R155H, A232E) did not cause detectable impairment in ubiquitin-dependant degradation by the proteasome (including the ERAD and UFD pathways) (Tresse *et al.*, 2010). Thus, to further validate my data, one could observe distribution of VCP and LC3 positive-vesicles in cells expressing expanded, aggregate-prone polyglutamines and treated with proteasome inhibitors (such as MG132 or Lactscystin). In such conditions, VCP vesicles would be expected to associate with LC3-positive autophagosomes, mirroring the results described in this study. In light of the hypothesis that VCP is a critical factor for the degradation of polyubiquitinated protein aggregates one could also observe the subcellular localisation/organisation of p62 and LC3 in cells treated with puromycin. Puromycin treatment increases formation of truncated and misfolded proteins in a cell, dramatically accelerating the formation of large cytoplasmic bodies containing polyubiquitinated proteins. The co-localisation of VCP to puromycin-induced inclusion bodies can also be examined by immunofluorescence.

However, Korolchuk and colleagues postulated that autophagy inhibition may in fact impact on flux through the ubiquitin-proteasome system (UPS) (Korolchuk *et al.*, 2009). This result being largely due to accumulation of p62 (normally degraded via autophagy), which in turn inhibits the clearance of ubiquitinated proteasome substrates (Korolchuk *et al.*, 2009). Conversely, impairment of the UPS leads to increased levels of the UPS client proteins, such as p53, and this result in the autophagy upregulation (Ding *et al.*, 2007; Du *et al.*, 2009). The p62 siRNA reduces ubiquitin-primed GFP (Ub^{G76V}-GFP, an ubiquitin-proteasome activity reporter) and p53 (endogenous proteasome substrate) levels in autophagy-deficient cells (Korolchuk *et al.*, 2009). In agreement with this, knockdown of p62 neither had an effect on autophagosome number nor did affected autophagic flux (by measuring levels of LC3-II) in cells in which autophagosome degradation was inhibited (Komatsu *et al.*, 2007; Korolchuk *et al.*, 2009). Likewise, p62 knockout mice had no

abnormalities in autophagy (Komatsu *et al.*, 2007). In relation to aggregate-prone, disease-associated polyglutamines, p62 overexpression increased aggregation and toxicity of polyglutamine-expanded huntingtin fragment (httQ74) in autophagy-deficient cells and this effect was abrogated via VCP overexpression (Korolchuk *et al.*, 2009). Knockdown of VCP in normal cells compromises the clearance of Ub^{G76V}-GFP and polyglutamine aggregates (Wojcik *et al.*, 2006; Kobayashi *et al.*, 2007). In contrast, increased expression of wild-type VCP reduces polyglutamine inclusion bodies in the *Drosophila* model (Koike *et al.*, 2010). Likewise, I have found that a sole over-expression of wild-type VCP decreases the concentration of insoluble, ubiquitinated protein aggregates in normal cells (possibly increasing the normal turnover of ubiquitinated client proteins), whereas R155H mutant VCP-expressing cells showed a significant increase in ubiquitinated aggregates. A recent study demonstrated that wild-type Cdc48 (Yeast VCP equivalent) helps maintain the solubility of the misfolded insoluble substrates after ubiquitination and prior to proteasomal degradation (Gallagher *et al.*, 2014). Similarly, VCP has been shown to prevent the aggregation of denatured luciferase *in vitro* and *in vivo* (Song *et al.*, 2007) and to re-solubilise heat denatured luciferase from insoluble aggregates as well as facilitate the clearance of pre-formed polyglutamine inclusions (Kobayashi *et al.*, 2007). Contrary, the loss of Cdc48 function led to increased misfolded protein insolubility and *in vivo* inclusion formation (Gallagher *et al.*, 2014). Similarly, my results demonstrate increased aggregation and reduced solubility of ubiquitinated substrates in cells expressing VCP mutant protein. These data further implies that VCP plays an important role in the degradation of aggregate-prone proteins and that mutation in VCP make cells more sensitive to protein aggregation. It was proposed that VCP competes with p62 for ubiquitin binding, thus overexpression of p62 may act by displacing VCP from complexes with ubiquitinated proteins (Korolchuk *et al.*, 2009). Perhaps, by skewing the VCP/p62 ratio it is likely to result in stopped/slowed transfer of ubiquitinated substrates from VCP to p62 and hence the activation of autophagy as shown by the increase of p62 in cells where autophagy is impaired.

The VCP forms a functionally active homo-hexameric complex with each monomer consisting of four specific domains: the N-terminal domain, 2 centrally located ATPase domains (D1 and D2) and C-terminal domain. The N-domain and the C-

terminus on VCP are mainly responsible for the interactions with various VCP binding partners. The N-terminal binding site was described a general site of interactions for many cofactors with the ubiquitin regulatory X (UBX) and ubiquitin D (UBD) domain-containing protein cofactors, such as Ubx2 and Ufd1/Npl4 respectively (Chapman *et al.* 2011). Nevertheless, mutations within the N-domain that result in either R93C, R95G or R155H amino acid changes did not affect the binding of cofactors in an *in vitro* protein binding assay (Huberts *et al.*, 2007; Fernandez-Saiz and Buchberger 2010). In fact, it was reported that R95G and R155H mutants have elevated binding affinities for p47 and UFD1-Npl4 complex *in vivo* (Fndez-Saiz and Buchberger 2010). While p62 has many motifs and binding domains it remains unknown if it contains any motifs or domains that have been identified in other proteins that bind to VCP. Although I have not identified any known VCP binding motifs/domains in p62, this did not rule out the potential of p62 to bind to VCP, either directly or indirectly. The finding that VCP co-precipitates with p62 in cells in which autophagy was induced with Torin 1 and in cells expressing pathogenic (Q79) polyglutamines, suggests that VCP plays a role in the early stages of autophagy (by interacting with p62) and that it has an active role in the degradation of ubiquitinated substrates by autophagy (Fig. 4.7). In addition, mutations in VCP did not appear to abrogate its affinity for binding to p62, though further studies are required to address this phenomenon in more detail. Nevertheless, these findings are significant as they directly link VCP with components of the autophagy pathway and for the first time show that p62 either is a VCP binding partner or at least forms a complex with VCP. This could have implications for other proteinopathies caused by mutations in either VCP or p62. Therefore, the future investigations would ideally elucidate which VCP regions/domains are involved in the binding of p62, and in the reverse which p62 regions/domains are involved in the binding of VCP. These experiments could utilise bacterial plasmids expressing truncated versions of VCP, which I have described in Chapter 4 of this study, translate them *in vitro* and subject to pull down experiments. It would also be interesting to see how the mutations in p62 affect its binding affinity for VCP as this will give the additional insight into p62-associated diseases. Although, the molecular lesions, caused by VCP mutations, seem to affect late autophagy, my data show that VCP uses ubiquitin based interactions as part of the early autophagy

(Fig. 4.7). Additionally, the extent of autophagy impairment may also dictate the severity of compromised flux through the UPS. I speculate that mutant VCP is more likely to sequester ubiquitinated UPS client proteins into aggregates preventing them from being delivered to or into the proteasome. This hypothesis would potentially explain accumulation of aggregates in cells expressing polyubiquitinated Q35 glutamine repeats, normally degraded by the proteasome, and also to some extent the cellular pathology observed in the IBMPFD patients. Indeed, inclusions containing ubiquitinated proteins are a common pathologic feature found in all mutant VCP disease-affected tissues (Weihl *et al.*, 2009). Overall, I propose that formation of altered VCP/p62 complexes, which lead to disease pathogenesis, result in an impairment of coordination between the UPS and autophagy. This in turn causes accumulation of ubiquitinated substrates and protein aggregates implied in the broad array of proteinopathies that result from mutations in either VCP or p62.

7.2 VCP stability is linked to p62 instability

Protein degradation is essential for the regulation of protein homeostasis (proteostasis) and triggers a variety of processes, such as cell cycle progression and cellular signalling. All eukaryotic cells use the following two systems for protein degradation: the ubiquitin-proteasome system (UPS) and the autophagy-lysosome system. The UPS is used for selective degradation of short lived and abnormal or misfolded proteins following labelling with Lys-48-linked polyubiquitin chains mediated by ubiquitin-protein ligases (Goldberg, 2003). Whereas the lysosome mainly degrades extracellular and plasma membrane proteins brought there by endocytosis and cytoplasmic components delivered by autophagy. VCP often acts between the ubiquitin-protein ligase and the proteasome, coordinating recruitment and targeting of ubiquitinated substrate proteins to the proteasome (Mayer *et al.*, 2012). The evidence also implies that VCP is necessary for lysosomal protein degradation via autophagy (Ju *et al.*, 2009; Tresse *et al.*, 2010) and I have shown that it interacts directly with key components of the autophagy pathway (specifically that it binds directly to p62). The p62 is an ubiquitin-binding protein, which targets ubiquitinated substrates to autophagosome, is itself degraded by autophagy and accumulates when autophagy is blocked (Bjorkoy *et al.*, 2005; Korolchuk *et al.*, 2009).

The VCP is an interesting protein which uses its ATPase activity to extract substrates from multiprotein complexes (Kobayashi *et al.*, 2007) and also to transport abnormal proteins into aggregates (Manno *et al.*, 2010). It binds to a variety of adaptor proteins (including p62) and carries out a multitude of processes within the cell, conducted through ubiquitin based interaction, but until now its degradation or stability has not been studied. I found that VCP availability in the cell is directly linked to the levels of p62 (is regulated in a p62 dependent manner). In p62-deficient cells, with functional autophagy (Komatsu *et al.*, 2007), VCP is sequestered into the insoluble aggregated fraction, likely as the result of VCP collecting and aggregating polyubiquitinated substrates to be degraded by autophagy in the absence of p62. This could partially explain why the knockdown of p62 neither had an effect on autophagosome number nor did affected autophagic flux – normal autophagy in these cells (Komatsu *et al.*, 2007; Korolchuk *et al.*, 2009). It was also significant that, in the absence of p62 over an extended time period, VCP is released back to the soluble fraction, possibly further compensating for the loss of p62 by shuttling substrates to the proteasome for degradation. This finding helps to explain how p62 siRNA rescues the increased levels of soluble ubiquitinated proteasome client proteins in autophagy-deficient cells (Korolchuk *et al.*, 2009). Whereas, whilst the proteasome is inhibited, the VCP levels stably decrease suggesting that proteasome inhibition might increase the efficiency of soluble VCP degradation and stop the release of the insoluble pool of VCP. Therefore, the likely hypothesis is that soluble pool of VCP is either being degraded by autophagy (and not the proteasome) or it is being sequestered to the growing (insoluble) aggresome (vimentin-positive, ubiquitinated large aggregates; Johnson *et al.*, 1998) resulting from the proteasomal inhibition. Interestingly, I have noted that overexpression of wild-type VCP in cells halts degradation of p62, possibly only for a limited time period (though further studies are required to address this) whilst it complexes with p62, to capture and deliver polyubiquitinated substrates to the autophagy-lysosome machinery for degradation. Thus, elimination of the effects of p62 overexpression by overexpressing the wild-type VCP (Korolchuk *et al.*, 2009) is likely to act through increased VCP/p62 complex formation, which in turn allows for normal degradation of both the UPS ubiquitinated substrates and protein aggregates. Therefore I favour a model in which VCP and p62, rather than compete for ubiquitin

binding are functionally coupled and dictate the fate of ubiquitinated proteins within the cell.

Disease-associated mutant VCP proteins are reported to retain a normal hexameric structure (Niwa *et al.* 2012) but exhibit altered communication between the N and D1 domains (Fernandez-Saiz and Buchberger 2010). This could manifest as a disruption in the normal control of the N-domain where many substrates bind (Fernandez-Saiz and Buchberger 2010) and result in either increased or decreased binding profile of VCP. Indeed, IBMPFD VCP mutants exhibit elevated binding affinities for Ufd1-Npl4 as well as for p47 *in vitro* (Manno *et al.*, 2010) but decreased binding to a UBX cofactor – UBXD1 (Ritz *et al.*, 2011). The enhanced cofactor binding ability also enhances binding of ubiquitinated protein substrates and potentially also the formation of polyubiquitinated aggregates (Manno *et al.*, 2010). Although, as outlined in the Chapter 4, the binding affinity of mutant VCP protein to p62 appears normal, result is increased aggregation of polyubiquitinated substrates. Instead, my hypothesis is that the mutant VCP is unable to release its substrates and hence is being aggregated as a result. The data presented in this study suggests that R155H-VCP is less likely to be released from the insoluble aggregate pool and as a consequence of this decrease the levels of soluble p62 (most likely by accumulation in autophagosomes). Previously it has been shown that Cdc48 (yeast VCP) requirement for facilitating the proteasomal degradation of some ubiquitin ligase San1 substrates correlates with the insolubility of this substrate (Gallagher *et al.*, 2014). It is possible that in cells in which autophagy is compromised and as result p62 is accumulated, VCP's requirement for the degradation of ubiquitinated substrates increases. An earlier study demonstrated that IBMPFD-causing mutant VCPs possessed elevated ATPase activities (tested biochemically) which the authors link to the acceleration of abnormal protein aggregate formation in cells; although this effect is not directly attributed to the VCP's cofactor-binding abilities (Manno *et al.*, 2010). Additionally, the A232E mutant VCP, which represents the severest clinical phenotypes (Watts *et al.*, 2004), demonstrated the highest ATPase activity (Manno *et al.*, 2010). It would be interesting to examine the availability of this particular mutant protein in the cell and its effect on p62 degradation/stability. Further work could also include an examination of p62 stability in cells in which VCP is down regulated.

7.3 P62/VCP – dependant autophagy regulates osteoclastogenesis

Since the identification of both VCP and p62 being involved in classical Paget disease of the bone (PDB), there has been a lot of speculation in how they cause the disease and what pathways/roles they have in common (Ralston, 2008; Chung *et al.*, 2011). The metabolic hyperactivity in focal bone resorption is the main feature of Paget's disease. This primary abnormality is believed to be a result of abnormal osteoclasts (the principal resorptive cells of the bone) which are increased in size, contain many more nuclei than normal osteoclasts and are overactive. Therefore, it has been believed that the common pathway was the RANKL-NF κ B pathway (responsible for osteoclast differentiation) as both p62 and VCP are involved at different points within this pathway (Daroszewska and Ralston, 2005). Furthermore, causative mutations in the VCP localise within or close to the region in the N-domain known to be involved in ubiquitin (ub) – binding (Dai and Li, 2001; Watts *et al.*, 2004). Likewise, PDB-causing mutations in the *SQSTM1* gene also affect the ub-binding domain of the gene product – p62 (Hocking *et al.*, 2004), suggesting that the disease processes in PDB and IBMPFD may be related. However, disease-causing mutations in the *SQSTM1* lead to various degrees of loss of ub-binding function of p62, in the context of full-length protein (Garner *et al.*, 2011). In contrast, there is no generalised increase or loss in binding affinity for ubiquitinated proteins by mutant VCP (Hubbers *et al.*, 2007; Manno *et al.*, 2010; Erzurumlu *et al.*, 2013). Nevertheless, I have shown that VCP and p62 interact either directly or indirectly as a complex during autophagy. In view of this, I speculate that the disruption of a non-canonical autophagy based pathway could lead to deregulation of NF κ B signalling resulting in aberrant bone phenotype in the IBMPFD (Fig. 7.1).

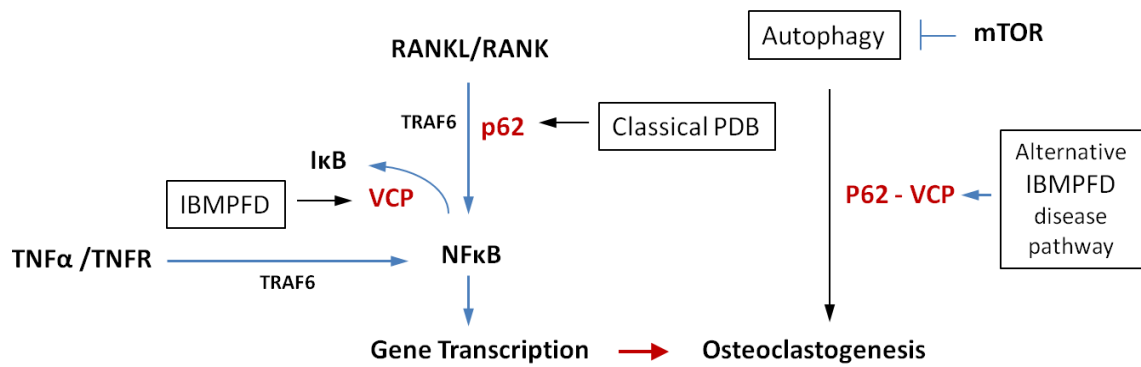


Figure 7.1. Mutations in p62 and VCP disrupt regulatory pathways resulting in over-activation of the NFκB signalling cascade and increased osteoclastogenesis. Mutations in p62 gene result in a Classical PDB and mutations in VCP result in the IBMPFD-associated PDB; both lead to elevated cytokine activation of NFκB. The pathogenic mechanism of VCP mutations may involve increased clearance of IκB and consequently increased downstream activation of NFκB with pathological consequences. Mutations in p62 may result in upregulation of downstream signalling from RANK receptor (activated via RANKL cytokine) and through TRAF6 association with both RANK and p62 that results in activation of target gene expression and initiation of osteoclast formation. Alternatively VCP and p62 may interact directly in a different pathway (autophagy-linked) that leads to IBMPFD - PDB when either is mutated.

Osteoclasts (OCL), which have been demonstrated as monocyte-macrophage derived multinuclear cells, are principal resorptive cells of bone (Maziere *et al.*, 2009). Osteoclasts originate from mononuclear progenitors of monocyte-macrophage lineage (hematopoietic precursors) which, upon cytokine stimulation, fuse into multinucleated non-dividing mature osteoclasts. Two characteristics in osteoclast differentiation are the expression of tartrate-resistant acid phosphatase (TRAP) and the presence of multiple nuclei, which are considered to be biomarkers of mature osteoclasts (Sakiyama *et al.*, 2001). The orchestrated process of osteoclast differentiation involves the rearrangement of the cytoskeleton and the degradation and renewal of intracellular proteins (Chen and Olson 2005; Oikawa *et al.*, 2013). Autophagy possesses pivotal roles in regulating the degradation of cellular proteins and organelles (Mizushima and Levine, 2010) and its activation in osteoclast differentiation has been implicated in several studies (Zhao *et al.*, 2012; Lin *et al.*, 2013; Lin *et al.*, 2014). It has been shown that autophagy has an essential regulatory role in the hypoxia-induced osteoclastogenesis (Zhao *et al.*, 2012). Increase in the

number of TRAP positive multinuclear cells was observed in RAW264.7 cells following hypoxia-induced autophagy and determined to be regulated via the HIF-1 α /BNIP3 dependent pathway (Zhao *et al.*, 2012). Conversely, genetic (with dominant negative Atg5 mutant – DN-Atg5^{K130R}) and chemical (with 3-methyladenine (MA)) suppression of autophagy dramatically attenuated hypoxia-induced osteoclast differentiation (Zhao *et al.*, 2012). Stimulatory effects of autophagy on osteoclastogenesis were also reported in patients with rheumatoid arthritis (RA) (Lin *et al.*, 2013). The key player in the pathogenesis of RA - TNF α increased expression of Atg7 and LC3II in murine osteoclasts, whereas inhibition of autophagy either by knockdown of Atg7 or by treatment with Bafilomycin A1, strongly impaired osteoclast differentiation and expression of osteoclast-associated genes (Lin *et al.*, 2013). In contrast to work recently published my data demonstrates that induction of autophagy during osteoclastogenesis has an inhibitory effect on osteoclast differentiation. Specifically, my study reveals that inhibition of the mTOR signalling (with either rapamycin or Torin 1) suppresses early stages of RANKL - dependent osteoclast differentiation of mouse macrophage-like RAW 264.7 cells. This could be because the mammalian target of rapamycin (mTOR) kinase is involved in the promotion of osteoclast formation and inactivation of the mTOR pathway with rapamycin results in a translational shift of the C/EBP β toward LAP isoform that in turn restricts osteoclast formation (Smink *et al.*, 2009). Furthermore, suppression of the m-TOR pathway is a requirement for osteoprotegerin (OPG)/ osteoclastogenesis inhibitory factor production in bone marrow stromal cells (Mogi and Kondo, 2009). Thus, inhibition of mTOR activity increases cell death rate of mature osteoclasts, and significantly reduces bone resorption (Glantsching *et al.*, 2003; Indo *et al.*, 2013). This is in contrast to the earlier work, where the authors claimed that rapamycin, alone or in synergy with TGF β , induce osteoclastogenesis of RAW264.7 cells in the presence of RANKL (Shui *et al.*, 2002). Moreover, preceding study proposed that rapamycin decreases protein levels of osteoprotegerin (OPG), a decoy receptor for RANKL, but increases RANKL production in bone marrow stromal cells (Hofbauer *et al.*, 2001). In addition, the mTOR is also a major switch between anabolic and catabolic processes (Glantschnig *et al.*, 2003), including regulation of autophagy. Inhibition of mTOR with drugs such as rapamycin or through nutrient deprivation induces autophagy in mouse

skeletal muscle (Ju *et al.*, 2010) and further worsens muscle pathology (decrease in muscle strength and significant increase in serum creatine kinase) in VCP-mutant mice (Ching *et al.*, 2013). Interestingly, VCP-mutant mice showed reduced levels of phosphorylated direct mTOR targets (p4EBP1, pp70S6 and pS6 kinase) and overall decrease in protein translation, as well as enhanced autophagosome biogenesis (Ching *et al.*, 2013). Further to this, chemical inhibition of VCP (with DBeQ) or expression of catalytically inactive VCP in U2OS cells attenuated activation of mTOR upon nutrient stimulation (Ching *et al.*, 2013). This is particularly interesting, since p62 was also shown to mediate mTOR activity (amino acid signalling for the activation of S6K and 4EBP1 kinase) upon nutrient stimulation, via its direct association with raptor and mTOR (Duran *et al.*, 2011). In view of this, I speculate that VCP/p62 complex coordinates mTOR signalling versus autophagy in response to nutrient availability and this action is impaired when either protein is mutated. Additionally, inhibiting mTOR at early stages of osteoclastogenesis mirrors response to the lack of nutrients in favour of autophagy and halts osteoclast differentiation in favour of cell survival. Therefore it is likely that action of rapamycin (and other mTOR inhibitors) varies in early and late stages of osteoclast differentiation. To further test this hypothesis, one could examine the effects of mTOR inhibition on osteoclasts differentiating from R155H-mutant VCP and p62-mutant hematopoietic precursors. If mTOR activity is impaired in VCP-mutants then perhaps restoring it would improve cellular pathology in IBMPFD. So far only two molecules have been shown as direct activators of mTOR signalling, these are the GTPase Ras homologue enriched in brain (Rheb) and the lipid second messenger phosphatidic acid (PA) (Goodman *et al.*, 2010; Jacobs *et al.*, 2014). GTP-bound Rheb can bind to the catalytic domain of mTOR and overexpression of Rheb is sufficient to activate mTOR signalling (Sato *et al.*, 2009), which in turn inhibits autophagy. In accordance with this, expression of Rheb effectively enhanced the phosphorylation of p70S6 kinase and increased the myofibre size in VCP-IBM mouse muscle (Ching *et al.*, 2013). Stimulation of cells with exogenous PA was also shown to increase mTOR signalling (You *et al.*, 2012). Mechanistically, PA binds to the FKBP12-Rapamycin binding (FRB) domain of mTOR, and like GTP-Rheb, it can directly activate mTOR kinase activity in-vitro (You *et al.*, 2012). Thus alternatively, one could determine if restoring mTOR activity in

rapamycin-treated and IBMPFD-VCP osteoclast precursors with either Rheb or PA would alter their response to osteoclastogenic cytokines.

The RANK ligand (RANKL; activator of both classical/canonical and non-canonical NF κ B) is considered to be a master regulator of physiologic osteoclastogenesis and is considered to act synergistically with TNF α (activator of classical NF κ B) to induce osteoclast differentiation (Zou *et al.*, 2001). Interestingly, a key feature of pagetic osteoclast precursors is that they are sensitive to lower levels of osteotropic factors than normal precursors. In marrow cultures from patients with Paget's disease, OCL are formed in response to 10-fold lower concentrations of the cytokines RANKL (Neale *et al.*, 2000; Roodman and Windle, 2005), TNF- α (Kurihara *et al.*, 2007) and hormonally active form of vitamin D (1, 25-dihydroxyvitamin D₃) (Menaar *et al.*, 2000) than normal cells. In accordance with this, I found that *R155H-mutant VCP* shows increased activation of NF κ B in response to both RANKL and TNF α cytokines. *It was suggested that mutant VCP amplifies* NF κ B activation through altered regulation of I κ B-ubiquitin-dependent degradation (Custer *et al.*, 2010). However, a recent report proposed that although a short term activation of NF κ B is mediated by the proteasomal degradation of I κ B α , persistently activated NF κ B state is achieved via the induction of autophagy at later phases, following stimulation with TNF α (Colleran *et al.*, 2011). As such, it would seem that the R155H mutation in VCP alone efficiently induces NF κ B activation, possibly due to disruption of the basal macroautophagy pathway. Likewise, osteoclast precursors from mice with a P394L p62 mutation (equivalent to P392L mutation causing PDB in humans) were noted to be not only over-sensitive to RANKL but also show an increased expression of autophagy-related genes, *atg5* and *lc3* (Daroszewszka *et al.*, 2011).

It was established that RANKL knockout mice exhibit irregularities in bone homeostasis (Boyle *et al.*, 2003) and that inhibition of RANKL/RANK signalling pathway will in turn inhibit bone resorption (Zhao *et al.*, 2011; Cordowa *et al.*, 2015). For example, local administration of RANK siRNA exerted a protective effect against polyethylene (PE) induced osteolysis, decreasing the bone loss and osteoclastogenesis (Cordowa *et al.*, 2015). Similarly, RANK antibody directly blocked RANKL/RANK signalling leading to inhibition of inflammatory osteolysis associated

with implant wearing particles (Zhao et al., 2011). Interestingly, knockdown of p62 in both RAW264.7 and in mouse bone marrow macrophages also significantly decreased RANKL-induced formation of TRAP-positive multinuclear cells (Li et al., 2014). Additionally, the key autophagy-related markers (Atg5, Atg12, Atg7 and LC3II) that were up-regulated in mature osteoclasts were found attenuated following the p62 siRNA in RAW264.7 cells (Li et al., 2014). The authors state that RANKL induces autophagy in osteoclasts and propose p62 to be a bridge protein between autophagy and RANKL-induced osteoclastogenesis (Li et al., 2014).

The results outlined in Chapter 6 of this study demonstrate that increased accumulation of protein aggregates in osteoclast precursor cells has stimulating effect on the activation of NF κ B signalling cascade. This implies that enhanced osteoclastogenic potential of the bone marrow derived macrophages (BMDM), clearly observed in the IBMPFD cases is indeed effect of compromised autophagy. Inhibition of the late phase of autophagy with Bafilomycin A1 dramatically increased NF κ B activation in osteoclast progenitor cells from wild-type mice and had significant effect on BMDM from VCP-mutant mice. Coinciding with the osteoclast differentiation effects, macrophages from mutant mice appear more sensitive to Bafilomycin A1 treatment, accumulating more lipidated LC3II than wild type cells. The assembly of the essential for autophagosome formation Atg5-Atg12-Atg16 complex is also elevated in mutant cells, suggesting up-regulated early autophagy signalling. Likewise, treatment with inhibitor of autophagy – Bafilomycin A1 increased LC3 II protein levels in osteoclasts from P394L p62 mutant mice, compared with wild type osteoclasts, suggesting deregulation of autophagy and enhanced autophagosome formation (Daroszewska et al., 2011). Interestingly, while inhibition of autophagy induces NF κ B activation, stimulation of this degradation pathway has little to no effect on the osteoclastogenic signalling cascade. Similarly, it was demonstrated that rapamycin treatment led to increased expression of LC3 II in RAW264.7 cells in time dependent manner (over 24 hour period), and also slightly enhanced osteoclast differentiation (Zhao *et al.*, 2012). Their study evaluated osteoclastogenic response over a long time period whereas my work monitored more immediate NF κ B pathway responses. Therefore, the increased sensitivity of mutant macrophages to either TNF α or RANKL appears to be a defect in early autophagy (potentially a new role for

VCP identified in Chapters 3 to 5) implied by the lack of autophagy induction in mutant cells after cytokine treatment. Since both p62 and VCP mutations cause the same molecular defect in cytokine induced activation of autophagy, it is tempting to speculate that the molecular lesion in PDB is a defect in actions of the p62/VCP complex, leading to deregulation of autophagy and ultimately PDB pathology. One possibility for the increased downstream signalling in pagetic osteoclasts is decreased RANK receptor recycling (mediated through the VCP/p62 complex). VCP has been previously associated with regulating lysosomal degradation and recycling of dNRAMP receptor (Panda *et al.*, 2013) and thus it would not be that surprising if VCP also mediated lysosomal degradation of RANK receptor. Under such circumstances, aberrant degradation of RANK receptor, due to impairment of VCP function (and hence compromise autophagy) would lead to increased downstream signalling and in turn enhanced osteoclast differentiation, though further studies are required to address this.

In summary, I have identified VCP as a new and important component of the autophagy pathway which may represent a major regulator of bone remodelling and maintenance. This would indicate that mutations in VCP, resulting in disruption of autophagic processes, cause an increase in osteoclast differentiation as a direct effect of an overactive NF κ B, causing bone pathology observed in the IBMPFD cases. In an effort to further understand autophagic dysfunction in IBMPFD-specific PDB one could go on to determine how mature osteoclasts respond to cell stress that challenges the UPS and macroautophagy pathways. To further delineate the mechanisms responsible for stimulating effects of mutant VCP on osteoclastogenesis one can examine the phosphorylation status of downstream signalling intermediates (such as I κ B α , MAPK, ERK1 and ERK2) during osteoclastogenesis mediated by RANKL or TNF α . A significant challenge in future IBMPFD research will be to further untangle the contribution of individual perturbations caused by VCP mutations to tissue-specific disease manifestations, and I believe that the mouse model presented in the present study provides an excellent resource in our further search for the molecular underpinnings of IBMPFD.

7.4 Concluding remarks

I have shown evidence that VCP is important in both the early and late stages of autophagy and that VCP does not just act as the main shuttle to the proteasome. I have also identified p62 as a new binding partner for VCP which not only links VCP to early autophagy but also potentially shows that both p62 and VCP mutations disrupt autophagy as the underlying cause of PDB. Importantly, I have provided evidence that not only does VCP and p62 co-localise to pathogenic inclusion bodies, but when autophagy is induced, p62 acts as a VCP binding partner. Here, either p62, VCP or both are binding to polyubiquitinated substrates with the LIR domain of p62 potentially being used to target the complex to the lipid bound LC3 in the nascent autophagosome. Significantly, this places VCP and p62 as having roles in the early stages of autophagy in addition to the previously reported disruption of late stage autophagy seen in IBMPFD. I have also demonstrated that mutations in VCP cause a reduction in autophagic efficiency of normal aggregate-prone autophagy substrates. Interestingly, the solubility of VCP is regulated in a p62 dependent manner, further supporting the notion that VCP and p62 cooperate in degradation of substrates by the proteasome or autophagy. I also examined the effects of VCP mutations on autophagic activity of osteoclasts and showed here that autophagy defect significantly regulates the osteoclast differentiation. Since, the induction of autophagy at any stage of osteoclastogenesis has an inhibitory effect; it would imply that cytokine activated autophagy has major regulatory role in NF κ B signalling during osteoclastogenesis. I investigated the molecular mechanisms by which autophagy mediates osteoclastogenesis through the NF κ B signalling pathway. The results of this study show that the increased NF κ B activation seen in mutant VCP macrophages could be due to a lack of early stage autophagy induction needed for the recycling (regulation of receptor availability) of the RANK receptor. This would also fit with the inhibitory effect induced autophagy had on RAW264.7 cell differentiation, where in this instance the RANK receptor (and signalling response) is greatly reduced due to increased turnover by autophagy. Furthermore, this would fit with the potential role of p62 in PDB and that both p62 and VCP mutations cause the same molecular defect in cytokine induced activation of autophagy resulting in decreased receptor recycling. Significantly, I have shown that mutations in VCP not only affect late stage autophagy

(as demonstrated by age dependent accumulations of LC3II in muscle of the IBMPFD mouse), but also the new role I have identified for VCP in early stage autophagy.

Currently there is no cure for PDB and therapies are aimed to reduce or stabilise the symptoms and make the life of the patient more comfortable. The bisphosphonates (BP) treatment is the most applied pharmacological treatment for PDB (Chung and Hul, 2012). BP's are anti-remodelling drugs that inhibit the function, activation and survival of osteoclasts but are known to initiate pro-inflammatory response (Chung and Hul, 2012). It is also plausible that over-suppression of the bone remodelling could lead to accumulation of microcracks or increase bone deformity due to unbalanced activity of osteoblasts. Therefore, I speculate that the manipulation of autophagy, or more specifically p62/VCP complex interaction, as a potential therapy in IBMPFD-disease could be promising. Activation of impaired autophagy in a mouse model of congenital muscular dystrophy using mTOR inhibition or dietary modifications improved strength and muscle pathology (Grumati et al., 2010). Perhaps modulating osteoclast differentiation through time-restricted treatment with rapamycin or with an alternative mTOR inhibitor may also be beneficial for management of the PDB. Nevertheless, inhibition of the mTOR pathway could have adverse side effects, potentiate cellular pathology in IBMPFD cases and worsen the disease. Of note, chronic rapamycin treatment significantly worsens the degenerative phenotype in VCP-IBM mice (Ching et al., 2013). Thus restoring mTOR activity with RHEB (Goodman *et al.*, 2010) may tender better prognosis in advanced cases. However, future studies are required to inspect effects of prolonged expression of Rheb (or PA) in IBMPFD-mice tissue. Also strategy aimed at controlled up-regulation of steady state levels of wild-type VCP may be feasible as means of improving prognosis of PDB. However, future studies must define the effects of modulating VCP function in the context of whole organism, before therapeutic compounds aimed at VCP can move into clinical trials.

REFERENCES

- Abedin M J, Wang D, McDonnell MA, Lehmann U, Kelekar A (2007). Autophagy delays apoptotic death in breast cancer cells following DNA damage. *Cell Death Differ.* 14, 500–510
- Abu-Amer Y1, Darwech I, Otero J.(2008). Role of the NF-kappaB axis in immune modulation of osteoclasts and bone loss. *Autoimmunity.* 41(3):204-11.
- Alexandru G, Graumann J, Smith GT, Kolawa NJ, Fang R, Deshaies RJ (2008). UBXD7 binds multiple ubiquitin ligases and implicates p97 in HIF1alpha turnover. *Cell* 134:804–816.
- Anderson P, Kedersha N (2009). Stress granules. *Curr Biol.* 19: R397–R398
- Ang E, Pavlos NJ, Rea SL, Qi M, Chai T, Walsh JP, Ratajczak T, Zheng MH, Xu J. (2009). Proteasome inhibitors impair RANKL-induced NF-kappaB activity in osteoclast-like cells via disruption of p62, TRAF6, CYLD, and IkkappaBalpha signaling cascades. *J Cell Physiol.* 220(2):450-9
- Babu JR, Geetha T, Wooten MW (2005). Sequestosome 1/p62 shuttles polyubiquitinated tau for proteasomal degradation. *J Neurochem.* 94:192-203
- Badadani M, Nalbandian A, Watts GD, Vesa J, Kitazawa M, Su H, Tanaja J, Dec E, Wallace DC, Mukherjee J, Caiozzo V, Warman M, Kimonis VE (2010). VCP associated inclusion body myopathy and paget disease of bone knock-in mouse model exhibits tissue pathology typical of human disease. *PLoS One* 5pii: e13183
- Baldwin AS (2001). Series Introduction: The transcription factor NF-κB and human disease. *J Clin Invest.* 107(1): 3–6.
- Ballar P, Pabuccuoglu A, Kose FA (2011). Different p97/VCP complexes function in retrotranslocation step of mammalian ER-associated degradation (ERAD). *Int J Biochem Cell Biol.* 43(4):613-21.
- Baron R (2008). Chapter 1. Anatomy and ultrastructure of bone – histogenesis, growth and remodelling.
- Berenson JR, Yellin O (2008). New drugs in multiple myeloma. *Curr Opin Support Palliat Care* 2:204-210
- Berke SJ, Schmied FA, Brunt ER, Ellerby LM, Paulson HL (2004). Caspase-mediated proteolysis of the polyglutamine disease protein ataxin-3. *J Neurochem.* 89(4):908-18
- Boyault C, Gilquin B, Zhang Y, Rybin V, Garman E, Meyer-Klaucke W, Matthias P, Mübller CW, Khochbin S (2006). HDAC6-p97/VCP controlled polyubiquitin chain turnover. *EMBO J.* 25:3357-3366
- Bjørkøy G, Lamark T, Brech A, Outzen H, Perander M, Overvatn A, Stenmark H, Johansen T (2005). p62/SQSTM1 forms protein aggregates degraded by autophagy and has a protective effect on huntingtin-induced cell death. *J Cell Biol* 171:603-614

- Bjørkøy G, Lamark T, Pankiv S, Øvervatn A, Brech A, Johansen T (2009). Monitoring autophagic degradation of p62/SQSTM1. *Methods Enzymol.* 452:181-97
- Botti J, Djavaheri-Mergny M, Pilatte Y, Codogno P (2006). Autophagy signaling and the cogwheels of cancer. *Autophagy* 2, 67–73
- Boyle WJ, Simonet WS, Lacey DL (2003). Osteoclast differentiation and activation. *Nature.* 423(6937):337-42.
- Bruderer RM, Brasseur C, Meyer HH (2004). The AAA ATPase p97/VCP interacts with its alternative co-factors, Ufd1-Npl4 and p47, through a common bipartite binding mechanism. *J Biol Chem.* 279(48):49609-16
- Buchan JR, Muhlrud D, Parker R (2008). P bodies promote stress granule assembly in *Saccharomyces cerevisiae*. *J. Cell Biol.* 183:441–455.
- Buchan JR, Parker Rn (2009). Eukaryotic stress granules: the ins and outs of translation. *Mol. Cell.* 36:932–941
- Buchan JR, Kolaitis RM, Taylor JP, Parker R (2013). Eukaryotic stress granules are cleared by autophagy and Cdc48/VCP function. *Cell* 153: 1461–1474.
- Buchberger A, Schindelin H, Hänzelmann P (2015). Control of p97 function by cofactor binding. *FEBS Lett.* 589(19 Pt A):2578-89.
- Bug M, Meyer H (2012). Expanding into new markets - VCP/p97 in endocytosis and autophagy. *J Struct Biol* 179(2):78-82
- Bukau B, Weissman J, Horwich A (2006). Molecular chaperones and protein quality control. *Cell* 125: 443–451
- Cao Y, Espinola JA, Fossale E, Massey AC, Cuervo AM, MacDonald ME, Cotman SL (2006.) Autophagy is disrupted in a knock-in mouse model of juvenile neuronal ceroid lipofuscinosis. *J Biol Chem* 281:20483–20493
- Chamoux E, Couture J, Bisson M, Morissette J, Brown JP, Roux S (2009). The p62 P392L mutation linked to Paget's disease induces activation of human osteoclasts. *Mol Endocrinol* 23:1668-1680
- Chang E, Kuret J (2008). Detection and Quantification of Tau Aggregation Using a Membrane Filter Assay. *Anal Biochem.* 373(2):330-336
- Chan S, Scheulen ME, Johnston S, Mross K, Cardoso F, Dittrich C, Eiremann W, Hess D, Morant R, Semiglazov V, Borner M, Salzberg M, Ostapenko V, Illiger HJ, Behringer D, Bardy-Bouxin N, Boni J, Kong S, Cincotta M, Moore L (2005). Phase II study of temsirolimus (CCI-779), a novel inhibitor of mTOR, in heavily pretreated patients with locally advanced or metastatic breast cancer. *J Clin Oncol* 23:5314-5322
- Chapman E, Fry AN, Kang M (2011). The complexities of p97 function in health and disease. *Mol Biosyst.* 7:700-710

Chen S, Ferrone FA, Wetzel R (2002). Huntington's disease age-of-onset linked to polyglutamine aggregation nucleation. *PNAS* 99(18): 11884-89

Chen EH, Olson EN (2005). Unveiling the mechanisms of cell-cell fusion. *Science* 308:369-373.

Cherra SJ 3rd, Dagda RK, Chu CT (2010). Review: autophagy and neurodegeneration: survival at a cost? *Neuropathol Appl Neurobiol* 36:125-132

Ching JK, Elizabeth SV, Ju JS, Lusk C, Pittman SK, Weihl CC (2013). mTOR dysfunction contributes to vacuolar pathology and weakness in valosin-containing protein associated inclusion body myopathy. *Hum Mol Genet.* 22(6):1167-79.

Choi AM, Ryter SW, Levine B (2013). Autophagy in human health and disease. *N Engl J Med.* 368(19):1845-6.

Chou TF1, Brown SJ, Minond D, Nordin BE, Li K, Jones AC, Chase P, Porubsky PR, Stoltz BM, Schoenen FJ, Patricelli MP, Hodder P, Rosen H, Deshaies RJ. (2011). Reversible inhibitor of p97, DBeQ, impairs both ubiquitin-dependent and autophagic protein clearance pathways. *Proc Natl Acad Sci U S A.* 108(12):4834-9

Chung PY, Beyens G, de Freitas F, Boonen S, Geusens P, Vanhoenacker F, Verbruggen L, Van Offel J, Goemaere S, Zmierzak HG, Westhovens R, Devogelaer JP, Van Hul W (2011). Indications for a genetic association of a VCP polymorphism with the pathogenesis of sporadic Paget's disease of bone, but not for TNFSF11 (RANKL) and IL-6 polymorphisms. *Mol Genet Metab* 103:287-292

Chung PY, Van Hul W (2012). Paget's disease of bone: evidence for complex pathogenetic interactions. *Semin Arthritis Rheum.* 41(5):619-41.

Chung YH, Yoon SY, Choi B, Sohn DH, Yoon KH, Kim WJ, Kim DH, Chang EJ (2012). Microtubule-associated protein light chain 3 regulates Cdc42-dependent actin ring formation in osteoclast. *Int J Biochem Cell Biol.* 44:989-97

Ciechanover A, Kwon YT (2015). Degradation of misfolded proteins in neurodegenerative diseases: therapeutic targets and strategies. *Exp Mol Med.* 13;47:e147.

Comb WC, Cogswell P, Sitcheran R, Baldwin AS (2011). IKK-dependent, NF- κ B-independent control of autophagic gene expression. *Oncogene.* 30(14):1727-32

Colleran A, Ryan A, O'Gorman A, Mureau C, Liptrot C, Dockery P, Fearnhead H, Egan LJ (2011). Autophagosomal I κ B α degradation plays a role in the long term control of tumor necrosis factor- α -induced nuclear factor- κ B (NF- κ B) activity. *J Biol Chem.* 286(26)

Colleran A, Ryan A, O'Gorman A, Mureau C, Liptrot C, Dockery P, Fearnhead H, Egan LJ (2011). Autophagosomal I κ B α degradation plays a role in the long term control of tumor necrosis factor- α -induced nuclear factor- κ B (NF- κ B) activity. *J Biol Chem* 286:22886-93

- Colombrita C, Zennaro E, Fallini C, Weber M, Sommacal A, Buratti E, Silani V, Ratti A. (2009). TDP-43 is recruited to stress granules in conditions of oxidative insult. *J Neurochem* 111(4): 1051-61
- Córdova LA, Trichet V, Escriou V, Rosset P, Amiaud J, Battaglia S, Charrier C, Berreur M, Brion R, Gouin F, Layrolle P, Passuti N, Heymann D (2015). Inhibition of osteolysis and increase of bone formation after local administration of siRNA-targeting RANK in a polyethylene particle-induced osteolysis model. *Acta Biomater.* 13:150-8.
- Criollo A, Senovilla L, Authier H, Maiuri MC, Morselli E, Vitale I, Kepp O, Tasdemir E, Galluzzi L, Shen S, Tailler M, Delahaye N, Tesniere A, De Stefano D, Younes AB, Harper F, Pierron G, Lavandro S, Zitvogel L, Israel A, Baud V, Kroemer G (2010). The IKK complex contributes to the induction of autophagy. *EMBO J* 29:619-31
- Cuervo AM, Stefanis L, Fredenburg R, Lansbury PT, Sulzer D (2004). Impaired degradation of mutant α -synuclein by chaperone-mediated autophagy. *Science* 305, 1292–1295
- Custer SK, Neumann M, Lu H, Wright AC, Taylor JP (2010). Transgenic mice expressing mutant forms VCP/p97 recapitulate the full spectrum of IBMPFD including degeneration in muscle, brain and bone. *Hum Mol Genet* 19:1741755
- Dai RM, Chen E, Longo DL, Gorbea CM, Li CC (1998). Involvement of valosin-containing protein, an ATPase Co-purified with I κ B α and 26 S proteasome, in ubiquitin-proteasome-mediated degradation of I κ B α . *J. Biol. Chem.* 273:3562–3573
- Dai RM, Li CC (2001). Valosin-containing protein is a multi-ubiquitin chain-targeting factor required in ubiquitin-proteasome degradation. *Nat Cell Biol* 3:740-4
- Daroszewska A, Van't Hof RJ, Rojas JA, Layfield R, Landao-Basonga E, Rose L, Rose K, Ralston SH (2011). A point mutation in the ubiquitin-associated domain of SQSTM1 is sufficient to cause a Paget's disease-like disorder in mice. *Hum Mol Genet.* 20:2734-2744
- Decker CJ, Teixeira D, Parker R (2007). Edc3p and a glutamine/asparagine-rich domain of Lsm4p function in processing body assembly in *Saccharomyces cerevisiae*. *J. Cell Biol.* 179:437–449.
- Demuro A, Mina E, Kaye R, Milton SC, Parker I, Glabe CG (2005). Calcium dysregulation and membrane disruption as a ubiquitous neurotoxic mechanism of soluble amyloid oligomers. *J Biol Chem.* 280(17):17294-300.
- DeSelm CJ, Miller BC, Zou W, Beatty WL, van Meel E, Takahata Y, Klumperman J, Tooze SA, Teitelbaum SL, Virgin HW (2011). Autophagy proteins regulate the secretory component of osteoclastic bone resorption. *Dev Cell* 21:966-974
- Dewey CM, Cenik B, Sephton CF, Johnson BA, Herz J, Yu G (2012). TDP-43 aggregation in neurodegeneration: are stress granules the key? *Brain Res.* 1462:16–25.
- Didiot MC, Subramanian M, Flatter E, Mandel JL, Moine H (2009). Cells lacking the fragile X mental retardation protein (FMRP) have normal RISC activity but exhibit altered stress granule assembly. *Mol. Biol. Cell.* 20:428–437.

- Ding H, Dolan PJ, Johnson GV (2008). Histone deacetylase 6 interacts with the microtubule-associated protein tau. *J Neurochem.*106:2119-2130
- Ding WX, Ni HM, Gao W, Yoshimori T, Stolz DB, Ron D, Yin XM (2007). Linking of autophagy to ubiquitin-proteasome system is important for the regulation of endoplasmic reticulum stress and cell viability. *Am J Pathol.* 171(2):513-24. Epub 2007 Jul 9.
- Dolan PJ, Jin YN, Hwang W, Johnson GV (2011). Decrease in the valosin-containing protein result in increased levels of tau phosphorylated at Ser262/356. *FEBS Lett* 585:3424-3429
- Dormann D, Rodde R, Edbauer D, Bentmann E, Fischer I, Hruscha A, Than ME, Mackenzie IR, Capell A, Schmid B, Neumann M, Haass C (2010). ALS-associated fused in sarcoma (FUS) mutations disrupt transportin-mediated nuclear import. *EMBO J* 29: 2841–2857
- Du Y, Yang D, Li L, Luo G, Li T, Fan X, Wang Q, Zhang X, Wang Y, Le W (2009). An insight into the mechanistic role of p53-mediated autophagy induction in response to proteasomal inhibition-induced neurotoxicity. *Autophagy*, 5(5):663-75.
- Duran A, Amanchy R, Linares JF, Joshi J, Abu-Baker S, Porollo A, Hansen M, Moscat J, Diaz-Meco MT (2011). p62 is a key regulator of nutrient sensing in the mTORC1 pathway. *Mol Cell.* 44(1):134-46.
- Erickson SL, Lykke-Andersen J (2011). Cytoplasmic mRNP granules at a glance. *J. Cell Sci.*124:293– 297.
- Erzurumlu Y, Kose FA, Gozen O, Gozuacik D, Toth EA, Ballar P (2013). A unique IBMPFD-related P97/VCP mutation with differential binding pattern and subcellular localization. *Int Biochem Cell Biol.* 45(4): 773-82
- Ewens CA1, Kloppsteck P, Förster A, Zhang X, Freemont PS (2010). Structural and functional implications of phosphorylation and acetylation in the regulation of the AAA+ protein p97. *Biochem Cell Biol.* 88(1):41-8
- Falchetti A, Di Stefano M, Marini F, Ortolani S, Olivieri MF, Bergui S, Masi L, Cepollaro C, Benucci M, Di Munno O, Rossini M, Adami S, Del Puente A, Isaia G, Torricelli F, Brandi ML; GenePage Project (2009). Genetic epidemiology of Paget's disease of bone in Italy: sequestosome1/p62 gene mutational test and haplotype analysis at 5q35 in a large representative series of sporadic and familial Italian cases of Paget's disease of bone. *Calcif Tissue Int* 84:20-37
- Fernandez-Saiz V, Buchberger A (2010). Imbalances in p97 co-factor interactions in human proteinopathy. *EMBO Rep* 11:479-485
- Forman MS, Farmer J, Johnson JK, Clark CM, Arnold SE, Coslett HB, Chatterjee A, Hurtig HI, Karlawish JH, Rosen HJ, Van Deerlin V, Lee VM, Miller BL, Trojanowski JQ, Grossman M (2006). Frontotemporal dementia: clinicopathological correlations. *Ann Neurol.* 59(6):952-62.
- Franz A, Ackermann L, Hoppe T (2014). Create and preserve: proteostasis in development and aging is governed by Cdc48/p97/VCP. *Biochim Biophys Acta.* 1843(1):205-15.

Fujita N, Itoh T, Omori H, Fukuda M, Noda T, Yoshimori T (2008). The Atg16L complex specifies the site of LC3 lipidation for membrane biogenesis in autophagy. *Mol Biol Cell* 19:2092-2100

Fujita K, Nakamura Y, Oka T, Ito H, Tamura T, Tagawa K, Sasabe T, Katsuta A, Motoki K, Shiwaku H, Sone M, Yoshida C, Katsuno M, Eishi Y, Murata M, Taylor JP, Wanker EE, Kono K, Tashiro S, Sobue G, La Spada AR, Okazawa H (2013). A functional deficiency of TERA/VCP/p97 contributes to impaired DNA repair in multiple polyglutamine diseases. *Nat Commun.* 4:1816.

Fushman D, Walker O (2010). Exploring the linkage dependence of polyubiquitin conformations using molecular modeling. *J Mol Biol.* 395(4):803-14.

Fu L, Sztul E (2009). ER-associated complexes (ERACs) containing aggregated cystic fibrosis transmembrane conductance regulator (CFTR) are degraded by autophagy. *Eur J Cell Biol* 88(4): 215-26.

Galassi G, Scholz SW, Taylor JP, Restagno G, Chiò A, Traynor BJ (2010). Exome sequencing reveals VCP mutations as a cause of familial ALS. *Neuron* 68:857-864

Gallagher PS1, Clowes Candadai SV, Gardner RG (2014). The requirement for Cdc48/p97 in nuclear protein quality control degradation depends on the substrate and correlates with substrate insolubility. *J Cell Sci.* 127(Pt9): 1980-91

Galson DL, Roodman GD (2014). Pathobiology of Paget's Disease of Bone. *J Bone Metab.* 21(2): 85–98.

Garner TP, Long J, Layfield R, Searle MS (2011). Impact of p62/SQSTM1 UBA domain mutations linked to Paget's disease of bone on ubiquitin recognition. *Biochemistry* 50:4665-4674

Geetha T, Wooten MW (2002). Structure and functional properties of the ubiquitin binding protein p62. *FEBS Lett.* 512(1-3):19-24

Gelman A, Elazar Z (2011). Autophagic factors cut to the bone. *Dev Cell* 21: 808-810

Glantschnig H, Fisher JE, Wesolowski G, Rodan GA, Reszka AA (2003). M-CSF, TNF α and RANK ligand promote osteoclast survival through mTOR/S6 kinase. *Cell Death Differ* 10:1165-1177

Gilks N, Kedersha N, Ayodele M, Shen L, Stoecklin G, Dember LM, Anderson P (2004). Stress granule assembly is mediated by prion-like aggregation of TIA-1. *Mol Biol Cell* 15: 5383–5398.

Goldberg AL (2003). Protein degradation and protection against misfolded or damaged proteins. *Nature.* 18;426(6968):895-9.

Goodman CA, Miu MH, Frey JW, Mabrey DM, Lincoln HC, Ge Y, Chen J, Hornberger TA (2010). A phosphatidylinositol 3-kinase/protein kinase B-independent activation of mammalian target of rapamycin signaling is sufficient to induce skeletal muscle hypertrophy. *Mol Biol Cell.* 21(18):3258-68.

Grumati P, Coletto L, Sabatelli P, Cescon M, Angelin A, Bertaggia E, Blaauw B, Urciuolo A, Tiepolo T, Merlini L, Maraldi NM, Bernardi P, Sandri M, Bonaldo P (2010). Autophagy is defective in collagen VI muscular dystrophies, and its reactivation rescues myofiber degeneration. *Nat Med.* 16(11):1313-20.

Halawani D, LeBlanc AC, Rouiller I, Michnick SW, Servant MJ, Latterich M (2009). Hereditary Inclusion Body Myopathy-Linked p97/VCP Mutations in the NH2 Domain and the D1 Ring Modulate p97/VCP ATPase Activity and D2 Ring Conformation. 29: 4484-4494

Hampe J, Franke A, Rosenstiel P, Till A, Teuber M, Huse K, Albrecht M, Mayr G, De La Vega FM, Briggs J, Günther S, Prescott NJ, Onnie CM, Häsler R, Sipos B, Fölsch UR, Lengauer T, Platzer M, Mathew CG, Krawczak M, Schreiber S (2007). A genome-wide association scan of nonsynonymous SNPs identifies a susceptibility variant for Crohn disease in ATG16L1. *Nat Genet.* 39(2):207-11.

Hanada T, Noda NN, Satomi Y, Ichimura Y, Fujioka Y, Takao T, Inagaki F, Ohsumi Y (2007). The Atg12-Atg5 conjugate has a novel E3-like activity for protein lipidation in autophagy. *J. Biol. Chem.* 282, 37298–37302

Han S, Shin D, Choi H, Lee S (2014) Molecular determinants of the interaction between Doa1 and Hse1 involved in endosomal sorting. *Biochem Biophys Res Commun.* 446(1):352-7

Hara T, Nakamura K, Matsui M, Yamamoto A, Nakahara Y, Suzuki-Migishima R, Yokoyama M, Mishima K, Saito I, Okano H, Mizushima N (2006). Suppression of basal autophagy in neural cells causes neurodegenerative disease in mice. *Nature* 441(7095):885-9

Hauer J, Püschner S, Ramakrishnan P, Simon U, Bongers M, Federle C, Engelmann H (2005) TNF receptor (TNFR)-associated factor (TRAF) 3 serves as an inhibitor of TRAF2/5-mediated activation of the noncanonical NF- κ B pathway by TRAF-binding TNFRs. *Proc Natl Acad Sci U S A.* 102(8):2874-9.

Hirabayashi M, Inoue K, Tanaka K, Nakadate K, Ohsawa Y, Kamei Y, Popiel AH, Sinohara A, Iwamatsu A, Kimura Y, Uchiyama Y, Hori S, Kakizuka A (2001). VCP/p97 in abnormal protein aggregates, cytoplasmic vacuoles, and cell death, phenotypes relevant to neurodegeneration. *Cell Death Differ.* 8(10): 977-84

Higashiyama H, Hirose F, Yamaguchi M, Inoue YH, Fujikake N, Matsukage A, Kakizuka A (2002). Identification of ter94, *Drosophila* VCP, as a modulator of polyglutamine-induced neurodegeneration. *Cell Death Differ.* 9(3):264-73

Hiruma Y, Kurihara N, Subler MA, Zhou H, Boykin CS, Zhang H, Ishizuka S, Dempster DW, Roodman GD, Windle JJ (2008). A SQSTM1/p62 mutation linked to Paget's disease increases the osteoclastogenic potential of the bone microenvironment. *Hum Mol Genet* 17:3708-3719

Hocking LJ, Lucas GJA, Daroszewska A, Mangion J, Olavesen M, Cundy T, Nicholson GC, Ward L, Bennett ST, Hul WV, Ralston SH (2002). Domain specific mutations in Sequestosome 1 (SQSTM1) cause familial and sporadic Paget's disease. *Human Molecular Genetics.* 11: 2735–2739.

Hocking LJ, Lucas GJ, Daroszewska A, Cundy T, Nicholson GC, Donath J, Walsh JP, Finlayson C, Cavey JR, Ciani B, Sheppard PW, Searle MS, Layfield R, Ralston SH (2004). Novel UBA domain mutations of SQSTM1 in Paget's disease of bone: genotype phenotype correlation, functional analysis, and structural consequences. *J Bone Miner Res.* 19(7):1122-7

Hocking LJ, Mellis DJ, McCabe PS, Helfrich MH, Rogers MJ (2010). Functional interaction between sequestosome-1/p62 and autophagy-linked FYVE-containing protein WDFY3 in human osteoclasts. *Biochem Biophys Res Commun.* 402(3):543-8

Hocking LJ, Whitehouse C, Helfrich MH (2012). Autophagy: a new player in skeletal maintenance? *J Bone Miner Res* 27:1439-47

Hoesel B, Schmid JA (2013). The complexity of NF- κ B signalling in inflammation and cancer. *Mol. Cancer* 12(86): 1476-4598

Hofbauer LC, Shui C, Riggs BL, Dunstan CR, Spelsberg TC, O'Brien T, Khosla S (2001) Effects of immunosuppressants on receptor activator of NF-kappaB ligand and osteoprotegerin production by human osteoblastic and coronary artery smooth muscle cells. *Biochem Biophys Res Commun* 280:334-339

Homma T, Ishibashi D, Nakagaki T, Satoh K, Sano K, Atarashi R, Nishida N (2014). Increased expression of p62/SQSTM1 in prion diseases and its association with pathogenic prion protein. *Sci Rep.* 4 (4504)

Hoppe T (2005). Multiubiquitylation by E4 enzymes: 'one size' doesn't fit all. *Trends Biochem. Sci.*, 30: 183–187

Hsu H, Lacey DL, Dunstan CR, Solovyev I, Colombero A, Timms E, Tan HL, Elliott G, Kelley MJ, Sarosi I, Wang L, Xia XZ, Elliott R, Chiu L, Black T, Scully S, Capparelli C, Morony S, Shimamoto G, Bass MB, Boyle WJ. (1999). Tumor necrosis factor receptor family member RANK mediates osteoclast differentiation and activation induced by osteoprotegerin ligand. *Proc Natl Acad Sci USA* 96:3540–3545.

Hubbard VM, Valdor R, Macian F, Cuervo AM (2012). Selective autophagy in the maintenance of cellular homeostasis in aging organisms. *Biogerontology.* 13:21–35.

Hübbers CU, Clemen CS, Kesper K, Böddrich A, Hofmann A, Kämäräinen O, Tolksdorf K, Stumpf M, Reichelt J, Roth U, Krause S, Watts G, Kimonis V, Reimann J, Thal DR, Biermann K, Evert BO, Lochmüller H, Wanker EE, Schoser BG, Noegel AA, Schröder R (2007). Pathological consequences of VCP mutations on human striated muscle. *Brain* 130:381-393

Hughes AE, Shearman AM, Weber JL, Barr RJ, Wallace RG, Osterberg PH, Nevin NC, Mollan RA (1994). Genetic linkage of familial expansile osteolysis to chromosome 18q. *Hum Mol Genet.* 3(2):359-61

Ichimura Y, Kumanomidou T, Sou YS, Mizushima T, Ezaki J, Ueno T, Kominami E, Yamane T, Tanaka K, Komatsu M (2008). Structural basis for sorting mechanism of p62 in selective autophagy. *J. Biol. Chem.* 283:22847–22857.

- Ikeda F, Dikic I (2008). Atypical ubiquitin chains: new molecular signals. 'Protein modifications: beyond the usual suspects' review series. *EMBO Rep.* 9, 536–542
- Imafuku I, Waragai M, Takeuchi S, Kanazawa I, Kawabata M, Mouradian MM, Okazawa H (1998). Polar amino acid-rich sequences bind to polyglutamine tracts. *Biochem. Biophys. Res. Commun.* 253, 16–20
- Indo Y, Takeshita S, Ishii KA, Hoshii T, Aburatani H, Hirao A, Ikeda K (2013). Metabolic regulation of osteoclast differentiation and function. *J Bone Miner Res.* 28(11):2392-9.
- Isakson P, Holland P, Simonsen A (2013). The role of ALFY in selective autophagy. *Cell Death Differ.* 20(1):12-20
- Itakura E, Mizushima N (2011). p62 Targeting to the autophagosome formation site requires self-oligomerization but not LC3 binding. *J Cell Biol.* 192(1):17-27
- Ito D, Suzuki N (2011). Conjoint pathologic cascades mediated by ALS/FTLD-U linked RNA-binding proteins TDP-43 and FUS. *Neurology.* 77:1636–1643.
- Jacobs BL, Goodman CA, Hornberger TA (2014). The mechanical activation of mTOR signaling: an emerging role for late endosome/lysosomal targeting. *J Muscle Res Cell Motil.* 35(1):11-21
- Janiesch PC, Kim J, Mouysset J, Barikbin R, Lochmuller H, Cassata G, Krause S, Hoppe T (2007). The ubiquitin-selective chaperone CDC-48/p97 links myosin assembly to human myopathy. *Nat Cell Biol* 9: 379–390
- Jentsch S, Rumpf S (2007). Cdc48 (p97): a "molecular gearbox" in the ubiquitin pathway? *Trends Biochem Sci.* 32(1):6-11
- Jing K, Lim K (2012). Why is autophagy important in human diseases? *Exp Mol Med* 29:69-72
- Johnson JO, Mandrioli J, Benatar M, Abramzon Y, Van Deerlin VM, Trojanowski JQ, Gibbs JR, Brunetti M, Gronka S, Wu J, Ding J, McCluskey L, Martinez-Lage M, Falcone D, Hernandez DG, Arepalli S, Chong S, Schymick JC, Rothstein J, Landi F, Wang YD, Calvo A, Mora G, Sabatelli M, Monsurrò MR, Battistini S, Salvi F, Spataro R, Sola P, Borghero G; ITALSGEN Consortium, Ju JS, Fuentealba RA, Miller SE, Jackson E, Piwnica-Worms D, Baloh RH, Weihl CC (2009). Valosin-containing protein (VCP) is required for autophagy and is disrupted in VCP disease. *J Cell Biol* 187: 875-88
- Johnson JO, Mandrioli J, Benatar M, Abramzon Y, Van Deerlin VM, Trojanowski JQ, Gibbs JR, Brunetti M, Gronka S, Wu J, Ding J, McCluskey L, Martinez-Lage M, Falcone D, Hernandez DG, Arepalli S, Chong S, Schymick JC, Rothstein J, Landi F, Wang YD, Calvo A, Mora G, Sabatelli M, Monsurrò MR, Battistini S, Salvi F, Spataro R, Sola P, Borghero G; ITALSGEN Consortium, Galassi G, Scholz SW, Taylor JP, Restagno G, Chiò A, Traynor BJ (2010). Exome sequencing reveals VCP mutations as a cause of familial ALS. *Neuron.* 68:857–864.
- Johnston JA, Ward CL, Kopito RR (1998). Aggresomes a cellular response to misfolded proteins *J. Cell Biol.* 143, 1883–1898

- Ju JS, Miller SE, Hanson PI, Weihl CC (2008). Impaired protein aggregate handling and clearance underlie the pathogenesis of p97/VCP-associated disease. *J Biol Chem* 283:30289-30299
- Ju JS, Varadhachary AS, Miller SE, Weihl CC (2010). Quantification of autophagic flux in mature skeletal muscle. *Autophagy* 6:929-935.
- Ju JS, Weihl CC (2010) Inclusion body myopathy, Paget's disease of the bone and frontotemporal dementia: a disorder of autophagy. *Hum Mol Genet* 19:R38-45
- Jung CH, Jun CB, Ro SH, Kim YM, Otto NM, Cao J, Kundu M, Kim DH (2009). ULK-Atg13-FIP200 complexes mediate mTOR signaling to the autophagy machinery. *Mol. Biol. Cell* 20, 1992–2003
- Jung CH, Ro SH, Cao J, Otto NM, Kim DH. (2010). mTOR regulation of autophagy. *FEBS Lett.* 2;584(7):1287-95
- Kakizuka A (2008) Roles of VCP in human neurodegenerative disorders. *Biochem Soc Trans.* 36:105-108
- Kaleem M, Zhao A, Hamshere M, Myers AJ (2007). Identification of a novel valosin-containing protein polymorphism in late-onset Alzheimer's disease. *Neurodegener Dis.* 4(5):376-81
- Kamada Y, Funakoshi T, Shintani T, Nagano K, Ohsumi M, Ohsumi Y (2000). Tor-mediated induction of autophagy via an Apg1 protein kinase complex. *J. Cell Biol.* 150, 1507–1513
- Kasagi S, Chen W (2013). GF-beta1 on osteoimmunology and the bone component cells *Cell Biosci.* 3: 4
- Khosla S (2001). Minireview: the OPG/RANKL/RANK system. *Endocrinology.* 142:5055
- Kimonis VE, Donkervoort S, Watts GD (2007-2011). Inclusion Body Myopathy with Paget Disease of Bone and/or Frontotemporal Dementia. *GeneReviews* 1993-2014
- Kimonis VE, Fulchiero E, Vesa J, Watts G (2008). VCP disease associated with myopathy, Paget disease of bone and frontotemporal dementia: review of a unique disorder. *Biochim Biophys Acta* 1782: 744-748
- Kimonis VE, Kovach MJ, Waggoner B, Leal S, Salam A, Rimer L, Davis K, Khardori R, Gelber D (2000). Clinical and molecular studies in a unique family with autosomal dominant limb-girdle muscular dystrophy and Paget disease of bone. *Genet Med* 2:232-241
- Kimonis VE, Mehta SG, Fulchiero EC, Thomasova D, Pasquali M, Boycott K, Neilan EG, Kartashov A, Forman MS, Tucker S, Kimonis K, Mumm S, Whyte MP, Smith CD, Watts GD (2008; 2nd). Clinical studies in familial VCP myopathy associated with Paget disease of bone and frontotemporal dementia. *Am J Med Genet A.* 146A (6):745-57
- Kimonis VE, Watts GD (2005). Autosomal dominant inclusion body myopathy, Paget disease of bone, and frontotemporal dementia. *Alzheimer Dis Assoc Disord* 19: S44-S47

Kimonis VE, Watts GD (2007). Inclusion Body Myopathy with Paget Disease of Bone and/or Frontotemporal dementia. GeneTests (www.genetests.org) and University of Washington, Seattle

Kim K, Kim JH, Lee J, Jin HM, Kook H, Kim KK, Lee SY, Kim N (2007). MafB negatively regulates RANKL-mediated osteoclast differentiation. *Blood* 109: 3253-3259

Kim J, Jung Y, Sun H, Joseph J, Mishra A, Shiozawa Y, Wang J, Krebsbach PH, Taichman RS (2012). Erythropoietin mediated bone formation is regulated by mTOR signaling. *J Cell Biochem* 113:220-228

Kim NC, Tresse E, Kolaitis RM, Molliex A, Thomas RE, Alami NH, Wang B, Joshi A, Smith RB, Ritson GP, Winborn BJ, Moore J, Lee JY, Yao TP, Pallanck L, Kundu M, Taylor JP (2013). VCP is essential for mitochondrial quality control by PINK1/Parkin and this function is impaired by VCP mutations. *Neuron*. 2013 Apr 10;78(1):65-80.

Kirkin, V. Lamark T, Sou YS, Bjørkøy G, Nunn JL, Bruun JA, Shvets E, McEwan DG, Clausen TH, Wild P, Bilusic I, Theurillat JP, Øvervatn A, Ishii T, Elazar Z, Komatsu M, Dikic I, Johansen T. (2009). A role for NBR1 in autophagosomal degradation of ubiquitinated substrates. *Mol. Cell* 33, 505–516

Klionsky DJ, Deretic V (2011). Autophagy: molecular mechanisms and disease outcomes. *Nature Rev.*

Klopsteck P, Ewens CA, Förster A, Zhang X, Freemont PS (2012). Regulation of p97 in the ubiquitin-proteasome system by the UBX protein-family. *Biochim Biophys Acta*. 1823(1):125-139

Kobayashi T, Manno A, Kakizuka A (2007). Involvement of valosin-containing protein (VCP)/p97 in the formation and clearance of abnormal protein aggregates. *Genes Cells* 12:889-901

Koike M, Shibata M, Waguri S, Yoshimura K, Tanida I, Kominami E, Gotow T, Peters C, Von Figura K, Mizushima N, Saftig P, Uchiyama Y (2005). Participation of autophagy in storage of lysosomes in neurons from mouse models of neuronal ceroid-lipofuscinoses (batten disease). *Am J Pathol* 167: 1713–1728.

Koike M, Fukushi J, Ichinohe Y, Higashimae N, Fujishiro M, Sasaki C, Yamaguchi M, Uchiyama T, Yagishita S, Ohizumi H, Hori S, Kakizuka A (2010). Valosin-containing Protein (VCP) in Novel Feedback Machinery between abnormal protein accumulation and transcriptional suppression. *J Biol Chem* 28:21736-21749

Komander D, Rape M (2012). The ubiquitin code. *Annu. Rev. Biochem.*, 81: 203–229

Komatsu J, Iwasa K, Yanase D, Yamada M (2013). Inclusion body myopathy with Paget disease of the bone and frontotemporal dementia associated with a novel G156S mutation in the VCP gene. *Muscle Nerve*.

Komatsu M, Waguri S, Chiba T, Murata S, Iwata J, Tanida I, Ueno T, Koike M, Uchiyama Y, Kominami E, Tanaka K (2006). Loss of autophagy in the central nervous system causes neurodegeneration in mice. *Nature* 441:880-884.

Komatsu M, Waguri S, Koike M, Sou YS, Ueno T, Hara T, Mizushima N, Iwata J, Ezaki J, Murata S, Hamazaki J, Nishito Y, Iemura S, Natsume T, Yanagawa T, Uwayama J, Warabi E, Yoshida H, Ishii T, Kobayashi A, Yamamoto M, Yue Z, Uchiyama Y, Kominami E, Tanaka K (2007). Homeostatic levels of p62 control cytoplasmic inclusion body formation in autophagy-deficient mice. *Cell* 131:1149-1163

Komatsu M, Waguri S, Ueno T, Iwata J, Murata S, Tanida I, Ezaki J, Mizushima N, Ohsumi Y, Uchiyama Y, Kominami E, Tanaka K, Chiba T (2005). Impairment of starvation-induced and constitutive autophagy in Atg7-deficient mice. *J Cell Biol.* 169(3): 425-34

Komatsu M, Ueno T, Waguri S, Uchiyama Y, Kominami E, Tanaka K (2007; 2nd). Constitutive autophagy: vital role in clearance of unfavorable proteins in neurons. *Cell Death Differ* 14:887-894

Kopito RR (2000). Aggresomes, inclusion bodies and protein aggregation. *Trends Cell Biol.*10(12):524-30.

Korolchuk VI, Mansilla A, Menzies FM, Rubinsztein DC (2009). Autophagy inhibition compromises degradation of ubiquitin-proteasome pathway substrates. *Mol Cell* 33:517-527

Korolchuk VI, Menzies FM, Rubinsztein DC (2010). Mechanisms of cross-talk between the ubiquitin-proteasome and autophagy-lysosome systems. *FEBS Lett.* 584(7):1393-1398

Kurihara N, Hiruma Y, Zhou H, Subler MA, Dempster DW, Singer FR, Reddy SV, Gruber HE, Windle JJ, Roodman GD (2007). Mutation of the sequestosome 1 (p62) gene increases osteoclastogenesis but does not induce Paget disease. *J Clin Invest.* 117:133-142.

Kwon S, Zhang Y, Matthias P (2007). The deacetylase HDAC6 is a novel critical component of stress granules involved in the stress response. *Genes & development.* 21:3381-3394

Lam J, Takeshita S, Barker JE, Kanagawa O, Ross FP, Teitelbaum SL (2000). TNF-alpha induces osteoclastogenesis by direct stimulation of macrophages exposed to permissive levels of RANK ligand. *J Clin Invest.* 106(12): 1481-8

Lamothe B, Webster WK, Gopinathan A, Besse A, Campos AD, Darnay BG (2007). TRAF6 ubiquitin ligase is essential for RANKL signaling and osteoclast differentiation. *Biochem Biophys Res Commun.* 359:1044-1049.

Lavoie C, Chevet E, Roy L, Tonks NK, Fazel A, Posner BI, Paiement J, Bergeron JJ (2000). Tyrosine phosphorylation of p97 regulates transitional endoplasmic reticulum assembly in vitro. *Proc Natl Acad Sci U S A* 97(25): 13637-42.

Layfield R, Ciani B, Ralston SH, Hocking LJ, Sheppard PW, Searle MS, Cavey JR (2004). Structural and functional studies of mutations affecting the UBA domain of SQSTM1 (p62) which cause Paget's disease of bone. *Biochem Soc Trans* 32:728-730

- Leach RJ, Singer FR, Ench Y, Wisdom JH, Pina DS, Johnston-Pais TL (2006). Clinical and cellular phenotypes associated with sequestosome 1 (SQSTM1) mutations. *J. Bone Miner. Res.* 21: 45–50
- Lee JJ, Park JK, Jeong J, Jeon H, Yoon JB, Kim EE, Lee KJ (2013). Complex of Fas-associated factor 1 (FAF1) with valosin-containing protein (VCP)-Npl4-Ufd1 and polyubiquitinated proteins promotes endoplasmic reticulum-associated degradation (ERAD). *J Biol Chem.* 288(10):6998-7011.
- Lee DH, Qi J, Bradner JE, Said JW, Doan NB, Forscher C, Yang H, Koeffler HP (2014). Synergistic effect of JQ1 and rapamycin for treatment of human osteosarcoma. *Int J Cancer.* doi: 10.1002/ijc.29269. [Epub ahead of print]
- Levine B, Deretic V (2007). Unveiling the roles of autophagy in innate and adaptive immunity. *Nature Rev. Immunol.* 7, 767–777.
- Levine B, Kroemer G (2008). Autophagy in the pathogenesis of disease. *Cell* 132:27-42
- Levine B, Yuan J (2005). Autophagy in cell death: an innocent convict? *J Clin Invest* 115:2679-2688
- Li RF, Chen G, Ren JG, Zhang W, Wu ZX, Liu B, Zhao Y, Zhao YF (2014). The adaptor protein p62 is involved in RANKL-induced autophagy and osteoclastogenesis. *J Histochem Cytochem.* 62(12):879-88
- Lin NY, Stefanica A, Distler JH (2013). Autophagy: a key pathway of TNF-induced inflammatory bone loss. *Autophagy.* 9(8):1253-5
- Long J, Gallagher TR, Cavey JR, Sheppard PW, Ralston SH, Layfield R, Searle MS (2008). Ubiquitin recognition by the ubiquitin-associated domain of p62 involves a novel conformational switch. *J Biol Chem.* 283(9):5427-40.
- Long J, Garner TP, Pandya MJ, Craven CJ, Chen P, Shaw B, Williamson MP, Layfield R, Searle MS (2010). Dimerisation of the UBA domain of p62 inhibits ubiquitin binding and regulates NF-kappaB signalling. *J Mol Biol.* 396(1):178-94.
- Lucas GJ, Metha SG, Hocking LJ, Stewart TL, Cundy T, Nicholson GC, Walsh JP, Fraser WD, Watts GD, Ralston SH, Kimonis VE (2006). Evaluation of the role of Valosin-containing protein in the pathogenesis of familial and sporadic Paget's disease of bone. *Bone* 38:280-285
- Madsen L, Seeger M, Semple CA, Hartmann-Petersen R (2009). New ATPase regulators--p97 goes to the PUB. *Int J Biochem Cell Biol* 41:2380-2388
- Manno A, Noguchi M, Fukushi J, Motohashi Y, Kakizuka A (2010). Enhanced ATPase activities as a primary defect of mutant valosin-containing proteins that cause inclusion body myopathy associated with Paget disease of bone and frontotemporal dementia. 15: 911-922
- Marino G, Salvador-Montoliu N, Fueyo A, Knecht E, Mizushima N, López-Otín C (2007). Tissue-specific autophagy alterations and increased tumorigenesis in mice deficient in Atg4C/autophagin-3. *J. Biol. Chem.* 282,18573–18583.

- Martinez-Vicente M, Cuervo AM (2007). Autophagy and neurodegeneration: when the cleaning crew goes on strike. *Lancet Neurol.* 6, 352–361.
- Maziere C, Louvet L, Gomila C, Kamel S, Massy Z, Maziere JC (2009). Oxidised low density lipoprotein decreased Rankl-induced differentiation of osteoclasts by inhibition of Rankl signalling. *J Cell Physiol.* 221:572-578
- Mehta SG, Khare M, Ramani R, Watts GD, Simon M, Osann KE, Donkervoort S, Dec E, Nalbandian A, Platt J, Pasquali M, Wang A, Mozaffar T, Smith CD, Kimonis VE (2013). Genotype-Phenotype studies of VCP-associated Inclusion Body Myopathy with Paget Disease of Bone and/or Frontotemporal Dementia. *Clin Genet.* 83(5): 422–431
- Mehta SG, Watts GD, Adamson JL, Hutton M, Umberger G, Xiong S, Ramdeen S, Lovell MA, Kimonis VE, Smith CD (2007). APOE is a potential modifier gene in an autosomal dominant form of frontotemporal dementia (IBMPFD). *Genet Med* 9:9-13
- Menea C, Barsony J, Reddy SV, Cornish J, Cundy T, Roodman GD (2000). 1,25-Dihydroxyvitamin D3 hypersensitivity of osteoclast precursors from patients with Paget's disease. *J Bone Miner Res* 15:228-236
- Menea C, Reddy SV, Kurihara N, Maeda H, Anderson D, Cundy T, Cornish J, Singer FR, Bruder JM, Roodman GD (2000). Enhanced RANK ligand expression and responsiveness of bone marrow cells in Paget's disease of bone. *J Clin Invest.* 105(12):1833-8
- Meyer H, Bug M, Bremer S (2012). Emerging functions of the VCP/p97 AAA-ATPase in the ubiquitin system. *Nat Cell Biol* 14:117-123
- Meyer HH, Kondo H, Warren G (1998). The p47 co-factor regulates the ATPase activity of the membrane fusion protein, p97. *FEBS Lett.* 437(3):255-7.
- Meyer HJ, Rape M (2014). Enhanced protein degradation by branched ubiquitin chains. *Cell.* 157(4):910-21.
- Michou L, Morissette J, Gagnon ER, Marqui A, Dellabadia M, Brown JP, Siris ES (2011). Novel SQSTM1 mutations in patients with Paget's disease of bone in an unrelated multiethnic American population. *Bone* 48:456-60;
- Mizuno Y, Hori S, Kakizuka A, Okamoto K (2003). Vacuole-creating protein in neurodegenerative diseases in humans. *Neurosci. Lett.* 343: 77-80
- Mizuno Y, Ikeda K, Tsuchiya K, Ishihara R, Shibayama H (2003). Two distinct subgroups of senile dementia of Alzheimer type: quantitative study of neurofibrillary tangles. *Neuropathology.* 23(4): 282-9
- Mizushima N, Levine B, Cuervo AM, Klionsky DJ (2008). Autophagy fights disease through cellular self-digestion. *Nature* 451:1069-1075
- Mizushima N, Yoshimori T, Levine B (2010). Methods in mammalian autophagy research. *Cell* 140(3):313-26

- Mogi M1, Kondo A (2009). Down-regulation of mTOR leads to up-regulation of osteoprotegerin in bone marrow cells. *Biochem Biophys Res Commun.* 384(1):82-6
- Morales-Piga AA, Rey-Rey JS, Corres-González J, García-Sagredo JM, López-Abente G (1995). Frequency and characteristics of familial aggregation of Paget's disease of bone. *J Bone Miner Res.* 10(4):663-70
- Mori-Konya C, Kato N, Maeda R, Yasuda K, Higashimae N, Noguchi M, Koike M, Kimura Y, Ohizumi H, Hori S, Kakizuka A (2009). p97/valosin-containing protein (VCP) is highly modulated by phosphorylation and acetylation. *Genes Cells.* 14(4):483-97
- Mori F, Tanji K, Toyoshima Y, Sasaki H, Yoshida M, Kakita A, Takahashi H, Wakabayashi K (2013). Valosin-containing protein immunoreactivity in tauopathies, synucleinopathies, polyglutamine diseases and intranuclear inclusion body disease. *Neuropathology* 33(6): 637-44
- Moscat J, Diaz-Meco MT (2009). p62 at the crossroads of autophagy, apoptosis, and cancer. *Cell* 137(6): 1001-4.
- Mukhopadhyay D, Riezman H (2007). Proteasome-independent functions of ubiquitin in endocytosis and signalling. *Science*, 315: 201–205
- Mullally JE, Chernova T, Wilkinson KD (2006). Doa1 is a Cdc48 adapter that possesses a novel ubiquitin binding domain. *Mol Cell Biol* 26:822-830
- Nakano, T., Nakaso, K., Nakashima, K. & Ohama, E (2004). Expression of ubiquitin-binding protein p62 in ubiquitin-immunoreactive intraneuronal inclusions in amyotrophic lateral sclerosis with dementia: analysis of five autopsy cases with broad clinicopathological spectrum. *Acta Neuropathol.* 107: 359–364
- Nakaso K, Yoshimoto Y, Nakano T, Takeshima T, Fukuhara Y, Yasui K, Araga S, Yanagawa T, Ishii T, Nakashima K (2004). Transcriptional activation of p62/A170/ZIP during the formation of the aggregates: possible mechanisms and the role in Lewy body formation in Parkinson's disease. *Brain Res*, 1012(1-2): 42-51
- Nakatsuka K, Nishizawa Y, Ralston SH (2003). Phenotypic Characterization of early onset Paget's disease of bone caused by a 27-bp duplication in the TNFRSF11A gene. *J Bone Miner. Res.* 18(8): 1381-1385
- Nalbandian A, Donkervoort S, Dec E, Badadani M, Katheria V, Rana P, Nguyen C, Mukherjee J, Caiozzo V, Martin B, Watts GD, Vesa J, Smith C, Kimonis VE (2011). The multiple faces of valosin-containing protein-associated diseases: inclusion body myopathy with Paget's disease of bone, frontotemporal dementia, and amyotrophic lateral sclerosis. *J Mol Neurosci* 45:522-531
- Nalbandian A1, Llewellyn KJ, Badadani M, Yin HZ, Nguyen C, Katheria V, Watts G, Mukherjee J, Vesa J, Caiozzo V, Mozaffar T, Weiss JH, Kimonis VE (2012). A progressive translational mouse model of human valosin-containing protein disease: the VCP(R155H/+) mouse. *Muscle Nerve.* 47(2): 260-70

Nalbandian A1, Llewellyn KJ, Kitazawa M, Yin HZ, Badadani M, Khanlou N, Edwards R, Nguyen C, Mukherjee J, Mozaffar T, Watts G, Weiss JH, Kimonis VE (2012; 2nd). The homozygote VCP R155/R155H mouse model exhibits accelerated human VCP-associated disease pathology. *PLoS ONE* 7(9): 1932-6203

Nalbandian A, Llewellyn KJ, Badadani M, Yin HZ, Nguyen C, Katheria V, Watts G, Mukherjee J, Vesa J, Caiozzo V, Mozaffar T, Weiss JH, Kimonis VE (2013). A progressive translational mouse model of human valosin-containing protein disease: the VCP(R155H/+) mouse. *Muscle Nerve*. 47(2):260-70

Neale SD, Smith R, Wass JA, Athanasou NA (2000). Osteoclast differentiation from circulating mononuclear precursors in Paget's disease is hypersensitive to 1,25-dihydroxyvitamin D(3) and RANKL. *Bone* 27:409-416

Neutzsky-Wulff AV, Sørensen MG, Kocijancic D, Leeming DJ, Dziegiel MH, Karsdal MA, Henriksen K (2010). Alterations in osteoclast function and phenotype induced by different inhibitors of bone resorption--implications for osteoclast quality. *BMC Musculoskelet Disord* 11:109

Niwa H, Ewens CA, Tsang C, Yeung HO, Zhang X, Freemont PS (2012). The Role of the N-Domain in the ATPase Activity of the Mammalian AAA ATPase p97/VCP. *J Biol Chem* 287: 8561-8570

NHS. (05/12/2014). Paget disease. Available: <http://www.nhs.uk/Conditions/Pagets-disease/Pages/Introduction.aspx>. Last accessed 01/01/2015

Nonhoff U, Ralser M, Welzel F, Piccini I, Balzereit D, Yaspo ML, Lehrach H, Krobitsch S (2007). Ataxin-2 interacts with the DEAD/H-box RNA helicase DDX6 and interferes with P-bodies and stress granules. *Mol. Biol. Cell*. 18:1385–1396.

Novack DV, Yin L, Hagen-Stapleton A, Schreiber RD, Goeddel DV, Ross FP, Teitelbaum SL (2003). The I κ B function of NF- κ B2 p100 controls stimulated osteoclastogenesis. *J Exp Med* 198(5):771-81.

Oikawa T, Kuroda Y, Matsuo K (2013). Regulation of osteoclasts by membrane-derived lipid mediators. *Cell Mol Life Sci* 70:3341-3353.

Otero JE, Chen T, Zhang K, Abu-Amer Y (2012). Constitutively active canonical NF- κ B pathway induces severe bone loss in mice. *PLoS One*.7(6):e38694. doi: 10.1371/journal.pone.0038694

Panda D, Rose PP, Hanna SL, Gold B, Hopkins KC, Lyde RB, Marks MS, Cherry S (2013). Genome-wide RNAi screen identifies SEC61A and VCP as conserved regulators of Sindbis virus entry. *Cell Rep*. 5(6): 1737-48

Pandey UB, Batlevi Y, Baehrecke EH, Taylor JP (2007). HDAC6 at the intersection of autophagy, the ubiquitin-proteasome system and neurodegeneration. *Autophagy* 3:643-645

Pankiv S, Clausen TH, Lamark T, Brech A, Bruun JA, Outzen H, Øvervatn A, Bjørkøy G, Johansen T (2007). p62/SQSTM1 binds directly to Atg8/LC3 to facilitate degradation of ubiquitinated protein aggregates by autophagy. *J Biol Chem* 282:24131-24145

- Parker R, Sheth U. P bodies and the control of mRNA translation and degradation (2007). *Mol. Cell.* 25:635–646.
- Pederson L, Ruan M, Westendorf JJ, Khosla S, Oursler MJ (2008). Regulation of bone formation by osteoclasts involves Wnt/BMP signaling and the chemokine sphingosine-1-phosphate. *Proc Natl Acad Sci U S A.* 105(52):20764–20769.
- Pennuto M, Sambataro F (2010). Pathogenesis of Polyglutamine Diseases. *Enc. Of Life Sci.* 1- doi: 10.1002/9780470015902.a0021486/pdf
- Peters JM, Franke WW, Kleinschmidt JA (1994). Distinct 19S and 20S subcomplexes of the 26S proteasome and their distribution in the nucleus and cytoplasm. *J Biol Chem.* 10(11): 7709-7718
- Perutz MF, Johnson T, Suzuki M and Finch JT (1994). Glutamine repeats as polar zippers: their possible role in inherited neurodegenerative diseases. *Proceedings of the National Academy of Sciences of the USA* 91: 5355–5358.
- Poksay KS, Madden DT, Peter AK, Niazi K, Banwait S, Crippen D, Bredesen DE, Rao RV (2011). Valosin-containing protein gene mutations: Cellular phenotypes relevant to neurodegeneration. *J Mol Neurosci.* 44:91-102
- Primer Design Guide (2012). <https://agctsequencing.wordpress.com/2012/05/14/primer-selection-guidelines-good-primers-important-for-pcr-and-automated-sequencing/> Accessed 20 Feb 2012
- Pye VE, Beuron F, Keetch CA, McKeown C, Robinson CV, Meyer HH, Zhang X, Freemont PS (2007). Structural insights into the p97-Ufd1-Npl4 complex. *PNAS* (104): 467–72
- Qin A, Cheng TS, Pavlos NJ, Lin Z, Dai KR, Zheng MH (2012). V-ATPases in osteoclasts: structure, function and potential inhibitors of bone resorption. *Int J Biochem Cell Biol.* 44(9):1422-35.
- Qu X, Yu J, Bhagat G, Furuya N, Hibshoosh H, Troxel A, Rosen J, Eskelinen EL, Mizushima N, Ohsumi Y, Cattoretti G, Levine B (2003). Promotion of tumorigenesis by heterozygous disruption of the beclin 1 autophagy gene. *J. Clin. Invest.* 112, 1809–1820.
- Rabinowitz JD, White E (2010). Autophagy and metabolism. *Science* 330:1344-1348
- Ralston SH (2008) .Pathogenesis of Paget’s disease of bone. *Bone* 43:819-825
- Ravikumar B, Acevedo-Arozena A, Imarisio S, Berger Z, Vacher C, O’Kane CJ, Brown SD, Rubinsztein DC (2005). Dynein mutations impair autophagic clearance of aggregate-prone proteins. *Nat Genet.* 37(7):771-6
- Ravikumar B, Duden R, Rubinsztein DC (2002). Aggregate-prone proteins with polyglutamine and polyalanine expansions are degraded by autophagy. *Hum Mol Genet.* 11(9): 1107-17
- Rea SL, Walsh JP, Ward L, Magno AL, Ward BK, Shaw B, Layfield R, Kent GN, Xu J, Ratajczak T (2009). Sequestosome 1 mutations in Paget’s disease of bone in Australia: prevalence, genotype/phenotype correlation, and a novel non-UBA domain mutation

(P364S) associated with increased NF-kappaB signaling without loss of ubiquitin binding. *J Bone Miner Res.* 24(7):1216-23

Rechsteiner M, Rogers SW (1996). PEST sequences and regulation by proteolysis. *Trends Biochem Sci.* 21(7): 267-71

Reijns MA, Alexander RD, Spiller MP, Beggs JD (2008). A role for Q/N-rich aggregation-prone regions in Pbody localization. *J. Cell Sci.* 121:2463–2472.

Ritson GP, Custer SK, Freibaum BD, Guinto JB, Geffel D, Moore J, Tang W, Winton MJ, Neumann M, Trojanowski JQ, Lee VM, Forman MS, Taylor JP (2010). TDP-43 mediates degeneration in a novel *Drosophila* model of disease caused by mutations in VCP/p97. *J Neurosci.* 20:7729-7739

Ritz D, Vuk M, Kirchner P, Bug M, Schütz S, Hayer A, Bremer S, Lusk C, Baloh RH, Lee H, Glatter T, Gstaiger M, Aebersold R, Wehl CC, Meyer H. (2011). Endolysosomal sorting of ubiquitylated caveolin-1 is regulated by VCP and UBXD1 and impaired by VCP disease mutations. *Nat Cell Biol* 13(9): 1116–1123.

Rodriguez-Ortiz CJ, Hoshino H, Cheng D, Liu-Yescevitiz L, Blurton-Jones M, Wolozin B, LaFerla FM, Kitazawa M (2013). Neuronal-specific overexpression of a mutant valosin-containing protein associated with IBMPFD promotes aberrant ubiquitin and TDP-43 accumulation and cognitive dysfunction in transgenic mice. *Am J Pathol.* 183(2):504-15.

Roodman GD, Windle JJ (2005). Paget disease of bone. *J Clin Invest.* 115(2):200-8.

Roy L, Bergeron JJ, Lavoie C, Hendriks R, Gushue J, Fazel A, Pelletier A, Morre DJ, Subramaniam VN, Hong W, Paiement J (2000). Role of p97 and syntaxin 5 in the assembly of transitional endoplasmic reticulum. *Mol Biol Cell.* 11:2529–42.

Rubino E, Rainero I, Chiò A, Rogaeva E, Galimberti D, Fenoglio P, Grinberg Y, Isaia G, Calvo A, Gentile S, Gentile S, Bruni AC, St George-Hyslop PH, Scarpini E, Gallone S, Pinessi L; TODEM Study Group (2012). SQSTM1 mutations in frontotemporal lobar degeneration and amyotrophic lateral sclerosis. *Neurology* 79:1556-62

Rubinsztein DC (2006). The roles of intracellular protein-degradation pathways in neurodegeneration. *Nature* 443, 780–786

Rumpf S, Jentsch S (2006). Functional division of substrate processing cofactors of the ubiquitin-selective Cdc48 chaperone. *Mol Cell.* 21(2):261-9

Sabharwal R, Gupta S, Sepolia S, Panigrahi R, Mohanty S, Subudhi SK, Kumar M (2014). An Insight in to Paget's Disease of Bone. *Niger J Surg.* 20(1): 9–15

Saitoh T, Fujita N, Jang MH, Uematsu S, Yang BG, Satoh T, Omori H, Noda T, Yamamoto N, Komatsu M, Tanaka K, Kawai T, Tsujimura T, Takeuchi O, Yoshimori T, Akira S (2008). Loss of the autophagy protein Atg16L1 enhances endotoxin-induced IL-1beta production. *Nature* 456(7219):264-8.

- Salajegheh M, Pinkus JL, Taylor JP, Amato AA, Nazareno R, Baloh RH, Greenberg SA (2009). Sarcoplasmic redistribution of nuclear TDP-43 in inclusion body myositis. *Muscle & nerve* 40:19–31.
- Sambandam Y, Townsend MT, Pierce JJ, Lipman CM, Haque A, Bateman TA, Reddy SV (2014). Microgravity control of autophagy modulates osteoclastogenesis. *Bone* 61:125-31
- Sasazawa Y, Kanagaki S, Tashiro E, Nogawa T, Muroi M, Kondoh Y, Osada H, Imoto M (2012). Xanthohumol impairs autophagosome maturation through direct inhibition of valosin-containing protein. *ACS Chem Biol.* 7(5):892-900.
- Sato T, Nakashima A, Guo L, Tamanoi F (2009). Specific activation of mTORC1 by Rheb G-protein in vitro involves enhanced recruitment of its substrate protein. *J Biol Chem.* 284(19):12783-91
- Scheffner M, Nuber U, Huibregtse JM (1995). Protein ubiquitination involving an E1–E2–E3 enzyme ubiquitin thioester cascade. *Nature*, 373: 81–83
- Schmid D, Pypaert M, Münz C (2007). Antigenloading compartments for major histocompatibility complex class II molecules continuously receive input from autophagosomes. *Immunity* 26:79–92.
- Schroder R, Watts GD, Mehta SG, Evert BO, Broich P, Fließbach K, Pauls K, Hans VH, Kimonis V, Thal DR (2005). Mutant valosin-containing protein causes a novel type of frontotemporal dementia. *Ann Neurol.* 57: 457–61.
- Searle MS, Garner TP, Strachan J, Long J, Adlington J, Cavey JR, Shaw B, Layfield R (2012). Structural insights into specificity and diversity in mechanisms of ubiquitin recognition by ubiquitin-binding domains. *Biochem Soc Trans.* 40(2):404-8
- Seibenhener ML, Geetha T, Wooten MW (2007). Sequestosome 1/p62 – More than just a scaffold. *FEBS let.* 581(2): 175-179
- Seguin SJ, Morelli FF, Vinet J, Amore D, De Biasi S, Poletti A, Rubinsztein DC, Carra S (2014). Inhibition of autophagy, lysosome and VCP function impairs stress granule assembly. *Cell Death Differ.* 21(12):1838-51.
- Singh R, Xiang Y, Wang Y, Baikati K, Cuervo AM, Luu YK, Tang Y, Pessin JE, Schwartz GJ, Czaja MJ (2009). Autophagy regulates adipose mass and differentiation in mice. *J Clin Invest* 119:3329-3339
- Shaw CE (2010). Capturing VCP: another molecular piece in the ALS jigsaw puzzle. *Neuron* 68:812-814
- Shvets E, Fass E, Scherz-Shouval R, Elazar Z (2008). The N-terminus and Phe52 residue of LC3 recruit p62/SQSTM1 into autophagosomes. *J Cell Sci* 121:2685-2695
- Schubert U, Anton LC, Gibbs J, Norbury CC, Yewdell JW, Bannink JR (2000). Rapid degradation of a large fraction of newly synthesized proteins by proteasomes. *Nature* 404: 770–774.

Shui C, Riggs BL, Khosla S (2002). The immunosuppressant rapamycin, alone or with transforming growth factor beta, enhances osteoclast differentiation of RAW264.7 monocyte-macrophage cells in the presence of RANK-Ligand. *Calcif Tissue Int* 71:437-446

Smink JJ, Begay V, Schoenmaker T, Sterneck E, de Vries TJ, Leutz A (2009). Transcription factor C/EBPbeta isoform ratio regulates osteoclastogenesis through MafB. *EMBO J* 28:1769-1781

Smink JJ, Leutz A (2010). Rapamycin and the transcription factor C/EBPbeta as a switch in osteoclast differentiation: implications for lytic bone disease. *J Mol Med* 88:227-233

Smink JJ, Tunn PU, Leutz A (2012). Rapamycin inhibits osteoclast formation in giant cell tumor of bone through the C/EBPbeta – MafB axis. *J Mol Med* 90:25-30

Song C, Wang Q, Song C, Lockett SJ, Colburn NH, Li CC, Wang JM, Rogers TJ (2015). Nucleocytoplasmic shuttling of valosin-containing protein (VCP/p97) regulated by its N-domain and C-terminal region. *Biochim Biophys Acta*.1853(1):222-32.

Song C, Wang Q, Li CC (2007). Characterization of the aggregation-prevention activity of p97/valosin-containing protein. *Biochemistry* 25; 46(51):14889-98.

Stapf C, Cartwright E, Bycroft M, Hofmann K, Buchberger A (2011). The general definition of the p97/valosin-containing protein (VCP)-interacting motif (VIM) delineates a new family of p97 cofactors. *J Biol Chem* 286:38670-38678

Stenbeck G, Horton MA (2004). Endocytic trafficking in actively resorbing osteoclasts. *J Cell Sci* 117:827-836

Srinivas V, Bohensky J, Shapiro IM (2009). Autophagy: A new phase in the maturation of growth plate chondrocytes is regulated by HIF, mTOR and AMP kinase. *Cell Tissue Organ* 189: 88-92

Song C, Wang Q, Li CC (2007). Characterization of the aggregation-prevention activity of p97/valosin-containing protein. *Biochemistry* 25; 46(51):14889-98.

Song C, Wang Q, Song C, Rogers TJ (2015). Valosin-containing protein (VCP/p97) is capable of unfolding polyubiquitinated proteins through its ATPase domains. *Biochem Biophys Res Commun*. 463(3):453-7.

Sowa ME, Bennett EJ, Gygi SP, Harper JW (2009). Defining the human deubiquitinating enzyme interaction landscape. *Cell* 138, 389-403

Soysa NS, Alles N, Aoki K, Ohya K (2012). Osteoclast formation and differentiation: an overview. *J Med Dent Sci*. 59(3):65-74

Sun SC (2011). Non-canonical NF- κ B signalling pathway. *Cell Res*. 21: 71-85

Suzuki T, Nakagawa M, Yoshikawa A, Sasagawa N, Yoshimori T, Ohsumi Y, Nishino I, Ishiura S, Nonaka I. (2002). The first molecular evidence that autophagy relates rimmed vacuole formation in chloroquine myopathy." *J Biochem* 131(5): 647-51.

- Takahashi Y, Coppola D, Matsushita N, Cualing HD, Sun M, Sato Y, Liang C, Jung JU, Cheng JQ, Mulé JJ, Pledger WJ, Wang HG (2007). Bif-1 interacts with Beclin 1 through UVRAG and regulates autophagy and tumorigenesis. *Nature Cell Biol.* 9, 1142–1151
- Tanida I, Waguri S (2010). Measurement of autophagy in cells and tissues. *Methods Mol Biol.* 648:193-214
- Tang WK, Li D, Li C, Esser L, Dai R, Guo L, Xia D (2010). A novel ATP-dependent conformation in p97 N–D1 fragment revealed by crystal structures of disease-related mutants. *The EMBO Journal*, 29(13), 2217–2229
- Tang WK, Xia D (2013). Altered intersubunit communication is the molecular basis for functional defects of pathogenic p97 mutants. *J Biol Chem.* 288(51):36624-35.
- Teitelbaum SL (2011). The osteoclast and its unique cytoskeleton. *Ann N Y Acad Sci* 1240:14-7
- Takeshita S, Fumoto T, Matsuoka K, Park KA, Aburatani H, Kato S, Ito M, Ikeda K (2013). Osteoclast-secreted CTHRC1 in the coupling of bone resorption to formation. *J Clin Invest.* 123(9):3914-24
- Thoreen CC, Kang SA, Chang JW, Liu Q, Zhang J, Gao Y, Reichling LJ, Sim T, Sabatini DM, Gray NS (2009). An ATP-competitive mammalian target of rapamycin inhibitor reveals rapamycin-resistant functions of mTORC1. *J Biol Chem* 284:8023–8032
- Thrower JS, Hoffman L, Rechsteiner M, Pickart CM (2000). Recognition of the polyubiquitin proteolytic signal. *EMBO J.* 19: 94–102
- Tresse E, Salomons FA, Vesa J, Bott LC, Kimonis V, Yao TP, Dantuma NP, Taylor JP (2010). VCP/p97 is essential for maturation of ubiquitin-containing autophagosomes and this function is impaired by mutations that cause IBMPFD. *Autophagy* 6:217-227
- Tung YT, Hsu WM, Lee H, Huang WP, Liao YF (2010). The evolutionarily conserved interaction between LC3 and p62 selectively mediates autophagy-dependent degradation of mutant Huntingtin. *Cell Mol Neurobiol* 30: 795-806
- Uchiyama K, Jokitalo E, Kano F, Murata M, Zhang X, Canas B, Newman R, Rabouille C, Pappin D, Freemont P, Kondo H (2002). VCIP135, a novel essential factor for p97/p47-mediated membrane fusion, is required for Golgi and ER assembly in vivo. *J Cell Biol.* 159(5):855-66
- Vandermoere, F., El Yazidi-Belkoura, I., Slomianny, C., Demont, Y., Bidaux, G., Adriaenssens, E., Lemoine, J. and Hondermarck, H. (2006). The valosin-containing protein (VCP) is a target of Akt signaling required for cell survival. *J. Biol. Chem.*, 281, 14307–14313.
- Vij N (2008). AAA ATPase p97/VCP: cellular functions, disease and therapeutic potential. *J ell Mol ed.* 12(6A): 2511-8
- Wang Q, Song C, Yang X, Li CC (2003). D1 ring is stable and nucleotide-independent, whereas D2 ring undergoes major conformational changes during the ATPase cycle of p97-VCP. *J Biol Chem* 278: 32784-32793

- Wang Q, Song C, Irizarry L, Dai R, Zhang X, Li CC (2005). Multifunctional roles of the conserved Arg residues in the second region of homology of p97/valosin-containing protein. *J Biol Chem.* 280(49):40515-23.
- Watts GD, Thomasova D, Ramdeen SK, Fulchiero EC, Mehta SG, Drachman DA, Weihl CC, Jamrozik Z, Kwiecinski H, Kaminska A, Kimonis VE (2007). Novel VCP mutations in inclusion body myopathy associated with Paget disease of bone and frontotemporal dementia. *Clin Genet.* 72(5):420-6.
- Watts GD, Wymer J, Kovach MJ, Mehta SG, Mumm S, Darvish D, Pestronk A, Whyte MP, Kimonis VE (2004). Inclusion body myopathy associated with Paget disease of bone and frontotemporal dementia is caused by mutant valosin-containing protein. *Nat Genet* 36:377-381
- Weihl CC, Dalal S, Pestronk A, Hanson PI (2006). Inclusion body myopathy-associated mutations in p97/VCP impairs endoplasmic reticulum-associated degradation. *15: 189-199*
- Weihl CC, Miller SE, Hanson PI, Pestronk A (2007). Transgenic expression of inclusion body myopathy associated mutant p97/VCP causes weakness and ubiquitinated protein inclusions in mice. *Hum Mol Genet* 16:919-928
- Weihl CC, Pestronk A, Kimonis VE (2009). Valosin-containing protein disease: inclusion body myopathy with Paget's disease of the bone and fronto-temporal dementia. *Neuromuscul Disord.* 9(5):308-15.
- Weitzmann MN, Pacifici R (2006). Estrogen deficiency and bone loss: an inflammatory tale *J Clin Invest.* 116(5): 1186–1194
- Whyte MP, Hughes AE (2002). Expansile skeletal hyperphosphatasia is caused by a 15-base pair tandem duplication in TNFRSF11A encoding RANK and is allelic to familial expansile osteolysis. *J Bone Miner Res.* 17(1):26-9
- Whyte MP, Obrecht SE, Finnegan PM, Jones JL, Podgornik MN, McAlister WH, Mumm S (2002). Osteoprotegerin deficiency and juvenile Paget's disease. *N Engl J Med.* 347(3):175-84.
- Woodman PG (2003). p97, a protein coping with multiple identities. *J Cell Sci* 116(Pt 21):4283-90
- Wullschleger, S. Loewith R, Hall MN (2006). TOR signaling in growth and metabolism. *Cell* 124, 471–484
- Wu YT, Tan HL, Shui G, Bauvy C, Huang Q, Wenk MR, Ong CN, Codogno P, Shen HM (2010). Dual role of 3-methyladenine in modulation of autophagy via different temporal patterns of inhibition on class I and III phosphoinositide 3-kinase. *J. Biol. Chem.* 285:10850–10861.
- Xiao G, Harhaj EW, Sun SC (2001). NF-kappaB-inducing kinase regulates the processing of NF-kappaB2 p100. *Mol Cell* 7:401-409.
- Xu J, Feng HT, Wang C, Yip KH, Pavlos N, Papadimitriou JM, Wood D, Zheng MH (2003). Effects of Bafilomycin A1: an inhibitor of vacuolar H (+)-ATPases on endocytosis and apoptosis in RAW cells and RAW cell-derived osteoclasts. *J Cell Biochem.* 88(6):1256-64.

- Yamanaka K, Okubo Y, Suzuki T, Ogura T (2004). Analysis of the two p97/VCP/Cdc48p proteins of *Caenorhabditis elegans* and their suppression of polyglutamine-induced protein aggregation. *J Struct Biol.* 146(1-2):242-50
- Yamanaka K, Sasagawa Y, Ogura T (2012). Recent advances in p97/VCP/Cdc48 cellular functions. *Biochim Biophys Acta* 1823:130-137
- Yang Z, Klionsky DJ (2010). Mammalian autophagy: core molecular machinery and signaling regulation. *Curr Opin Biol* 22:124-131
- Yao Z, Xing L, Boyce BF (2009). NF- κ B p100 limits TNF-induced bone resorption in mice by a TRAF3-dependent mechanism. *J Clin Invest.* 119(10):3024-34
- Yeung HO, Kloppsteck P, Niwa H, Isaacson RL, Matthews S, Zhang X, Freemont PS (2008). Insights into adaptor binding to the AAA protein p97. *Biochem Soc Trans.* 36(Pt1): 62-7
- Ye Y (2006). Diverse functions with a common regulator: ubiquitin takes command of an AAA ATPase. *J Struct Biol.* 156(1):29-40.
- Ye Y, Meyer HH, Rapoport TA (2003) Function of the p97-Ufd1-Npl4 complex in retrotranslocation from the ER to the cytosol: dual recognition of nonubiquitinated polypeptide segments and polyubiquitin chains. *J Cell Biol.* 162(1):71-84
- You JS, Frey JW, Hornberger TA (2012). Mechanical stimulation induces mTOR signaling via an ERK-independent mechanism: implications for a direct activation of mTOR by phosphatidic acid. *PLoS One.* 7(10):e47258.
- Yue Z., Jin S, Yang C, Levine AJ, Heintz N (2003). Beclin 1, an autophagy gene essential for early embryonic development, is a haploinsufficient tumor suppressor. *Proc. Natl Acad. Sci. USA* 100, 15077–15082 .
- Zhao S, Cheng T, Peng X, Zhang X (2011). Inhibition of aseptic loosening by receptor activator of nuclear factor kappa B ligand antibody in osteolysis model of mouse. *Zhongguo Xiu Fu Chong Jian Wai Ke Za Zhi.* 25(6):656-60.
- Zhao Y, Chen G, Zhang W, Xu N, Zhu JY, Jia J, Sun ZJ, Wang YN, Zhao YF (2012). Autophagy regulates hypoxia-induced osteoclastogenesis through the HIF-1 α /BNIP3 signalling pathway. *J. Cell. Physiol.* 227: 639-648
- Zhang X, Gui L, Zhang X, Bulfer SL, Sanghez V, Wong DE, Lee Y, Lehmann L, Lee JS, Shih PY, Lin HJ, Iacovino M, Wehl CC, Arkin MR, Wang Y, Chou Tf (2015). Altered cofactor regulation with disease-associated p97/VCP mutations. *Proc Natl Acad Sci U S A.* pii: 201418820. [Epub ahead of print]
- Zhou H, Luo Y, Huang S (2010). Updates of mTOR inhibitors. *Anticancer Agents Med Chem.* 10(7):571-81.
- Zou W, Hakim I, Tschoep K, Endres S, Bar-Shavit Z (2001). Tumor necrosis factor-alpha mediates RANK ligand stimulation of osteoclast differentiation by an autocrine mechanism. *J Cell Biochem.* 25;83(1):70-83.

APPENDIX

APPENDIX

Homo sapiens VCP/TERA/p97 (Gene ID 7415); Accession Number: NM_007126;

```
ATGGCTTCTGGAGCCGATTCAAAGGTGATGACCTATCAACAGCCATTCTCAAACAGAAGAACCGTCCC
AATCGGTTAATTGTTGATGAAGCCATCAATGAGGACAACAGTGTGGTGTCTTGTCCCAGCCCAAGATG
GATGAATTGCAGTTGTTCCGAGGTGACACAGTGTGCTGAAAGGAAAGAAGAGACGAGAAGCTGTTTGC
ATCGTCTTTTCTGATGATACTTGTCTGATGAGAAGATTTCGGATGAATAGAGTTGTTTCGGAATAACCTT
CGTGTACGCCTAGGGGATGTCATCAGCATCCAGCCATGCCCTGATGTGAAGTACGGCAAACGTATCCAT
GTGCTGCCCATTTGATGACACAGTGAAGGCATTACTGGTAATCTCTTCGAGGTATACCTTAAGCCGTAC
TTCTTGAAGCGTATCGACCCATCCGAAAGGAGACATTTTTCTTGTCCGTGGTGGGATGCGTGTGTG
GAGTTCAAAGTGGTGGAAACAGATCCTAGCCCTTATTGCATTGTTGCTCCAGACACAGTATCCACTGC
GAAGGGGAGCCTATCAAACGAGAGGATGAGGAAGAGTCCCTTGAATGAAGTAGGGTATGATGACATTGGT
GGCTGCAGGAAGCAGCTAGCTCAGATAAAGGAGATGGTGGAACTGCCCTGAGACATCTGCCCTCTTT
AAGGCAATTGGTGTGAAGCCTCTAGAGGAATCCTGCTTTACGGACCTCCTGGAACAGGAAAGACCCTG
ATTGCTCGAGCTGTAGCAAATGAGACTGGAGCCTTCTTCTTCTTGATCAATGGTCTGAGATCATGAGC
AAATTGGCTGGTGTGAGTCTGAGAGCAACCTTCGTAAAGCCTTTGAGGAGGCTGAGAAGAATGCTCCTGCC
ATCATCTTCATTGATGAGCTAGATGCCATCGCTCCCAAAGAGAGAAAACATGCGGAGGTGGAGCGG
CGCATTGTATCACAGTTGTTGACCCTCATGGATGGCTAAAGCAGAGGGCACATGTGATTGTTATGGCA
GCAACCAACAGACCCAACAGCATTGACCCAGCTCTACGGCGATTTGGTCGCTTTGACAGGGAGGTAGAT
ATTGGAATTCCTGATGCTACAGGACGCTTAGAGATTCTTCAGATCCATACCAAGAACATGAAGCTGGCA
GATGATGTGGACCTGGAACAGGTAGCCAATGAGACTCACGGGCATGTGGGTGCTGACTTAGCAGCCCTG
TGCTCAGAGGCTGCTCTGCAAGCCATCCGCAAGAAGATGGATCTCATTGACCTAGAGGATGAGACCATT
GATGCCGAGGTCATGAACTCTCTAGCAGTTACTATGGATGACTTCCGGTGGGCCTTGAGCCAGAGTAAC
CCATCAGCACTGCGGGAAACCGTGGTAGAGGTGCCACAGGTAACCTGGGAAGACATCGGGGGCCTAGAG
GATGTCAAACGTGAGCTACAGGAGCTGGTCCAGTATCCTGTGGAGCACCCAGACAAAATTCCTGAAGTTT
GGCATGACACCTTCCAAGGGAGTTCTGTTCTATGGACCTCCTGGCTGTGGGAAAACCTTTGTTGGCCAAA
GCCATTGCTAATGAATGCCAGGCCAACTTCATCTCCATCAAGGGTCTGAGCTGCTCACCATGTGGTTT
GGGGAGTCTGAGGCCAATGTCAGAGAAATCTTTGACAAGGCCCGCCAAGCTGCCCCCTGTGTGCTATTC
TTTGATGAGCTGGATTTCGATTGCCAAGGCTCGTGGAGGTAACATTGGAGATGGTGGTGGGGCTGCTGAC
CGAGTCATCAACCAGATCCTGACAGAAATGGATGGCATGTCCACAAAAAAAAAATGTGTTTCATCATTGGC
GCTACCAACCGCCTGACATCATTGATCCTGCCATCCTCAGACCTGGCCGCTTTGATCAGTCATCTAC
ATCCCCTTCTGATGAGAAGTCCCGTGTGCCATCCTCAAGGCTAACCTGCGCAAGTCCCCAGTTGCC
AAGGATGTGGACTTGGAGTTCTGGCTAAAATGACTAATGGCTTCTCTGGAGCTGACCTGACAGAGATT
TGCCAGCGTGTGCAAGCTGGCCATCCGTGAATCCATCGAGAGTGAGATTAGGCGAGAACGAGAGAGG
CAGACAAACCCATCAGCCATGGAGGTAGAAGAGGATGATCCAGTGCCTGAGATCCGTGAGATCACTTT
GAAGAAGCCATGCGCTTTGCGCGCCGTTCTGTGTCAGTGACAATGACATTCGGAAGTATGAGATGTTTGCC
CAGACCCTTCAGCAGAGTGGGGCTTTGGCAGCTTCAGATTCCCTTCAGGGAACAGGGTGGAGCTGGC
CCCAGTCAGGGCAGTGGAGGGGCACAGGTGGCAGTGTATACACAGAAGACAATGATGATGACCTGTAT
GGCTAA
```

Figure A1. *The coding sequence of Human VCP cDNA.*

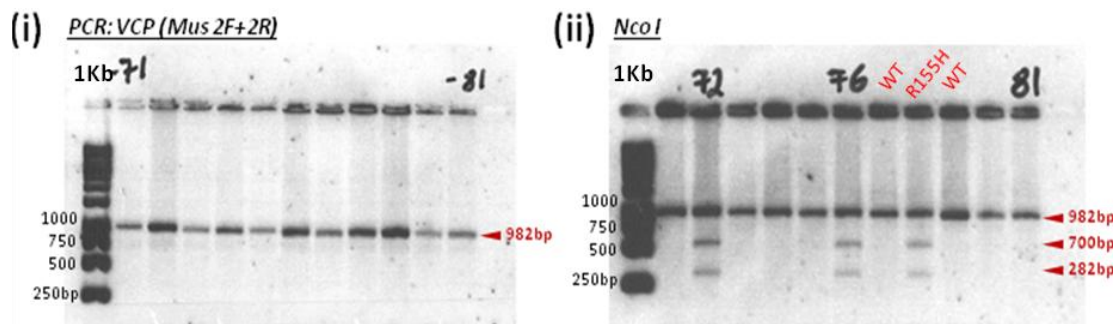
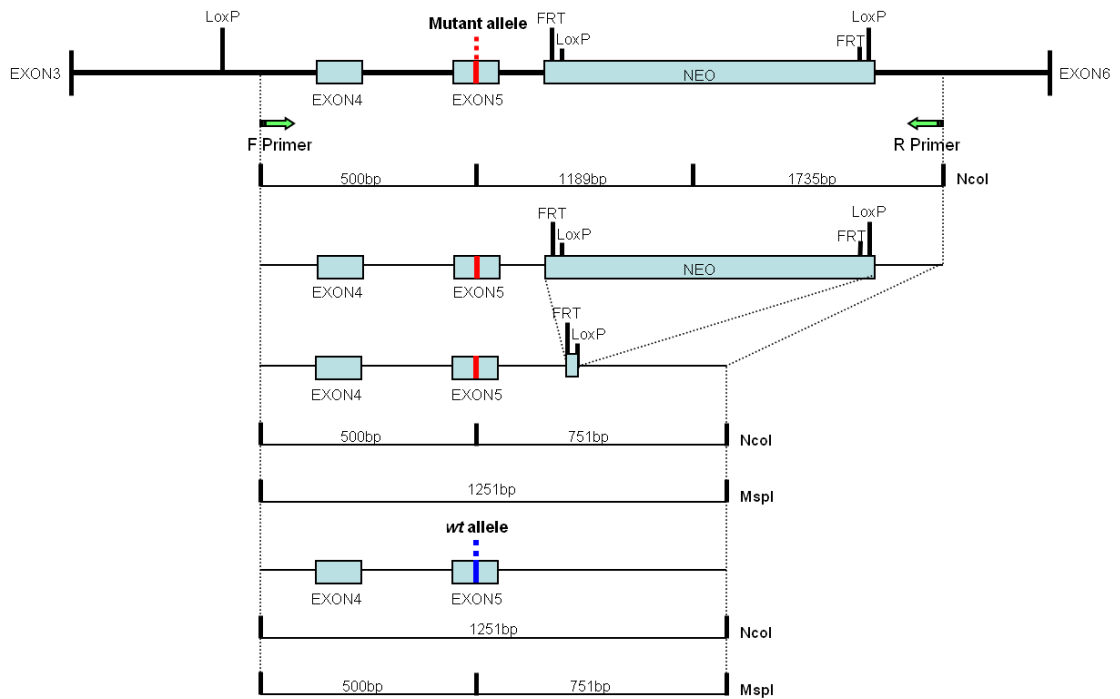


Figure A2. Genotype analyses of $VCP^{R155H/+}$ knock-in mice. Mutant VCP construct is shown at the top. Neomycin-cassette is marked by Neo. Green arrows indicate the locations of primers used in genotyping. After Neomycin cassette is removed we can test for presence of either wild-type or mutant allele. The *Nco* I restriction enzyme cuts mutant allele, conversely *Msp* I will cut wild-type allele. (i) Subjecting the extracted genomic DNA to a PCR protocol results in the generation of DNA fragments of 982bp in size. (ii) Digestion of the PCR product with the *Nco* I restriction enzyme results in three fragments (982bp, 700bp and 282bp) in the heterozygous $VCP^{R155H/+}$ mouse extracts only. The heterozygous $VCP^{R155H/+}$ mouse has a cut (700bp and 282bp) and uncut (982bp) band indicating that both the mutant and wild-type alleles are expressed in this animal. The wild-type mice have uncut (982bp) band only.

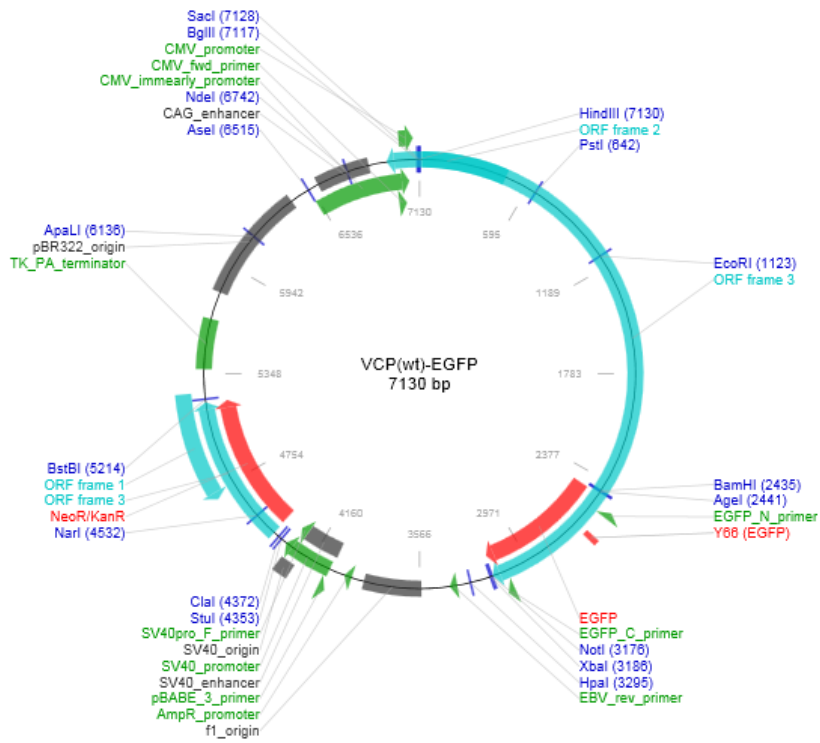


Figure A3. Plasmid map of EGFP-tagged wt VCP including restriction sites.

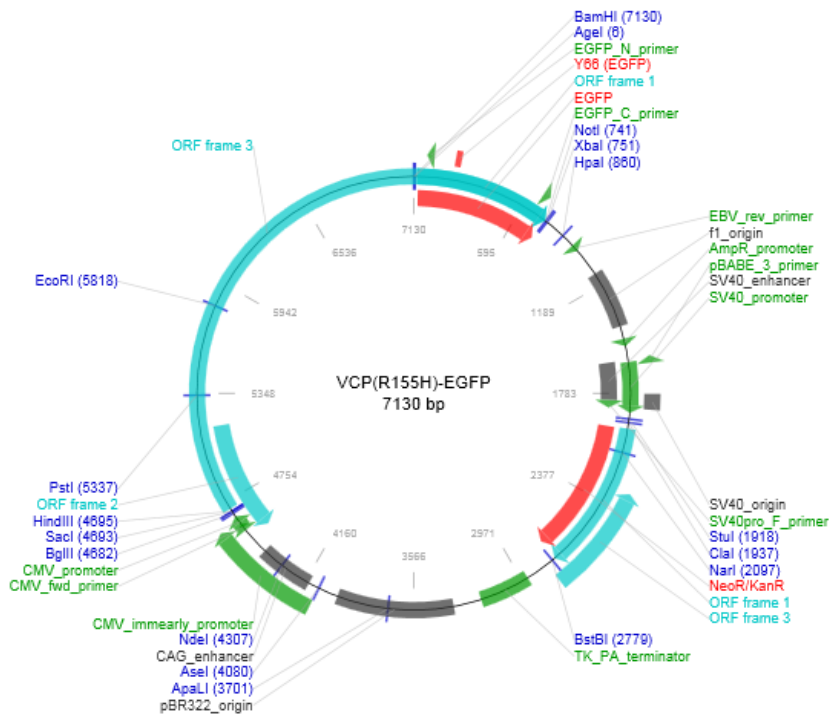


Figure A4. Plasmid map of EGFP-tagged R155H/+ VCP with restriction sites.

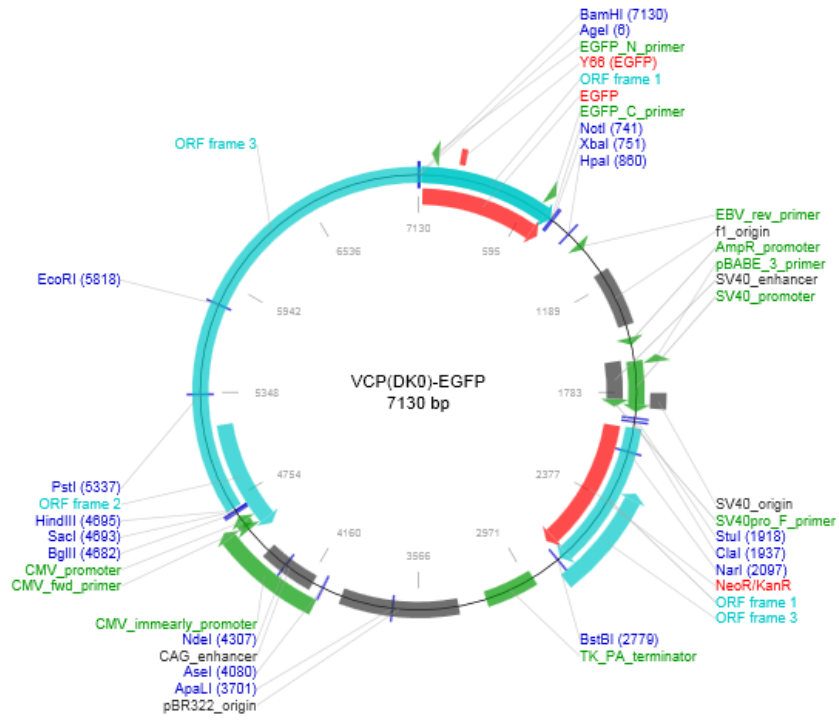
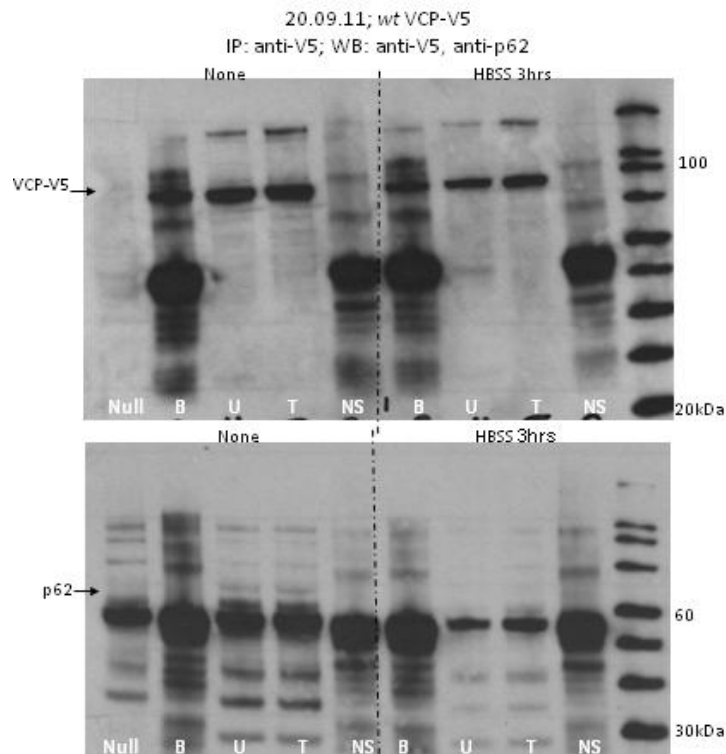
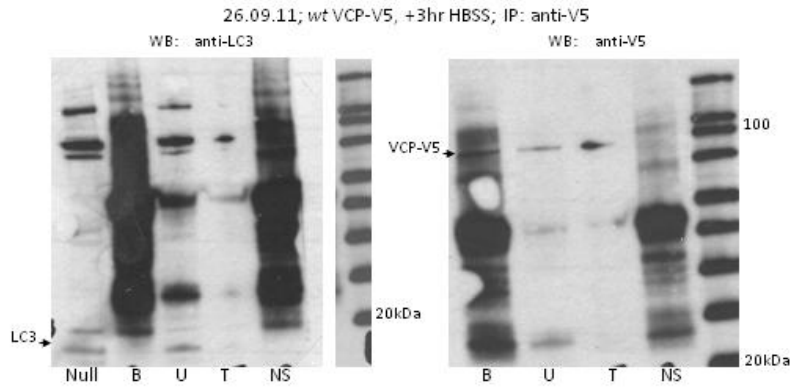


Figure A5. Plasmid map of EGFP-tagged DKO VCP indicating restriction sites.

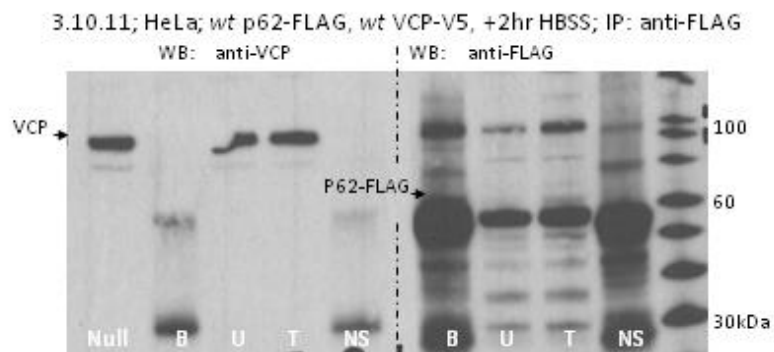
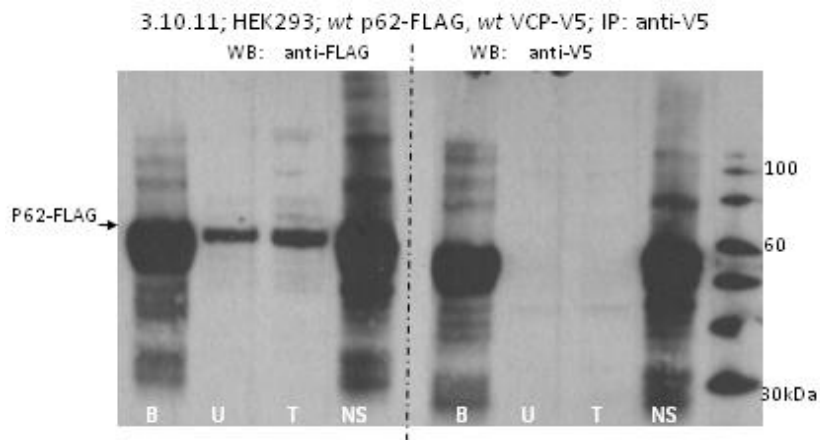
No. 4



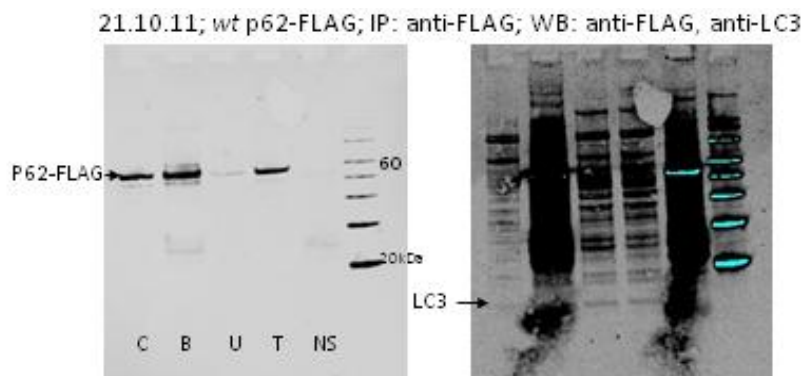
No.5



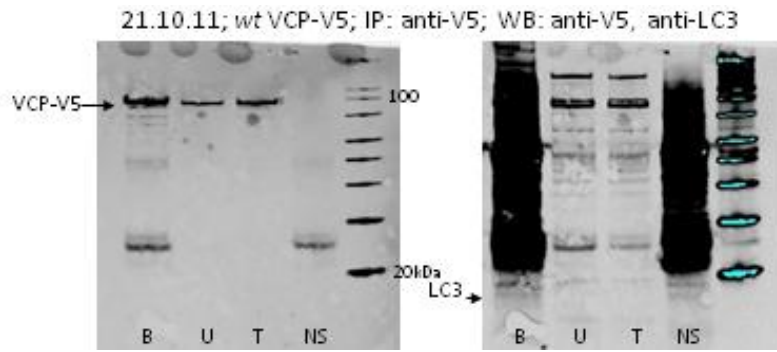
No.6 and 7



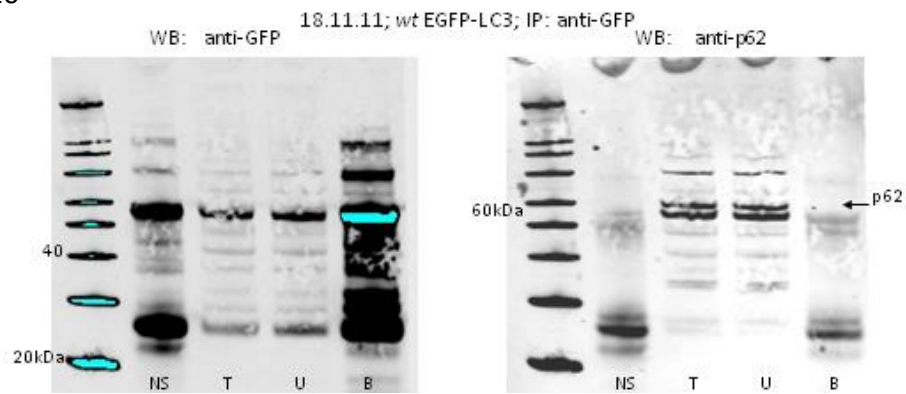
No.8



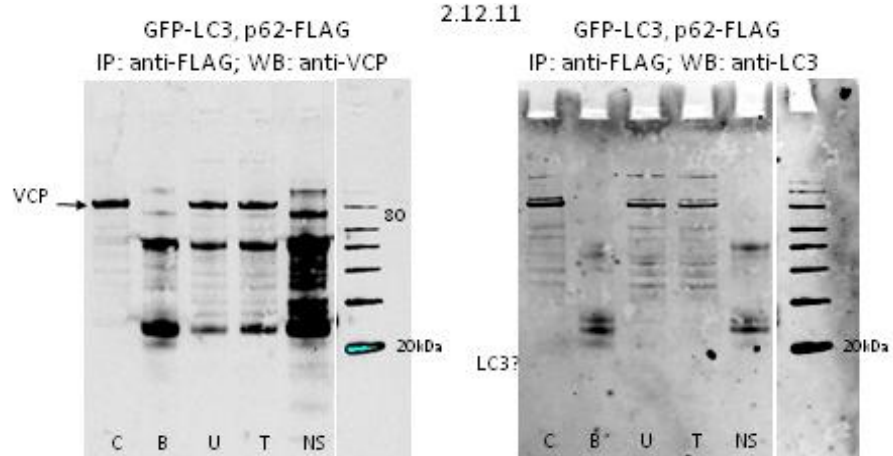
No.9



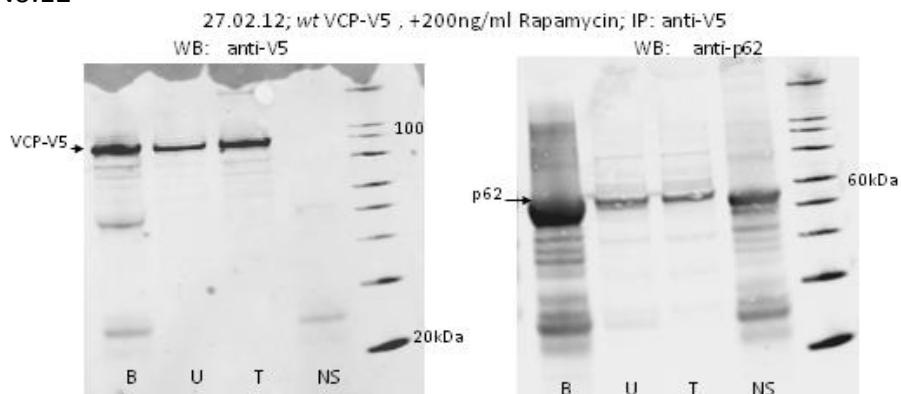
No.10



No.11



No.12



No.13

15.03.12; wt p53-hLC3, +200ng/ml Rapamycin; IP: anti-p62

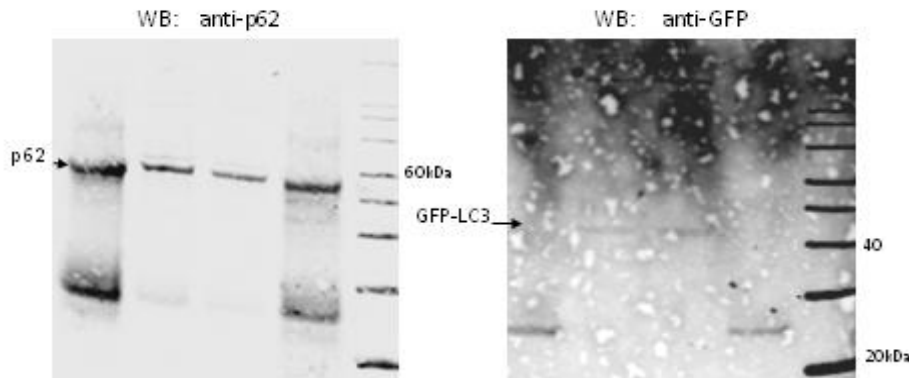


Figure A6. Immunoprecipitation (IP) of VCP and autophagic markers p62 and LC3.

Main areas addressed to trouble shoot the inconsistency of the IP results were: plasmid DNA used for the cell transfection and its concentration, amount of the transfection reagent used, number of plasmids used, timeline of transfection (in hours), additional exposure to stress-inducing reagents and cell line exposed. Additional reagents, such as Rapamycin, were used to directly activate autophagy pathway within the exposed cells. Induction of starvation through 2-3hrs incubation in Hanks Balanced Salt Solution (HBSS) was to trigger starvation-induced-autophagy response. Figures below correspond to 4-13 transfection variants described in Table 4.2 (Chapter 4). NS – IP: IgG; T - total input, B - bound IP fraction, Null – Non-transfected cell lysate, C – non-IP cellular extract.

HeLa, HEK293 and MEF cells were cultured in DMEM supplemented with 10% heat inactivated FBS and 0.5 units/ml penicillin and 50 µg/ml streptomycin.

24h transfection with pCMx-Q79 or pCMx-Q79 + wt VCP-EGFP
IP: anti-p62; WB: anti-VCP, anti-p62

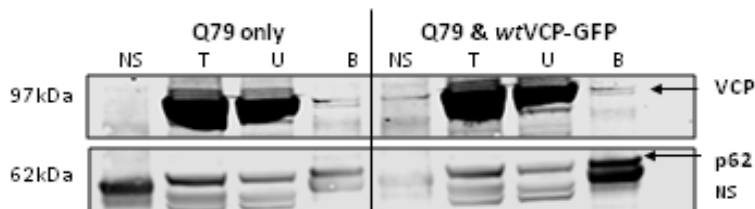


Figure A7. Wild-type (wt) VCP Immunoprecipitates (IP) with wt p62 in cells expressing pathogenic polyglutamines. Pathogenic poly-(Q) 79 glutamines were expressed in MEF cells with or without wt VCP-EGFP for 24h and analysed for co-IP of

VCP with p62 using anti-p62 antibody (Sigma #P0067). Presence of pulled down proteins was determined by Western blotting with anti-p62 and anti-VCP antibodies.

1 μ M Torin1 for 5h; wt VCP-EGFP + wt p62-FLAG IP: anti-p62;
 1 μ M Torin1 for 4h; wt VCP-V5 + wt p62-FLAG IP: anti-FLAG;
 WB: anti-p62 mouse, anti-VCP rabbit, anti-actin mouse

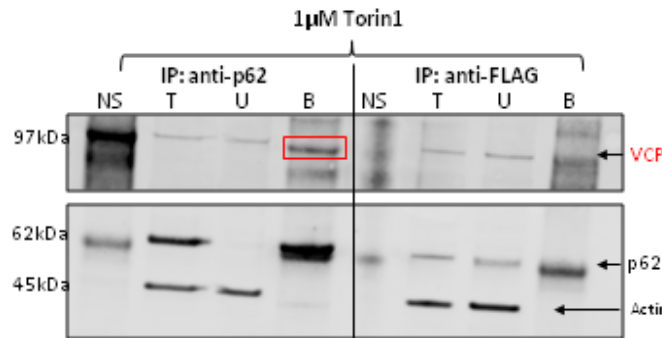


Figure A8. Wild-type VCP Immunoprecipitates (IP) with wt p62 in the mTOR/Autophagy - dependant manner. MEF cells were co-transfected with wt p62-FLAG and wt VCP-EGFP or wt VCP-V5 and after 20h, treated with 1 μ M Torin1 for 4-5 hours. Cell lysates were then subject to Immunoprecipitation by either anti-p62 (Sigma #P0067) or anti-FLAG antibody (Sigma/F7425). Pulled down proteins were analyzed by Western blotting with anti-actin, anti-p62 and anti-VCP antibodies.

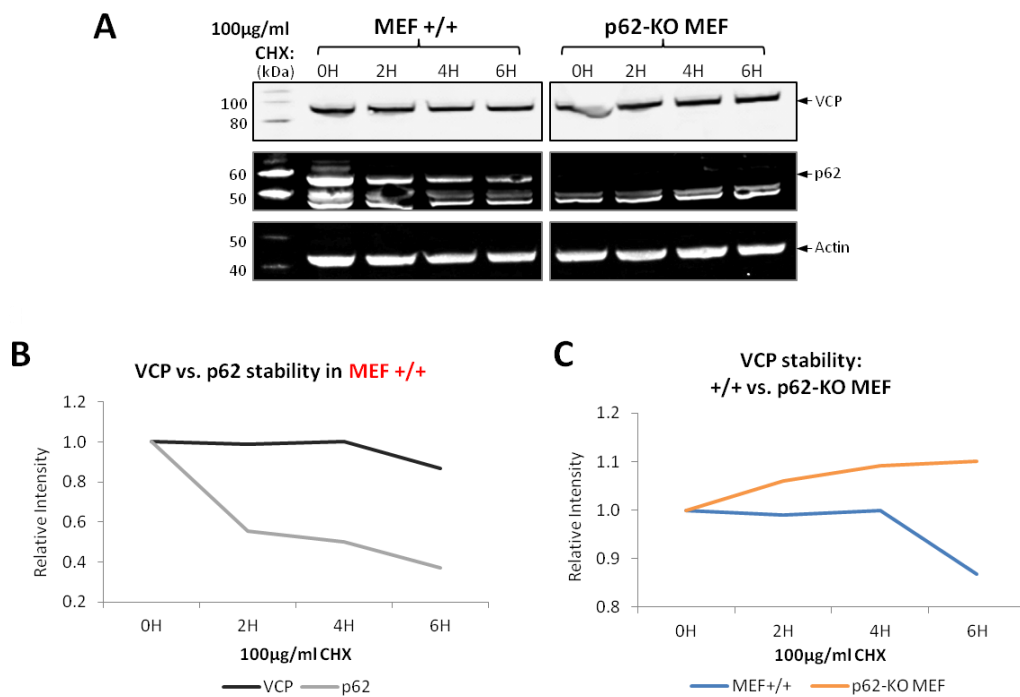
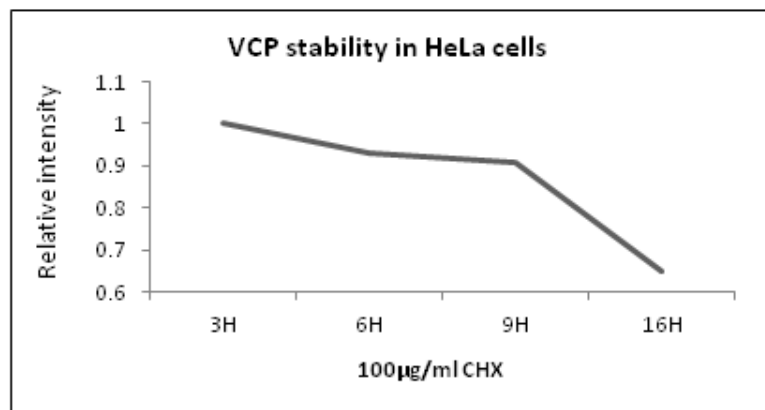


Figure A9. VCP stability increases in cells lacking p62. Immunoblot from cellular extracts of p62-expressing (MEF +/+) and p62-knockout (p62-KO) MEFs exposed to

100 μ g/ml Cycloheximide (CHX) for 0-6hrs (A). Densitometry analysis of normalized to actin p62 and VCP expression from MEF +/+ immunoblot in A (B), and comparison of normalized to actin VCP expression in p62-KO versus VCP expression in normal (p62 expressing) MEF cells (C). Figures presented in B and C show the relative intensity readings (with intensity at 0h=1.0) calculated from arbitrary optical density results normalized to loading control-actin from immunoblots presented in A.

Densitometry of VCP immunoblot from HeLa cells treated with 100 μ g/ml Cycloheximide (CHX) for 3-16 hours.



Densitometry of VCP and p62 immunoblots from HeLa cells treated with a mix of 20 μ M MG132, 6 μ M Torin1 and 100 μ g/ml Cycloheximide (CHX) in a standard growth media for 0-6 hours.

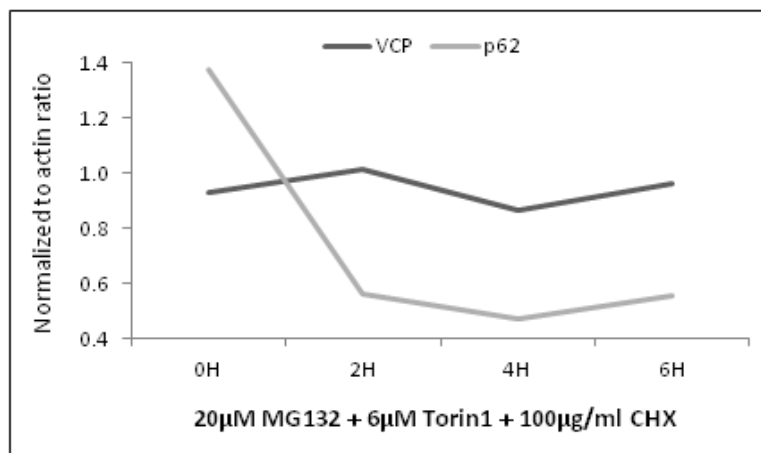


Figure A10. VCP stability in differentiated cells. Densitometry analysis of normalized to actin VCP (Top graph) or p62 and VCP (Bottom graph) expression from immunoblots of HeLa cells treated with 100 μ g/ml cycloheximide for either 3-16 (top) or 0-6(bottom) hours. Additional cell treatment details are included in the overheads. Figures presented show the relative intensity readings calculated from arbitrary optical density results normalized to loading control - actin.

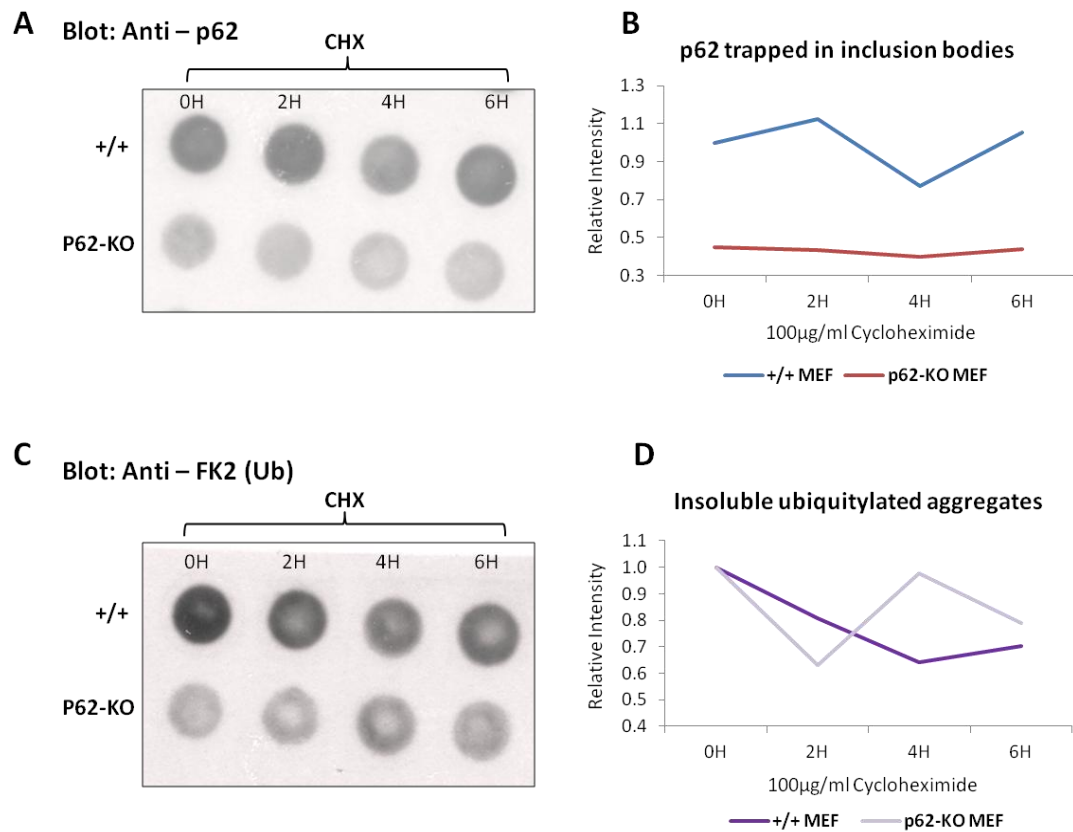


Figure A11. Insoluble aggregates in cells lacking p62. Filter-trap analysis of the p62 insoluble content (A) and insoluble ubiquitinated aggregates (C) generated in p62-expressing (wild-type; +/+) and p62-KO MEFs exposed to 100µg/ml Cycloheximide (CHX) for 0-6hrs. The signal intensity from the p62 (B) and ubiquitin (D) immunoblot was quantified and presented as a relative intensity values of the control at 0hrs exposure (0H).

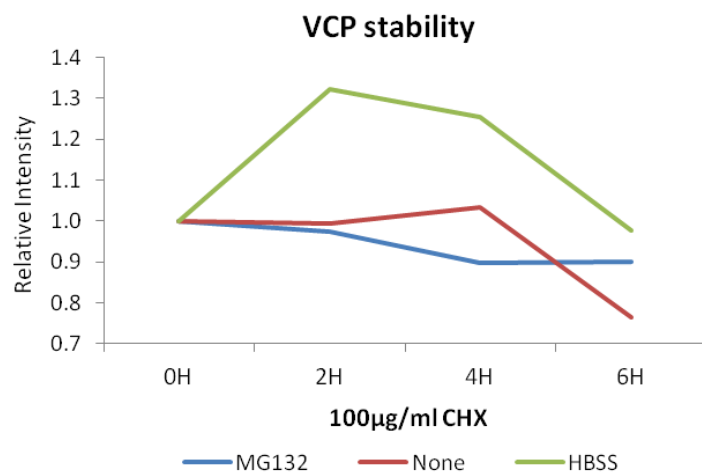


Figure A12. VCP stability in cells. Comparison of normalized VCP levels in MEF cells exposed to 100µg/ml Cycloheximide (CHX) alone (None), incubated in HBSS media

containing 100µg/ml CHX or treated with 25µM MG132 and 100µg/ml CHX for 0-6 hrs .

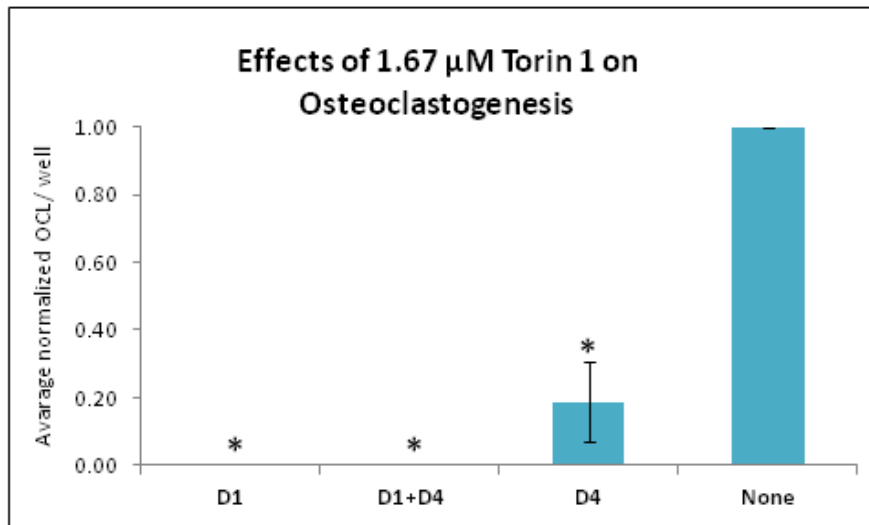


Figure A13. Inhibition of the mTOR signalling with 1.67µM Torin 1 suppresses both early and late stages of osteoclast differentiation. Differentiating RAW264.7 cells were treated with 1.67µM Torin 1 (mTOR signalling inhibitor) on either day 1, day 4 or both day 1 and day 4. Cells were then fixed, stained for TRAP activity and scored for osteoclast-like cells (OCL) per well. Each bar represents the normalized mean \pm SEM of OCL per well from four samples, *p<0.05.

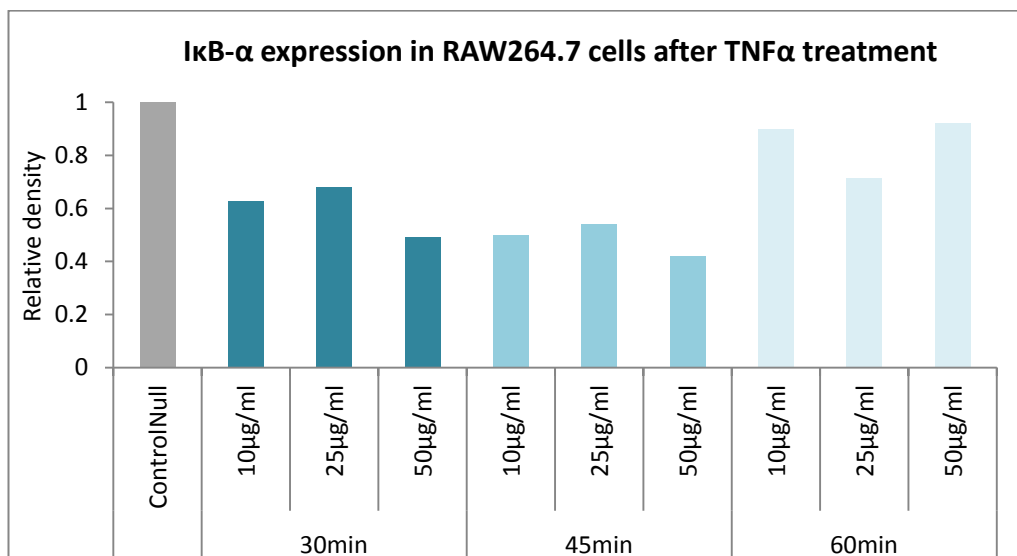


Figure A14. IkB-α expression in RAW264.7 cells after TNFα treatment. Optimising NFκB activation with 10, 25 and 50µg/ml TNFα for 30 – 60 minutes. Bar chart shows results of the analysis of post-treatment IkBα expression in RAW264.7 cells.